

Tassilo Schröder

**Investigation of the rotational vibration
response of human hand-arm systems in the
context of user-centered product development**

Untersuchung des rotatorischen
Schwingungsverhaltens des menschlichen
Hand-Arm-Systems im Kontext der
nutzerzentrierten Produktentwicklung

Band 173

Systeme ■ Methoden ■ Prozesse

Univ.-Prof. Dr.-Ing. Dr. h.c. A. Albers
Univ.-Prof. Dr.-Ing. S. Matthiesen
(Hrsg.)

Forschungsberichte



Tassilo Schröder

Investigation of the rotational vibration response of human hand-arm systems in the context of user-centered product development

Untersuchung des rotatorischen Schwingungsverhaltens des menschlichen Hand-Arm-Systems im Kontext der nutzerzentrierten Produktentwicklung

Band 173

Herausgeber Univ.-Prof. Dr.-Ing. Dr. h.c. A. Albers
Univ.-Prof. Dr.-Ing. S. Matthiesen

Copyright IPEK - Institut für Produktentwicklung, 2024
Karlsruher Institut für Technologie (KIT)
Die Forschungsuniversität in der Helmholtz-Gemeinschaft
Alle Rechte vorbehalten

ISSN 1615-8113

Investigation of the rotational vibration response of human hand-arm systems in the context of user-centered product development

Zur Erlangung des akademischen Grades eines
DOKTORS DER INGENIEURWISSENSCHAFTEN (Dr.-Ing.)
von der KIT-Fakultät für Maschinenbau des
Karlsruher Instituts für Technologie (KIT)

angenomme

DISSERTATION

von

M.Sc. Tassilo Schröder

Tag der mündlichen Prüfung	21.03.2024
Hauptreferent	Univ.-Prof. Dr.-Ing. Sven Matthiesen
Koreferent	Univ.-Prof. Dr.-Ing. Robert Weidner

Vorwort der Herausgeber

Wissen ist einer der entscheidenden Faktoren in den Volkswirtschaften unserer Zeit. Der Unternehmenserfolg wird mehr denn je davon abhängen, wie schnell ein Unternehmen neues Wissen aufnehmen, zugänglich machen und verwerten kann. Die Aufgabe eines Universitätsinstitutes ist es, hier einen wesentlichen Beitrag zu leisten. In den Forschungsarbeiten wird ständig Wissen generiert. Dieses kann aber nur wirksam und für die Gemeinschaft nutzbar werden, wenn es in geeigneter Form kommuniziert wird. Diese Schriftenreihe dient seit mehr als 20 Jahren als eine Plattform zum Transfer und macht damit das Wissenspotenzial aus aktuellen Forschungsarbeiten am IPEK - Institut für Produktentwicklung Karlsruhe* am Karlsruher Institut für Technologie (KIT) verfügbar. Die Forschung des IPEK ist dabei strukturiert in die Kategorien Systeme, Methoden und Prozesse, um so der Komplexität heutiger Produktentwicklung ganzheitlich gerecht zu werden. Erst die Verknüpfung dieser drei Kategorien ermöglicht die Synthese innovativer Systeme durch Nutzung neuester Methoden und Prozesse. Gleichzeitig werden durch die Systemsynthese die erforschten neuen Methoden und Prozesse validiert und deren Mehrwert für die Praxis abgesichert. Dieses Forschungskonzept prägt nicht nur das IPEK-Leitbild, sondern auch den Charakter dieser Schriftenreihe, da immer alle drei Kategorien und deren Wechselwirkungen berücksichtigt werden. Jeder Band setzt hier individuelle Schwerpunkte und adressiert dabei folgende Forschungsgebiete des IPEK:

- das Entwicklungs- und Innovationsmanagement,
- die Entwicklungs- und Konstruktionsmethodik,
- der Leichtbau von der Ebene des ganzen Systems bis hinunter zur Optimierung des Bauteils,
- die Validierung technischer Systeme auch unter Berücksichtigung der NVH Aspekte (Noise, Vibration, Harshness) mit dem Fokus auf Schwingungen und Akustik an Komponenten und in den Gesamtsystemen sowie deren subjektiver Beurteilung durch den Menschen,
- die Antriebssystemtechnik mit den Schwerpunkten komplette Antriebslösungen für Fahrzeuge und Maschinen,
- das Design, die Tribologie und Erprobung von Kupplungen und Bremsen sowie
- die Gerätetechnik mit dem Schwerpunkt auf Power-Tools.

Die Forschungsberichte stellen Ergebnisse unserer Forschung sowohl anderen Wissenschaftlern als auch den Unternehmen zu Verfügung, um damit die Produktentwicklung in allen ihren Facetten mit innovativen Impulsen zu optimieren.

Albert Albers und Sven Matthiesen

* Eh.: Institut für Maschinenkonstruktionslehre und Kraftfahrzeugbau, Universität Karlsruhe (TH)

Vorwort zu Band 173

Technische Systeme erfüllen ihre Funktion in Interaktion mit ihrer Umwelt. Für die Entwicklung von Mensch-Maschine-Systemen ist es wichtig, die Wechselwirkungen zwischen dem technischen System und dem Menschen zu kennen und zu berücksichtigen. Vibrationen und Schwingungen, die auf das Hand-Arm System eines Menschen aufgebracht werden, führen zu Wechselwirkungen, die auf das mit dem Hand-Arm System interagierende technische System einwirken. Für translatorische Schwingungsanregungen kann die Biodynamik des menschlichen Hand-Arm Systems im Stand der Forschung als umfassend untersucht angesehen werden. Für rotatorische Schwingungsanregungen ist die Biodynamik des menschlichen Hand-Arm Systems weitgehend unbekannt.

Die vorliegende Arbeit „Investigation of the rotational vibration response of human hand-arm systems in the context of user-centered product development“ von Tassilo Schröder befasst sich mit der Untersuchung der Biodynamik des menschlichen Hand-Arm Systems bei rotatorischer Schwingungsanregung. Dabei liefert sie drei zentrale Ergebnisse.

- Ergebnis 1 betrifft die Biodynamik des Menschen bei rotatorischer Anregung,
- Ergebnis 2 einen Messgriff, der die Biodynamik des Hand-Arm Systems überhaupt erst untersuchbar macht,
- Ergebnis 3 eine Methode, die die Entwicklung generischer Griffformen für die Untersuchung von Hand-Arm Systemen bei Vibrationsanregung ermöglicht.

Dabei konnte die rotatorische mechanische Impedanz des menschlichen Hand-Arm Systems bei rotatorischer Vibrationsanregung um die dorsale Achse der Hand mit verschiedenen Griffgeometrien bzw. Greifarten ermittelt werden. Im Rahmen der Messungen konnte der Einfluss der Greif- und Andruckkraft auf die rotatorische Impedanz des Hand-Arm Systems herausgearbeitet werden. Damit wird der Stand des Wissens zur physikalischen Beschreibung des biodynamischen Schwingungsverhaltens des Hand-Arm Systems deutlich erweitert und eine experimentelle Datenbasis geschaffen, um Simulationsmodelle oder physische Hand-Arm Modelle zu parametrisieren. Aus den Messergebnissen hat Tassilo Schröder ein übertragbares Erklärungsmodell abgeleitet, welches die dämpfende Wirkung von primär reibschlüssig gegriffenen Griffformen auf die Impedanz beschreibt.

Das Erklärmodell unterstützt die Entwicklung von Power Tools, indem es Möglichkeiten aufzeigt, wie durch die spezifische Griffgestaltung die Vibrationsbelastung des Anwenders potentiell verringert werden kann.

Mit dem zweiten zentralen Ergebnis der Arbeit wird ein Beitrag zum Testing von Mensch-Maschine-Interaktionen geleistet. Ein neuartiger knaufförmiger Messgriff eröffnet der Forschung zum Schwingungsverhalten des menschlichen Hand-Arm-Systems erstmalig die Möglichkeit, Greifkräfte beim Greifen eines knaufförmigen Griffes zu messen und ihren Einfluss auf die Impedanz zu erforschen.

Die zur Entwicklung des knaufförmigen Messgriffes verwendete datengetriebene Methode ist auf andere generische Griffformen übertragbar. Die Arbeit erweitert somit den Stand der Forschung um ein methodisches Vorgehensmodell zur Ableitung von Messmitteln aus Anwendungsdaten. Zusammenfassend liefern die gemessenen rotatorischen Impedanzwerte des menschlichen Hand-Arm-Systems eine experimentelle Grundlage für die Entwicklung von rotatorischen und multiaxialen Hand-Arm-Modellen. Derartige Modelle umfassen dabei sowohl Simulation wie auch physische wirkungsäquivalente Modelle. Die Verwendung solcher Modelle bei der Validierung von Power Tools ermöglicht reproduzierbare Tests anhand derer Aussagen zum Systemverhalten getroffen werden können und Entwicklung von technischen Systemen zielgerichtet erfolgen kann.

März 2024

Sven Matthiesen

Kurzfassung

In der vorliegenden Arbeit wird die Biodynamik des menschlichen Hand-Arm-Systems bei rotatorischer Schwingungsanregung untersucht. Für translatorische Schwingungsanregungen kann die Biodynamik des menschlichen Hand-Arm-Systems im Stand der Forschung als umfassend untersucht angesehen werden, jedoch fehlt es an Wissen zur Biodynamik bei rotatorischer Anregung. In der Arbeit wird daher die rotatorische, mechanische Impedanz des Hand-Arm-Systems und der Einfluss von Greif- und Andruckkraft sowie Körperhaltung auf diese in mehreren Probandenstudien untersucht. Die Untersuchungen der Arbeit erfolgen im Kontext der Power-Tool-Entwicklung und bilden die Grundlage zur Modellierung schwingungstechnischer Hand-Arm-Ersatzmodellen, die eine höhere Anzahl reproduzierbarer Testzyklen ermöglichen als manuelle Tests. Die Arbeit umfasst dabei drei vorveröffentlichte Probandenstudien, die entsprechend zitiert werden. Die erste Studie behandelt die datengetriebene Konstruktion eines knauf-förmigen Messgriffs zur Greifkraftmessung. Die zweite Studie untersucht die Impedanz des Hand-Arm-Systems mit Hilfe des entwickelten Messgriffs. Die Studienergebnisse zeigen, dass bei der Anregung durch einen knauf-förmigen Griff das Hand-Arm-System ein Feder-Dämpfer-Verhalten aufweist und die Impedanz von der Greifkraft, aber nicht von der Andruckkraft beeinflusst wird. Die dritte Studie der Arbeit untersucht die rotatorische Impedanz des Hand-Arm-Systems beim Greifen eines zylindrischen Messgriffs, der um seine Längsachse rotatorisch schwingt. Die Ergebnisse der dritten Studie zeigen, dass auch für diese Anregung das Hand-Arm-System ein Feder-Dämpfer-Verhalten aufweist. Die Impedanz wird hierbei ebenfalls von der Greifkraft beeinflusst und ist von der Andruckkraft und der Körperhaltung unabhängig. Aus den Ergebnissen der zweiten und dritten Studie wird der schwingungsdämpfende Effekt von primär reibschlüssigen Hand-Griff-Kontakten abgeleitet, der durch die höheren Normalkräfte im Hand-Griff-Kontakt bei stärkerer Greifkraft verringert wird. Der fehlende Einfluss der Andruckkraft auf die Impedanz ergibt sich dabei aus der parallelen Ausrichtung der Andruckkraft zur rotatorischen Anregungsachse. Die Ergebnisse der Arbeit erweitern im Stand der Forschung das Wissen zur rotatorischen Impedanz des Hand-Arm-Systems, die abgeleiteten Erkenntnisse zur Vibrationsdämpfung von reibschlüssigen Hand-Griff-Kontakten sind in der Power-Tool-Entwicklung als Grundlage vibrationsdämpfender Griffdesigns verwendbar. Die in der Arbeit entwickelte Methode zur datengetriebenen Konstruktion des knauf-förmigen Messgriffs ist auf andere Griff-Geometrien übertragbar und kann ebenfalls für die Griffentwicklung genutzt werden. Der in diesem Zusammenhang entwickelte knauf-förmige Messgriff, erweitert die Hand-Arm-Vibrationsforschung um ein zusätzliches Messmittel, in dem er die Greifkraftmessungen bei Vibrationsanregung in einer aufliegenden, umschließenden Handhaltung ermöglicht.

Abstract

The present study investigates the biodynamics of the human hand-arm system during rotational vibration excitation. For translational vibration excitation, the biodynamics of the human hand-arm system can be regarded as widely investigated in the state of research, but there is a lack of knowledge about the biodynamics of rotational excitation. This thesis therefore conducts subject studies to investigate rotational mechanical impedance of the hand-arm system and the influences of gripping force, push force and body posture. Obtained data can be used in research and power tool development for modeling simulative or physical, vibration-related hand-arm models, which allow for more reproducible test cycles than manual tests. The investigations of the thesis are carried out in the context of power tool development. The thesis comprises three pre-published subject studies, which are cited. The first study is concerned with the data-driven design of a knob-shaped measuring handle for gripping force measurement.

This measuring handle is used in the second study to investigate the impedance of the hand-arm system. Results of this study show that when excited by a knob-shaped handle, the hand-arm system indicates a spring-damper dynamic and its impedance is influenced by the gripping force while influences by the push force are negligible. The third study of the thesis investigates the rotational impedance of the hand-arm system when gripping a cylindrical measuring handle that vibrates rotationally around its lateral axis. This study's results demonstrate that this kind of excitation also leads to a spring-damper dynamic in the hand-arm system. Under these circumstances impedance is influenced by the gripping force and is independent of the push force and body posture. From the results of the second and third study, the vibration damping effect of primarily frictional hand-handle contacts is derived. Higher normal forces in hand-handle contacts with stronger gripping force reduce this effect.

The missing influence of the push force on the impedance is a result of the parallel alignment of the rotational excitation axis and the direction of the push force. This work broadens the knowledge about rotational impedance of the hand-arm system in the state of research. Newly derived insights concerning vibration damping of frictional hand-handle contacts can be used in power tool development as a basis for vibration damping handle designs. The method used for the data-driven design of the knob-shaped measuring handle can be applied to other handle geometries and can also contribute to the development of ergonomic handle designs. The knob-shaped measuring handle developed in this context extends the research on hand-arm vibrations by providing an additional measuring device that allows gripping force measurements during vibration excitation in a mounted, enclosing hand position.

Danksagung

Diese Arbeit entstand im Rahmen meiner Tätigkeit als wissenschaftlicher Mitarbeiter am IPEK-Institut für Produktentwicklung des Karlsruher Instituts für Technologie (KIT).

Mein besonderer Dank gilt daher meinem Doktorvater Prof. Sven Matthiesen, der durch meine Anstellung als wissenschaftlicher Mitarbeiter, die Grundlage für diese Arbeit geschaffen hat und sie durch seine Betreuung mit zum Erfolg geführt hat. Für die Möglichkeit zur Promotion sowie für die sehr guten fachlichen und persönlichen Gespräche und meiner damit verbundene wissenschaftliche und persönliche Weiterentwicklung möchte ich mich noch einmal bedanken. In diesem Zusammenhang möchte ich auch Prof. Robert Weidner für die Übernahme des Korreferats danken, womit er ebenfalls den erfolgreichen Abschluss meiner Promotion ermöglicht hat.

Weiterhin will ich dem gesamten IPEK-Team danken. Sowohl die wissenschaftliche Diskussion mit meinen Kollegen, als auch die Unterstützung durch die technischen Dienste und die Administration trugen einen wichtigen Teil zum Entstehen dieser Arbeit bei. Ich danke auch meinem früheren Gruppenleiter Jan Robens für die Bereitstellung der notwendigen Freiräume zur Ausarbeitung dieser Arbeit. Des weiteren möchte ich meinem Freund und Kollegen Dr.-Ing. Andreas Lindenmann dafür danken, dass er mich immer wieder fachlich beraten und unterstützt hat, wodurch er den Erfolg meiner Forschung maßgeblich beeinflusst hat, auch meinem Kollegen Dr.-Ing. Thomas Gwosch möchte ich danken. Durch die Betreuung meiner Masterarbeit am IPEK, hat Thomas Gwosch die Voraussetzung für meine Promotion geschaffen und mir dabei die fachlichen Kenntnisse vermittelt auf denen diese Arbeit u.a. aufbaut. Außerdem möchte ich allen studentischen Hilfskräften und Abschlussarbeiter*innen danken, die durch ihre Arbeit ebenfalls zu meiner Forschung und damit zu dieser Arbeit beigetragen haben.

Neben meinen wissenschaftlichen und beruflichen Wegbegleitern möchte ich auch meinen Freunden und meiner Familie für ihre Unterstützung danken. Hier gilt mein Dank vor allem Dr.-Ing. Miriam Batkowiak und Dr.-Ing. Christoph Breuner mit denen ich gemeinsam die Studien- sowie Promotionszeit verbracht habe. Beiden möchte ich dabei sowohl für die konstruktiven Kommentare zu meiner Arbeit, als auch für die Motivation und Unterstützung während meiner Promotion danken.

Zuletzt möchte ich noch meiner Familie für die Unterstützung danken, die mir das Studium und damit schlussendlich die Promotion ermöglicht hat. Mein Dank gilt hierbei vor allem meiner Mutter. Leider war es meiner Mutter nicht mehr vergönnt meine erfolgreiche Promotion mitzerleben, doch ich denke, sie würde sich darüber freuen und ich möchte mich daher für alles bedanken was sie für mich getan und mir ermöglicht hat, „Danke Mama.“

„Der Mensch ist das Modell der Welt“
Leonardo da Vinci, 1452-1519

Contents

Kurzfassung	i
Abstract	iii
Contents	ix
List of Figures	xiii
List of Tables	xxi
List of Abbreviations	xxiii
Equation Symbols	xxv
1 Introduction	1
1.1 Motivation	1
1.2 Structure of the thesis	3
2 Basics and state of research on the mechanical impedance	5
2.1 Description of the mechanical impedance, apparent mass and apparent stiffness of the human hand-arm system	5
2.2 Overview of the influences on the translational MI	12
2.3 Directions of vibration excitation and the coordinate systems of the hand-arm system	17
2.4 Description of the coupling forces	20
2.5 Description of the body posture	26
2.6 Measurement of the MI and the applied coupling forces	27
2.7 Interim conclusion	33
3 State of research on the measurements of the rotational impedance of the human hand-arm system	35
3.1 State of research on the rotational excitation of the human hand-arm system around the xh –axis and yh –axis	41
3.1.1 Vibration excitation in xh –direction with the hand-arm system in the “palm” position	41
3.1.2 Vibration excitation in yh –direction with the hand-arm system in the “hand grip” position	45
3.2 Overall conclusion on the state of research	50
4 Objective of the thesis	53

5	Research questions and research design.....	57
5.1	Research Questions	57
5.2	Research design.....	61
6	Study on Hypothesis 1: Derivation of the measuring handle design	67
6.1	Thesis specific introduction	67
6.2	Methods	68
6.2.1	Test Subjects	69
6.2.2	Test Setup	70
6.2.3	Test Procedure	72
6.2.5	Analysis of the Grip Force and Influence of the Pressing Force	74
6.3	Results.....	80
6.3.1	Determination of the Separation Plane.....	80
6.3.2	Influence of the Pressing Force and Deviation to the Vertical ...	84
6.5	Discussion	86
6.5.1	Splitting of the Knob-shaped Measuring Handle	86
6.5.2	Influence of the Subjects' Handedness and the Applied Pressing Forces	87
6.5.3	Design and Implementation of the Knob-shaped Measuring Handle	89
6.6	Limitations	90
6.7	Conclusion	92
6.8	Acknowledgment	93
6.9	Thesis specific conclusion	93
7	Study on Hypothesis 2: Rotational impedance around the xh –axis.....	95
7.1	Thesis specific introduction	95
7.2	Methods	96
7.2.1	Test Subjects	96
7.2.2	Test Apparatus.....	97
7.2.3	Test Procedure	101
7.2.4	Data Analysis	102
7.3	Results.....	105
7.3.1	Qualitative results on the influence of the gripping and the push forces on the RMI.....	105
7.3.2	Statistical results on the influence of the gripping and the push forces on the RMI.....	108
7.4	Discussion	109
7.4.1	The plots of the magnitude and the phase angle of the RMI across the applied frequency spectrum.....	109
7.4.2	Influence of the gripping and push force on the RMI	112

7.4.3	Relevance of the results for hand-arm modeling, power tool applications, and risk assessment	114
7.5	Limitations	116
7.6	Conclusion.....	117
7.7	Acknowledgment	118
7.8	Thesis specific conclusion	118
8	Study on Hypothesis 3: Rotational impedance around the <i>yh</i> –axis	121
8.1	Thesis specific introduction.....	121
8.2	Methods	124
8.2.1	Test Subjects.....	124
8.2.2	Test Apparatus	125
8.2.3	Test Procedure	130
8.2.4	Data Evaluation	133
8.3	Results	134
8.3.1	Influence of the Gripping Force on the RMI	134
8.3.2	Influence of the Push Force on the RMI.....	137
8.3.3	Influence of the Body Posture on the RMI	138
8.4	Discussion.....	140
8.4.1	How is the Course of the RMI of the HAS for Rotational Vibration Excitation around the <i>yh</i> -axis?	140
8.4.2	How is the RMI in <i>yh</i> Direction Influenced by the Gripping Forces?	146
8.4.3	How is the RMI in <i>yh</i> Direction Influenced by the Push Forces?	148
8.4.4	How is the RMI in <i>yh</i> direction influenced by the Body Posture?	150
8.4.5	Relevance of the Results to Industrial Applications	150
8.5	Limitations	151
8.6	Conclusion.....	152
8.7	Thesis specific Conclusion	154
9	Summary Overall Discussion and Outlook.....	157
9.1	Summary.....	157
9.2	Overall Discussion.....	160
9.3	Overall Conclusion on the obtained Results	164
9.4	Outlook.....	165
	References	I
	Glossary	XV
	Appendix A.....	XVII

Appendix B	XVIII
Publikationen die unter der Mitautorenschaft des Autors dieser Forschungsarbeit entstanden sind:.....	XXI

List of Figures

Figure 2.1:	Example of a schematic plot of the magnitude $Y1Nsm$ and phase angle $Y2$ (degrees) of the MI of the HAS across the frequency spectrum X (Hz) for translational vibrations excited along the axis of the forearm taken from the ISO 10068 (ISO - International Organization for Standardization, 2012).....	8
Figure 2.2:	Linear, rotational single-mass oscillator with one degree of freedom excited by the external torque T with the inertia J , the rotational spring constant k and the rotational damping constant d . The rotation angel is given by φ , the angular velocity by $\dot{\varphi}$ and the acceleration by $\ddot{\varphi}$	9
Figure 2.3:	Exemplary representation of magnitude and phase angle of the RMI for the mass-, spring- and damper-dominated vibration dynamics of a single-mass oscillator.	12
Figure 2.4:	Basic centric coordinate system for the measuring of the biodynamic response of the HAS according to (ISO - International Organization for Standardization, 2012).....	17
Figure 2.5:	Basic-centric and biodynamic coordinate system defined in the DIN EN ISO 5349-1 within the “hand-grip”- and the “palm”- posture, both figures are taken from the DIN EN ISO 5349-1 and with the description translated into English (DIN Deutsches Institut für Normung e. V., 2001b).	18
Figure 2.6:	Examples from ISO 15230 for the application of the push force F_{pu} and the pull force F_{pu} . Example of the push force acting downwards orthogonally to the guiding force F_g on a knob-shaped handle, the illustration is taken from ISO 15230 (below) (ISO - International Organization for Standardization, 2007).....	22
Figure 2.7:	Schematic application of the guiding force F_g acting orthogonally to the push force F_{pu} on the knob-shaped handle of a sander, the illustration is taken from ISO 15230 (ISO - International Organization for Standardization, 2007).....	23
Figure 2.8:	Example of the gripping force F_{gr} when gripping a cylindrical handle, taken from ISO 15230. Illustration a) on the left side: pressure field p of the gripping. Illustration b) on the right side: the gripping force F_{gr} as clamp-like force acting towards the	

	dividing plane. the dividing plane is oriented by the hand-oriented angle α and the machine oriented angle β with the z –axis along the forearm (ISO - International Organization for Standardization, 2007).....	25
Figure 2.9:	Two examples for torque and friction forces from ISO 15230 a) Moment applied to a cylindrical handle b) Torque applied to a cylindrical handle Key: 1 moment, 2 push or pull force, 3 friction, 4 torque (ISO - International Organization for Standardization, 2007).....	25
Figure 2.10:	Side and top view (left to right) of the schematic illustration of the body posture defined in the ISO 10068 as condition over which the translational MI data were obtained with the corresponding allowable joint angle ranges below (ISO - International Organization for Standardization, 2012).	26
Figure 2.11:	Schematic drawing of a shaker equipped test bench for MI measurement. Own illustration based on (DIN Deutsches Institut für Normung e. V., 2001b; ISO - International Organization for Standardization, 2012, 2013).....	28
Figure 2.12:	Assembly drawing from ISO 10819 of the cylindrical measuring handle. Key: 1 base aluminium, 2 feed force transducer, 3 rear bracket, 4 handle Ø 40mm, 5 accelerometer base, 6 accelerometer, 7 front bracket, 8 handle cover Ø 40mm, 9 grip force transducer (ISO - International Organization for Standardization, 2013).....	29
Figure 2.13:	Examples of handles and surfaces used for translational MI measurement from the state of research (The markings on the sixth picture refer to the positions, where the acceleration was measured via a laser accelerometer (Xu et al., 2011)): 1. (Dong, Welcome, McDowell, & Wu, 2006), 2. (Besa et al., 2007), 3 (Concettoni & Griffin, 2009), 4. (Zhang et al., 2021), 5. (P. Marcotte et al., 2005), 6. (Xu et al., 2011).....	30
Figure 2.14:	Test setup of Matthiesen et al. (2018) for the translational and rotational MI measurement (Matthiesen et al., 2018). Key (translated by the author): 1. Frame, 2. Shaker mount, 3. Lifting drive, 4. Rotation drive, 5. Translational shaker, 6. Rotational shaker, 7. Handle, 8 Gear rack-gear arrangement.	32
Figure 3.1:	The conversion used by Mangold (2019) to convert the rotational excitation of the impulse wrench into a translational excitation of the HAS. The figure was put together by the author	

of the thesis from two figures by Mangold (2019). From left to right: Schematic drawing of the side view of the impulse wrench with the hand gripped, free cut from the rear view of the angular deflected impulse wrench with the hand gripped, rear view of the impulse wrench with the HAS illustrated as single mass oscillator. **Key:** r_{Hand} = radius from the rotation axis to the center of the hand, T = torque of the impulse wrench, x = displacement of the pistol, θ = angular deflection at the center of the hand, m = mass of the HAS in xh –direction, k = spring constant of the HAS in xh –direction, d = damping constant of the HAS in xh –direction.37

Figure 3.2: Left side: Rotational vibration excitation around the yh –axis in the “hand grip” position, according to ISO 10068. Right side: Rotational vibration excitation around the xh –axis in the “palm” position, according to DIN EN ISO 5349-1. The illustration of the hand positions are taken from both standards, the forces and were added by the author of the thesis. **Key:** (xh, yh, zh) = basic centric coordinate axis, TRV +/- = positive and negative torque applied by the rotational vibration, FTx +/- = tangential forces between hand and handle in positive and negative xh –direction, FTy +/- = tangential forces between hand and handle in positive and negative yh –direction, FTz +/- = tangential forces between hand and handle in positive and negative zh –direction.40

Figure 3.3: Comparison between the gripping of a one-handed random orbital sander from Nouri (2019) (left) and the “palm” position from DIN EN ISO 5349-1 (right). A description of the coordinate axes can be found in Figure 2.5 on page 1742

Figure 3.4: Test setup used by Xu et al. (2011) to excite the HAS in the “palm” position via a flat aluminum platform. The photo is taken from Xu et al. (2011). The labels in the photo were added by the author of the thesis.....43

Figure 3.5: Comparison between the gripping of an in-line electric assembly screwdriver taken by the author (left) and the schematic hand position according to ISO 10068 (right). The illustration from ISO 10068 is twisted about 156°.46

Figure 3.6: Position of the accelerometer on the hand of the subject (top) and test setup (bottom) from Chih-Hung Chang and Wang

	(2001) with the biodynamic coordinate system of DIN EN ISO 5349-1 added by the author of the thesis.....	48
Figure 5.1:	Orientation of the main direction of the gripping force (blue) and the corresponding separation plane (transparent blue) within the coordinate system of a generic knob-shape handle. 1: three-dimensional view, 2: Front view, 3: Top view, 4: Rear view	58
Figure 5.2:	Overview of the introduced research problem, the specified objective of the thesis and the derived hypotheses with their corresponding sub-research questions.....	61
Figure 5.3:	Proceeding and results for the investigation of Hypothesis 1: Derivation of the measuring handle design	63
Figure 5.4:	Proceeding and results for the investigation of Hypothesis 2: Rotational impedance around the xh –axis	64
Figure 5.5:	Proceeding and results for the investigation of Hypothesis 3: Rotational impedance around the yh –axis	65
Figure 6.1:	Anthropometric characteristic of the human hand according to DIN EN ISO 7250-1. The illustration of the hand is based on DIN EN ISO 7250-1 (DIN - Deutsches Institut für Normung, 2017).	70
Figure 6.2:	The left side shows the random orbital sander, which was used in the study, surrounded by the projection planes according to the initial coordinate system of the sander. The planes used for the determination of the grip force are highlighted in red. The right side shows the corresponding coordinate directions defined for the used orbital sander and the dimensions of the sander handle. The 3D model of the sander handle was created using the HandySCAN-3D provided by Creaform GmbH, Egenhausen, Germany.....	71
Figure 6.3:	Schematic drawing of the test setup und photo of the random orbital sander with the applied force measuring foil gripped by subject 12 (Schróder et al., 2020).	72
Figure 6.4:	Graphical surface of the pattern to be ground by the subject. The red dot shows the predefined position of the sander on the pattern. The green bar shows the remaining time of measurement.....	73
Figure 6.5:	Schematic presentation of the projection of the force measurement foil values onto the 3D model of the orbital	

	sander handle. The left side of Figure 6.5 shows the graphical representation of the sensor matrix of the force measurement foil. While each rectangle represents a sensor element, the colors characterize the pressure applied to the respective sensor element from blue (low pressure) to yellow (high pressure) (Schröder et al., 2020).....	74
Figure 6.6:	Rotation of the reference frame $n' - l'$ by the angle $\alpha \in 0, \pi$ in the x-y- and the x-z-planes of the initial coordinate system of the sander handle. The angle between the vertical y- or z-axis and the angular position of the specific sensor element f_i of the force measurement foil is given by ϑ_i	76
Figure 6.7:	Splitting of the sensors set into the <i>A</i> and <i>B</i> group (red and gray) exemplified for one subject with the resulting separation planes of each group oriented by $\alpha_{opt A}$ and $\alpha_{opt B}$ the intervening separation plane of α_{sep} for both projections.	78
Figure 6.8:	Resulting angular orientation $\alpha_{res xy}$ of the separation plane's edge in the x-y plane for all three tasks performed.	81
Figure 6.9:	Resulting angular orientation $\alpha_{res xz}$ of the separation plane's edge in the x-z plane for all three tasks performed.	83
Figure 7.1:	Knob-shaped measuring handle used in the conducted study.	98
Figure 7.2:	Test bench with measuring handle and visual force feedback.	99
Figure 7.3:	RMS-values of the acceleration magnitudes used to calibrate the measuring handle and to excite the subjects' HAS in the RMI measurements.	100
Figure 7.4:	The magnitude of the RMI according to Equation 2.3 of the used measuring handle across the excited frequencies	101
Figure 7.5:	Schematic overview of the conducted data evaluation for the determination of the RMI and the influence of the coupling forces.	104
Figure 7.6:	The median and interquartile range of the magnitude (above) and the phase angle (below) of the RMI over all subjects. The RMI was measured for the gripping forces of $F_{gr} = 14 N$ and $F_{gr} = 24 N$ at a gripping force of $F_{pu} = 32.5 N$. The RMI was calculated according to equation 2.3 and refers to steps 7 and 8 of the overview in Figure 7.5	105
Figure 7.7:	The median and interquartile range of the magnitude (above) and the phase angle (below) of the RMI over all subjects. The RMI was measured for the gripping forces of $F_{gr} = 14 N$ and	

	<i>Fgr</i> = 24 N at a gripping force of <i>Fpu</i> = 42.5 N. The RMI was calculated according to equation 2.3 and refers to steps 7 and 8 of the overview in Figure 7.5.....	106
Figure 7.8:	The median and the interquartile range of the magnitude (above) and the phase angle (below) of the RMI over all subjects. The RMI was measured for the gripping forces of <i>Fpu</i> = 32.5 N and <i>Fpu</i> = 42.5 N at a gripping force of <i>Fgr</i> = 14 N. The RMI was calculated according to equation 2.3 and refers to steps 7 and 8 of the overview in Figure 7.5.....	107
Figure 7.9:	The median and the interquartile range of the magnitude (above) and the phase angle (below) of the RMI over all subjects. The RMI was measured for the gripping forces of <i>Fpu</i> = 32.5 N and <i>Fpu</i> = 42.5 N at a gripping force of <i>Fgr</i> = 24 N. The RMI was calculated according to equation 2.3 and refers to steps 7 and 8 of the overview in Figure 7.5.....	107
Figure 8.1:	Comparison of the frictional closure hand and handle for the rotational excitations in the "palm" position investigated in Chapter 7 and for the excitations in the "hand-grip" position investigated in Chapter 8 based on the figures from DIN EN ISO 5349-1	122
Figure 8.2:	Illustrations of the carrier mechanism and the shaker system. Key: 1. Frame, 2. holder of the shakers, 3. electric motor for height adjustment, 4. electric motor for tilt angle adjustment, 5. translational shaker, 6. rotational shaker, 7. measuring handle, 8. rack and pinion gear, and 9. measuring flange.	126
Figure 8.3:	a): A photo of the handle used in the study. b): A schematic of the measuring handle	128
Figure 8.4:	Calibration measurement of the measuring handle's apparent mass determined for the frequencies excited in the study. The magnitude (a) and phase angle (b) of the apparent mass indicated the dynamic characteristic of a constant mass, without any natural frequencies.as their value is almost the same for every excited frequency.....	129
Figure 8.5:	Body postures in which the RMI of the subjects was measured: standing posture with angled arm (a), sitting with extended arm (b). The left side also shows the display with the visual force feedback.....	131
Figure 8.6:	Boxplots and median trend lines of the magnitude of the RMI at gripping forces of <i>Fgr</i> = 5.5 N and <i>Fgr</i> = 24 N (standing	

	posture) and $F_{gr} = 10\text{ N}$ (sitting posture) at a push force of $F_{pu} = 15\text{ N}$ (a) and $F_{pu} = 32.5\text{ N}$ (b).	134
Figure 8.7:	Boxplots and median trend lines of the RMI phase angle for gripping forces of $F_{gr} = 5.5\text{ N}$ and $F_{gr} = 24\text{ N}$ (standing posture) and $F_{gr} = 10\text{ N}$ (sitting posture) at a push force of $F_{pu} = 15\text{ N}$ (a) and $F_{pu} = 32.5\text{ N}$ (b).	135
Figure 8.8:	Boxplots and median trend line of the RMI's magnitude (a) and phase angle (b) for push forces of 15 N, 32.5 N, and 50 N at a gripping force of $F_{gr} = 24\text{ N}$ provided in the standing posture.	137
Figure 8.9:	Boxplots and median trend line of the RMI's magnitude (a) and phase angle (b) for the standing and the sitting postures at a push force of $F_{pu} = 50\text{ N}$ and a gripping force of $F_{gr} = 24\text{ N}$	139
Figure 8.10:	a): Magnitude plot of the MI for vibration excitation along the yh -axis from ISO 10068, b): Phase angle plot of the MI for vibration excitation along the yh -axis from ISO 10068. Key: X: frequency [Hz], Y1: modulus (corresponds to the magnitude) N_{sm} , Y2: Phase angel (degree) (ISO - International Organization for Standardization, 2012)	146
Figure 8.11:	Schematic of the relationship between hand position and rotational axis on the basis of the "hand-grip" position from ISO 10068, where yellow indicates contact surface between hand and handle, blue indicates deflection angle and tangential force of excitation, and green indicates normal and friction force, resulting from the gripping force of the test subject (ISO - International Organization for Standardization, 2012). Key: r = radius of the handle, φ = deflection angle of rotational vibration excitation, FT = tangential force on the handle surface conferred by rotational vibration excitation acting on the HAS, FN = normal force, and FR = frictional force.....	147
Figure 8.12:	Schematic drawing of the relationship between the rotational axis and the direction of the push force on the basis of the "hand-grip" position from ISO 10068, where blue indicates torque of the rotational vibration excitation and red indicates the push force applied by the subject (ISO - International Organization for Standardization, 2012). Key: F_{pu} = push force, $T_j\omega$ = torque of the rotational vibration excitation acting on the hand.	149

Figure 8.13: (a) Top view from Figure 4.1 where yellow indicates contact surface between hand and handle, blue indicates deflection angle and tangential force of excitation, and green indicates normal and frictional force resulting from the gripping force of the test subject. (b) Side view from Figure 4.2, where blue indicates torque of the rotational vibration excitation and red indicates push force applied by the subject. **Key:** r = radius of the handle, ϕ = deflection angle of the rotational vibration excitation, FT = tangential force on the handle's surface conferred by rotational vibration excitation acting on the HAS, FN = normal force, FR = frictional force, Fpu = push force, and $T(j\omega)$ = torque of the rotational vibration excitation acting on the hand" 153

Figure 9.1: Graphical illustration of the explanation model derived from the findings of Chapter 7 and Chapter 8 presented in this thesis.162

List of Tables

Table 2.1:	Representative list of scientific publications on the influence of certain factors in the translational MI 13
Table 6.1:	Clustering of age, bodyweight, and body height. 69
Table 6.2:	Physical characteristics of the subjects, M. Sc Tassilo Schröder 70
Table 6.3:	Minimum, maximum, and the 5th and 95 th percentile of the subject-specific separation planes' orientations in the x-y plane over all three tasks performed in the study. 80
Table 6.4:	Minimum, maximum, and the 5th and 95 th percentile of the subject-specific separation planes' orientations in the x-z plane over all three tasks performed in the study. 82
Table 6.5:	The minimum, maximum, and mean values of the percentage deviations between the resulting grip force acting on the separation plane oriented by <i>asep</i> and the one acting on the vertically oriented separation plane. The deviation is calculated separately for the corresponding planes <i>asep_{xy}</i> and <i>asep_{xz}</i> in the x-y and x-z planes. 85
Table 7.1:	Distribution of the anthropometric properties of the subjects' HAS, which were measured according to DIN EN ISO 7250-1 (DIN - Deutsches Institut für Normung, 2017)..... 97
Table 7.2:	Factor levels of the gripping force and push force 102
Table 7.3:	The mean and the maximum percentage deviations between the requested gripping and push force levels and the applied gripping and push forces 104
Table 7.4:	Effect of the gripping force on the magnitude of the RMI, level of significance $p = 0.05$, MW-U= Mann-Whitney-U test, r = effect strength. The table refers to step 9 of the overview in Figure 7.5. The effect strength r is considered as small for $r \leq .30$, as moderate for $.30 < r < .50$, and as high for $r \geq .50$ (Cohen, 1992)..... 108
Table 8.1:	Median, upper and lower quartiles of the subjects' anthropometric properties. 125

Table 8.2:	Distribution of the maximum gripping forces of the subjects in each body posture.	131
Table 8.3:	Overview of the different factor combinations assessed in this study.....	132
Table 8.4:	Mean percentage deviation between the applied gripping and push forces and the predefined force levels across all frequencies and subjects. Gripping force: F_{gr} ; push force: F_{pu}	133
Table 8.5:	Overview of the different factor combinations performed in the study.....	136

List of Abbreviations

AM	Apparent Mass
AS	Apparent Stiffness
HAM	Hand-Arm Model
HAS	Hand-Arm System
MI	Mechanical Impedance
RAM	Rotational Apparent Mass
RAS	Rotational Apparent Stiffness
RMI	Rotational Mechanical Impedance

Equation Symbols

α	Angle of the rotating separation plane in <i>rad</i>
$\Delta\alpha$	Increment of the angle with which the separation plane rotates.
$\alpha_{opt A}$	Angular orientation at which $I(\alpha)$ form the <i>A group</i> reaches its maximum on the separation plane
$\alpha_{opt B}$	Angular orientation at which $I(\alpha)$ form the <i>B group</i> reaches its maximum on the separation plane
α_{sep}	Task and subject specific angle of the separation plane in $^{\circ}$
α_{xy}	Angle of the rotating separation plane in the x-y plane
α_{xz}	Angle of the rotating separation plane in the x-z plane
$\alpha_{mean xy}$	Angle of the total separation plane in the x-y plane
$\alpha_{mean xz}$	Angle of the total separation plane in the x-z plane
γ	Coefficient of the push force for calculation of the contact force according to ISO 15230
ϑ_i	Angle of the force sensor element in polar coordinates in <i>rad</i>
δ	Coefficient of the gripping force for calculation of the contact force according to ISO 15230
φ	Rotation angel
$\dot{\varphi}$	First time derivation of the rotation angle in $\frac{rad}{s}$
$\ddot{\varphi}$	Second time derivation of the rotation angle in $\frac{rad}{s^2}$
ϕ_0	Phase angle referred to time zero in <i>rad</i>
$\hat{\phi}$	Amplitude of the rotational oscillation in <i>rad</i>
μ_h	Friction coefficient
ω	Angular frequency in $\frac{1}{s}$
Φ	Fourier transformed of the rotation angle in <i>rad</i>
$\dot{\Phi}$	Fourier transformed of the first time derivation of the rotation angle in $\frac{rad}{s}$

$\ddot{\Phi}$	Fourier transformed of the second time derivation of the rotation angle in $\frac{rad}{s^2}$
$\widehat{\Phi}$	Fourier transformed of the amplitude of the rotational oscillation in rad
Ω	Fourier transformed of the angular velocity in $\frac{rad}{s}$
$\dot{\Omega}$	Fourier transformed of the angular acceleration $\frac{rad}{s^2}$
d	Damping constant in $\frac{Ns}{m}$
$\vec{e}_{n'}$	Unit vector aligned normal to the separation plane
f	Frequency in Hz
f_i	Counter variable of the force sensor elements
f_r	Reference frequency of 1000 Hz
j	Imaginary unit
k	Stiffness in $\frac{N}{m}$
l'	Lateral direction of the rotating reference frame
n'	Normal direction of the rotating reference frame
$\vec{n}_{i,(x-y)}$	Vector of the force sensor element in the Cartesian coordinate system
$\vec{n}_{i,(n'-l')}$	Vector of the force sensor element in the transformed into the reference frame $n' - l'$
p	p-Value, correlation coefficient
r	Effect strength
q	Displacement in m
\dot{q}	First time derivation of the displacement in $\frac{m}{s}$
\ddot{q}	Second time derivation of the displacement in $\frac{m}{s^2}$
t	Time in s
x, y, z	Cartesian coordinates
x_h, y_h, z_h	Coordinates of the basic-centric coordinate system of ISO 10068 and DIN EN ISO 5349-1
AM	Apparent mass
AS	Apparent stiffness

$D_{res\ xy/xz-A/B}$	Percentage deviation between the resulting forces from the A and B groups in the x-y and x-z plane
$\mathcal{F}(\ast)$	Fourier transformation of the argument \ast
F_c	Contact force in N
F_N	Normal force in N
F_{gr}	Gripping force in N
$F_{p\ res}$	Resulting pressing force in N
F_{pu}	Push force in N
F_q	Force applied for the displacement q in N
F_R	Friction force in N
$F_{res\ xy/xz-A/B}$	Resultant gripping force of the A or the B group acting normal to the separation plane in the x-y or x-z plane, respectively.
$F_{Tx+/-}$	Tangential forces between hand and handle in positive and negative x_h -direction
$F_{Ty+/-}$	Tangential forces between hand and handle in positive and negative y_h -direction
$F_{Tz+/-}$	Tangential forces between hand and handle in positive and negative z_h -direction
I	Integral over the resulting forces F_{res} acting on the separation plane
J	Inertia
MI	Mechanical impedance
$MW - U$	Test statistics of the Mann-Whitney U test
RAM	Rotational apparent mass
RAS	Rotational apparent stiffness
RMI	Rotational mechanical impedance
T	Torque in Nm

1 Introduction

1.1 Motivation

The interaction between humans and machines is one central aspect in product development (Matthiesen et al., 2014; Matthiesen et al., 2015; Matthiesen & Uhl, 2017b). Particularly in view of the technical development towards Industry 5.0, this interaction is increasingly becoming the focus of technical development. In 2021 the European commission announced a guiding principle for industry 5.0, which focuses on the wellbeing of people in the production process and the individualization of human-machine-interaction (European Commission et al., 2021). Several studies have shown that user productivity correlates with user interaction with the device (Kuijt-Evers, Bosch, et al., 2007; Kuijt-Evers, Vink, & Looze, 2007; Looze et al., 2001; Päivinen & Heinimaa, 2009). Consequently, improving human-machine interaction would lead to an increase in user productivity. Therefore extending the scientific knowledge on human-machine interaction is relevant for the engineering research in product development.

One aspect of this human-machine interaction is the exposure of the human hand-arm system (HAS) to vibration by technical systems. One example of such a technical system in which this aspect is particularly pronounced are power tools. Users usually guide power tools by hand and in turn create a physical coupling. Consequently, vibrational properties of the human hand-arm system such as damping, stiffness, and inertia, influence the power tool and its components and vice versa (Matthiesen et al., 2012; Matthiesen & Uhl, 2017b). Since early validation of product functionality is essential for detecting malfunctions and adjusting predicted product behavior, the influence of the user's HAS needs to be considered during power tool development (Forsteneichner et al., 2015). Validation of these vibration interactions through manual testing requires a fully designed prototype, is less reproducible due to the physical condition and physiological properties of the user (e.g., height, weight), and the number of test repetitions is limited by the user fatigue. Contrary to that simulative or physical substitute models that simulate the vibration behavior of the hand-arm system (so-called hand-arm models, abbreviated HAM), are more reproducible, unlimited in their number of repetitions and do not require a physical user interface. However, the parameterization of these models requires experimental data of the biodynamic properties, of the HAS.

A basis from, which these parameters can be derived is the mechanical impedance (hereafter referred to as MI) of the HAS, which describes the mechanical resistance against vibration excitation (Matysek & Kern, 2009). For translational vibration excitation the translational impedance of the hand-arm system has been widely investigated and several different HAM and corresponding simulations exist in the state of research so far (Adewusi et al., 2012; Dong et al., 2013; Lindenmann, 2023; P. Marcotte et al., 2010; Rakheja et al., 2002; D. Welcome et al., 2004). However, the excitation of the HAS in three translational directions does not represent the complete description of the biodynamics of the HAS because rotational excitation is not considered. For multiaxial vibrational modeling of the HAS, knowledge of the rotational biodynamic response of the HAS is required to enable complete and accurate modeling of the HAS. A statement of Dong et al. (2013) on modeling the HAS for multiaxial vibrations shows the need for this knowledge in the state of research: "Not directly accounting for the cross-axis responses and rotational responses in these models may also contribute to discrepancies." (Dong et al., 2013, p. 1139). For the example of power tools, this multiaxial vibration excitation of the HAS is particularly true, as noted by Dong et al. (2012): "Powered hand tools are known to generate and transmit multi-axes vibrations. Due to the non-uniform distributions of the mass, elastic, and viscous properties in the human hand-arm system, it could respond to such multi-axes vibrations in a highly complex manner a long all the translational and rotational axes." (Dong et al., 2012, p. 1193). In addition many power tools mainly excite the HAS in a rotational direction, such as the random orbital sander or the pneumatic assembly screwdriver (Chih-Hong Chang et al., 1999; Chih-Hung Chang & Wang, 2001). Thus, power tools represent a suitable exemplary technical system for the investigation of the MI of the HAS for rotational vibration excitation (so-called rotational mechanical impedance, abbreviated RMI). Nevertheless in the state of research, there are only a few studies investigating the biodynamics of the HAS during rotational vibration excitation and, accordingly, there are also only a few rotational HAM (Joshi et al., 2008; Lin et al., 2003; Mangold, 2019). Due to the lack of knowledge about the biodynamics of the HAS for rotational vibration excitation these HAM only represent the biodynamics in certain frequency ranges (Joshi et al., 2008; Lin et al., 2003; Mangold, 2019).

Research Problem

The state of research lacks data on the rotational mechanical impedance of the human hand-arm system, which is required for the parametrization and the development of hand-arm models, such as those used in power tool development.

1.2 Structure of the thesis

The following thesis consists of nine main chapters. The first chapter is the introduction of the thesis, which contains the motivation and the current subchapter on the structure of the thesis. Chapter 2 contains the relevant basics for understanding the thesis. Chapter 3 presents the state of research on the rotational mechanical impedance of the hand-arm system and the rotational vibration excitation of the hand-arm system by power tools. Chapter 3 ends with an overall conclusion on the state of research. Based on this overall conclusion Chapter 4 defines the objective of the thesis. This objective comprises three hypotheses, which are investigated in this thesis. To this end, Chapter 5 derives research questions from the hypotheses of the objective and provides the corresponding research design to answer the derived questions. Chapter 6, Chapter 7, and Chapter 8 each present one scientific study conducted by the author of the thesis to investigate one of the hypotheses from the objective. In this context, each study has been pre-published as a journal article. Therefore, the methods used the results obtained and the discussion of the findings in Chapters 6, 7, and 8 are cited entirely from the corresponding journal articles. However, each chapter is specifically introduced and the cited text is placed in the context of the thesis. At the end of each of the Chapters 6 to 8 a conclusion is drawn as to how the conducted and pre-published study contributes to the specific hypothesis and thus to the objective of the thesis. Chapter 9 summarizes and discusses Chapters 6, 7, and 8 in terms of results and findings and thus forms the conclusion of the thesis. The thesis ends with an outlook, which provides an overview of further possible research as well as additional studies to be conducted

2 Basics and state of research on the mechanical impedance

This chapter provides the physical definition of mechanical impedance, apparent mass and apparent stiffness of the HAS and describes the resulting properties. Furthermore, previously established measurement methods and test setups suitable for the determination of these quantities are presented. Hereinafter the influences of gripping force, push force and body posture on the MI will be explained.

2.1 Description of the mechanical impedance, apparent mass and apparent stiffness of the human hand-arm system

The following subchapter provides a basic overview of the mathematical and physical description of mechanical impedance (MI) and rotational mechanical impedance (RMI) of the HAS. In addition, the subchapter explains how these quantities provide information about the biodynamics of the HAS in terms of stiffness, damping and mass properties. In this context the subchapter provides basic knowledge and explanations to understand obtained results of this thesis and the conclusions drawn.

For describing the biodynamic response of the human HAS to translational vibration, the quantities apparent mass $AM(j\omega)$, apparent stiffness $AS(j\omega)$ and mechanical impedance $MI(j\omega)$ are used. These are complex functions, which depend on the excitation frequency (Dong, Welcome, McDowell, & Wu, 2006). Equation 2.1 and 2.2 show the corresponding equations for translational vibration excitation.

$$AM(j\omega) = \frac{F_q(j\omega)}{\ddot{q}(j\omega)} ; MI(j\omega) = \frac{F_q(j\omega)}{\dot{q}(j\omega)} ; \quad 2.1$$

$$AS(j\omega) = \frac{F_q(j\omega)}{q(j\omega)} ; j = \sqrt{-1} ; \omega = 2\pi * f \quad 2.2$$

In equation 2.1 all quantities are represented in the frequency domain. Accordingly, all quantities are functions of the frequency f , which is given as the angular frequency ω of the applied oscillation, where j denotes the imaginary part of the oscillation. The displacement is denoted by q with the dots above it referring to the derivative with respect to time. Consequently, the apparent mass (AM), described by

the quotient of the force F_q and the acceleration \ddot{q} , can be calculated as the time derivative of the mechanical impedance (MI). The MI, in turn, is the quotient of the force F_q and the velocity \dot{q} and can be derived from the apparent stiffness (AS), which is the quotient of the force F_q and the distance q . In the context of the human HAS, MI can be regarded as analogous to electrical impedance, that is to say, as a resistance against vibrational excitation (Matysek & Kern, 2009). The MI of the HAS thus describes the resistance of the HAS against mechanical vibration excitation. Since the biodynamics of the hand-arm system are primarily damper-dominated, the MI has established itself as the main descriptive variable in the state of research (Reynolds & Soedel, 1972). In this context, MI of the HAS for translational vibration excitation has been investigated in several studies in the state of research (Aldien et al., 2006; Besa et al., 2007; Concettoni & Griffin, 2009; Dong et al., 2012; Dong, Welcome, McDowell, & Wu, 2006; Griffin, 1996; Lindenmann et al., 2022; P. Marcotte et al., 2005; Pan et al., 2018; Xu et al., 2011; Zhang et al., 2021). Based on these studies, different value ranges for the magnitude and the phase angle of the MI of the HAS for translational vibration excitation are specified in the standardization. ISO 10068 and DIN 45677 are standards that specify such value ranges for different directions of excitation as well as corresponding multibody models of the HAS.

As mentioned above, Equation 2.1 describes the calculation of the apparent mass $AM(j\omega)$, apparent stiffness $AS(j\omega)$ and mechanical impedance $MI(j\omega)$ of the HAS in the case of translational vibration excitation. For rotational vibration excitation, Matysek and Kern (2009) describe the rotational MI (RMI) as the complex, frequency-dependent quotient of the torque $T(j\omega)$ and the angular velocity $\Omega(j\omega)$ of the rotational vibration. As for the translational MI both quantities are measured at the vibration initiation point of the hand (Matysek & Kern, 2009). According to Matysek and Kern (2009). Equation 2.3 shows the equation of the mechanical impedance for rotational vibration excitation as indicated by the additional R (Matysek & Kern, 2009). The indication of the angular velocity by Ω has been adopted from Matysek and Kern (2009).

$$RMI(j\omega) = \frac{T(j\omega)}{\Omega(j\omega)} ; j = \sqrt{-1} ; \omega = 2\pi * f \quad 2.3$$

Like translational MI, RMI is also a complex function of the angular frequency ω , in which j denotes the imaginary part of the vibration. Following the mathematical relationship between MI, AM and AS for translational vibrations, a corresponding re-

relationship between the rotational mechanical impedance $RMI(j\omega)$, the rotational apparent inertia, $RAM(j\omega)$ and the rotational apparent stiffness $RAS(j\omega)$ can be derived. Equation 2.4 shows the corresponding equations for the RAM and RAS.

$$RAM(j\omega) = \frac{T(j\omega)}{\dot{\Omega}(j\omega)} \quad 2.4$$

$$RAS(j\omega) = \frac{T(j\omega)}{\Phi(j\omega)}; \dot{\Phi} = \Omega; \ddot{\Phi} = \dot{\Omega} \quad 2.5$$

In correspondence with the translational AM, the RAM can be derived from the RMI via the derivative with respect to time of the angular velocity Ω , resulting in the angular acceleration $\dot{\Omega}$. Consequently, the rotational apparent stiffness is the quotient of the torque T and the antiderivative of the angular velocity, indicated by the rotation angle Φ .

As a complex quantity, the MI and the RMI can be characterized by their magnitude and phase angle. If these have been determined for several specific frequencies, the magnitude and phase angle of the MI or RMI can be plotted across an applied frequency spectrum. According to the ISO 10068, the frequency spectrum on the x-axis is scaled logarithmically while magnitude and phase angle on the y-axis are scaled linearly (ISO - International Organization for Standardization, 2012). Figure 2.1 shows an example of a schematic plot of the magnitude of the MI of the HAS for translational vibration excitation along the axis of the forearm taken from ISO 10068. The representation of translational MI as plots of the magnitude and the phase angle in Figure 2.1 is the most commonly used type of representation in the state of research and in standardization (ISO - International Organization for Standardization, 2012). Accordingly, this thesis is representing RMI in this way.

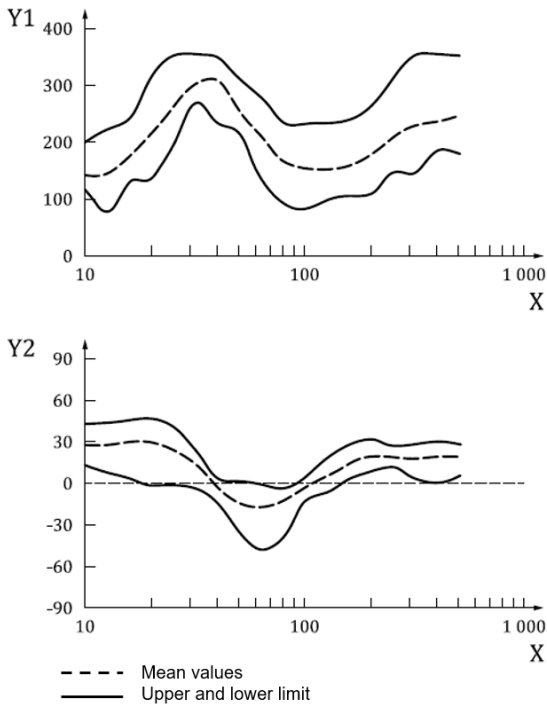


Figure 2.1: Example of a schematic plot of the magnitude $Y1 \left(\frac{Ns}{m} \right)$ and phase angle $Y2$ (degrees) of the MI of the HAS across the frequency spectrum X (Hz) for translational vibrations excited along the axis of the forearm taken from the ISO 10068 (ISO - International Organization for Standardization, 2012)

From the shape of magnitude and the phase angle curves, conclusions can be drawn about the dynamic behavior of a vibrating object. For rotational vibrations, this interpretation of magnitude and phase angle of the RMI is explained below using a harmonic, linear, single-mass rotational oscillator, excited by a torque. Oscillator dynamics are described based on DIN 1311-2 (DIN Deutsches Institut für Normung e. V., 2002). Figure 2.2 shows a schematic view of a linear, rotational single-mass oscillator.

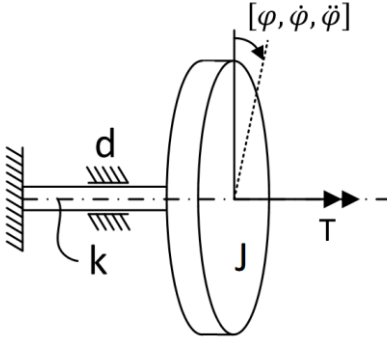


Figure 2.2: Linear, rotational single-mass oscillator with one degree of freedom excited by the external torque T with the inertia J , the rotational spring constant k and the rotational damping constant d . The rotation angle is given by φ , the angular velocity by $\dot{\varphi}$ and the acceleration by $\ddot{\varphi}$.

The harmonic oscillation of the rotational single mass oscillator can be described by a sine respectively cosine function, which is shown below in equation 2.6. To avoid confusion with the phase angle the rotation angle is given as φ or Φ in the frequency domain and the phase angle is given as ϕ_0 .

$$\varphi(t) = \hat{\varphi} * \sin(\omega t + \phi_0) = \hat{\varphi} * \cos\left(\omega t + \phi_0 - \frac{\pi}{2}\right) \quad 2.6$$

In equation 2.6, $\hat{\varphi}$ is the amplitude of the rotational oscillation, ω the angular frequency and ϕ_0 the phase angle. Based on the linear, rotational single mass oscillator in Figure 2.2, the following equation of motion can be derived.

$$J\ddot{\varphi}(t) + d\dot{\varphi}(t) + k\varphi(t) = T(t) \quad 2.7$$

The equation of motion in equation 2.7 consists of a mass component given by the inertia J , a rotational acceleration $\ddot{\varphi}(t)$, a damping component given by damping constant d , an angular velocity $\dot{\varphi}(t)$, a spring component given by a spring constant k and a rotation angle $\varphi(t)$. The sum of these components equals the external torque $T(t)$, which deflects the single-mass oscillator rotationally.

Assuming a harmonic vibration excitation with an angular frequency ω the equation of motion from equation 2.7 can be transferred into the frequency domain by using the Fourier transformation, resulting in equation 2.8.

$$(J(j\omega)^2 + dj\omega + k)\Phi(j\omega) = T(j\omega) \quad 2.8$$

The Fourier-transformation of the time-depending rotation angle $\varphi(t)$ or of the angular velocity $\dot{\varphi}(t)$ and acceleration $\ddot{\varphi}(t)$ is denoted with $\Phi(j\omega)$. The Fourier-transformation of the external torque $T(t)$ is given by $T(j\omega)$. Consequently, the time derivation of $\Phi(j\omega)$ in the frequency domain results in equation 2.9.

$$\mathcal{F}\left(\frac{d(\varphi(t))}{dt}\right) = j\omega\Phi(j\omega) = \dot{\Phi}(j\omega) = \Omega(j\omega) \quad 2.9$$

Combining equation 2.3 of the RMI with equations 2.8 and 2.9, RMI can be represented as a sum of inertia, spring and damper components in the frequency domain.

$$RMI(j\omega) = \frac{T(j\omega)}{\Omega(j\omega)} = Jj\omega + d + \frac{k}{j\omega} \quad 2.10$$

With regard to the phase angle ϕ_0 , the first part of equation 2.10 for the general case can be written as

$$RMI(j\omega) = \frac{T(j\omega)}{\Omega(j\omega)} = \frac{\hat{T}(j\omega)}{\hat{\Phi}(j\omega)} * e^{j(\phi_{0T}(\omega) - \phi_{0\Omega}(\omega))} \quad 2.11$$

In equation 2.11, \hat{T} and $\hat{\Phi}$ are the amplitude of the torque and the rotation angle, while ϕ_{0T} and $\phi_{0\Omega}$ indicate the corresponding initial phase angles at a given frequency.

In addition to RMI, rotational AM can also be represented as combination of inertia, spring, and damper components in the frequency domain by combining equations 2.4, 2.8 and 2.9.

$$RAM(j\omega) = \frac{RMI(j\omega)}{j\omega} = \frac{T(j\omega)}{\Omega(j\omega)} = J + \frac{d}{j\omega} + \frac{k}{(j\omega)^2} \quad 2.12$$

Using equation 2.10, conclusions about the dynamic behavior of a vibrating object can be drawn from variations of magnitude and phase angle of the RMI at different frequencies. Figure 2.3 shows example plots of magnitude and phase angle of RMI for mass-, spring- and damper-dominated vibration dynamics of a single-mass oscillator, as shown in Figure 2.2 on page 9. In Figure 2.3, the magnitude plot of the RMI increases across the frequency spectrum for mass-dominated vibrational dynamics. The double logarithmic scaling makes the proportional increase appear linear. According to equation 2.10 this is plausible, because for rotational vibration excitation of a constant mass, the damping and spring component are zero and the remaining mass component has constant inertia resulting in a linear increase of the magnitude across the frequency spectrum. Also, the magnitude plot of the RMI for the spring dominated vibration dynamic in Figure 2.3 can be explained by equation 2.10. Since damping and mass components are zero for rotational vibration excitation of a torsion spring, the quotient of the spring constant and the complex angular frequency remains, resulting in a proportionally decreasing magnitude, which appears linear due to the double logarithmic representation. In case of a damping dominated vibration dynamic the only remaining component of equation 2.10 is the damping constant of the rotational damper, resulting in a constant magnitude of the RMI. The phase angles of Figure 2.3 correspond to the plots of the magnitude.

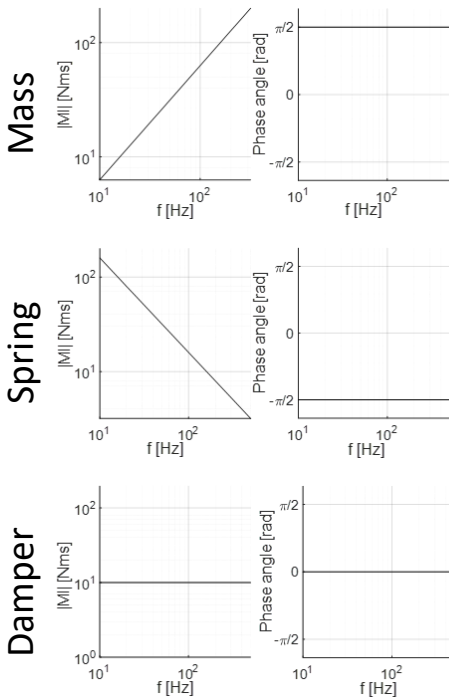


Figure 2.3: Exemplary representation of magnitude and phase angle of the RMI for the mass-, spring- and damper-dominated vibration dynamics of a single-mass oscillator.

2.2 Overview of the influences on the translational MI

Subchapter 2.2 provides an overview of the state of research regarding factors influencing translational MI. Since these factors corresponding influence the MI a corresponding influence on the RMI can be assumed. Therefore, based on this overview, factors that influence RMI are identified and derived accordingly.

According to ISO 10068, MI is influenced by several factors, the most important of which are listed below. (ISO - International Organization for Standardization, 2012).

- The direction from which the vibration excites the HAS. The three spatial axes are designated as x_h , y_h and z_h .
- The coupling forces, i.e. the gripping and push forces applied to the handle that excites the vibration.
- The body posture, especially the hand and arm posture of the person being exposed to the vibration.
- The geometry of the handle that excites the vibration.
- The individual anthropometric properties and physical characteristics of the person being exposed to the vibration.
- The acceleration of the vibration excitation.

For translational vibrations, the effects of these influences on MI have been widely investigated in several studies, as the representative list of publications in **Table 2.1** shows.

Table 2.1: Representative list of scientific publications on the influence of certain factors in the translational MI

Authors	Investigated influencing factor	Direction of excitation	Investigated frequency range	Number of subjects
(Aldien et al., 2005)	Gripping force; Push force; Body Posture; Handle size	x_h -axis	8-1000 Hz	7
(Aldien et al., 2006)	Gripping force; Push force; Body Posture; Handle size	z_h -axis	8-1000 Hz	7
(Besa et al., 2007)	Push force, Gripping force	x_h -, y_h -, z_h - axis	1-700 Hz	5
(Burström, 1997)	Gripping force; Push force; Body Posture;	x_h -, y_h -, z_h - axis	4-2000 Hz	10

Table 2.1 continued

			100-200 Hz (x_h -axis)	
(Dong et al., 2012)	Excitation direction	x_h -, y_h -, z_h -axis	60-120 Hz (y_h -axis)	7
			160-300 Hz (z_h -axis)	
(Lindenmann et al., 2022)	Gripping force; Push force; Body posture	z_h -axis	10-500 Hz	30
(P. Marcotte et al., 2005)	Gripping force; Push force; Handle size	z_h -axis	8-1000 Hz	7
(Pan et al., 2018)	Gripping force; Push force	z_h -axis	4-500 Hz	9
(Zhang et al., 2021)	Gripping force; Push force; Body posture	z_h -axis	10-1000 Hz	7

Translational MI has been investigated along all three coordinate axes in the state of research for different frequency ranges, as exemplified by studies of Besa et al. (2007), Burström (1997) and Dong, Welcome, McDowell, and Wu (2006) from **Table 2.1**. As in ISO 10068, the results of the studies show that translational MI of the HAS is also under vibration excitation along different coordinate axes. The results obtained by Burström (1997) further indicate that the influence of gripping force, push force and body posture on MI also depends on the excitation direction. Based on the state of research on translational MI, it can be assumed that RMI is also different for different excitation directions. Furthermore, the influence of gripping force, push force and body posture on RMI could also depend on excitation direction.

As the representative collection of studies in **Table 2.1** illustrate, the state of research on translational MI mainly focuses on excitation along the z_h -axis. The ratio of the excitation directions investigated in the studies in **Table 2.1** can be considered representative of the state of research in this regard.

The influence of the gripping force on translational MI upon vibration excitation along the z_h -axis has been investigated for various frequency spectra by, e.g., Aldien et al. (2006), Besa et al. (2007), Burström (1997), Lindenmann et al. (2022), P. Marcotte et al. (2005), Pan et al. (2018) and Zhang et al. (2021).

Concerning the influence of gripping force on translational MI for excitation along the z_h -axis, all authors agree that a higher gripping force result in a stronger coupling of the HAS to the vibration source and therefore result in a higher MI magnitude. However, the increase in magnitude of MI due to gripping force depends on the frequency range. The results of Lindenmann et al. (2022) show that below 50 Hz and beyond 150 Hz the gripping force has a strong effect on the MI, whereas the effect between 50 Hz and 150 Hz is only moderate to low. Regarding excitation in x_h - and y_h -direction the studies of Aldien et al. (2005), Besa et al. (2007) and Burström (1997) show a similar effect of gripping force on MI magnitude. Since a higher gripping force leads to a stronger coupling of the HAS to the source of vibration excitation, an increase in the magnitude due to gripping force can also be expected for RMI. Following this logic, the effect size of gripping force could also differ depending on the frequency range.

As with the gripping force, the results from the current state of research on translational MI also indicate a comparable effect of the push force on the RMI. From the representative collection of studies in **Table 2.1** the works Aldien et al. (2006), Besa et al. (2007), Burström (1997), Lindenmann et al. (2022), P. Marcotte et al. (2005), Pan et al. (2018) and Zhang et al. (2021) show that a higher push force in z_h -direction also leads to an MI increase. Aldien et al. (2005) demonstrated a comparable effect of push force on MI for excitation in x_h -direction. As with gripping force, the effect of push force on MI differs across the frequency spectrum. Regarding the effect of push force on MI in different frequency ranges, the effect size in certain frequency ranges differs from that of gripping force, as shown by the results of Lindenmann et al. (2022). In the frequency range between 50 Hz and 150 Hz push force has a strong effect on MI, while the effect size is moderate to low outside of this range. As with gripping force, the influence of push force on RMI may be the same as that described for translational MI.

Regarding the influence of body posture on translational MI, the influence on MI seems to depend less on the position of the HAS and more on its flexion. In their studies Lindenmann et al. (2022) distinguished between a posture in which the hand was held in front of the body with the forearm horizontal and one in which the hand was held above the head with the forearm vertical. In both postures investigated by Lindenmann et al. (2022), the elbow joint was flexed to 90°. The statistical results of Lindenmann et al. (2022) only show a low effect size of the body posture on MI. In

contrast, the studies of Aldien et al. (2005), Aldien et al. (2006), Besa et al. (2007) and Zhang et al. (2021) distinguish between a posture with the HAS outstretched and a posture, with the elbow flexed, in both cases the hand is held in front of the body. In all studies, the magnitude plots of MI measured with the HAS outstretched was remarkably higher in the frequency range below 100 Hz (Aldien et al., 2005; Aldien et al., 2006; Besa et al., 2007; Zhang et al., 2021). Consequently, it can be assumed that the flexion of the HAS has a greater influence on the MI than its position. This assumption may also apply for the RMI.

Furthermore, the state of research on translational MI, exemplified by the studies in **Table 2.1**, shows that MI is also influenced by handle size. To investigate the influence of the handle size on MI, Aldien et al. (2005), Aldien et al. and P. Marcotte et al. (2005) changed the diameter of a cylindrical handle through which vibration was transmitted to the HAS. All three studies agree that a greater handle diameter results in a higher magnitude of translational MI, especially at high frequencies (Aldien et al., 2005; Aldien et al., 2006; P. Marcotte et al., 2005). Based on these findings, it can be assumed that both the handle size and the handle geometry via which the vibration is excited can have an influence on MI. A similar influence of handle size and geometry seems plausible for rotational vibration excitation, since the vibration movement is transmitted differently with handle geometries. Depending on the vibration movement (rotational or translational), parts of the handle surface can transmit the vibration excitation to the HAS in a positive or frictional manner.

Overall, based on the state of research on factors influencing translational MI, it can be assumed that these factors also have an influence on RMI. Of the factors mentioned above the direction of vibration excitation, the applied coupling forces, the body posture, and geometry of the handle were investigated in this thesis. These factors are addressed in the following Subchapters 2.3, 2.4, 2.5 and 2.6.

2.3 Directions of vibration excitation and the coordinate systems of the hand-arm system

ISO 10068 specifies MI for the three orthogonal, translational directions of excitation. To describe these directions of excitation, ISO 10068 defines a base-centric coordinate system, which refers to a cylindrical handle gripped by the hand. The center of the axis or midpoint of this cylindrical handle is the origin of this coordinate system (ISO - International Organization for Standardization, 2012). Figure 2.4 shows the corresponding coordinate system from ISO 10068.

— · — · — Basic-centric (device-related, grip-oriented) coordinate system

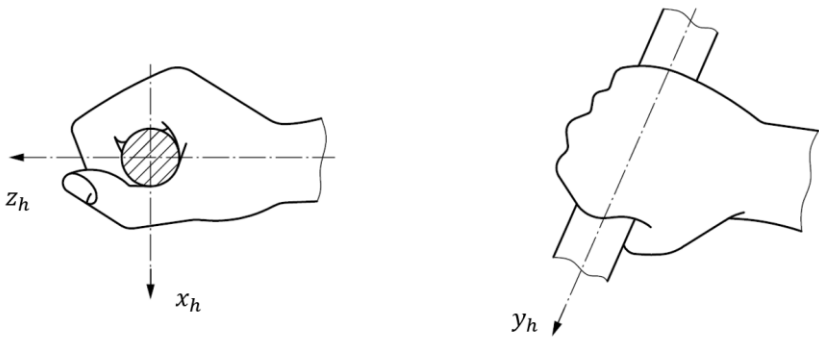
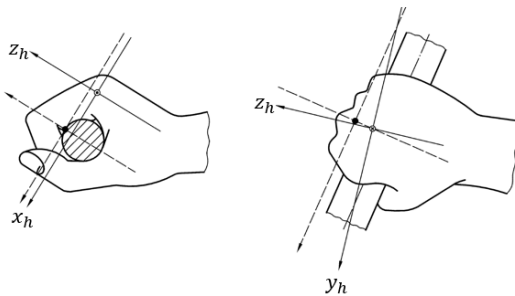


Figure 2.4: Basic centric coordinate system for the measuring of the body-dynamic response of the HAS according to (ISO - International Organization for Standardization, 2012).

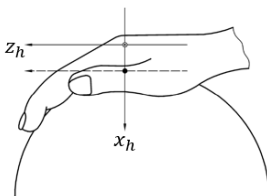
Although ISO 10068 refers only to translational vibration, the coordinate system used is independent of the type of excitation (ISO - International Organization for Standardization, 2012). Accordingly, the coordinate axes of ISO 10068 can also be defined as the rotational axes for the rotational vibration excitation. Beside the coordinate system of ISO 10068, DIN EN ISO 5349-1 proposes two additional coordinate systems, which are mainly used for measuring exposure of the HAS to vibration caused by devices (DIN Deutsches Institut für Normung e. V., 2001b). As in ISO 10068, the first coordinate system in DIN EN ISO 5349-1 is basic-centric, while the second one is biodynamic and refers to the hand. Furthermore, the DIN EN ISO 5349-1 distinguishes between two basic hand positions. Hand position a) in Figure

2.5 is referred to as the "hand grip" position that correspond to the hand position in ISO 10068 (DIN Deutsches Institut für Normung e. V., 2001b; ISO - International Organization for Standardization, 2012). Posture b) is described as the "palm" position and refers to a resting hand position in which the hand lies on the top of a hemispherical surface (DIN Deutsches Institut für Normung e. V., 2001b). Figure 2.5 shows the basic and the biodynamic coordinate system of the HAS within the two hand positions.



a) "Hand grip" position

(In this position, the hand embraces a cylindrical handle in the commonly used manner)



—— Biodynamic coordinate system
 - - - - Basic-centric (device-related, grip-oriented) coordinate system

b) "Palm" position

(In this position, the hand pushes on a spherical surface)

Figure 2.5: Basic-centric and biodynamic coordinate system defined in the DIN EN ISO 5349-1 within the "hand-grip"- and the "palm"-posture, both figures are taken from the DIN EN ISO 5349-1 and with the description translated into English (DIN Deutsches Institut für Normung e. V., 2001b).

ISO 10068 defines MI of the three spatial directions of the HAS as independent of each other. In this context the ISO 10068 states: "The components of impedance in the three directions are treated as being independent." (ISO - International Organization for Standardization, 2012, p. 1). However, ISO 10068 also states: "The hand and arm are usually treated as a system in which translational vibrations in the three mutually perpendicular directions are independent. In reality, some coupling effects can be involved in the response." (ISO - International Organization for Standardization, 2012, p. 36). This statement of ISO 10068 is supported by a study by Dong et al. (2012). In the study Dong et al. (2012) measured MI of the HAS for vibration excitations along the three basic-centric spatial axes of ISO 10068 (Dong et al., 2012). From the results obtained, Dong et al. (2012) concluded cross-axis responses of MI are possible (Dong et al., 2012). In another study on the modeling of biodynamic responses of the HAS in three spatial directions Dong et al. (2013) concluded that a lack of modeling of cross-axis and rotational responses of the HAS may contribute to discrepancies. Overall, this shows that the biodynamic response of the HAS also occurs along rotational axes and cross-axial, especially with multi-axial excitation.

In this context Tarabini et al. (2013) suggest to substitute the description of MI in x_h – and z_h –direction in ISO 10068 by a common radial MI r_h to describe the MI of the HAS for stimulus with an unknown vibration direction in the x_h - z_h -plane. According to Tarabini et al. (2013) the use of radial MI r_h as general MI in the x_h - z_h -plane, would be practical in the context of power tools, since the cylindrical handle of power tools can be gripped in different angels in the x_h - z_h -plane regardless of the direction of vibration excitation (Tarabini et al., 2013). Therefore the approach of Tarabini et al. (2013) is to expressed magnitude and phase angle of the radial MI as linear a combination of the relative angles that position the limbs of the HAS to each other, rather than by the direction the HAS is exited in (Tarabini et al., 2013). For this purpose, Tarabini et al. (2013) conducted a subject study in which the HAS of 8 subjects was excited vertically in different body postures. They then calculated the radial impedance according to equation 2.1 as the complex ratio between the frequency-weighted force and velocity for a vertical excitation direction. In this way the magnitude of r_h was calculated as the root mean square for the respective excitation frequencies. The obtained magnitudes and phase angles of r_h were statistically evaluated by an analysis of variance (ANOVA). The corresponding regression model expressed the magnitude, and phase angle as linear combinations of influencing factors with corresponding sensitivity coefficients. Among other things the linear combination consists of six angles describing the position of the HAS (Tarabini et al., 2013). The evaluation of the model for octave bands of center frequencies of 16, 31.5, 63, 125, 250, and 500 Hz showed that all of these angles have an influence on radial MI.

The conclusion presented by Dong et al. (2012) and the study by Tarabini et al. (2013) suggest that translational MI of the HAS probably cannot be regarded as independent from each other for different spatial excitation directions, as ISO 10068 proposes. Furthermore, it can be concluded that for exact modeling of the HAS under multiaxial vibration exposure, as it occurs in power tool applications, more knowledge on the rotational biodynamic response is required. Since RMI is a characteristic of this biodynamic response it is purposeful to use the established coordinate systems from ISO 10068 and DIN EN ISO 5349-1 as reference systems in this thesis, so that the results are transferable and can be used in further work without conversion for modeling. In this context, the use of a coordinate system such as the one proposed by Tarabini et al. (2013) would be impractical, as it is not yet established in the state of research. Therefore, in this thesis, the basic-centric coordinate systems of ISO 10068 are used as a reference for hand positions enclosing cylindrical handles in the “hand grip” position¹. For hand positions that can be referred to the “palm” position of DIN EN ISO 5349-1 (see Figure 2.5, page 18), the basic-centric coordinate system of DIN EN ISO 5349-1 is used as reference, since the ISO 10068 does not propose a corresponding coordinate system for such a posture (DIN Deutsches Institut für Normung e. V., 2001b; ISO - International Organization for Standardization, 2012).

2.4 Description of the coupling forces

The coupling forces refer to all forces, which the user applies to a vibrating surface or handle (DIN Deutsches Institut für Normung e. V., 2013; ISO - International Organization for Standardization, 2007). According to DIN 45679 and ISO 10068 as well as the state of research, the coupling force are influencing the MI of the HAS (DIN Deutsches Institut für Normung e. V., 2001a; ISO - International Organization for Standardization, 2012). In this thesis, the coupling forces are divided according to ISO 15230 into the pushing/pulling force, the guiding force, the lifting force, the gripping force, the feeding force and the contact forces (DIN Deutsches Institut für Normung e. V., 2001a; ISO - International Organization for Standardization, 2007). Based on these forces, the thesis focuses on the influence of the push/pull force and

¹ In the following the term “hand grip” position is used to refer to the hand position of DIN EN ISO 5349-1 and to the hand position of ISO 10068, although the term can only be found in DIN EN ISO 5349-1. An extension of this term to the hand position of ISO 10068 is practical, since the hand position in both standards is the same and and the term refers only to the hand position and not to the coordinate system used.

the gripping force on the RMI. In addition the guiding force and the torque and friction force will be explained in the beyond part of the basic chapter as both are necessary for a complete understanding of the thesis's studies and findings.

The lifting and feed force are not addressed below, as they were not represented in the test setup of the thesis, since those forces refer to a power tool or device moved by the user (ISO - International Organization for Standardization, 2007). In this context Subchapter 2.6 provides further information on the established test setup for the measurement of the MI of the HAS, from which the test setups of this thesis were derived.

Contact forces are also not specifically measured or considered as an influencing factor on RMI in this thesis. The contact forces can be calculated by integrating the pressure distribution between the hand and the handle. Furthermore, it can be described by a linear combination of the push force F_{pu} and the gripping force F_{gr} with the coefficients δ and γ as Equation 2.13 shows (DIN Deutsches Institut für Normung e. V., 2013; ISO - International Organization for Standardization, 2007)

$$F_c = \delta F_{gr} + \gamma F_{pu} \quad 2.13$$

Since the pressure distribution between the hand and a vibrating handle is difficult to measure, and the contact forces can also be described by the push and gripping force, a measurement of these forces is more practical.

Push/pull force²

According to the ISO 15230 and the DIN 45679 the push/pull force F_{pu} is defined as the resulting force, the user applies with each hand on a vibrating surface that is not compensated within the coupling surface of the hand (DIN Deutsches Institut für Normung e. V., 2013; ISO - International Organization for Standardization, 2007). A force applied away from the shoulder is defined as push force, a force applied towards the shoulder is defined as pull force (DIN Deutsches Institut für Normung e. V., 2013; ISO - International Organization for Standardization, 2007). In this context

² In the following thesis the terms push force, press force, pressing force and thrust force will be used synonymously as these terms are also used synonymously in the state of research, according to ISO - International Organization for Standardization, 2012. Thereby, all terms refer to the force described in the current subchapter and the definition in ISO - International Organization for Standardization, 2007.

the push force can be directed differently as Figure 2.7 on page 23 from ISO 15230 show, where the push/pull force is denoted by F_{pu} (DIN Deutsches Institut für Normung e. V., 2013; ISO - International Organization for Standardization, 2007).

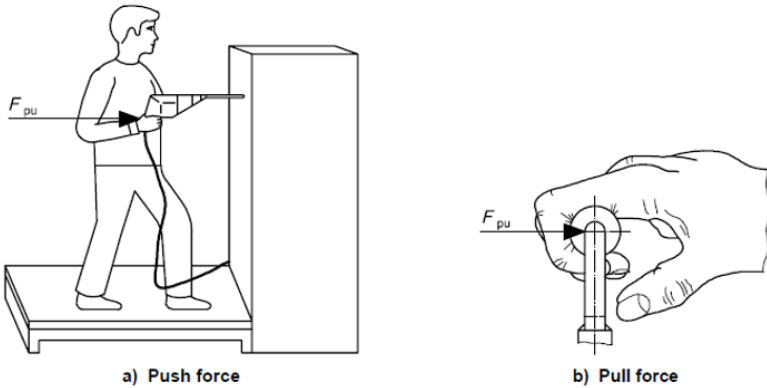


Figure 2.6: Examples from ISO 15230 for the application of the push force F_{pu} and the pull force F_{pu} . Example of the push force acting downwards orthogonally to the guiding force F_g on a knob-shaped handle, the illustration is taken from ISO 15230 (below) (ISO - International Organization for Standardization, 2007).

Guiding force

According to ISO 15230 the guiding force F_g is defined as a force applied by the user that moves a machine in a planar or horizontal movement. Thereby the guiding force is aligned orthogonal to the push force, as the schematic illustration of a sanding application in Figure 2.7 shows.

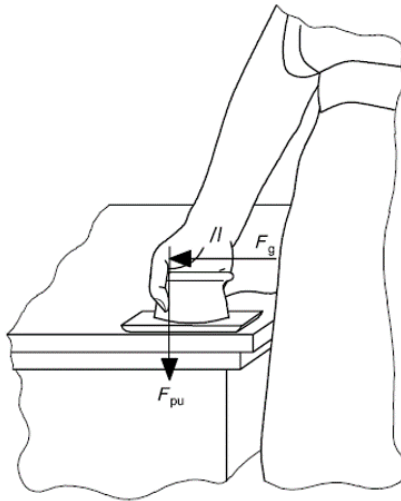


Figure 2.7: Schematic application of the guiding force F_g acting orthogonally to the push force F_{pu} on the knob-shaped handle of a sander, the illustration is taken from ISO 15230 (ISO - International Organization for Standardization, 2007).

In the case of the schematic sanding application from Figure 2.7 the push force is directed downwards while the power tool is moved plantar with the guiding force aligned orthogonal to the push force. For this purpose the coupling forces are applied by a knob-shaped handle. In the resulting hand position, the push force is aligned normal to the palm, resting on the top of the knob-shaped handle, while guiding force is aligned normal to the fingers on the side of the knob-shaped handle.

Gripping force³

The ISO 15230 and the DIN 45679 define the gripping force F_{gr} as a clamp-like force, which occurs when the hand encloses a handle (DIN Deutsches Institut für Normung e. V., 2013; ISO - International Organization for Standardization, 2007). The individual force components acting on the surface of the handle compensate each other in the center of the palm, as they are directed against each other. Consequently, the individual force components are summed into two opposing force vectors directed towards a dividing plane, with the gripping force F_{gr} being half the sum of the individual force components (DIN Deutsches Institut für Normung e. V., 2013; ISO - International Organization for Standardization, 2007). For this purpose ISO 15230 refers to the enclosed gripping of a cylindrical handle, for which the angular orientation of the dividing plane can be defined by the hand-oriented angle α or by the machine-oriented angle β (ISO - International Organization for Standardization, 2007). The angular orientation of the dividing plane depends on the distribution of the individual pressure field over the handle's surface. In the context of the gripping force, ISO 15230 only refers to the cylindrical handle geometry (ISO - International Organization for Standardization, 2007). Based on the push and guiding force applied to the knob-shaped handle of the sander in the schematic illustration in Figure 2.7, a corresponding gripping force can be assumed. However, the distribution of and direction of the gripping force applied to this knob-shaped handle are unknown.

Figure 2.8 shows the pressure field p and the resulting gripping force F_{gr} according to ISO 15230. Illustration a) on the left side shows the pressure field p . Illustration b) on the right side shows the resulting gripping force F_{gr} as clamping like force acting towards the dividing plane. Thereby the orientation of the dividing plane can be described by the hand-oriented angle α or the machine oriented angle β .

³ In the following thesis the terms gripping force and grip force will be used synonymously as these terms are also used synonymously in the state of research, according to ISO - International Organization for Standardization, 2012. Thereby, all terms refer to the force described in the current subchapter and the definition in ISO - International Organization for Standardization, 2007.

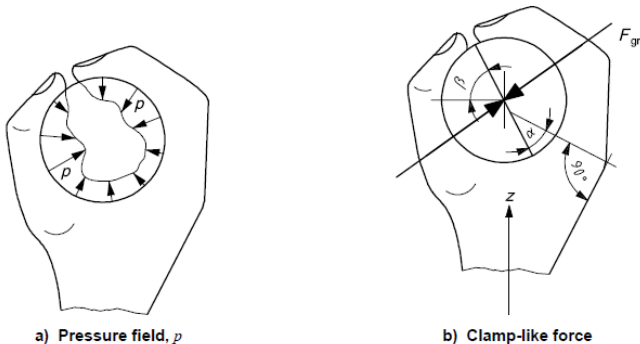


Figure 2.8: Example of the gripping force F_{gr} when gripping a cylindrical handle, taken from ISO 15230. Illustration a) on the left side: pressure field p of the gripping. Illustration b) on the right side: the gripping force F_{gr} as clamp-like force acting towards the dividing plane. the dividing plane is oriented by the hand-oriented angle α and the machine oriented angle β with the z -axis along the forearm (ISO - International Organization for Standardization, 2007)

Torque and friction force

ISO 15230 does not explicitly address forces, acting tangentially to the hand like surface forces resulting from an applied torque or moment. Nevertheless ISO 15230 gives two examples of these forces, that are visible in Figure 2.9

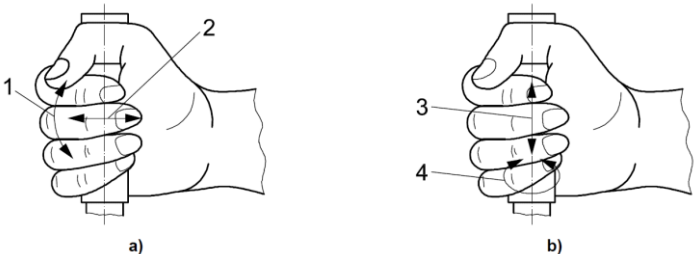


Figure 2.9: Two examples for torque and friction forces from ISO 15230 a) Moment applied to a cylindrical handle b) Torque applied to a cylindrical handle **Key:** 1 moment, 2 push or pull force, 3 friction, 4 torque (ISO - International Organization for Standardization, 2007).

In this context ISO 15230 states that the moment and torque in Figure 2.9 a) and b) are not possible without a gripping forces, a push/pull force or a lifting force (ISO - International Organization for Standardization, 2007).

2.5 Description of the body posture

The values of the MI of the HAS for translational vibration excitation given in DIN 45677 and ISO 10068 refer to a body posture specified as the arrangement of the limbs of the HAS within an allowable joint angle range (ISO - International Organization for Standardization, 2012). Accordingly, Figure 2.10 shows the referred arrangement of the limbs of the HAS with the joint specific angle ranges defined in the ISO 10068.

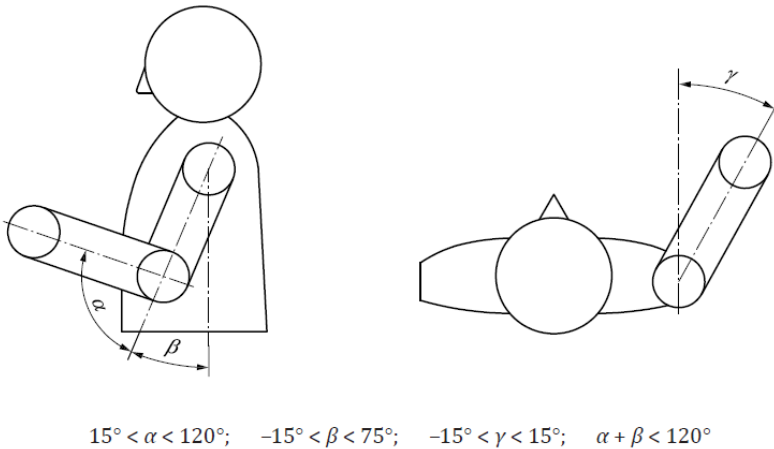


Figure 2.10: Side and top view (left to right) of the schematic illustration of the body posture defined in the ISO 10068 as condition over which the translational MI data were obtained with the corresponding allowable joint angle ranges below (ISO - International Organization for Standardization, 2012).

2.6 Measurement of the MI and the applied coupling forces

The established method for the measurement of the MI of the human HAS under laboratory conditions are subject studies in which the subjects' HAS is excited by a specific frequency spectrum (ISO - International Organization for Standardization, 2012, 2013). The corresponding frequency spectrum from ISO 10068 and ISO 10819 consist of the one-third-octave band in the range from 10 Hz up to 500 Hz, respectively in the range from 25 Hz up to 1600 Hz. Equation 2.14 shows the calculation rule for calculating the frequencies of the one-third-octave band, according to DIN EN ISO 266.

$$f = 10^{\frac{n}{10}} * f_r \quad 2.14$$

In Equation 2.14 f_r is the reference frequency of 1000 Hz, while n is a positive or negative number (DIN Deutsches Institut für Normung e.V., 1997). For the calculation of the norm frequencies of the one-third-octave band n is defined by the R10-sequence of ISO 3.

For the excitation of those frequencies, ISO 10819 recommends an electromagnetic shaker whose frequency range is controlled by an amplified signal controller connected to a real-time analyzer (ISO - International Organization for Standardization, 2013). A schematic drawing of the described test setup from ISO 10819 is shown in Figure 2.11. Although the test setup from ISO 10819 refers to the measurement of the vibration transmissibility of vibration-reducing gloves, the test setup can be taken as reference, because for the measurement of the MI the same elements are required. For transmitting the vibration to the subject's HAS a cylindrical instrumented handle is attached to the shaker's shaft (ISO - International Organization for Standardization, 2013). This measuring handle is equipped with accelerometers, to measure the acceleration of the HAS when vibrational excited (ISO - International Organization for Standardization, 2013). Additionally the measuring handle has several force transducers to measure dynamic reaction forces of the HAS as well as the push force and the gripping force applied to the handle.

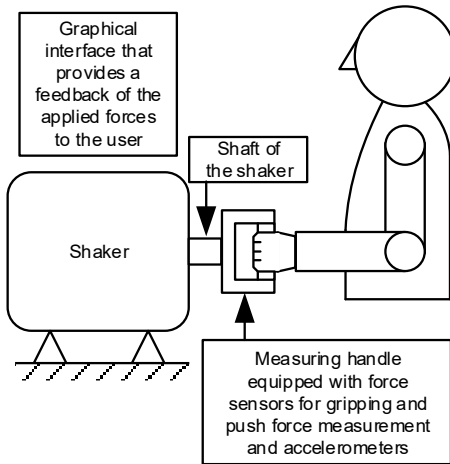


Figure 2.11: Schematic drawing of a shaker equipped test bench for MI measurement. Own illustration based on (DIN Deutsches Institut für Normung e. V., 2001b; ISO - International Organization for Standardization, 2012, 2013)

For the measuring handle in Figure 2.11, ISO 10819 suggests a handle design which is depicted in Figure 2.12. According to the gripping force-related dividing plane shown in Figure 2.8 on page 25 in Subchapter 2.4, the measuring handle from ISO 10819 is divided into a rear handle frame with a half-cylindrical inlay and two force sensors in between.

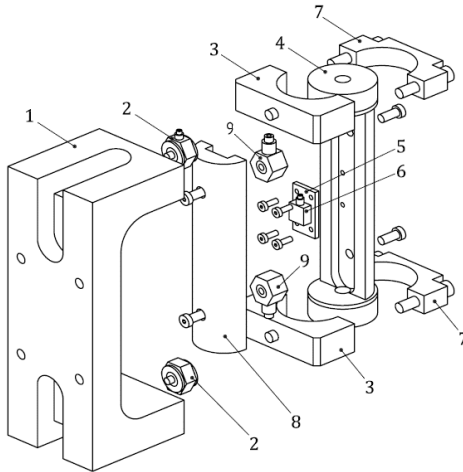


Figure 2.12: Assembly drawing from ISO 10819 of the cylindrical measuring handle. **Key:** 1 base aluminium, 2 feed force transducer, 3 rear bracket, 4 handle \varnothing 40mm, 5 accelerometer base, 6 accelerometer, 7 front bracket, 8 handle cover \varnothing 40mm, 9 grip force transducer (ISO - International Organization for Standardization, 2013).

The measuring handle from the ISO 10819 can be regarded as reference, on the basis of which different variants are used in the state of research for translational MI measurement. In this context, also the influence of different handle diameters hand been investigated, as the geometry of the handle also affects the MI of the HAS (Aldien et al., 2006; P. Marcotte et al., 2005). Beside this cylindrical handle MI of the HAS has also been investigated for translational vibration excitation via a flat platform, on which the hand was placed (Concettoni & Griffin, 2009; Xu et al., 2011). These hand positions roughly correspond to the “palm” position of Figure 2.5 on page 18 from DIN EN ISO 5349-1. However, these flat platforms do not allow the application of gripping forces. Figure 2.13 shows several exemplary handles and surfaces used in the state of research for translational MI measurement.

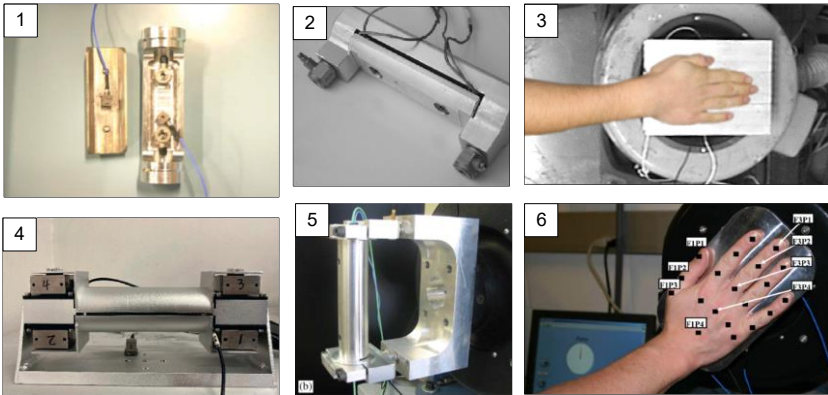


Figure 2.13: Examples of handles and surfaces used for translational MI measurement from the state of research (The markings on the sixth picture refer to the positions, where the acceleration was measured via a laser accelerometer (Xu et al., 2011)): 1. (Dong, Welcome, McDowell, & Wu, 2006), 2. (Besa et al., 2007), 3 (Concettoni & Griffin, 2009), 4. (Zhang et al., 2021), 5. (P. Marcotte et al., 2005), 6. (Xu et al., 2011)

The pictures in Figure 2.13 show that in the state of research the different variants of the measuring handle from ISO 10819 had been used for the measurement of the translational MI. Also the influence of the handle diameter on the MI has been investigated. Here, a larger handle diameter in combination with the body posture and coupling forces resulted in a higher magnitude of the translational MI in z_h -direction (Aldien et al., 2006; P. Marcotte et al., 2005). Furthermore, the translational excitation of the HAS via a flat surface results in a different MI than the excitation via a cylindrical handle (Concettoni & Griffin, 2009; Xu et al., 2011). Taken these findings concerning the influence of the handle geometry on the translational MI as reference, a similar effect of the handle geometry on the RMI can be assumed.

The basic test setup from the state of research for measuring the MI by vibrating the HAS with an electromagnetic shaker via an instrumented measuring handle can be adopted for measuring RMI. However, the measurement of the RMI requires a shaker system that excites rotational vibrations. In order to determine the RMI according to equation 2.3 the handle must be capable of measuring the torque and the angular acceleration. For this purpose, Matthiesen et al. (2018) describe a test setup, which enables the transmission of translational and rotational vibrations to HAS and the determination of the corresponding MI (Matthiesen et al., 2018).

The test setup of Matthiesen et al. (2018) consists of two independent shakers⁴, one for translational and one for rotational vibration excitation. Both shakers provide vibration to an output shaft. The shaker responsible for the translational vibration is aligned coaxial to the common output shaft (Matthiesen et al., 2018). The shaker responsible for rotational vibration excitation is aligned orthogonal to the common output shaft. A pretensioned gear rack attached to the shaker's shaft transmits the linear motion of the shaker to a gear attached to the common output shaft, resulting in an angular oscillation of the common output shaft without any ply. A spline connection between the common output shaft and the gear in combination with a bearing of the gear enables the common output shaft to move translationally while being rotationally oscillated. Therefore, the shaker system is capable to excite the common output shaft with superimposed rotational and translational vibrations (Matthiesen et al., 2018). To adjust the height and the tilt angle of the common output shaft to the subjects' height and body posture, the shaker system is attached to a carrier mechanism. The carrier mechanism can position the shaker system in a range from 0.7 m up to 2.8 m via two ball screw drives driven by electric motors. The tilt angle of the shaker system is also electromotive adjustable in the range from 0° up to 180° (Matthiesen et al., 2018). Figure 2.14 shows the described test setup of Matthiesen et al. (2018).

⁴ Both shakers are manufactured by ETS Solutions Europe (Loffenau, Germany), the translational vibration excitation is provided by the M124M model and the rotational vibration by the L215M model.

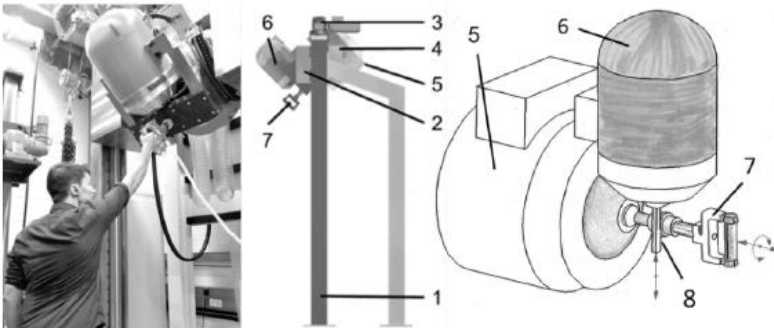


Figure 2.14: Test setup of Matthiesen et al. (2018) for the translational and rotational MI measurement (Matthiesen et al., 2018). **Key** (translated by the author): 1. Frame, 2. Shaker mount, 3. Lifting drive, 4. Rotation drive, 5. Translational shaker, 6. Rotational shaker, 7. Handle, 8. Gear rack-gear arrangement

In order to measure the MI, Matthiesen et al. (2018) instrumented the cylindrical measuring handle with two triaxial force transducers⁵ and two triaxial accelerometers⁶ (Matthiesen et al., 2018). The triaxial force transducers and accelerometers enable the determination of the torque and the angular acceleration of the handle from the tangential forces and accelerations of the rotational vibrations. The RMI can then be calculated from the torque and the angular acceleration. For this purpose, the force transducers and the accelerometers were amplified⁷ (Matthiesen et al., 2018). The sensor signals were recorded by a measuring board⁸ (Matthiesen et al., 2018). As the studies in this thesis were conducted with the same shaker system and a similar sensor setup, the torque and the angular acceleration were also calculated from the tangential forces and accelerations of the rotational vibration.

⁵ Kistler 9027C

⁶ PCB 356A02

⁷ Kistler 5073A411 and PCB 483C15

⁸ MIO-4-ET1 by Jäger-ADwin

2.7 Interim conclusion

According to Matysek and Kern (2009), the RMI of the HAS can be described, analogue to the translational MI, as complex, frequency depending quotient of the torque and the angular velocity. In correspondence to the translational MI, the RMI can occur for rotational vibration excitation around the spatial coordinate axes of the coordinate systems from DIN EN ISO 5349-1 and ISO 10068. In this context, an extend knowledge on the RMI of the HAS could also enable further investigation of cross-axial effects that occur when modeling the biodynamic response of the HAS for multi-axial vibration excitations. Thus, analogous to the translational MI, it can be assumed that the RMI of the HAS is also different for different spatial directions of vibration excitation. Further, the influencing factors on the translational MI reported in standardization and the state of research like coupling forces and body posture probably also affect the RMI. Following the established studies, a corresponding influence of the gripping and the push force as well as the body posture on the RMI can be assumed in this context. This assumption is supported by ISO 15230, which states, that for the application of torque around the y_h -axis in the "hand grip" position the application of gripping force is mandatory, as it generates friction between the hand and the handle. Accordingly, the gripping force also influences the RMI when the handle is loaded in the "hand grip" position by rotational vibrations with torque around the y_h -axis. Hence, the effect of the gripping force, the push force and the body posture on the RMI, have to be determined in experimental studies. To conduct such studies on the RMI, a shaker based test setup is required that corresponds to the setup for translational MI measurements. An appropriate test setup for the measurement of the RMI is suggested by Matthiesen et al. (2018). The test setup has a carrier mechanism that enables adjusting the shaker position and orientation. Such an adjustment is necessary for comparable arm and body postures among various human subjects. Since this test setup is appropriated and available the rotational shaker component and the sensor arrangement from Matthiesen et al. (2018) was used in the studies of this thesis. For the measurement of the gripping force Matthiesen et al. (2018) used a cylindrical measuring handle equivalent to those used for translational MI measurement in the state of research. However, the cylindrical measuring handle does not adequately represent vibration excitation of the HAS in the "palm" position from DIN EN ISO 5349-1. Therefore, in the state of research on translational MI, the "palm" position is represented by flat surfaces. The flat surface does not allow gripping forces to be applied, as it cannot be enclosed. Accordingly, studies on the influence of the gripping force on the MI or RMI of the HAS in the "palm" position are lacking in the state of research and standardization, as there is no suitable measuring grip for this.

3 State of research on the measurements of the rotational impedance of the human hand-arm system

The following chapter provides an overview of the state of research on the RMI measurement and the modeling of biodynamic response of the HAM for rotational vibration exposure.

A study of Lin et al. (2003) focuses on the modeling of the biodynamic response of the HAS to impulsive torque loads, as they occur when using pneumatic screwdrivers (Lin et al., 2003). For this purpose, Lin et al. (2003) conducted a study with 25 subjects from which a model with lumped parameters and one rotational degree of freedom was derived. To parametrize inertia, stiffness and damping of this model, Lin et al. (2003) excited the subject's HAS via a cylindrical handle with various rotational harmonic vibrations around the axis of the forearm (Lin et al., 2003). The harmonic vibrations were generated by oscillating different inertial masses connected to a torsional spring. Based on the angular deflection of the handle and the applied torque, Lin et al. (2003) determined the apparent stiffness of the HAS, from which the inertia, damping and stiffness of the HAS was derived (Lin et al., 2003). The similar approach of a rotational lumped parameter model with one degree of freedom was used by Joshi et al. (2008) for determining the biodynamic of the HAS in the context of fastening operations with a pistol grip pneumatic torque driver (Joshi et al., 2008). In the studies of Joshi et al. (2008), the subjects gripped a pistol grip, which was angularly displaced by an impulsive torque load. The inertia, damping and stiffness of the HAS were determined from the measured angularly deflection and applied torque (Joshi et al., 2008).

However, the biodynamic response of the HAS to single torque impact as investigated in the studies of Lin et al. (2003) and Joshi et al. (2008) are not comparable to the biodynamic response of the HAS during continuous, rotational vibrations. This is especially true, since the frequencies of the applied harmonic angular oscillation in the studies conducted by Lin et al. (2003) and Joshi et al. (2008) were below the frequency of 10 Hz, which is the lowest recommended frequency from ISO 10068. Furthermore, in the studies of Lin et al. (2003) and Joshi et al. (2008) the effect of influencing factors like the coupling forces was not considered.

Mangold (2019) investigated a physical, rotational HAM using a pistol grip impulse wrench as an example. To parametrize the stiffness, damping and inertia of the HAM based on the MI of the HAS, Mangold (2019) conducted a subject study using an instrumented, modified impulse wrench. For this purpose, the pistol grip of the impulse wrench was equipped with a triaxial accelerometer and a triaxial force transducer as well as two additional force transducers for the measurement of the gripping forces. The motor of the impulse wrench was actuated by an external trigger. In the test setup used by Mangold (2019), the drive shaft of the instrumented impulse wrench was attached to a model workpiece, simulating a tightened screw. As this model workpiece connected the impulse wrench to the environment, the pistol grip excited the HAS rotationally around the z_h -axis at the device specific frequency of 23 Hz when the external trigger was pressed.

Mangold used a full-factorial study design with two subjects to investigate the influence of grip force, push force, and body posture on the biodynamic response of the HAS. In this full-factorial study design, the gripping force levels were 20 N and 95 N, the push force levels were 7 N and 30 N and the body posture distinguished whether the impulse wrench was held at chest level or overhead. Overall, the full factorial design of the study resulted in eight different factor combinations per subject, with each factor combination being conducted in eleven trials (Mangold, 2019). In order to ensure a constant application of the requested coupling force levels, Mangold installed a display with an graphical feedback that visualized the applied coupling forces of the subject in relation to the requested coupling force levels.

Mangold (2019) determined the MI from the obtained acceleration and force data by converting the rotational excitation of the impulse wrench into a translational excitation of the HAS. This approach is based on a publication by Matthiesen et al. (2016) with co-authorship by Mangold. Figure 3.1 illustrates the conversion used by Mangold (2019).

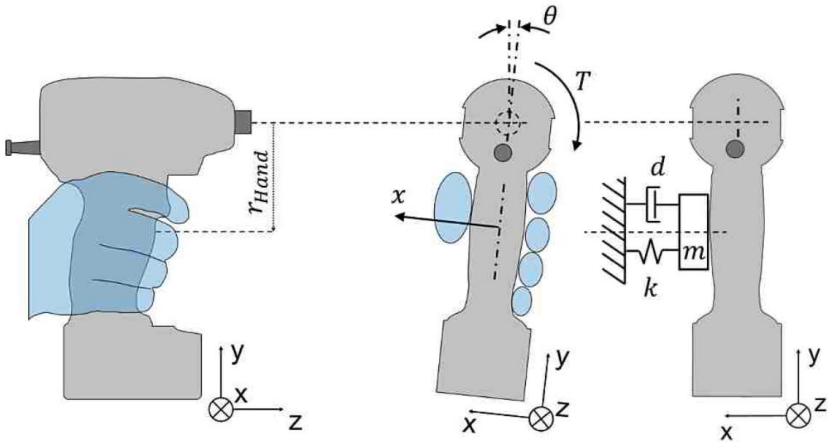


Figure 3.1: The conversion used by Mangold (2019) to convert the rotational excitation of the impulse wrench into a translational excitation of the HAS. The figure was put together by the author of the thesis from two figures by Mangold (2019). From left to right: Schematic drawing of the side view of the impulse wrench with the hand gripped, free cut from the rear view of the angular deflected impulse wrench with the hand gripped, rear view of the impulse wrench with the HAS illustrated as single mass oscillator. **Key:** r_{Hand} = radius from the rotation axis to the center of the hand, T = torque of the impulse wrench, x = displacement of the pistol, θ = angular deflection at the center of the hand, m = mass of the HAS in x_h –direction, k = spring constant of the HAS in x_h –direction, d = damping constant of the HAS in x_h –direction.

As shown in Figure 3.1, the angular deflection of the impulse wrench can be interpreted as translational displacement of the HAS in x_h –direction. Using the force measured on the sides of the pistol grip and the measured acceleration in x_h –direction, Mangold (2019) calculated the MI of the HAS in x_h –direction. Prior to the study, Mangold also determined the impedance of the unloaded impulse wrench with no HAS interaction before the study in several calibration trials. This impedance was later subtracted from the MI measured in the study, to obtain the MI of the subjects' HAS without the influence of the test setup's inertia, damping and stiffness.

In this context Matthiesen et al. (2016) used the conversion from Figure 3.1 to parametrize the stiffness, damping and inertia of a simulated HAM by the corresponding parameters given in ISO 10068 for excitation in x_h –direction. Matthiesen et al. (2016) thereby used a multibody model with lumped parameters and two degrees of

freedom based on Equation 2.7. Similar to the approach of Mangold (2019), Matthiesen et al. (2016) substituted the angular deflection trigonometrically by the translational displacement of the pistol grip center in x_h –direction and the corresponding radius. The substitution enabled a coefficient comparison between the rotational equation of motion of the model and the corresponding translational equation of motion in x_h –direction from ISO 10068. Based on this coefficient comparison, mass, damping and stiffness parameters given for excitation along the x_h –direction in ISO 10068, were converted into inertia, rotational damping and rotational stiffness to parametrize the rotational HAM (Matthiesen et al., 2016). In this context, Matthiesen et al. (2016) already refer to the upcoming experimental setup of Matthiesen et al. (2018), which was presented in Subchapter 2.6.

The study of Mangold is a first approach to determine the influence of the body posture as well as the coupling forces on the RMI. However, the study is limited in its significance, since Mangold conducted the study with only two subjects and due to the test setup with the impulse wrench, the HAS of the subjects was only exposed to the excitation frequency of the impulse wrench. These limitations are also mentioned by Mangold, who in this context recommended further studies on the RMI conducted with a greater number of subjects and for a larger frequency spectrum. In this context, Mangold recommended the test setup form Matthiesen et al. (2018) as it is suitable for this kind of investigations (Mangold, 2019).

In 2019, Lindenmann and Matthiesen conducted a study, in which the RMI of the HAS of 10 subjects was measured. For this purpose Lindenmann and Matthiesen used the test setup described in Matthiesen et al. (2018). Lindenmann and Matthiesen excited the HAS of the subjects with a frequency spectrum similar to the spectrum of ISO 10068, via a cylindrical measuring handle oriented on the handle of ISO 10819. The subjects applied a gripping and a push force of 50 N to the handle. Like in the study of Mangold (2019) the constant application of the coupling forces, was ensured by a graphical feedback on a display.

The study was conducted with three trials per subject. Within those trials the coupling forces and the body posture were not varied. The RMI from the obtained torque and acceleration data was determined using Matlab⁹. The corresponding evaluation algorithm of Lindenmann and Matthiesen (2019) consists of an identification of the applied frequencies by a spectrogram using short-time Fourier transform and an iterative filtering of the torque and acceleration data with a Butterworth-

⁹ MATLAB© The MathWorks, Inc, Natick MA, USA

band-pass-filter for the corresponding identified frequency. The frequency-filtered remaining torque and acceleration data was evaluated with a sinusoidal fitting algorithm, to obtain the magnitude of the corresponding vibration. From the obtained magnitudes of the torque and the acceleration, the RMI was calculated as a complex value by using equation 2.3 for the identified frequency. This evaluation was conducted for every applied frequency. Mangold (2019), Lindenmann and Matthiesen (2019) also subtracted the calibrated, rotational impedance of the unloaded measuring handle from the results obtained. Overall Lindenmann and Matthiesen (2019) determined the RMI of the HAS for 18 frequencies in the frequency range between 10 and 500 Hz, which were based on the one-third octave band of ISO 10068.

The course of the phase angle of the RMI constantly decreases across the applied frequency spectrum from 0 at 10 Hz to approximately $-\pi$ at 500 Hz, which probably indicates a spring-damper dynamic of the HAS. The magnitude of the RMI increases across the applied frequency spectrum. In reference to the conversion used by Matthiesen et al. (2016) and Mangold (2019), Lindenmann and Matthiesen (2019) compared the obtained magnitude plot to the magnitude plot for translational excitation along the x_h -axis from ISO 10068. In this comparison, Lindenmann and Matthiesen state that the course of the plot is similar, but considerably lower. Therefore, Lindenmann and Matthiesen concluded that the HAS is less resistant against rotational vibration excitation. These results of Lindenmann and Matthiesen show that rotational vibration excitation of the HAS, the corresponding MI cannot fully be derived from the values of the translational MI given in the ISO 10068.

Overall, the knowledge in the state of research on the rotational biodynamic response of the HAS is far smaller than on the translational. In this context, several approaches exist to convert the angular deflection into a displacement and to represent the RMI of the HAS by the translational MI. However, the results of Lindenmann and Matthiesen (2019) show that the RMI cannot be represented fully and with sufficient accuracy by the translational MI. Furthermore, the substitution of the RMI with the translational MI only works if the vibrational torque and angular acceleration acts normally on the palm via a lever arm, as it is the case in Figure 3.1.

For a rotational excitation around the y_h -axis in the "hand grip" position, an equivalent substitution with the translational MI does not work. With this constellation of hand position and excitation direction, the handle is angularly deflected around its centerline. Therefore, the acceleration and the force resulting from the torque act tangential to the handle's circumference and thus tangential to the palm, as Figure 3.2 shows. Consequently, the HAS would be translational excited along the z_h -axis as well as along the x_h -axis. Thus, a clear assignment to one translational excitation direction is not possible. Furthermore, it is questionable whether tangential force

and acceleration transfer to the HAS can be represented by translational MI values measured for force and acceleration transfer normal to the palm and fingers.

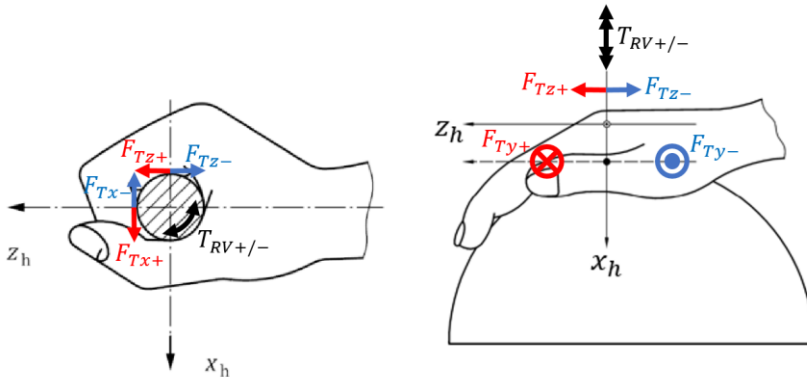


Figure 3.2: Left side: Rotational vibration excitation around the y_h –axis in the “hand grip” position, according to ISO 10068. Right side: Rotational vibration excitation around the x_h –axis in the “palm” position, according to DIN EN ISO 5349-1. The illustration of the hand positions are taken from both standards, the forces and were added by the author of the thesis. **Key:** (x_h, y_h, z_h) = basic centric coordinate axis, $T_{RV+/-}$ = positive and negative torque applied by the rotational vibration, $F_{Tx+/-}$ = tangential forces between hand and handle in positive and negative x_h –direction, $F_{Ty+/-}$ = tangential forces between hand and handle in positive and negative y_h –direction, $F_{Tz+/-}$ = tangential forces between hand and handle in positive and negative z_h –direction.

As the right side of Figure 3.2 shows these problems also occur for the rotational vibration excitation around the x_h –axis in the “palm” position of DIN EN ISO 5349-1. Therefore, the RMI of the HAS for excitations around the x_h – and y_h –axis in the “palm” and “hand grip” position cannot be represented by the substitution of translational MI values. However, no studies on the RMI for excitations around the x_h –axis or y_h –axis exist in the state of research so far. In addition, the influence of the coupling forces or the body posture on the RMI in general has only been investigated to a limited extend concerning the applied frequencies and subject numbers. Thus, the current state of research on the RMI of the HAS only considers the rotational vibration excitation around the z_h –axis in the “hand-grip” position and the influence of the coupling forces and body posture on the RMI has only been investigated to a limited extend.

3.1 State of research on the rotational excitation of the human hand-arm system around the x_h –axis and y_h –axis

Since the state of research on the RMI of the HAS only refers to the vibration excitation of the HAS by rotational vibrations around the z_h –axis, the following chapter should clarify whether a similar rotational vibration exposure of the HAS around the x_h –axis or y_h –axis occurs when using power tools. In this context the subchapter focuses on the rotational excitation of the HAS around the x_h –axis in the “palm” position of DIN EN ISO 5349-1 and the rotational excitation around the y_h –axis in the “hand grip” position as in ISO 10068. As described in Subchapter 2.3, the applied torque in both hand positions acts on the palm and fingers via a tangential force transmission. For this reason, the RMI cannot be substituted by existing values of the translational MI or by a corresponding measurement as performed by Mangold (2019). As a result, for rotational vibration excitations in these directions, the RMI of the HAS is considered to be particularly relevant, since it is not possible to derive it from existing translational MI values.

3.1.1 Vibration excitation in x_h –direction with the hand-arm system in the “palm” position

In the context of power tool applications, the “palm” position of DIN EN ISO 5349-1 can be interpreted as the corresponding use of a power tool with a knob-shaped main handle that is gripped one-handed in a resting hand position. Consequently, a representative power tool of this hand position is the one-handed gripped random orbital sander or a palm sander. Figure 3.3 shows the gripping of a random orbital sander taken from Nouri (2019)¹⁰ and the “palm” position from DIN EN ISO 5349-1 for comparison.

¹⁰ Unpublished Master thesis

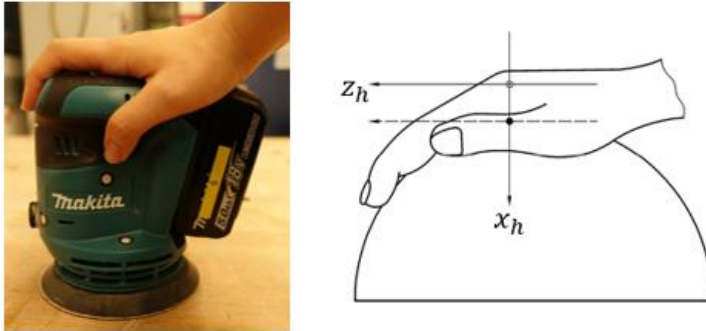


Figure 3.3: Comparison between the gripping of a one-handed random orbital sander from Nouri (2019) (left)¹¹ and the “palm” position from DIN EN ISO 5349-1 (right). A description of the coordinate axes can be found in Figure 2.5 on page 18

Figure 3.3 shows that the “palm” position of DIN EN ISO 5349-1 corresponds very closely to the one-handed gripping of the knob-shaped handle of a random orbital sander¹². In the state of research, the “palm” position is also related to the gripping of an orbital sander. Xu et al. (2011) excite the HAS in the “palm” position along the x_h –axis via a flat aluminum platform. In this context, Xu et al. (2011) referred to this type of excitation as an approximate simulation for the use of random orbital or palm sanders (Xu et al., 2011). The test setup used by Xu et al. is shown in Figure 3.4.

¹¹ The photo was taken from an unpublished master thesis and adopted by the author

¹² In the following the terms one handed palm sander, random orbital sander, orbital sander are used synonymously, all terms refer to the power tool type shown on the left side of Figure 3.3.

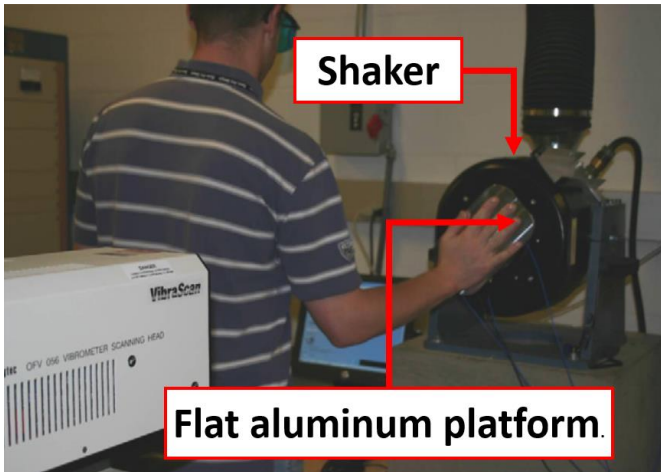


Figure 3.4: Test setup used by Xu et al. (2011) to excite the HAS in the “palm” position via a flat aluminum platform. The photo is taken from Xu et al. (2011). The labels in the photo were added by the author of the thesis.

The test setup of Xu et al. (2011) in Figure 3.4 shows that the flat aluminum platform oscillates the hand translationally along the x_h -axis. In consequence, the vibration of the vertical oriented platform moves the hand back and forth. However, it is questionable, whether the excitation of the HAS in the test setup of Xu et al. (2011) appropriately represents the vibration exposure of a random orbital sander. As Figure 3.3 shows, the axis of rotation of the grinding disc of the random orbital sanders is oriented perpendicular to the knob-shaped handle and thus to the palm of the hand. Therefore, it can be assumed that the main excitation direction of a random orbital sander is primarily the rotation around the x_h -axis. DIN EN ISO 28927-3 (2010b) and DIN EN ISO 5349-2 (2015) support this assumption, as they suggest positioning the accelerometer on the knob-shaped handle and eccentric to the axis of rotation of the motor shaft for measuring the vibration exposure of sanders. From the suggested sensor position eccentric to the axis of rotation it can be concluded that both standards consider the occurrence of tangential accelerations due to the rotation of the motor shaft.

Furthermore, a study by Shi and Sun (2018) on the vibrational response of an orbital sander verifies the assumption of mainly rotational vibration excitation (Shi & Sun, 2018). For the vibrational optimization of an orbital sander, Shi and Sun (2018) equipped the knob-shaped handle of the sander with accelerometers. The sander was hung on a string and driven in free-running mode for 120 s. The measurement

of the vibrational responses of the orbital sander shows that the RMS-value¹³ of the angular acceleration around the three spatial axes is much higher than the RMS-value of the translational acceleration along these axes. In this context the measured angular acceleration around the x_h –axis was the highest at $861.4 \frac{rad}{s^2}$ (Shi & Sun, 2018)¹⁴. In a further work by Shi and Sun on the modeling of the vibration response of a random orbital sander, the authors also state that the housing of the random orbital sander does not have large displacement motion (Shi & Sun, 2019). The results obtained by Shi and Sun show that orbital sanders excite the HAS primarily rotationally, with the main excitation direction around the x_h –axis. Thus, the translational vibration excitation of the HAS in the study by Xu et al. probably does not represent the main excitation direction of a random orbital sander.

Furthermore, Xu et al. (2011) use a flat platform for the exaction of the HAS. However, the hand is curved when gripping a knob-shaped handle as well as in the “palm” position of DIN EN ISO 5349-1 the hand is curved. As a result, the vibration excitation by a flat platform does not fully correspond to “palm” position of DIN EN ISO 5349-1 or the hand position when gripping a random orbital sander. Since the hand does not enclose anything, the flat platform also does not allow the application of gripping forces, which, however, influence the MI of the HAS according to the state of research (Besa et al., 2007; Lindenmann et al., 2022; Pan et al., 2018; D. Welcome et al., 2004; Zhang et al., 2021). In this regard Xu et al. state “While it is expensive and time-consuming to replicate the exact contact geometries of palm sanders or orbital sanders, such a test setup can be considered as an approximate simulation of the hand vibration exposure in the operations of these tools.” (Xu et al., 2011, p. 419). From this, it can be concluded that in the state of research lacks a suitable measuring handle that represents the knob-shaped handle geometry of orbital sanders. Accordingly the state of research also lacks corresponding studies on the rotational vibration excitation of the HAS with such a handle, which simulates the excitation of the HAS by a random orbital sander.

¹³ RMS = root mean square

¹⁴ For comparison the RMS-value of the translational acceleration along the x_h –axis was about 16.1 m/s^2 (Shi and Sun (2018))

In summary the following conclusions can be drawn from the state of research on the vibration excitation in the “palm” position.

- The “palm” position of DIN EN ISO 5349-1 can be interpreted as the gripping of a knob-shaped handle, where the hand rest on the top of the handle as it is the case with power tools such as the palm sander or the orbital sander.
- The orbital sander primarily emits rotational vibrations around the x_h –axis.
- The studies conducted for the purpose of measuring the MI of the HAS in the “palm” position with reference to orbital sanders excited the HAS translational. However, a rotational excitation would correspond more closely to the vibration excitation of an orbital sander, which would make the RMI to a more appropriated measure for this excitation.
- The test setup used in the studies to investigate MI in the “palm” position does not allow the application of gripping forces, although these forces got an influences on the MI.
- The state of research lacks an appropriate knob-shaped measuring handle, as its derivation from power tool handles is too expensive and too time-consuming.

3.1.2 Vibration excitation in y_h –direction with the hand-arm system in the “hand grip” position

So far in the state of research on the RMI, the "hand grip" position of DIN EN ISO 5349-1 or ISO 10068 was excited around the z_h –axis, using the measuring handle of ISO 10819. With regard to power tool applications, however, a rotational excitation around the y_h –axis may also be relevant, since the hand position corresponds to the use of a pneumatic or electrical operated in-line assembly screwdriver¹⁵. Figure 3.5 shows the hand position when holding an in-line assembly screwdriver compared to the hand position from ISO 10068 for comparison.

¹⁵ In the following the terms in-line clutch screwdriver, assembly screwdriver, in-line impact wrench, electric screwdriver and pneumatic screwdriver are used synonymously with each other. Hereby all terms refer to a cylindrical power tool with a motor shaft coaxial to the centerline of the cylinder, which is used for screwing tasks as in the Figure 3.5.

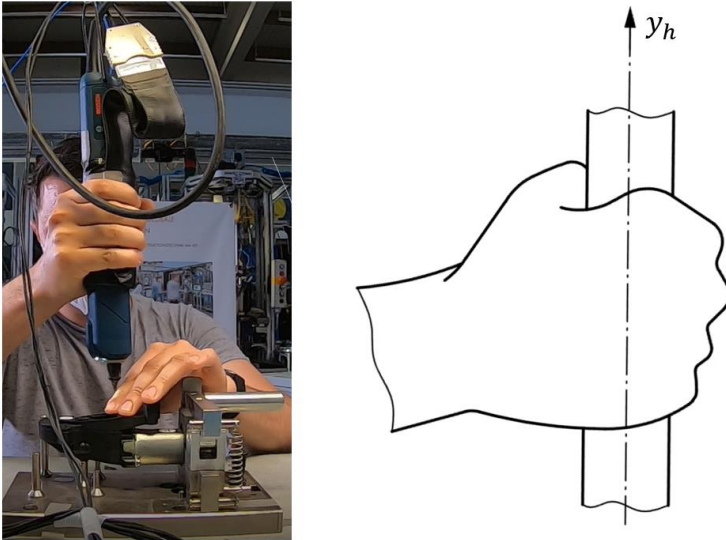


Figure 3.5: Comparison between the gripping of an in-line electric assembly screwdriver taken by the author (left) and the schematic hand position according to ISO 10068 (right). The illustration from ISO 10068 is twisted about 156° .

Figure 3.5 shows that the hand position when holding an in-line assembly screwdriver corresponds to the grip position from ISO 10068. As a result the rotation axis of the screwdriver's motor shaft and the y_h –axis are aligned in a coaxial way with each other. Due to this alignment, when tightening screws, the motor shaft might excite the HAS rotationally around the y_h –axis. The state of research on the vibration emissions of assembly screwdrivers seems to confirm this assumption.

In a field study on the vibration exposure of assembly line workers, Radwin and Armstrong (1985) measured the vibration emission of an in-line pneumatic screwdriver. For this purpose, a single-axis accelerometer was attached to the screwdriver with sensitivity tangential to the circumference. Using this sensor arrangement

Radwin and Armstrong (1985) measured vibrations in tangential direction with acceleration magnitudes that were five times the gravitational constant¹⁶ when bolts were tightened. These magnitudes correspond to an acceleration of approximately $50 \frac{m}{s^2}$. Following on from this, Radwin and Armstrong (1985) investigated the vibration emission of the pneumatic screwdriver under laboratory conditions using a triaxial accelerometer, which was attached to the power tool with the x-axis tangential to the screwdriver's circumference. In the laboratory study the vibration exposure of the screwdriver was investigated during free running and when tightening a screw using two separate test setups. The measured acceleration spectra when tightening the screw were higher in the x-direction than in the y- or z-direction. Due to the tangential alignment of the accelerometer, the results of Radwin and Armstrong (1985) indicate a primarily rotational vibration excitation of the in-line pneumatic screwdriver.

In three other publications Chih-Hong Chang et al. (1999), C. H. Chang and Wang (2000) and Chih-Hung Chang and Wang (2001) the vibration exposure of an in-line pneumatic screwdriver was also measured via a triaxial accelerometer. In all three studies the accelerometer was attached on the skin of the third proximal phalanx¹⁷ of the dominant hand. According to Chih-Hong Chang et al. (1999) and Chih-Hung Chang and Wang (2001), the attached accelerometers were aligned according to the coordinate system in DIN EN ISO 5349-1. Since the accelerometers were attached to the hand, hand it can be assumed that Chih-Hong Chang et al. (1999) and Chih-Hung Chang and Wang (2001) refer to the biodynamic coordinate system of DIN EN ISO 5349-1, but this is not explicit mentioned. In C. H. Chang and Wang (2000) the alignment of the accelerometers is not mentioned, but due to the same positioning of the accelerometer an equivalent alignment can be assumed. Figure 3.6 shows the test setup of Chih-Hung Chang and Wang (2001) with the biodynamic coordinate system of DIN EN ISO 5349-1 added by the author of the thesis, according to Figure 2.5 on page 18.

¹⁶ The plots in the publication of Radwin and Armstrong (1985) were scaled in multiples of the gravitational constant.

¹⁷ First finger limb of middle finger

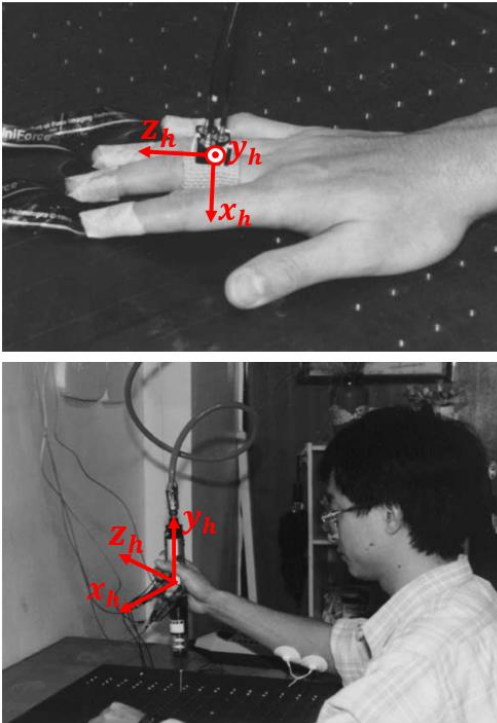


Figure 3.6: Position of the accelerometer on the hand of the subject (top) and test setup (bottom) from Chih-Hung Chang and Wang (2001) with the biodynamic coordinate system of DIN EN ISO 5349-1 added by the author of the thesis.

All three studies were conducted with 13 subjects, of which each tightened 300 screws with the in-line pneumatic screwdriver. The results of the studies have in common that the main vibrations occur along the y_h -axis and the z_h -axis. As Figure 3.6 shows the y_h -axis of the accelerometer was aligned along the shaft of the screwdrivers. The z_h -axis was parallel to the axis of the forearm and thus approximately tangential to the circumference of the assembly screwdriver, as also shown in Figure 3.6.

The first study of Chih-Hong Chang et al. (1999) aimed for the evaluation of vibration reducing gloves and wrist support when using pneumatic screwdrivers. The results obtained in the study show, among other things, that the highest vibration acceleration occurred in z_h -direction.

The other two studies of C. H. Chang and Wang (2000) and Chih-Hung Chang and Wang (2001) investigated the vibration exposure of the HAS by an electric screwdriver¹⁸ and two pneumatic screwdrivers¹⁹ for different body postures. In both studies the main vibrations occur in the y_h – and z_h –directions, with the vibration acceleration in the y_h –direction being about 20% higher than the vibration acceleration in the z_h –direction (C. H. Chang & Wang, 2000; Chih-Hung Chang & Wang, 2001). In all three studies the z_h –direction of the attached accelerometer is approximately tangential to the circumference of the assembly screwdrivers. Consequently, the vibration acceleration in this direction can be interpreted as rotational vibration excitation by the assembly screwdrivers.

The vibration acceleration in the y_h –direction along the centerline of the assembly screwdrivers, which was even higher than the acceleration in z_h –direction in two studies, was maybe due to the tightening process of the screw. First, the lowering of the screw into the hole, which results in a downward movement of the assembly screwdriver lead to an acceleration in the y_h –direction. Second, the bit of the assembly screwdriver can slip out of the screw head during tightening, causing the bit to bounce in the screw head and accelerate the assembly screwdriver in y_h –direction. Chih-Hung Chang and Wang (2001) seem to confirm this assumption as they state: “ While operating powered screwdrivers, the hand-transmitted vibrations were caused not only from the running motor, but also from the sway along the barrel, driving bit and screw. The more slant the driving pivot, the greater the sway, and thus greater vibration was induced.” (Chih-Hung Chang & Wang, 2001, p. 177).

In summary the following conclusions can be drawn from the state of research on the vibration excitation in in y_h –direction.

- The rotational excitation of the HAS around the y_h –axis in the „hand grip” position corresponds to the use of an assembly screwdriver.
- The main measured vibration excitation directions of the assembly screwdriver are tangential to the circumference of the assembly screwdriver and along the centerline of the screwdriver’s body.
- The measured vibration excitation tangential to the circumference of the assembly screwdriver indicates a rotational vibration excitation of the assembly screwdriver.

¹⁸ C. H. Chang and Wang (2000)

¹⁹ Chih-Hung Chang and Wang (2001)

3.2 Overall conclusion on the state of research

In the state of research the RMI of the HAS is far less investigated than the translational MI of the HAS. However, for a complete description and modeling of the HAS, knowledge of the rotational biodynamic response of the HAS is required. This knowledge is not only required for the description of the biodynamics of the HAS under rotational excitation, but also to represent the coupling effects described in ISO 10068 which occur in reality. In particular the modeling of cross-axial effects, with multiaxial excitations, requires knowledge of the rotational vibration biodynamics of the HAS. Therefore, in order to model and fully describe the vibrational behavior of the HAS, it is necessary to know its biodynamics in all six possible excitation directions. On this basis, several specific gaps in the state of research can be identified, each of which is mutually dependent on the other to be filled.

In the case of power tools, the state of research on the RMI mainly focuses on the impulse wrenches or comparable screwing power tools with a pistol grip, which excite the HAS around the forearm axis. However, there are many applications and scenarios where an excitation along other spatial directions or different handle geometries can occur. In this context the RMI of the HAS for excitation around the x_h -axis or y_h -axis in the "palm" or "hand grip" position has not been investigated in the state of research yet. A power tool application that represents the rotational vibration excitation around the x_h -axis in the "palm" position is the use of a one-handed random orbital sander. A power tool application that corresponds to the rotational vibration excitation around the y_h -axis in the "hand grip" position is the use of an inline assembly screwdriver. From the state of research on inline assembly screwdrivers it can be concluded that the HAS is rotationally excited around the y_h -axis during the use of such screwdrivers. Consequently, the measurement of the RMI for these excitation directions and hand positions can be considered relevant for the description and modeling of the vibrational human-machine-interaction in power tool applications. Thereby, both hand positions have in common that the applied rotational vibration acts partially or exclusively tangentially on the palm and fingers of the hand via a frictional connection between the hand and the handle. Therefore the following gap can be identified in the state of research:

The state of research lacks investigations on the biodynamics of the HAS under rotational vibration excitation. This lack concerns in particular excitations around the x_h -axis or y_h -axis in the "palm" or "hand grip" position.

It is known from the state of research that the coupling forces and the body posture have an influence on the MI of the HAS. However, in case of the RMI these influences have not been investigated for a larger range of excitation frequencies or

subject numbers. In consequence, the effect of these influencing factors have to be considered and determined when investigating the RMI for vibration excitations around the x_h – and y_h –axis in the "palm" and the "hand grip" position. In this, a further gap can be identified in the state of research:

The state of research lacks investigations on the influence of the coupling forces and the body posture on the RMI of the HAS.

For the measurement of the gripping force in the "hand grip" position the standardization and the state of research suggest the established handle design of a cylindrical measuring handle. For the measurement of gripping forces in the "palm" position when gripping power tools with knob-shaped handles, the state of research lacks a suitable measuring handle design, as the construction of such handles is considered too expensive and time-consuming. The distribution of gripping forces when gripping knob-shaped handles in the "palm" position has also not been sufficiently investigated to derive a suitable measuring handle. However, to measure the RMI in the "palm" position the development of such a measuring handle is required, resulting in a gap in the state of research:

The state of research lacks of measuring handle to measure gripping forces applied in the "palm" position.

4 Objective of the thesis

Based on the introduced research question and the overall objective of the thesis will be derived in this chapter. The research problem introduced in Subchapter 1.1 was:

Research Problem

The state of research lacks data on the rotational mechanical impedance of the human hand-arm system, which is required for the parametrization and the development of hand-arm models, such as those used in power tool development.

The overall conclusion on the state of research in Subchapter 3.2 confirms the relevance of this research problem, and shows that the existing studies on the RMI mainly focus on the rotational excitation around the z_h -axis. For excitations around the x_h -axis and the y_h -axis no corresponding investigations exist so far. Therefore, the investigation of these excitation directions can be considered particularly required. With regard to power tools excitation around the x_h -axis occurs mainly in applications where the hand is held in the “palm” position, while for the excitation around the y_h -axis the “hand-grip” position is more relevant. Under the perspective of an application-related investigation, it is therefore appropriate to investigate the RMI of the HAS in x_h -direction when excited in the “palm” position and the RMI in x_h -direction when excited in the “hand-grip” position. Furthermore, the rotational excitation of the HAS around the x_h -axis in the “palm” position and the rotational excitation around the y_h -axis in the “hand-grip” position are comparable to a certain degree. In both hand positions the rotational vibration around the corresponding axes is particularly or fully frictionally transmitted between the hand and the handle, as can be seen in Figure 2.4 and Figure 2.5 on page 17 and 18 from the ISO standards. The applied push force is also directed along the excitation axis in both cases. Therefore, this commonalities in terms of vibration transmission and push force direction can be expected to have a similar influence on the RMI of the HAS for both types of vibration excitation. For these reasons the following objective of the thesis can be derived.

Objective

The objective of this thesis is the investigation of the rotational mechanical impedance of the human hand-arm-system for rotational excitations around the x_h -axis in the „palm“ position, and around the y_h -axis in the „hand-grip“ position.

The investigation of the RMI for excitation around the x_h –axis in the “palm” position requires a corresponding measuring handle, which enables the measurement of the gripping force. The state of research lacks of such a suitable measuring handle. Such a measuring handle is mandatory, for the investigation of the RMI in the “palm” position in x_h –direction, because the gripping force has an influence on the MI according to the state of research. Therefore, this gap in the state of research must first be filled, by the development of a suitable measuring handle. Accordingly, the **first sub-objective** of the thesis is the development of a measuring handle that enables the measurement of the gripping force during RMI measurements of the HAS in the “palm” position for rotational vibration excitation around the x_h –axis. For the development of such a knob-shaped measuring handle, the main gripping force direction must be known in order to place the force transducers for gripping force measurement within this direction. As the knob-shaped handle has a generic geometry, the main gripping force direction and thus the position of the force transducers cannot be derived from the cylindrical measuring handle from the state of research. Consequently, the working hypothesis to achieve this sub-objective is:

Hypothesis 1: Derivation of the measuring handle design

From the distribution of gripping forces on a knob-shaped power tool handle, a measuring handle for excitations in the "palm" position can be derived, which is suitable for measuring gripping forces.

The development of a suitable measuring handle leads to the achievement of the **first sub-objective** and provides the basis for the determination of the influence of the gripping and the push force on the RMI. Accordingly the **second sub-objective** is the measurement of the RMI in magnitude and phase angle for the rotational vibration excitation of the HAS around the x_h –axis in the “palm” position. The investigation of the RMI around the x_h –axis measured in the “palm” position is a new approach with reference to the measured biodynamic data. In addition, the newly developed measuring handle from the first hypothesis is used, which enables the measurement of gripping forces. The sub-objective focuses on coupling forces as the main factors influencing the RMI, since their influence on MI is already known

from the state of research on translational MI. In order to reduce the test duration per subject and thus enable a higher number of subjects in the study the influence of the body is not investigated in the second sub-objective. Accordingly the second working hypothesis is:

Hypothesis 2: Rotational impedance around the x_h -axis

The rotational mechanical impedance for excitations around the x_h -axis in the „hand-grip“ position is influenced by the applied gripping force, push force.

The **third sub-objective** addresses the measurement of the RMI of the HAS for excitations around the y_h -axis in the “hand-grip” position. Thereby the measurement of the RMI in y_h -direction also includes the determination of the influence of the gripping and the push force on the RMI. For measuring these coupling forces in the “hand-grip” position the established measuring handle from ISO 10819 can be used. Furthermore, the **third sub-objective** also investigates the body posture as factor influencing the RMI.

Since there are no comparable investigations on the RMI in the state of research so far, the **third sub-objective** also serves as a reference for comparison with the results from the second sub-objective. This comparison is about the influence of the frictional hand-handle contact on the RMI and the alignment of the push force direction.

Consequently, the findings and conclusion drawn from the result of the **second sub-objective** must also be reflected in the results of the **third sub-objective**. The **third sub-objective** therefore also includes a review of the extent to which the results and findings of the **second sub-objective** are transferable. In the following the third working hypothesis is:

Hypothesis 3: Rotational impedance around the y_h -axis

The rotational mechanical impedance for excitations around the y_h -axis in the „hand-grip“ position is influenced by the applied gripping force, push force and body posture and the observed effects are comparable to hypothesis 2.

5 Research questions and research design

This chapter describes the research design that was used to achieve the objective of the thesis from Chapter 4. The chapter first provides an overview of how the three hypotheses from the objective have been investigated. For this purpose corresponding research questions are derived from the hypotheses. Based on these research questions the research design of the thesis is outlined, which consists of three studies. In this context the three studies as well as their results and the findings obtained from them have already been pre-published in the form of three journal articles.

In order to investigate the rotational mechanical impedance (RMI) of the HAS for excitations around the x_h -axis and the y_h -axis in the "palm" and "hand-grip" positions, the development of a knob-shaped measuring handle for measuring gripping forces in the "palm" position was first investigated. The description of the applied method and the resulting design of the corresponding knob-shaped measuring handle are the content of Chapter 6 in this thesis. The resulting knob-shaped measuring handle enables the measurement of gripping force during rotational vibration excitation around the x_h -axis in the "palm" position. Based on these measurements, Chapter 7 of the thesis presents a subject study in which the influence of the gripping and push force on the RMI of the HAS was investigated during excitation around the x_h -axis in the "palm" position. The results of this study lead to several conclusions and findings regarding the frictional and positive fit between hand and handle during rotational excitation. Following on from this Chapter 8 addressed two aspects. Firstly it presents an investigation of the RMI for the excitation around the y_h -axis in the "hand-grip" position, and secondly it served as a reference to investigate whether the findings from Chapter 7 are transferable to a different excitation direction and hand position.

5.1 Research Questions

The first hypothesis addresses the difference in the main gripping force direction for a knob-shaped handle compared to a cylindrical handle and the resulting unknown position of the force transducers for gripping force measurement on knob-shaped handles. Following the established cylindrical measuring handle from ISO 10819, the knob-shaped handle must also be divided into two handle halves, between which the force transducers are positioned. The same also applies for knob-shaped handles, but since knob-shaped handles have a generic geometry, the distribution of the individual force components across the handle's surface is unclear. As a result, the orientation of the main gripping force direction as well as the orientation of the

handle separation has to be determined. This orientation refers to the three-dimensional orientation of the main gripping force direction or to the angular alignment of the separation plane of the handle relative to the spatial coordinate axes of the handle. For a better illustration Figure 5.1 shows an example of how the main direction of the gripping force and the angular alignment of the resulting generic separation plane in a knob-shaped handle may look like. Hereby the model of the knob-shaped handle with the corresponding spatial coordinate system is based on the model used in Chapter 6. The coordinate system shown in Figure 5.1, does not correspond to the coordinate system of DIN EN ISO 5349-1. The coordinate system used in Figure 5.1 refers to the coordinate system of the mapped CAD model, which was more practical in the context of the method described in Chapter 6.

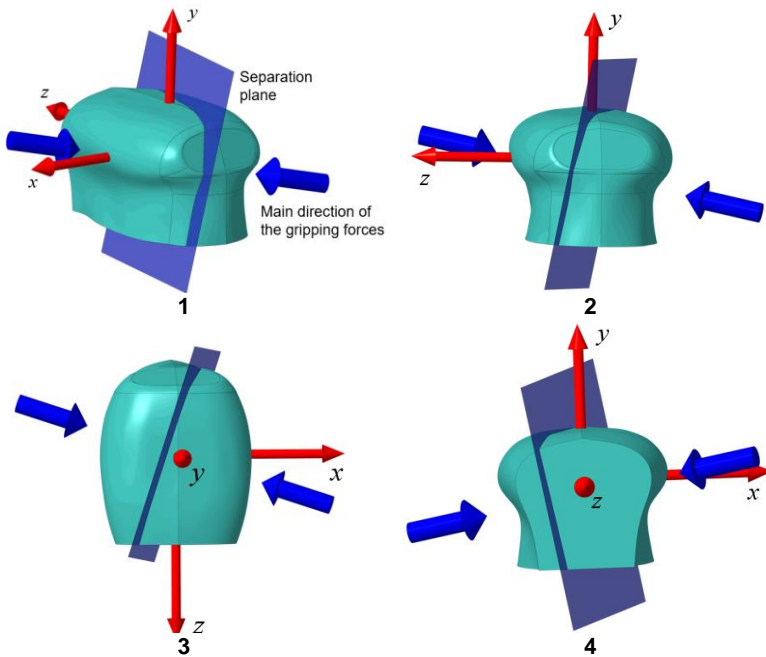


Figure 5.1: Orientation of the main direction of the gripping force (blue) and the corresponding separation plane (transparent blue) within the coordinate system of a generic knob-shape handle. 1: three-dimensional view, 2: Front view, 3: Top view, 4: Rear view

Concerning the orientation of the main direction of the gripping force and the angular alignment of the separation plane, the following research questions can be derived from **Hypothesis 1: Derivation of the measuring handle design**.

- **Sub-research question 1.1:** How can the distribution of the gripping force direction on a knob-shaped handle in the “palm” position be determined with a force sensing foil and projected onto the handle geometry in such a way that the main direction of the gripping force can be determined?
- **Sub-research question 1.2:** What is the angular orientation of the separation plane in which the force transducers are positioned in the x-y plane or the rearview of the knob-shaped handle?
- **Sub-research question 1.3:** What is the angular orientation of the separation plane in which the force transducers are positioned in the x-z plane or the top view of the knob-shaped handle?

The objective of **sub-research question 1.1** is to develop a method on how the distribution of the gripping force on a knob-shaped handle can be measured and projected as force vectors onto the surface of the handle. Based on this projection, the angular orientation of the separation plane in the spatial sphere of the handle should be determined. For this, the edges of the separation plane must be determined in two coordinate planes of the handle in order to span the separation plane three-dimensionally in the spatial sphere of the handle with these edges. The objectives of **sub-research questions 1.2** and **1.3** are therefore to experimentally determine the orientation of the separation plane for gripping force measurement. The determination of the separation plane, in which the force transducers for the gripping force measurement had to be positioned, enabled the development of the knob-shaped measuring handle.

The measuring handle in turn enables the measurement of the RMI in the “palm” position for excitation around the x_h –axis, as well as the determination of the influences of the gripping and the push force. Accordingly, the corresponding research questions to **Hypothesis 2: Rotational impedance around the x_h –axis** are:

- **Sub-research question 2.1:** What is the course of the magnitude and the phase angle of the RMI across the excited frequencies for rotational vibration excitation around the x_h –axis via a knob-shaped handle in the “palm” position?
- **Sub-research question 2.2:** How is the magnitude of the RMI influenced by the applied gripping force?
- **Sub-research question 2.3:** How is the magnitude of the RMI influenced by the applied push force?

The objective of **sub-research question 2.1** is to determine the general course of the RMI of the HAS for excitation around the x_h –axis in the “palm” position across the frequency spectrum from ISO 10068. The objectives of **sub-research questions 2.2** and **2.3** are to determine the influence of the gripping force and the push force on this course, since they are known to influence the translational MI.

As mentioned above, the investigation of the RMI for excitations around the y_h –axis in the “hand-grip” position involves two aspects, the extension of knowledge about the RMI of the HAS and the transferability of the effects inferred in the investigation of the RMI at the knob-shaped handle. These two aspects are also addressed in the corresponding research questions to **Hypothesis 3: Rotational impedance around the y_h –axis:**

- **Sub-research question 3.1:** What is the course of the magnitude and the phase angle of the RMI for rotational vibration excitation around the y_h –axis in the “hand-grip” position and can this course be related to the excitation around the x_h –axis in the “palm” position?
- **Sub-research question 3.2:** How is the magnitude of the RMI influenced by the applied gripping force and can this influence be related to the excitation around the x_h –axis in the “palm” position?
- **Sub-research question 3.3:** How is the magnitude of the RMI influenced by the applied push force and can this influence be related to the excitation around the x_h –axis in the “palm” position?
- **Sub-research question 3.4:** How is the magnitude of the RMI influenced by the body posture?

The objective of **sub-research questions 3.1 to 3.4** is to extend the knowledge on the RMI for excitations around y_h –axis in the “hand-grip” position. However **sub-research questions 3.1 to 3.3** also address the transferability of the assumptions and conclusions drawn from the results of the sub-research questions 2.1 to 2.3. The objective of **sub-research question 3.4** only focus on the extension of the knowledge on the RMI for excitations around y_h –axis, by determining the influence of the body posture on the RMI.

5.2 Research design

This chapter presents the research design that used to investigate hypothesis 1 to 3 and answer their corresponding sub-research questions. In order to classify the hypotheses and connect them to the objective and the research problem presented, Figure 5.2 provides a graphical overview.

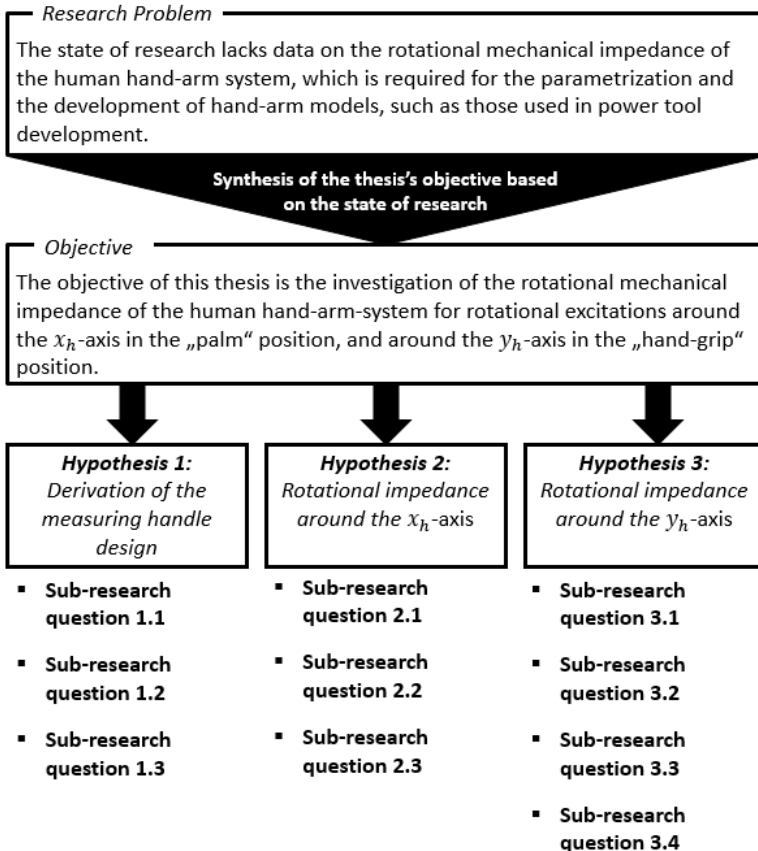


Figure 5.2: Overview of the introduced research problem, the specified objective of the thesis and the derived hypotheses with their corresponding sub-research questions.

As the overview shows the introduced research problem has been transformed into the specific objective of the thesis based on the state of research. To fulfill the objective, it has been divided into three hypotheses, each with corresponding sub-research questions. With the answering of these hypotheses or the sub-research questions, the objective of the thesis can therefore be considered fulfilled.

The procedure for investigating the hypotheses and answering the sub-research questions is shown Figure 5.3 to Figure 5.5. The figures show the hypothesis with the corresponding sub-research questions and present the derived sub-objectives, the research method, and the expected result.

To answer the sub-research questions 1.1 to 1.3 the distribution of the gripping force when gripping the knob-shaped handle was determined on the example of a random orbital sander. The random orbital sander was defined as suitable, since the state of research from Subchapter 3.1.1 shows that these power tools are gripped by a knob-shaped handle and emit rotational vibration. Furthermore, the work of Xu et al. (2011) on the MI refers in particular to the vibrational exposure of the HAS by a random orbital sander and to the lack of a corresponding measuring handle. The sub-results of the sub-research questions include a method of projecting the distribution of the forces measured in the study as force vectors onto the surface of the knob-shaped handle and, based on this, determining the edges of the separation plane in the x-y and x-z planes. The overall result of the study concerning **Hypothesis 1: Derivation of the measuring handle design** is the determination of the three-dimensional angular alignment of the separation plane and thus of the force transducers' position within the spatial sphere of the knob-shaped handle. Figure 5.3 shows an overview of the proceeding to answer the sub-research questions 1.1 to 1.3 of **Hypothesis 1: Derivation of the measuring handle design**.

Hypothesis 1: Derivation of the measuring handle design	
Sub-research question 1.1	
Sub-objective	Determination of the distribution of the gripping force when gripping a knob-shaped handle in the "palm"-position and projecting the distribution onto the geometry of the handle, so that the main direction of the gripping force can be calculated
Method	Measurement of the gripping force distribution across the surface of a knob-shaped handle in a subject study using a random orbital sander. Projecting the individual force components of the gripping force from the study onto the 3D scan of the knob-shaped handle
Sub-result	Projection of the gripping force distribution onto the geometry of the knob-shaped handle as vectors in the spatial coordinate system of a knob-shaped handle, from which the main gripping force direction can be calculated.
Sub-research questions 1.2 and 1.3	
Sub-objective	Determination of the separation plane's angular orientation in the x-y plane (rear view) and the x-z plane (top view) in the coordinate system of the knob-shaped handle.
Method	Calculation of the resulting gripping force, acting on the projection of the separation plane in the x-y plane and the x-z plane and determination of the angular position of the separation plane in which the resulting gripping force is maximum.
Sub-result	Angle at which the separation plane is aligned perpendicular to the main direction of the gripping force in the x-y plane and the x-z plane in the coordinate system of the knob-shaped handle.
Result	Determination of the separation of the knob-shaped measuring handle and the position of the force transducers, through the vectorial calculation of the separation plane based on their angular orientation in the x-y and x-z planes

Figure 5.3: Proceeding and results for the investigation of **Hypothesis 1: Derivation of the measuring handle design**

The investigation of **Hypothesis 2: Rotational impedance around the x_h -axis** and the answer to sub-research questions 2.1.to 2.3 is based on the derivation of the measuring handle design from hypothesis 1.

To answer the sub-research questions 2.1.to 2.3 a subject study was conducted using the derived knob-shaped measurement handle from hypothesis 1 on the shaker test bench described by Matthiesen et al. (2018). The sub-results of the study are the course of the RMI in magnitude and phase angle for rotational excitation around the x_h -axis in the "palm" position as well as the statistical determined influence of the gripping and the push force on the RMI. The overall result are a description of the RMI and the influence of the grip and push force on it, as well as the conclusions that can be drawn regarding the relationship between the hand-handle-contact, the hand position and the RMI of the HAS. Figure 5.4 shows the corresponding overview of the proceeding to answer the sub-research questions 2.1 to 2.3 of **Hypothesis 2: Rotational impedance around the x_h -axis**.

Hypothesis 2: Rotational impedance around the x_h –axis

	Sub-research question 2.1	Sub-research question 2.2	Sub-research question 2.3
Sub-objective	Determination of the course of the RMI of the HAS in magnitude and phase angle for rotational excitation around the x_h –axis in the "palm" position.	Determination of the influence of the gripping force on the RMI.	Determination of the influence of the push force on the RMI
Method	Experimental measurement of the RMI of the HAS in a subject study conducted on a shaker test bench using a knob-shaped measuring handle derived from the proposed design of Hypothesis 1: Derivation of the measuring handle design.		
Sub-result	Plots of the magnitude and the phase angle of the RMI of the HAS at different applied factor combinations of gripping and push force.	Statistical evaluation of the influence of the gripping force on the RMI.	Statistical evaluation of the influence of the push force on the RMI.
Result	Description of the RMI of the HAS and the influence of the gripping and push force acting on it when excited around the x_h –axis in the "palm" position, from which conclusions can be drawn about the relationship between the handle contact and the RMI of the HAS.		

Figure 5.4: Proceeding and results for the investigation of **Hypothesis 2: Rotational impedance around the x_h –axis**

To answer research questions 3.1 to 3.4, a study similar to the one used to investigate **Hypothesis 2: Rotational impedance around the x_h –axis** was conducted. The study primarily aimed for the extension of the knowledge of the RMI for excitation around the y_h –axis. However, the study also serves as a reference to compare the results of **Hypothesis 2: Rotational impedance around the x_h –axis** and thus investigate the transferability of the findings of this hypothesis. These findings are mainly related to the relationship between the hand-handle contact and the orientation of the rotational excitation axis to the hand position, and how these aspects may affect the RMI and the transmission of rotational vibrations. The sub-results of the study are the course of the RMI in magnitude and phase angle for rotational excitation around the y_h –axis in the "hand-grip" position as well as the statistical determined influence of the gripping and the push force and the body posture on the RMI. These result regarding the course of the RMI and the influence of the gripping and the push force are compared to the corresponding results of the second hypothesis regarding the transferability of the obtained findings. Figure 5.5 shows the corresponding overview of the proceeding to answer the sub-research questions 3.1 to 3.4 of the third hypothesis.

Hypothesis 3: Rotational impedance around the y_h –axis

	Sub-research question 3.1	Sub-research question 3.2	Sub-research question 3.3	Sub-research question 3.4
Sub-objective	Determination of the course of the RMI of the HAS in magnitude and phase angle for rotational excitation y_h –axis in the "hand-grip" position.	Determination of the influence of the gripping force on the RMI.	Determination of the influence of the push force on the RMI	Determination of the influence of the body posture on the RMI
Method	Experimental measurement of the RMI of the HAS in a subject study conducted on a shaker test bench with a cylindrical measuring handle derived from the design proposed in ISO 10819.			
Sub-result	Plots of the magnitude and the phase angle of the RMI of the HAS at different applied factor combinations of gripping and push force.	Statistical evaluation of the influence of the gripping force on the RMI and comparison to the findings of hypothesis 2.	Statistical evaluation of the influence of the push force on the RMI and comparison to the findings of hypothesis 2.	Statistical evaluation of the influence of the body posture on the RMI and comparison to the findings of hypothesis 2.
Result	Description of the RMI of the HAS and the influence of gripping force, pressure force, and body posture acting on it for excitation around the y_h –axis in the "hand-grip" position and comparison to the findings from Hypothesis 2: Rotational impedance around the x_h –axis for another axis, leading to a transferable explanation of the influence of the excitation axis, hand position, and hand-handle contact on the RMI.			

Figure 5.5: Proceeding and results for the investigation of **Hypothesis 3: Rotational impedance around the y_h –axis**

6 Study on Hypothesis 1: Derivation of the measuring handle design

6.1 Thesis specific introduction

The following chapter deals with **Hypothesis 1: Derivation of the measuring handle design** and its corresponding sub research questions. By answering the sub research questions, the hypothesis can be regarded as investigated. The hypothesis and the corresponding research questions from Subchapter 5.1 are:

Hypothesis 1: Derivation of the measuring handle design

From the distribution of gripping forces on a knob-shaped power tool handle, a measuring handle for excitations in the "palm" position can be derived, which is suitable for measuring gripping forces.

- **Sub-research question 1.1:** How can the distribution of the gripping force direction on a knob-shaped handle in the "palm" position be determined with a force sensing foil and projected onto the handle geometry in such a way that the main direction of the gripping force can be determined?
- **Sub-research question 1.2:** What is the angular orientation of the separation plane in which the force transducers are positioned in the x-y plane or the rearview of the knob-shaped handle?
- **Sub-research question 1.3:** What is the angular orientation of the separation plane in which the force transducers are positioned in the x-z plane or the top view of the knob-shaped handle?

According to the structure of the thesis described in Subchapter 1.2 and the research design from Subchapter 5.2 research questions from Subchapter 5.1 are answered by a subject study in the following Chapter 6. The presented study was pre-published in the *Journal of Applied Ergonomics* entitled *Use of data-driven design for the development of knob-shaped handles in the context of impedance measurements* (Schröder et al., 2022) and are cited in full below from that journal article.

In this context the following chapter presents a new approach on the development of a knob-shaped measuring handle for RMI measurement. This development addresses the angular orientation of the separation plane in which the force transducers of the knob-shaped measuring handle must be positioned. The force transducers must be aligned so that they are orthogonal to the main direction of the gripping force, as shown in Figure 5.1 on page 58 shows. This requires the distribution of the

gripping force over the surface of a knob-shaped handle. For this purpose the gripping force distribution on the knob-shaped handle of a random orbital was measured in a subject study using a force sensing foil. To determine the angular orientation of the separation plane, a new data-driven method was used to project the measured gripping force distribution onto a 3D scan of the random orbital sander handle. Thus, in the context of the thesis, this first chapter can be regarded virtually as the methods chapter.

The following subchapters: 6.2 *Methods*, 6.3 *Results*, 6.4 *Discussion*, 6.6 *Limitations*, 6.7 *Conclusion* and 6.8 *Acknowledgment* are full citations from the publication *Use of data-driven design for the development of knob-shaped handles in the context of impedance measurements* (Schröder et al., 2022). For this purpose, the numbering of the chapters, figures and tables were adapted to the numbering of the thesis. In addition the term “pressing” or “pressing force” is used in the publication to refer to the push force described in Subchapter 2.4 according to ISO 15230. As mentioned in footnote 2 within this thesis the term “pressing force” is considered equivalent to the push force described in ISO 15230.

6.2 Methods

“A study for three-dimensional determination of the separation plane was already published in Schröder et al., 2020 through a two-dimensional perspective. This manuscript aims to analyze the results from a three-dimensional perspective. This section describes the test setup, the test subjects, and the test procedure. The data of the study is analyzed more in depth, as the method of evaluation is extended from a 2D to a 3D approach. The study considers 30 subjects, whose grip forces were measured in the gripping of an orbital sander through use of a force measuring foil. The measured forces were evaluated in the main direction of the resulting grip force. Since the components of the grip force cancel each other out in the center of the palm (DIN Deutsches Institut für Normung e. V., 2013), the main direction of the grip force includes two force vectors directed against each other. In the data analysis, the angular orientation of these vectors was determined in regard to the x-y and x-z planes. This analysis leads to a median angle of the separation plane for splitting²⁰ of the measuring handle over all 30 subjects.

²⁰ The terms “splitting of the measuring handle” and “division of the measuring handle” are used synonymously within this thesis.

6.2.1 Test Subjects

The study was conducted with 30 healthy subjects (27 male and 3 female) aged 18 to 40 years. To record the subjects' age, bodyweight, and body size, we used a clustering which split the age, bodyweight, and body size into five different range clusters. This clustering was done in respect of a higher anonymization of the subjects' data, since the subjects only had to sort themselves into a range cluster instead of revealing their specific age, bodyweight, and body size. The number of subjects in each cluster is given in Table 6.1.

All subjects were right-handed and said that they were using power tools regularly (1 daily, 7 weekly, 18 monthly, 4 yearly). The data on the subjects' regular use of power tools is limited in its explanatory power since we only asked the subjects' experience in using power tools in general. The test setup used contained two static tasks with a switched-off sander and a grinding task in which only one pattern had to be followed. The use of power tools was only generally queried among the subjects. We considered that under these testing conditions, the subjects' experience in using power tools had little influence on the forces applied. No further questions were therefore asked regarding the use of specific power tools. For each subject, a set of anthropometric properties as given in DIN EN ISO 7250-1 and depicted in Figure 6.1 were recorded (DIN - Deutsches Institut für Normung, 2017). Table 6.2 lists the values for the anthropometric properties for all subjects. The anthropometric characteristics of the test subjects are within the range of standard values for German subjects given in DIN; CEN; ISO 7250-2 (DIN - Deutsches Institut für Normung, 2013). All recorded data were anonymized. The subjects were informed about their rights as well as the form of data acquisition.

Table 6.1: Clustering of age, bodyweight, and body height.

Age [years]	Number of subjects	Body height [cm]	Number of subjects	Bodyweight [kg]	Number of subjects
14-18	0	<160	1	<55	0
18-25	14	160-170	1	55-70	9
25-40	16	170-180	15	70-85	14
40-60	0	180-190	8	85-100	6
60-80	0	>190	5	>100	1
Sum	30	Sum	30	Sum	30

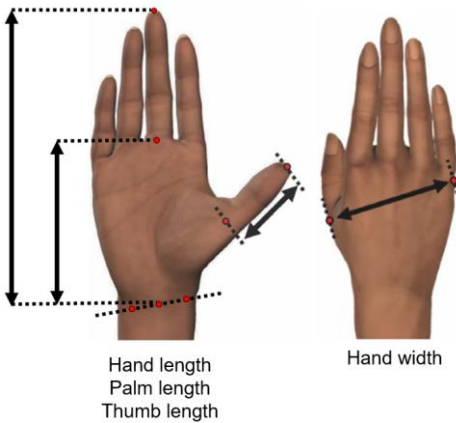


Figure 6.1: Anthropometric characteristic of the human hand according to DIN EN ISO 7250-1. The illustration of the hand is based on DIN EN ISO 7250-1 (DIN - Deutsches Institut für Normung, 2017).

Table 6.2: Physical characteristics of the subjects, M. Sc Tassilo Schröder

Characteristic	Lower [mm]	quantile Median [mm]	Upper quantile [mm]	Standard deviation [mm]
Hand Width	100	102.5	109.25	6.2
Hand Length	181	190	191.2	9.9
Palm Length	103	106.5	110	6.7
Thumb Length	60	65	67	6.9

6.2.2 Test Setup

For determination of the grip forces on power tools, previous studies by Kalra et al. (Kalra et al., 2015a) and Welcome et al. (D. Welcome et al., 2004) investigated the suitability of force measuring foils which can be applied to the power tool handles. The study conducted by Kalra et al. showed that resistive force measuring foils lack reproducibility. On the other hand, the study conducted by Welcome et al. who used capacitive sensor foils showed low scattering. Further studies conducted by Kaulbars (U. Kaulbars, 2006) and Kaulbars and Lemerle P. (Kaulbars & Lemerle, 2007) showed the use of capacitive force sensing foils for determination of grip forces on grinders, tampers, and demolition hammers. Furthermore, Matthiesen et al. used a force measuring foil for measurement of grip force at an orbital sander in 2017 (Matthiesen & Uhl, 2017a).

For the present study on the determination of grip forces on knob-shaped, battery-powered orbital sanders, DBO180U (Makita Corporation, Anjo, Aichi, Japan) was used. The technical data of the sander can be found in (Makita Werkzeug GmbH, 2021) The device and a 3D model of its handle geometry together with the defined coordinate directions is given in Figure 6.2. The left side of Figure 6.2 shows the device used in the study. The device's handle is surrounded by the projection planes of the initial coordinate system, the planes highlighted in red are the x - y and x - z planes that were considered for the determination of the grip forces. The right side of Figure 6.2 shows a 3D model with the corresponding dimensions of the sander handle. The 3D model shown was obtained by scanning the handle geometry with a 3D scanner²¹.

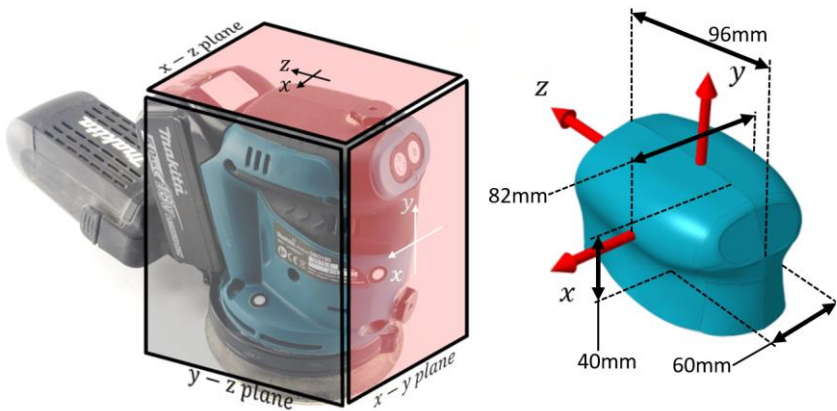


Figure 6.2: The left side shows the random orbital sander, which was used in the study, surrounded by the projection planes according to the initial coordinate system of the sander. The planes used for the determination of the grip force are highlighted in red. The right side shows the corresponding coordinate directions defined for the used orbital sander and the dimensions of the sander handle. The 3D model of the sander handle was created using the HandySCAN-3D provided by Creaform GmbH, Egenhausen, Germany.

²¹ HandySCAN-3D, Creaform GmbH, Egenhausen, Germany

For the manual experiment, the device was equipped with a capacitive force measuring foil on the main gripping surface (pliance-xf-32 with 16x10 element foil, novel GmbH, Munich, Germany). The foil consists of individual pressure elements in a grid arrangement. The elements can measure the mechanical pressure acting on it. The sensor foil was carefully oriented in order to achieve full surface coverage for all subjects. No adjustments were made during the study so that the foil element location and orientation remained consistent for all subjects. The test setup is depicted in Figure 6.3. The subjects were standing upright and were working on a level plywood board. The workpiece was raised at a height of 800 mm for all subjects. The subjects were provided with an instructional display guiding them through the individual steps of the study. The data for the force measuring foils was acquired by the control unit of the force measuring foil itself at a rate of 60 Hz.

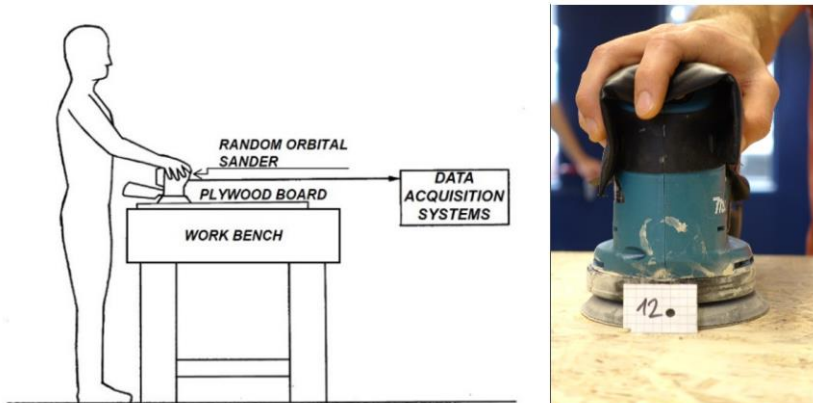


Figure 6.3: Schematic drawing of the test setup und photo of the random orbital sander with the applied force measuring foil gripped by subject 12 (Schröder et al., 2020).

6.2.3 Test Procedure

At the beginning of the experiment, the subjects were introduced to the general test procedure and aim of the study. Then, the anthropometric properties were recorded. Next, the subjects were allowed to familiarize themselves with the test setup. The subjects were allowed to freely work on the plywood board for two minutes with an unmodified sander in order to get a sensation of the gripping and pushing forces required for operation. In the subsequent step, the participants were handed the orbital sander with the force sensing foil. As part of the study, the subjects had to

perform three different tasks with the random orbital sander. The first task involved holding the sander statically with outstretched arm for 10 seconds. In the second task, the subjects gripped the switched-off device while pressing on the plywood plate for 20 seconds. In this pressing task, only the first trial was recorded to assess the intuitive, unaffected gripping manner of the subject. In the third task, the sander equipped with the sensor foil was switched on and the subject ground the plywood plate according to a specified pattern based on DIN EN ISO 28927-3 and corresponding to a horizontal figure of eight with a circular diameter of 100 mm (DIN Deutsches Institut für Normung e. V., 2010a). According to DIN EN ISO 28927-3, this pattern had to be ground within 4 seconds. For this purpose, the direction and the moving speed of the grinder were specified via a graphic interface on a screen. In total, the subject had to grind the pattern four times in a row without pausing. Thus, we achieved a total measurement time of 16 seconds, which corresponds to DIN EN ISO 28927-3 (DIN Deutsches Institut für Normung e. V., 2010a). Figure 6.4 shows a picture of the graphical interface with the pattern the subject had to follow. Due to a defect in the random orbital sander, the number of subjects in the sanding task was only 26. The defective sander was replaced with a new one of the same model and manufacturer. In all three tasks of holding, pressing, and grinding, no force feedback was provided to achieve unaffected gripping behavior.

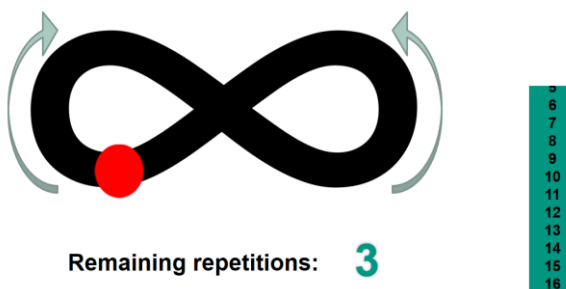


Figure 6.4: Graphical surface of the pattern to be ground by the subject. The red dot shows the predefined position of the sander on the pattern. The green bar shows the remaining time of measurement.

6.2.5 Analysis of the Grip Force and Influence of the Pressing Force

a) General description of the method used

To determine the grip forces, we used the 3D model of the grip obtained by 3D scanning of the grip geometry. The force values given by the sensor foil must be allocated and oriented to the 3D geometry of the handle. This is done by manually probing all sensor elements on the physical device and matching the location on the 3D scan. The spatial sensor element orientation is determined numerically from the scan geometry with the element direction being perpendicular to the handle surface. As a result of the above-mentioned step, each sensor element is assigned to a set of spatial coordinates and a normal vector in the 3D scan. An overview of the procedure is given in Figure 6.5.

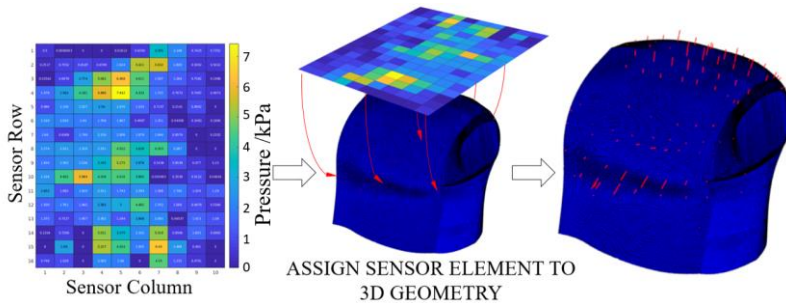


Figure 6.5: Schematic presentation of the projection of the force measurement foil values onto the 3D model of the orbital sander handle. The left side of Figure 6.5 shows the graphical representation of the sensor matrix of the force measurement foil. While each rectangle represents a sensor element, the colors characterize the pressure applied to the respective sensor element from blue (low pressure) to yellow (high pressure) (Schröder et al., 2020).

The procedure for finding a separation plane is based on (Schröder et al., 2020). To find the optimal handle separation, two separate but analogous analyses were performed for each task of the study. In order to find a three-dimensional representation of the handle separation, the problem is reduced to two-dimensional analyses. To do so, the 3D geometry and the force vectors from the sensor foil are projected onto the x-y and x-z planes, which represent the front and the top views of the handle. It should be mentioned that for projection in the x-z plane, the entire depth along the y-axis of the handle is taken into account. This means that the sensors of the force measurement foil, which are positioned on the curved surface below the top of the handle, are also projected in the x-z plane.

The angular position of the separation plane in the z-y plane is negligible, since the projections in the x-y and x-z planes cover any direction in which the vectors of the force sensors could potentially be oriented.

b) Detailed description of the mathematical model used for the determination of the handle separation

The determination of the angular position of the separation plane described below was performed in the same way for all three tasks.

The angular position of the separation plane in the x-y and x-z planes was determined separately here, but the same data evaluation method was used in both cases.

In a first step, the geometric center of all points to which the sensor elements are assigned is calculated. As depicted in Figure 6.6, the reference coordinate systems $x - y$ and $x - z$ are placed in the geometric center 0. In these initial reference frames, the edge of the separation plane is defined with an angle α relative to the vertical axis. The edge of the separation plane is described by a rotating reference frame with a normal (n') and lateral direction (l').

For a given angle α , the sensor elements f_i are separated into two groups at the edge given by the angle α . Elements with a relative angle ϑ_i in the range $\alpha \leq \vartheta_i \leq \alpha + \pi$ are combined in the *A group*, while elements outside of this range are assigned to the *B group*. The normal vectors n_i of each sensor element f_i , are normally expressed in the global coordinate system. For the given angle α , these normal vectors n_i , are transformed to the reference frame ($n' - l'$).

$$\begin{aligned} \vec{n}_{i,(n'-l')} &= \begin{pmatrix} \sin \alpha & -\cos \alpha \\ \cos \alpha & \sin \alpha \end{pmatrix} * \vec{n}_{i,(x-y)} \\ \vec{n}_{i,(n'-l')} &= \begin{pmatrix} \sin \alpha & -\cos \alpha \\ \cos \alpha & \sin \alpha \end{pmatrix} * \vec{n}_{i,(x-z)} \end{aligned} \tag{6.1}$$

For each angle α for $\alpha \in [0, \pi]$ in $\Delta\alpha = \pi/180$, increments of the normal vectors are transformed to the rotated reference frame.

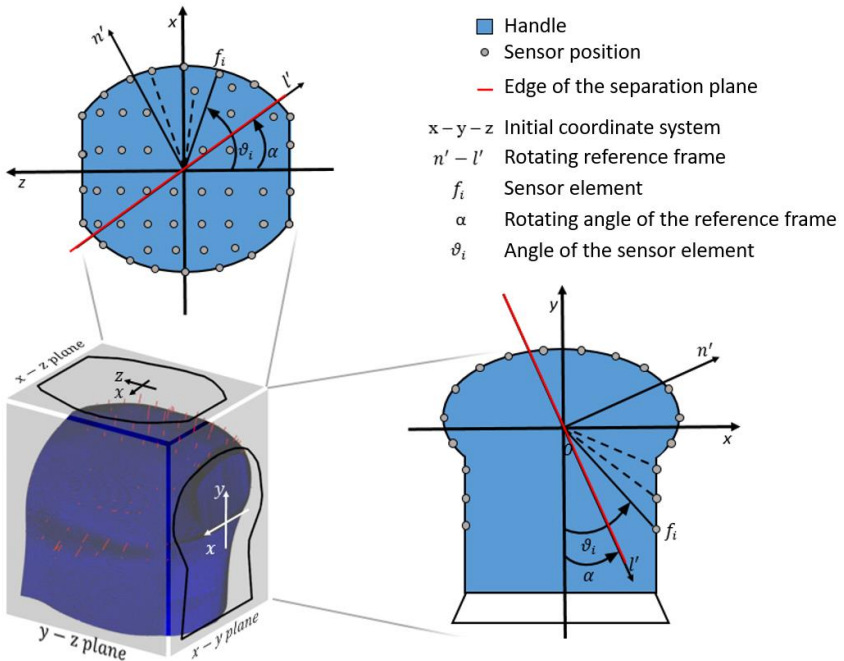


Figure 6.6: Rotation of the reference frame $n' - l'$ by the angle $\alpha \in [0, \pi]$ in the x - y - and the x - z -planes of the initial coordinate system of the sander handle. The angle between the vertical y - or z -axis and the angular position of the specific sensor element f_i of the force measurement foil is given by ϑ_i .

After transformation of the normal vectors for each angle $\alpha \in [0, \pi]$, the rotated normal vectors are fitted with the force measurement foil sensor data for each subject. This results in a course of the normal forces over the test duration projected onto the separation plane for each α .

To find the optimum separation angle α_{res} within the specific projection of the separation plane, all force vector components normal to the plane are added by

$$F_{res}(t, \alpha) = \sum_i f_i(t) \vec{n}_{i,(n'-l')}(\alpha) \cdot \vec{e}_{n'}(\alpha) \quad 6.2$$

This step is done for the *A* and *B groups* separately. This results in a time course of the resulting force normal to the separation plane. The vector $\vec{e}_{n'}(\alpha)$ denotes the unit vector normal to the separation plane and (\cdot) denotes the scalar product. The scalar product with $\vec{e}_{n'}(\alpha)$ ensures that only the part of $\vec{n}_{i,(n'-l')}(\alpha)$ which acts parallel to n' and normal to the separation plane is taken into account

To find the optimal angular orientation of the separation plane, it is assumed that the time integral

$$I(\alpha) = \int F_{res}(t, \alpha) dt \quad 6.3$$

is at its maximum at α_{opt} . Using Equations 6.2 and 6.3, the specific angle α_{opt} at which $I(\alpha)$ reaches its maximum is calculated for the *A* and *B groups* for each subject. The angle $\alpha_{opt A}$ is the angular orientation at which $I(\alpha)$ from the *A group* reaches its maximum on the separation plane. The angle $\alpha_{opt B}$ refers to the *B group* in the same way. The two angles $\alpha_{opt A}$ and $\alpha_{opt B}$ may deviate slightly from each other.

Referring to Equation 6.2, $I(\alpha)$ depends on two factors. The first factor is the measured value of each sensor element $f_i(t)$. The second factor is the amount of sensor elements belonging to the *A* or the *B group* for a specific rotation angle of the separation plane. The edge of the separation plane rotates in discrete steps with $\Delta\alpha = \pi/180$. Thus, belonging of a particular sensor element to the *A* or the *B group* may change within one increment step of $\Delta\alpha = \pi/180$. Therefore, the amount of sensor elements and hence $I(\alpha)$ of the *A* and $I(\alpha)$ of the *B group* varies for each α . This variation causes the deviation between $\alpha_{opt A}$ and $\alpha_{opt B}$. For these specific angles $\alpha_{opt A}$ and $\alpha_{opt B}$, the amount of sensor elements in the *A* and the *B groups* is slightly larger.

As the components of the grip force cancel each other out in the center of the palm, the value of $I(\alpha)$ from the *A* and *B groups* must be the same for a specific rotational angle α_{sep} of the separation plane's edge. Since the angle α_{sep} should also be the angle at which the maximum normal forces act on the separation plane, it has to be in the range of $\alpha_{opt A}$ and $\alpha_{opt B}$. Therefore, we calculated α_{sep} by the arithmetic mean of $\alpha_{opt A}$ and $\alpha_{opt B}$ for each subject. The result of this procedure is the edge of the separation plane in the x-y respectively x-z plane at the subject-specific angle $\alpha_{sep xy}$ respectively $\alpha_{sep xz}$. Figure 6.7 shows the splitting of the sensor foil's sensors

into the *A* and the *B* group for their projection in the x-y and the x-z planes. In addition, the figure shows the resulting angles $\alpha_{opt A}$ and $\alpha_{opt B}$ for the separation planes of both groups, where α_{sep} is located in between for both projections.

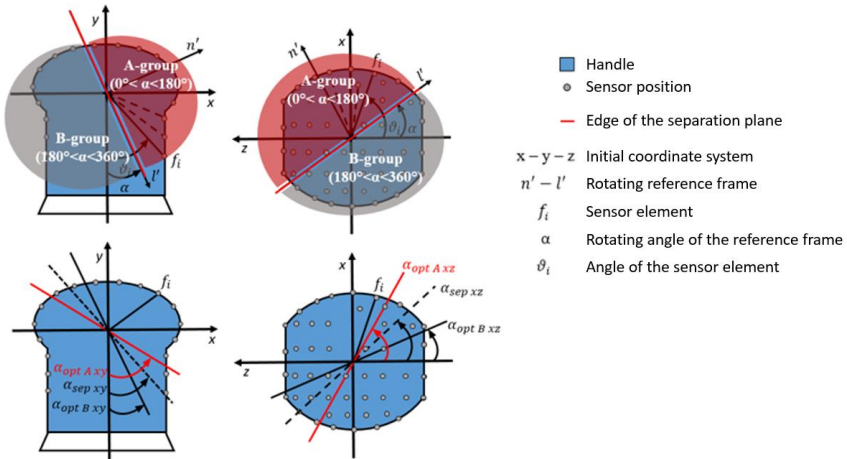


Figure 6.7: Splitting of the sensors set into the *A* and *B* group (red and gray) exemplified for one subject with the resulting separation planes of each group oriented by $\alpha_{opt A}$ and $\alpha_{opt B}$ the intervening separation plane of α_{sep} for both projections.

We subsequently calculated $\alpha_{res xy}$ and $\alpha_{res xz}$ as the median of $\alpha_{sep xy}$ and $\alpha_{sep xz}$ over all 30 subjects. Since this method was applied in the same way for all three tasks performed in the study, we obtained the angular orientation of the separation plane in the x-y and x-z projections. In the following, we calculated the arithmetic mean over the task-specific angles of $\alpha_{res xy}$ and $\alpha_{res xz}$ to obtain the angular orientation α_{xy} and α_{xz} of the resulting separation plane edges in each projection.

The resulting two edges of the separation plane can be understood as two vectors spanning a separation plane which is defined by Equation 6.4:

$$x = y * \sin(\alpha_{xy}) + z * \sin(\alpha_{xz}) \quad 6.4$$

c) *Evaluation of the influencing factors in the determination of the separation plane*

In this chapter, we compared the resulting grip force of a separation plane oriented only by the angles $\alpha_{res\ xy}$ and $\alpha_{res\ xz}$ to a vertically oriented separation plane. This comparison was done to determine how the angular offset of the separation plane affects the resulting grip force. For this purpose, we calculated the resulting force vectors of the *A* and *B groups* for the separation plane oriented by α_{xy} and α_{xz} over all subjects for each task separately. For comparison, we calculated the resulting force vectors in the same way for the *A* and *B groups* in the case of a vertically oriented separation plane. Subsequently, the percentage deviation between the resulting forces from the *A* and *B* groups was calculated separately for the x-y and x-z projections using Equation 6.5.

$$D_{res\ xy/xz-A/B} = 100 * \left| \left(1 - \frac{F_{res\ xy/xz-A/B}}{F_{res\ xy/xz-A/B}(\alpha_{xy/xz})} \right) \right| \quad 6.5$$

In Equation 6.5, $F_{res\ xy/xz-A/B}(\alpha_{xy/xz})$ stands for the resultant grip forces acting normal to the determined separation plane. $F_{res\ xy/xz-A/B}(\alpha_{xy/xz})$ was calculated separately for the *A* and the *B groups* and for the projections in the x-y and x-z planes. Consequently, $F_{res\ xy/xz-A/B}$ stands for the corresponding resultant grip forces acting normal to a vertical separation plane and was calculated in the same manner. The specific percentage deviation between the resulting forces is also divided by group and projection plane and is indicated by $D_{res\ xy/xz-A/B}$.

In addition to the deviation to a vertical plane, the influence of the pressing force on the angular alignment of the determined separation plane was also analyzed. In the pressing and grinding tasks, the gripping force distribution and thus the angular alignment of the separation plane can possibly be influenced by the pressing force exerted by the subject. Hence, we calculated the pressing force by summing all y-components of all vectors in both tasks. Since the upward and downward vectors of the grip force cancel each other out in this case, the result of this sum corresponds to the pressing force $F_{p\ res}$. This calculation was performed for each subject for the pressing and grinding tasks. The pressing force $F_{p\ res}$ was matched with the respective task specific angles $\alpha_{sep\ xy}$ of the separation plane individually for each task and subject. The pressing force $F_{p\ res}$ acts in negative y-direction, thus it can only influence the orientation of the separation plane in the x-y plane. The orientation in the x-z plane seen from above is not influenced, since the vector of the pressing force is directed into the viewing plane and cannot act on the projection of the separation plane.

Based on this subject-wise matching of $\alpha_{sep\ xy}$ and $F_{p\ res}$, we made a Spearman correlation analysis with the software SPSS. The Spearman correlation was used since the number of subjects performing the grinding task was less than 30 and we could not prove normal distributions for either the values of $F_{p\ res}$ or the values of $\alpha_{sep\ xy}$ using the Shapiro-Wilk test.

6.3 Results

6.3.1 Determination of the Separation Plane

The first part of the results chapter showcases the angular orientation of the separation plane's edge in the x-y-plane and x-z plane for the different tasks. Following from this, the three-dimensional orientation of the separation will be shown at the end of the results chapter. Table 4.3 shows the task-related distribution of $\alpha_{sep\ xy}$ over all subjects. Hereby Table 4.3 lists the minimum, maximum and median angel $\alpha_{res\ xy}$ as well as the percentiles.

Table 6.3: Minimum, maximum, and the 5th and 95th percentile of the subject-specific separation planes' orientations in the x-y plane over all three tasks performed in the study.

	Holding [°]	Pressing [°]	Grinding [°]
Minimum	-15	-17.5	-14
Maximum	2	4.5	2
Median ($\alpha_{res\ xy}$)	-7	-0.25	-2.5
5 th percentile	-13	-15.5	-13.62
95 th percentile	1.5	4	1.25

Regarding the minimum and maximum values and the percentiles of Table 4.3, it can be seen that the separation planes' edges are oriented in the same range over all tasks performed. The values of Table 4.3 show that the angles of the separation planes in the x-y plane are slightly shifted into the negative range, as the absolute value of the minimum is larger than the absolute value of the maximum, which is consistent with the values of the 95th and 5th percentiles. Figure 6.8 shows, a projection in the x-y plane of the task-specific separation plane edges, which are specifically oriented through their resulting median angel $\alpha_{res\ xy}$.

The edges are represented as lines in the x-y projection of the sensor positions of the force measurement foil with the geometric center 0' being the center of rotation. Through the orientation of the position vectors of sensors from the force measuring foil shown in blue, the shape of the orbital sander handle in the x-y plane is apparent. Therefore, it can be concluded that the foil was correctly positioned on the orbital sander handle

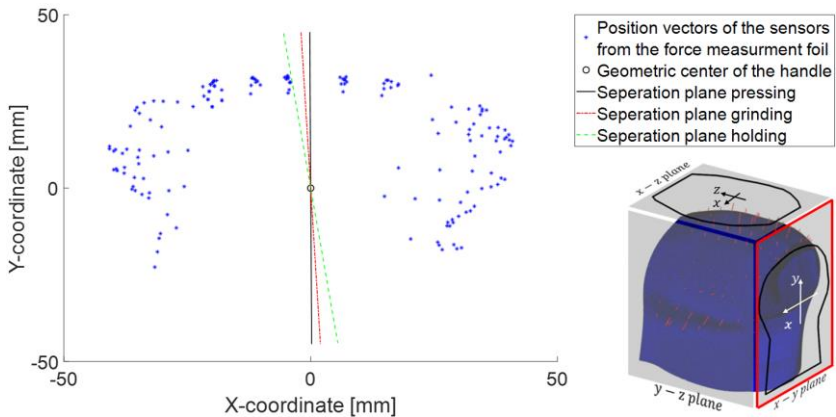


Figure 6.8: Resulting angular orientation $\alpha_{res\ xy}$ of the separation plane's edge in the x-y plane for all three tasks performed.

The edges of the resulting separation planes shown in Figure 6.8 are nearly vertical, as the values of the median respectively $\alpha_{res\ xy}$ from Table 4.3 are close to zero. In particular, the planes' edges of the grinding and pressing tasks are very close to the vertical with a value of $\alpha_{res\ xy} = -0.25^\circ$, the edge resulting from the pressing task is almost vertical. The plane's edge from the holding task has an angle of $\alpha_{res\ xy} = -7^\circ$, which deviates from the two other angles. This is also visible in Figure 6.8, since the gap between the line of the holding task and the two others is larger than their gap to each other. Following Figure 6.8, Table 6.4 shows the task-related distribution of $\alpha_{sep\ xz}$ over all subjects. As for the resulting angles of $\alpha_{sep\ xy}$ in the x-y plane, the minimum, maximum, and median values and the 5th and 95th percentiles are given

Table 6.4: Minimum, maximum, and the 5th and 95th percentile of the subject-specific separation planes' orientations in the x-z plane over all three tasks performed in the study.

	Holding [°]	Pressing [°]	Grinding [°]
Minimum	-22	-14	-30.5
Maximum	7	9	4
Median ($\alpha_{res\ xy}$)	-6	-5.75	-4.75
5 th percentile	-15	-14	-13.5
95 th percentile	6.5	0.5	0.5

According to Table 6.4, the separation plane edges in the x-z plane tend to be vertically oriented with a slight shift to the negative. For the percentiles of Table 6.4, a slight shift of $\alpha_{sep\ xz}$ into the negative range as in the case of $\alpha_{sep\ xy}$ can be seen. This is visible by the absolute values of the 5th percentiles of all tasks being larger than the corresponding absolute values of the 95th percentiles. In this context it can be assumed that the maximum value of 9° the pressing task in Table 6.4, refers to the outlier, since it is much bigger than the 95th percentile. Consequently the median angles of the respective tasks in Table 6.4 also deviate slightly from the vertical into the negative and are very close to each other. In the following, Figure 6.9 presents the separation planes' edges of each task oriented by the median angle $\alpha_{res\ xz}$. which represents the angular orientation of the separation plane in the top view of the handle. Since the whole top side of the handle is covered with the measurement foil, the sensor positions are distributed all over the plot as shown in Figure 6.9. From the shape of this blue dotted cloud, it is possible to guess the shape of the handle of the random orbital sander viewed from above. Therefore, it can be assumed that positioning of the force measurement foil and the calculation of the sensor positions on the handle were correct.

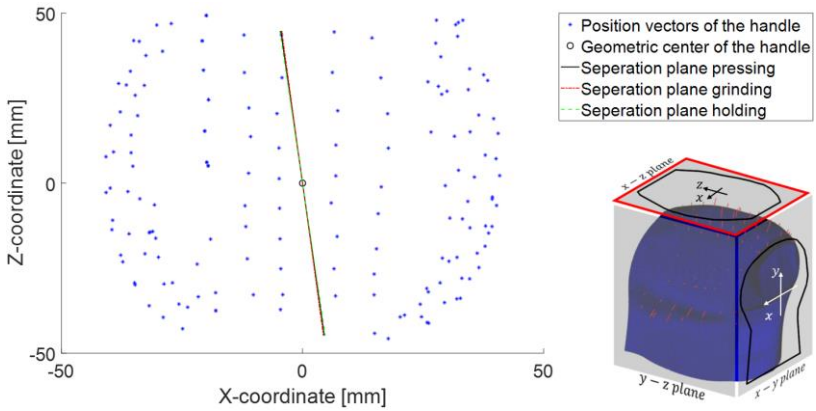


Figure 6.9: Resulting angular orientation $\alpha_{res\ xz}$ of the separation plane's edge in the x-z plane for all three tasks performed.

As expected from the values of the median angles $\alpha_{res\ xz}$ in Table 6.4, the task-specific separation plane edges in Figure 6.9 lie nearly on top of each other with a slight angular offset of minus five degrees from the vertical. With the angular orientations of the separation planes' edges in the x-y and x-z planes from Figure 6.8 and Figure 6.9, a three-dimensional representation of each separation plane can be calculated by using Equation 6.4. Based on these three task specific separation planes the total separation plane over all three tasks performed was determined. Therefore the arithmetic mean angle of $\alpha_{res\ xy}$ and $\alpha_{res\ xz}$ over all tasks was calculated. The angular orientation of this total separation plane is given by $\alpha_{mean\ xy} = -3.25^\circ$ and $\alpha_{mean\ xz} = -5.5^\circ$. A three-dimensional representation of the task specific separation planes passing through the sander's handle as well as a three-dimensional representation of the calculated total separation plane can be found in the appendix of the manuscript²².

²² The appendix of the corresponding manuscript can be found in the appendix of this thesis

6.3.2 Influence of the Pressing Force and Deviation to the Vertical

The second part of the results chapter shows the percentage deviation of the grip force with respect to the calculated separation plane compared to a fully vertical separation plane. In addition, the influence of the pressing force on the angular orientation of the separation plane will be presented.

The separation planes' orientations in the x-y and x-z planes are approximately vertically across all tasks. Therefore, it has to be evaluated whether a vertically oriented separation plane respectively a vertical splitting of the measurement handle is sufficient. Under the conditions of an easy-to-manufacture design, a vertically oriented splitting of the measurement handle would be less expensive and easier to manufacture. Thus, Table 6.5 shows the maximum, the minimum, and the median value of the deviations $D_{res\ xy-A/B}$ and $D_{res\ xz-A/B}$ between the resulting grip force for the task-specific determined separation plane and a vertically oriented separation plane. These characteristic values of $D_{res\ xy-A/B}$ and $D_{res\ xz-A/B}$ are divided into those of the x-y and x-z projections to allow separate evaluation. Furthermore, the values are divided into the *A* and *B groups*. This is due to the fact, that the components of the grip force cancel each other out in the center of the palm. Therefore, the resulting grip force of each subject for each task and the percentage deviation were calculated separately for both groups. The percentage deviation between the resulting grip force acting on the determined separation planes and the one acting on a vertical separation plane is overall below 10%. Furthermore, this deviation is smaller in the x-y plane than in the x-z plane across all tasks. Regarding the different tasks, it can be seen that the resulting grip force from the pressing task has the smallest percentage deviation compared to the resulting grip force that would act on a vertical separation plane. This trend is visible for the values of both groups and for both projections, except for the minimum value of the *B group* which is the largest in both projections compared to that of the other tasks. Defining the range of the percentage deviation as the range between the minimum and the maximum value, Table 6.5 shows that this range is the largest for the holding task and the smallest for the pressing task. This observation can be made across all tasks and projections except of the *B group* in the x-z plane where the range of the grinding task is slightly larger.

To determine the influence of the pressing force $F_{p\ res}$ on the separation planes' angular orientation $\alpha_{res\ xy}$ in the x-y plane, a Spearman correlation analyses was carried out. The results of this analysis indicate a significant correlation of $p=0.03$ between the pressing force and the angular orientation of the separation plane of the pressing task (The correlation is significant at the 0.05 level (two-sided)). In the case of the grinding task, no significant correlation between the pressing force and the angular orientation of the separation plane could be detected. Regarding the effect size of $F_{p\ res}$ on $\alpha_{res\ xy}$ for the pressing task, a value of $r=0.4$ indicates a medium effect.

Table 6.5: The minimum, maximum, and mean values of the percentage deviations between the resulting grip force acting on the separation plane oriented by α_{sep} and the one acting on the vertically oriented separation plane. The deviation is calculated separately for the corresponding planes $\alpha_{sep\ xy}$ and $\alpha_{sep\ xz}$ in the x-y and x-z planes.

			Holding task [%]	Pressing task [%]	Grinding task [%]
x-y plane	A group	Minimum $D_{res\ xy-A}$	0.40	0.00	0.01
		Maximum $D_{res\ xy-A}$	2.10	0.07	0.75
		Median $D_{res\ xy-A}$	1.30	0.02	0.23
	B group	Minimum $D_{res\ xy-B}$	0.03	0.06	0.3
		Maximum $D_{res\ xy-B}$	1.20	0.18	1.30
		Median $D_{res\ xy-B}$	0.45	0.10	0.92
x-z plane	A group	Minimum $D_{res\ xz-A}$	0.13	0.09	0.49
		Maximum $D_{res\ xz-A}$	8.73	5.20	7.09
		Median $D_{res\ xz-A}$	1.96	1.59	2.66
	B group	Minimum $D_{res\ xz-B}$	0.17	0.34	0.00
		Maximum $D_{res\ xz-B}$	8.33	6.50	8.30
		Median $D_{res\ xz-B}$	2.18	3.00	2.64

6.5 Discussion

6.5.1 Splitting of the Knob-shaped Measuring Handle

With the method used, it was possible to extract design parameters for a knob-shaped measurement handle from the experimental data of a subject study using a numeric algorithm. Based on the results obtained,²³ the angular orientation of the separation plane in the knob-shaped handle will be discussed and compared to the cylindrical measurement handle.

Across all tasks performed and subjects participating, the results show that the separation plane for a knob-shaped handle is predominantly vertically oriented with an overall orientation $\alpha_{mean\ xy} = -3.25^\circ$ and $\alpha_{mean\ xz} = -5.5^\circ$. This angular orientation of the separation plane shows that the grip force on a knob-shaped handle acts predominantly horizontally.

In this case, the alignment of the separation plane to the pressing force and to the respective power tool movement deviates from the established cylinder handle. With the cylindrical handle, the separation plane is perpendicular to the pressing force and to the axis of the forearm and the direction of a representative power tool movement. In contrast to this, the separation plane of the knob-shaped handle is oriented parallel to the direction of the pressing force and to the axis of the forearm.

Hence, for a knob-shaped handle, the relations between coupling forces and power tool movements are more complex than in the case of power tools with a mainly cylindrical handle such as the hammer drill. The power tool movement of the orbital sander is planar, while the pressing force is perpendicular to this movement as it presses the grinding disc against the surface of the plywood plate. Moreover, the grip force is perpendicular to the pressing force and mostly independent of the power tool movement. Evidence of this independence is provided by the values in Table 6.4 and Table 6.5, where the 5th and 95th percentiles of the grinding and static pressing tasks are in the same range. In addition, the 95th and 5th percentiles of

²³ In this sentence a passage from the original publication has been deleted to avoid confusion in the context of the thesis. The deleted passage refers to the main question of the introduction of the original publication, which is not cited in the thesis. At this point the deleted passage reads “[...] the first main question of the manuscript concerning [...]” Schröder et al. (2022)

both projections range from -15.5° to 6.5° across all tasks, which is consistent with a separation plane that is slightly negative to the vertical.

The scatter of the individual separation planes, which can be seen by the percentiles in Table 6.4 and Table 6.5 may be due to the scatter of the subjects' hand and finger sizes shown in Table 2. The scatter may also be due to the shape of the grip. Compared to the unidirectional gripping of a cylindrical handle or a power grip, the knob-shaped handle allows more flexible positioning of the palm and fingers on the handle surface. This may lead to a higher variability of the gripping position across the subjects.

6.5.2 Influence of the Subjects' Handedness and the Applied Pressing Forces

Regarding the separation planes in Figure 6.8 and Figure 6.9 it has to be mentioned that in all tasks, the planes are slightly shifted negative to the vertical. This negative angular offset from the vertical is also evident from the values of $\alpha_{res\ xy}$ and $\alpha_{res\ xz}$ in Table 6.4 and Table 6.5. In the x-z plane, this negative angular offset has a similar magnitude in all tasks in the range of -5.5 as is shown in Figure 6.9, where the separation planes are oriented almost on top of each other. In the x-y plane, the separation planes of the different tasks differ more from each other. While the negative offset to the vertical in the holding task is about the same in the x-y and x-z planes, the separation planes of the pressing and the grinding tasks are oriented clearly more vertically in the x-y plane than in the x-z plane.

Overall, the negative angular offset is more pronounced in the x-z plane, firstly, because it is approximately the same for all three tasks, and secondly, because on average, it is greater than the offset in the x-y plane. Accordingly, it can be assumed that the offset has the same cause in all three tasks.

A possible explanation of the negative angular offset in the x-z plane could be that the subjects in the study were only right-handed. In the case of a knob-shaped handle, the subject's hand is mounted on the top of the handle and the arm is oriented backwards to the handle as an extension of the palm. Therefore, the subject must rotate the hand slightly so that the index finger is on the front of the handle, while the thumb and other fingers are on either side of the knob-shaped handle, facing each other. Such way of gripping can be seen in Figure 6.3, a similar type of gripping is also described in (Wakula et al., 2009). In this type of gripping, the grip axis of the thumb and fingers runs diagonally across the palm from the index finger to the wrist. For a right-handed person, this diagonal gripping axis has a negative angular offset because, from the user's point of view, the gripping axis runs from the left front side

to the right rear side of the orbital sander handle. With reference to the results in Table 6.4 and Figure 6.9, the angular offset of the separation planes from the vertical in the x-z plane would correspond to the gripping axis of a right-handed subject. Therefore, the connection between the angular offset of the separation plane in the x-z-plane and the only right-handed subjects of the study is a reasonable assumption.

According to this assumption, the angular offsets in the x-y plane must also be discussed. In the x-y plane, the assumed influence of the subjects' right-handedness only affects the separation plane of the holding task, whose angular orientation $\alpha_{res\ xy}$ is nearly the same as in the x-z plane, as is shown in Table 6.4 and Table 6.5. In contrast, Figure 6.8 and the values of $\alpha_{res\ xy}$ in Table 4.3 show that the separation planes of the pressing and grinding tasks are oriented approximately vertically in the x-y plane. A possible explanation for these differences in the x-y plane is that no pressing force was applied to the random orbital sander during the holding task. The grip force could thus act uninfluenced on the sander without being stabilized by being pressed against the plywood. This uninfluenced acting of the grip force leads to a stronger effect of the right-handedness of the subjects in the holding task. This explanation is supported by the similar angular orientations of the different separation planes in the x-z plane in Figure 6.9 and Table 6.4. Since the vector of the pressing force is directed downward into the x-z plane, it cannot act normally on the projection of the separation plane and does not contribute to its orientation. Therefore, the separation planes' orientations in the x-z plane are only influenced by the grip force. In consequence, the separation planes of the pressing and grinding tasks are oriented in a similar angle as the separation plane from the holding task. In the x-y plane, on the other hand, the applied pressing force causes the separation planes of the pressing and grinding tasks to be more vertically aligned, while the separation plane of the holding task has a similar angle as in the x-z plane, since no pressing force was applied. In the case of the pressing task, this explanation is supported by the results of the Spearman correlation analyses, which show a medium effect size for a significant correlation between $\alpha_{res\ xy}$ and the resulting pressing force $F_{p\ res}$. In the case of the grinding task, no significant correlation could be shown. The fact that no significant correlation between $\alpha_{res\ xy}$ and the resulting pressing force $F_{p\ res}$ could be shown for the grinding task may be due to the task itself and the corresponding test procedure. In the pressing task, the subjects only had to apply static force to the sander while in the grinding task, the sander was moved. In consequence, the subjects had to apply less pressing force in the grinding task. Furthermore, in the pressing task, the subjects were instructed to press the random orbital sander against the plywood plate. This instruction can lead to a more intentional application of the pressing force, as the subjects only had to pay attention

to it. In the grinding task, the subjects had to pay attention to the grinding of the pattern, hence they possibly paid less attention to the application of the pressing force. In consequence, no correlation between the applied pressing force in the grinding task and the specific angle of the separation plane in the x-y plane could be shown. A possible indication of this assumption could be that the pressing force of the grinding task is not normally distributed across the subjects.

²⁴The results show that in the pressing task, the applied pressing force reduces the value of $\alpha_{res\ xy}$ to a more vertical orientation of the separation plane in the x-y plane. Hereby, the assumed effect of the subjects' right-handedness is compensated. A similar effect can be assumed for the grinding task, but could not be proven by the correlation analyses, which is probably due to the test procedure. In further studies, this assumption had to be analyzed. A possible test procedure for this would be to give the subjects several different values for the pressing force during the grinding task. Regarding the assumed effect of right-handedness, it would be interesting to also consider left-handed subjects in the study, since a shift of $\alpha_{res\ xy}$ to the positive would be expected.

6.5.3 Design and Implementation of the Knob-shaped Measuring Handle

Based on the results obtained concerning the orientation of the separation plane and the influence of the pressing force, it has to be evaluated how the splitting of the knob-shaped measurement handle has to be implemented.

Assuming a negative separation plane shift for right-handers and a positive shift for left-handers, a vertical splitting of the knob-shaped measuring handle would be a possible suitable design, as it would be suitable for both right- and left-handers.

Considering the effect of the pressing force on the separation plane orientation in the x-y plane, a vertical splitting of the knob-shaped measuring handle would also make sense. Based on the results obtained, it can be assumed that the application of the pressing force causes a rather vertical alignment of the separation plane.

²⁴ In this sentence a passage from the original publication has been deleted to avoid confusion in the context of the thesis. The deleted passage refers to the main question of the introduction of the original publication, which is not cited in the thesis. At this point the deleted passage reads “[...] To answer the second main question of the manuscript, [...]” Schröder et al. (2022)

Since the pressing force is also applied during the impedance measurement on shaker-based test benches, a vertical splitting of the handle would be a reasonable option. Therefore, it has to be evaluated how much a vertical splitting of the knob-shaped measurement handle would influence the resulting grip force. The results of the percentage deviation between the pressing forces acting on the determined and on the vertical separation plane in Table 6.5 are overall below 10% including both projections, all tasks, and both groups. In this context, it can be seen that the values of the maximum and median percentage deviation in the x-z plane are greater than in the x-y plane across all tasks. This trend corresponds to the separation plane angles in Figure 6.8 and Figure 6.9, where the angular deviation from the vertical in the x-z plane is also greater than in the x-y plane across all tasks. Furthermore, Table 6.5 shows that the percentage deviation of the grip force is lowest for the pressing task, especially as far as the deviation in the x-y plane is concerned. This deviation also coincides with the alignment of the separation plane of the pressing task, as this has the smallest angular deviation from the vertical. With regard to the intended use of the measuring handle, this is most likely represented by the pressing task. Following on from this, the maximum percentage deviation between the gripping forces applied to the different separation planes is lowest for the pressing task in both projections. If one also takes into account that the measuring handle should be suitable for right- and left-handed subjects, a vertical splitting of the measuring handle would be an acceptable and easy-to-manufacture design.

6.6 Limitations

The results of the study only refer to one specific random orbital sander. Although the analyzed gripping position is representative of this type of sander, the results obtained are limited to the specific geometry of the sander handle. Since this geometry may vary slightly for a different random orbital sander, different results are possible. With a wider handle, the fingers of the subject's hand would close less around the handle and rest more on the top than on the side of the handle. In this case, the applied grip force would act more vertically than horizontally. The subjects' grip force could also be affected by the thickness of the force measurement foil as it increases the dimensions of the handle. Since the foil's measurement works by compressing a layer of elastomer, a certain thickness is required for the measurement. For determination of the separation plane, the foil's sensor elements were evaluated relative to each other. The influence of the film thickness on the angular position of the separation plane can thus be considered minor, since it affects all sensors and the grip force distribution of all subjects in the same way.

In this context, it also has to be considered that the height of the plywood plate was fixed, which caused variations in the arm posture depending on the standing height of the subject. For tall subjects, a plywood plate that is too low could possibly cause the subjects to bend over the plywood plate more and add parts of their body weight to the pressing force. Considering the correlation between the subject's handedness, the separation plane's angular orientation, and the pressing force derived from the results obtained, the resulting higher pressing force would lead to a more vertical separation plane. Conversely, a plywood plate that is too high would result in small subjects applying less pressing force as they would not be able to align their arms properly, resulting in a less vertical separation plane. With regard to the study carried out, these correlations have probably influenced the obtained alignments of the separation planes' orientation, but the height of the subjects was predominantly in a relatively small range between 1.70 m and 1.90 m (23 out of 30 subjects). Therefore, the influence of the varying standing height of the subjects on the results obtained may be less than would be the case if the height of the subjects was normally distributed. Consequently, in further studies, the height of the plywood plate must be adjusted to the scatter of the subjects' body size.

Furthermore, only right-handed subjects were considered in this study. It would be wise to include left-handed subjects as well. In this context, the obtained results of the study are also limited by the scatter of the calculated individual subject-specific separation planes. This scatter is possibly caused by the different hand sizes of the subjects. Therefore, further studies using the same method of evaluation are required, since the subjects of the conducted study were only right-handed and not normally distributed in their anthropometric properties. Hereby, the study focused on the direction and orientation of the subjects' grip forces. Therefore, the force distribution across the handle was more relevant than the absolute value of the applied grip force. In consequence, the measurement of the subjects' anthropometric properties included only the hand dimensions according to DIN EN ISO 7250-1, since the dimensions and kinematics of the hand are related to the force distribution on the handle. The muscle strength and capacity play a minor role in determining this force distribution, therefore specific measurement of the subject's muscle strength was not necessarily required. However, it would be interesting to measure the muscle strength of the subjects in further studies, as it cannot be assumed that it is the same over all subjects. In this regard, measuring the subject's maximum voluntary isometric contraction (MVIC) would be a good indicator for the subject's muscle strength (Meldrum et al., 2007). In addition the data analyses could be combined with the ability of the novel force measurement foil to segment its force sensors. This segmentation sums up the applied force of a defined amount of sensors located in a certain area to one total value. Implementing this ability into the evaluation algorithm could possibly reduce the effort of assigning the sensor positions to the 3D

scan and lower the computing time. Through this optimization, a greater amount of handles could be evaluated faster.

Furthermore, the subjects' experience in the use of power tools considered only the use in general and did not refer to specific power tools. A possible connection between the angular orientations of the separation planes and the subjects' explicit power tool experience was not analyzed.

Nevertheless, further studies are required to analyze the relationship between the subjects' experience in handling certain power tools and the forces applied to these power tools. Therefore, the subjects' performance of a specific task related to one power tool would be a possible appropriate test setup. Hereby, not only the grip force and its distribution, but also the pressing force and the movement of the power tool have to be recorded. In this context, a more specific query on the subjects' experience in handling power tools is necessary, as there are large differences in the use of certain power tools.

6.7 Conclusion

The manuscript introduces a novel approach to the data-based design of a new knob-shaped measuring handle for the measurement of grip force in the context of impedance measurement. Since no comparable design of a measuring grip exists according to the current state of research, the significant design parameters for a knob-shaped measuring handle were extracted from the data of a subject study. The subject study was conducted with 26 subjects whose gripping force on a random orbital sander was measured during various tasks performed. Based on the results of the study, a separation plane was calculated to divide the new knob-shaped measuring handle in order to integrate the force sensors for grip force measurement. The force sensors of the knob-shaped measuring handle have to be placed in a vertically oriented separation plane, since the grip force of the test subjects acts mainly horizontally on the sander handle. The separation plane shows a slight angular offset to the vertical, which may be due to the handedness of the subjects, since only right-handed subjects participated in the study. This angular offset caused by the handedness seems to be reduced by the pressing force.

In future studies, the approach has to be validated with different knob-shaped handles both for right- and left-handed subjects.

6.8 Acknowledgment

This work was supported by the German research foundation Deutsche Forschungsgemeinschaft (DFG) under the funding number 408254169. The authors of this publication are responsible for its content. We want to thank the DFG for funding and the support of our research, which enabled this publication. We would like to emphasize that the presented results and conclusions do not necessarily reflect the opinion of the DFG.”

6.9 Thesis specific conclusion

In the following, it will be assessed whether and to what extent the results and findings of the study presented in this chapter contribute to the investigation of **Hypothesis 1: Derivation of the measuring handle design**. The study was pre-published in the *Journal of Applied Ergonomics* under the title *Use of data-driven design for the development of knob-shaped handles in the context of impedance measurement*. The assessment is based on how the conducted study answer the corresponding sub-research questions of the hypothesis.

Hypothesis 1: Derivation of the measuring handle design

From the distribution of gripping forces on a knob-shaped power tool handle, a measuring handle for excitations in the "palm" position can be derived, which is suitable for measuring gripping forces.

- **Sub-research question 1.1:** How can the distribution of the gripping force direction on a knob-shaped handle in the “palm” position be determined with a force sensing foil and projected onto the handle geometry in such a way that the main direction of the gripping force can be determined?
 - In the study of the cited article, a method was presented, in which a force measuring foil was attached to a knob-shaped handle and the measured distribution of the gripping force could be projected onto a 3D-scan of the handle, as shown in Figure 6.5. Based on this projection, the main direction of the gripping force could be calculated vectorially. Hence **Sub-research question 1.1** can be regarded as answered.

- **Sub-research question 1.2:** What is the angular orientation of the separation plane in which the force transducers are positioned in the x-y plane or the rear view of the knob-shaped handle?
 - From the measured and projected gripping force distribution the angular orientation of the separation plane was iteratively calculated by an optimization algorithm. Using this algorithm, it was possible to determine the angular position of the separation plane where the force transducers are positioned in the x-y plane, as shown Figure 6.8. Hence **Sub-research question 1.2** can be regarded as answered.

- **Sub-research question 1.3:** What is the angular orientation of the separation plane in which the force transducers are positioned in the x-z plane or the top view of the knob-shaped handle?
 - Following **Sub-research question 1.2** the same algorithm was used to determine the angular position of the separation plane in the x-y plane, as shown by the results in Figure 6.9. Hence **Sub-research question 1.3** can be regarded as answered.

From the angular orientation in the x-y and x-z plane of the separation plane, a three-dimensional representation of the separation plane within the knob-shaped handle was derived, which is shown in appendix A. This representation and the calculated angles of the separation plane enable the angular positioning of the force transducers and thus the derivation of the design of a knob-shaped measuring handle for excitations on the “palm” position. Accordingly, **Hypothesis 1: Derivation of Measurement Handle Design** can be considered investigated and confirmed by the current chapter and the cited pre-published study.

7 Study on Hypothesis 2: Rotational impedance around the x_h –axis

7.1 Thesis specific introduction

In order to achieve the objective of this thesis, the following chapter will answer the research questions, which is linked to the **Hypothesis 2: Rotational impedance around the x_h –axis**. By answering the sub research questions the hypothesis can be regarded as investigated. The hypothesis and the corresponding research questions from Subchapter 5.1 are:

Hypothesis 2: Rotational impedance around the x_h -axis

The rotational mechanical impedance for excitations around the x_h -axis in the „hand-grip“ position is influenced by the applied gripping force, push force.

- **Sub-research question 2.1:** What is the course of the magnitude and the phase angle of the RMI for rotational vibration excitation around the x_h –axis via a knob-shaped handle in the “palm” position?
- **Sub-research question 2.2:** How is the magnitude of the RMI influenced by the applied gripping force?
- **Sub-research question 2.3:** How is the magnitude of the RMI influenced by the applied push force?

According to the structure of the thesis described in Subchapter 1.2 and the research design from Subchapter 5.2 the research questions from Subchapter 5.1 are answered by a subject study in the following Chapter 7. The presented study was pre-published in the *Journal of Industrial Ergonomics* entitled *Influence of coupling forces on the mechanical impedance of the hand-arm system during rotational vibration excitation around the x_h –axis* (Schröder, Lindenmann, Resch, et al., 2023) and are cited in full below from that journal article.

In the presented subject study the RMI of the HAS was measured during rotational vibration excitation around the x_h –axis in the “palm” position. The influence of the gripping force and the push force on the RMI was also investigated in the study. For this purpose the proposed design for the knob-shaped measuring handle from Chapter 6 was adopted. In this context the handle design was slightly modified, as mentioned in the discussion in Subchapter 6.5.2. The subjects with whom the study

was conducted in Chapter 6 were exclusively right-handed. Due to this handedness the calculated separation plane of the knob-shaped handle had a slightly angular offset.

In order to make the measuring handle suitable for right and left handed subjects the angular offset of the separation plane of the knob-shaped measuring handle was neglected and the handle split vertically, as suggested in Subchapter 6.5.3. The resulting knob-shaped measuring handle was manufactured in GRP²⁵, with an aluminum plate in each half of the handle, between which two force transducers (8435, Burster GmbH & co kg, Gernsbach, Germany) were mounted. The measuring handle was attached to the measuring flange of the shaker test bench from Matthiesen et al. (2018) via an aluminum adapter component.

The following Subchapters: 7.2 *Methods*, 7.3 *Results*, 7.4 *Discussion*, 7.5 *Limitations*, 7.6 *Conclusion* and 7.7 *Acknowledgment* are full citations from the publication *Influence of coupling forces on the mechanical impedance of the hand-arm system during rotational vibration excitation around the x_h -axis* (Schrüder, Lindenmann, Resch, et al., 2023). For this purpose, the numbering of the chapters, figures and tables were adapted to the numbering of the thesis.





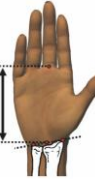

7.2 Methods

7.2.1 Test Subjects

“The study was conducted with 21 subjects (4 females; 17 males). The subjects’ age ranged from 17 to 34 years, with a median value of 26 years. Furthermore, the heights and weights of the subjects were recorded. The heights ranged from 1.58 m to 1.93 m with a median of 1.79 m. The weights ranged from 57 kg to 100 kg with a median of 77 kg. Within this range of weights, the subjects’ body mass index (BMI) were determined to be ranging from $19.7 \frac{kg}{m^2}$ to $28.8 \frac{kg}{m^2}$ with a median value of $23.4 \frac{kg}{m^2}$. In addition to this, the anthropometric properties according to DIN EN ISO 7250-1 were measured. **Table 7.1** shows the lower and the upper quartiles as well as the median values of these measurements (DIN - Deutsches Institut für Normung, 2017).

²⁵ GRP = Glass Reinforced Polyester, English designation for the German GFK

Table 7.1: Distribution of the anthropometric properties of the subjects' HAS, which were measured according to DIN EN ISO 7250-1 (DIN - Deutsches Institut für Normung, 2017)

	Arm length [cm]	Fore-arm length [cm]	Thumb length [mm]	Hand length [mm]	Palm length [mm]	Hand width [mm]
						
Median	73.5	35	61.5	185	101	100
Lower quartile	72	34.5	60	179.25	100	100
Upper quartile	74.5	36	65.5	190	105	105

7.2.2 Test Apparatus

For the study, a shaker test bench equipped with a measuring handle was used. The test bench allows the vibration of a measuring handle by two independent shakers (M124M and L125M; ETS Solutions Europe, Loffenau, Germany). While the M124M shaker provides translational oscillation, the L125M shaker provides angular oscillation through a gearbox, varying depending on its mode. Both shakers are adjustable in height and tilt angle via a carrier mechanism. This carrier mechanism allows the translational and angular oscillation of the shakers to occur in any spatial direction and at any height. In the presented study, only the angular oscillation of the L125M shaker was used. The L125M shaker excited the subject's HAS with a rotational vibration around the x_h -axis of the HAS, according to the coordinate system shown in Figure 2.5 on page 18²⁶. Two triaxial force transducers (9027C; Kistler

²⁶ In the original publication, the figure refers to Figure 1, which is part of the introduction to the publication and is not cited in this thesis. Therefore, the reference has been changed to Figure 2.5, which is equivalent to the original.

Instrumente AG, Winterthur, Switzerland) underneath the equipped handle measured the torque of the shaker's angular oscillation, as well as the push force applied by the subject. The acceleration of the handle was measured by two accelerometers (PCB 356A15; PCB Piezotronics, Depew - NY, USA) attached to a flange on which the measuring handle was mounted. The hemisphere geometry, described in DIN EN ISO 5349-1, does not allow for the application of gripping forces and does not represent a realistic power tool handle. Therefore, the geometry of a knob-shaped handle derived from the handle geometry of a random orbital sander for the measuring handle was used. The measuring handle used in the study is visible in Figure 7.1 and is described by Schröder et al. (Schröder et al., 2022).

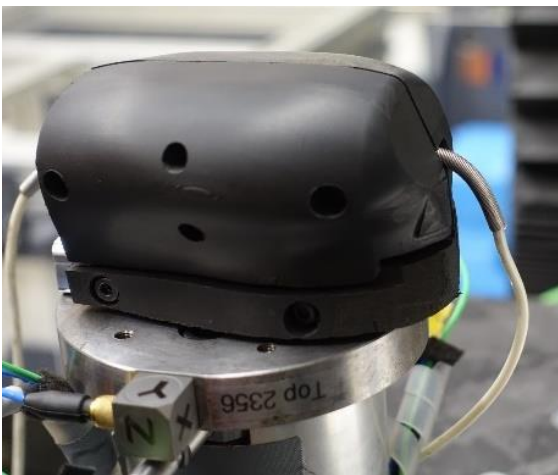


Figure 7.1: Knob-shaped measuring handle used in the conducted study.

Following DIN EN ISO 10819, the measuring handle is divided into two halves with two force sensors (8435, Burster GmbH & co kg, Gernsbach, Germany) placed in between. The orientation of the force sensors, and the division of the handle depending on the main gripping direction, were determined by the data-based evaluation of experimental data from manual studies with a random orbital sander (Schröder et al., 2020; Schröder et al., 2022). To provide visual feedback on the applied gripping and push forces, a display with a graphical interface was attached to the carrier mechanism of the shakers. Figure 7.2 shows the test bench with the visual force feedback on the display.

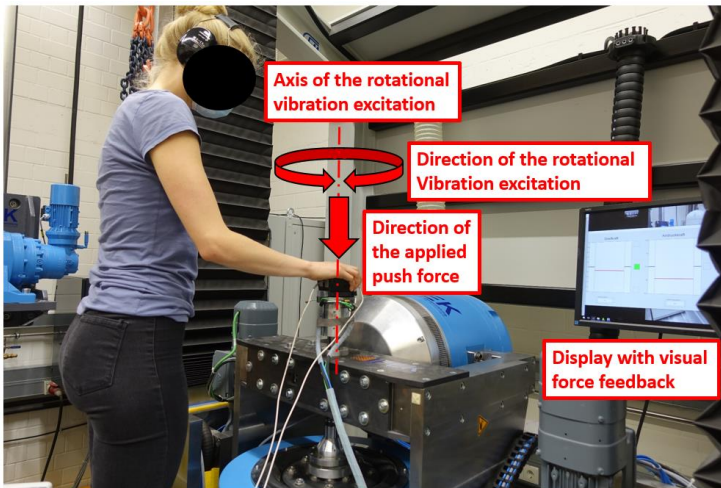


Figure 7.2: Test bench with measuring handle and visual force feedback.

To calibrate the measuring handle, the RMI of the measuring handle was measured. For this purpose, the unloaded, empty handle was excited in three trials using the frequency spectrum applied in the study. The spectrum used is based on the spectrum of ISO 10068 and was applied up to a frequency of 250 Hz. The pre-studies showed that using the same acceleration magnitude across the entire frequency spectrum leads to a rapid and large displacement of the measuring handle at low frequencies. Due to this displacement, the subjects were not able to apply a constant gripping force to the handle at low frequencies. However, a lower acceleration of the handle was difficult to detect at high frequencies, because it has to be set apart from the noise level. Therefore, in order to match the excitation magnitude to the subjects' abilities, the acceleration of the measuring handle had to be adjusted to the excited frequency. Accordingly, the acceleration of the measuring handle was linearly increased from an RMS-value of ca. $3 \frac{m}{s^2}$ ($62.5 \frac{rad}{s^2}$) at 10 Hz, up to an RMS-value of ca. $40 \frac{m}{s^2}$ ($834 \frac{rad}{s^2}$) at 65 Hz, remained almost constant up to 160 Hz, and was then increased again linearly up to an RMS-value of ca. $65 \frac{m}{s^2}$ ($1354.2 \frac{rad}{s^2}$) at 250 Hz.. Lindenmann and Matthiesen (2019) already used a similar approach in response to an identical problem. Lindenmann and Matthiesen also increased the RMS value of the acceleration linearly up to 81 Hz, and then kept this at a constant value (Lindenmann & Matthiesen, 2019). Furthermore, a similar approach has also been used for the measurement of translational MI (Burstrom, 1997). Figure 7.3 shows the frequency-weighted RMS values of the acceleration with which the measuring handle was excited

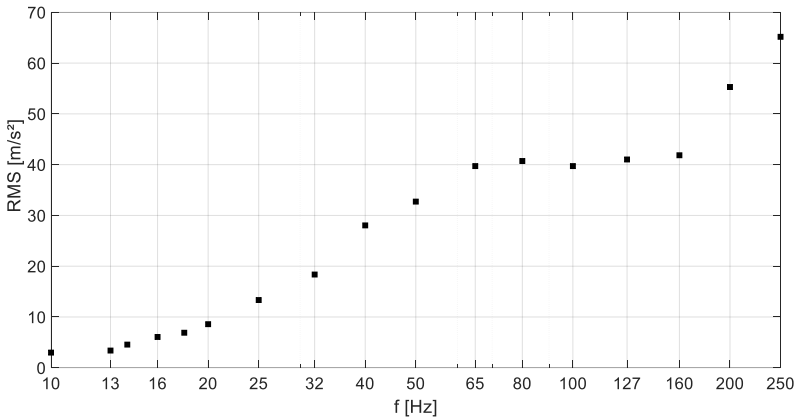


Figure 7.3: RMS-values of the acceleration magnitudes used to calibrate the measuring handle and to excite the subjects' HAS in the RMI measurements.

The described RMS values shown in Figure 7.3 were applied to the measuring handle in three calibration trials, resulting in corresponding values of the measured torque. The overall deviation of the handle's magnitude and phase angle, when comparing the three calibration trials against each other, was less than 1%. Figure 7.4 shows an example of the magnitude and the phase angle of the RMI of the measuring handle for one trial.

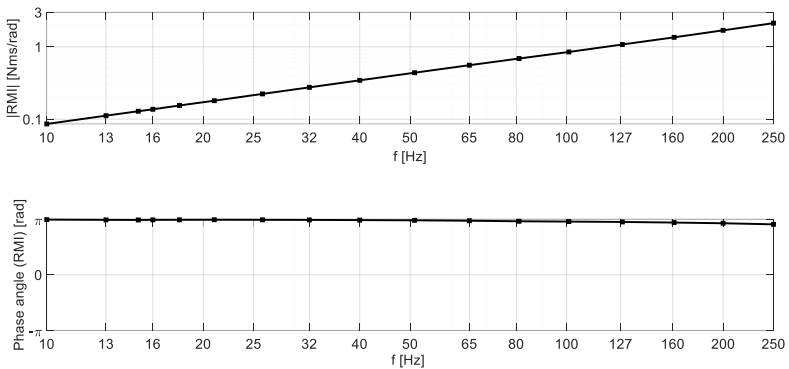


Figure 7.4: The magnitude of the RMI according to Equation 2.3²⁷ of the used measuring handle across the excited frequencies

7.2.3 Test Procedure

This research complied with the tenets of the Declaration of Helsinki and had human subject approval (World Medical Association, 2013). In this regard, we obtained informed consent from the subjects at the beginning of the study. In the first step of the test procedure, the subjects were informed about the duration and the procedure of the study. During the entire study, the subject had the option to interrupt or terminate the study at any time. After this briefing, the weight, height, and age of the subjects were noted, and the anthropometric properties of the hand-arm system were measured according to DIN EN ISO 7250-1 (DIN - Deutsches Institut für Normung, 2017). To keep the body posture constant in every experiment, the shakers were adjusted to the height of the subject. The specific body posture of the subjects is shown in Figure 7.2 and was taken from DIN EN ISO 28927-3 and DIN 45677 (DIN Deutsches Institut für Normung e. V., 2001a, 2010b). For this purpose, the subjects had to grip the handle in an angled arm posture with the forearm horizontal. To evaluate the influence of the gripping force (F_{gr}) and the push force (F_{pu}) on the RMI, both forces were investigated in a full factorial experimental design, using two different force sets. Table 7.2 shows the force sets of the gripping force and the push force the subjects had to apply.

²⁷ In the original publication, the figure refers to Equation 1, which is part of the introduction to the publication and is not cited in this thesis. Therefore, the reference has been changed to Equation 2.3, which is equivalent to the original.

Table 7.2: Factor levels of the gripping force and push force

Level	Gripping Force [N]	Push Force [N]
1	$F_{gr} = 14 N$	$F_{pu} = 32.5 N$
2	$F_{gr} = 24 N$	$F_{pu} = 42.5 N$

The chosen force sets were based on the measured forces of an application study conducted with a random orbital sander (Schröder et al., 2020). Due to the full factorial design using two force sets, each subject had to participate in four experiments with four different force combinations of gripping and push force. Hereby, the order of the factor combinations was randomized for each subject. For each force set, each subject applied the specific gripping and push force combination while the vibration of the measuring handle was set to the discrete frequency spectrum depicted in Figure 7.4. For this purpose, the order of the frequencies shown in Figure 7.4 was randomized. The magnitude of acceleration with which each frequency was excited corresponded to the description laid out in the Test Apparatus chapter. Each frequency of the spectrum was applied for 7 seconds with 5 seconds rest in between. Additionally, the subjects could interrupt the experiment at any time by releasing a hand trigger. If the trigger was pressed again, the vibration sequence was continued at the point where it was interrupted. Between experiments, subjects were given a break of at least 10 minutes, to prevent subject fatigue. In total, the test duration for performing all factor combinations was approximately 42 Minutes per subject, including breaks. To reduce the test duration per subject and to prevent subject fatigue, only one trial per force combination was performed.

7.2.4 Data Analysis

The data were evaluated with MATLAB (The MathWorks, Inc, Natick MA, USA) and SPSS (IBM SPSS Statistics 25, IBM, Armonk NY, USA). For the evaluation of the rotational mechanical impedance (RMI), the method used was based on one used earlier by Lindenmann and Matthiesen (2019). In this method, the excited frequencies were determined using a fast Fourier transformation. Subsequently, the torque and angular acceleration data were filtered using a Butterworth band pass filter, with cutoff frequencies 0.8 and 1.2 of the determined frequency, respectively. Hereinafter the filtered torque and acceleration data of each frequency were fitted to a sinusoid using a curve-fitting algorithm, from which the corresponding coefficients of the torque and the angular acceleration were obtained as complex values. Using Equation 1, the RMI was calculated as the complex ratio of the determined coefficients for each applied frequency, and the magnitude and phase angle were determined.

To compensate for the mass of the measuring handle, its calibrated RMI was subtracted from the results obtained. The determined RMI of each subject was grouped according to the applied factor combinations of the gripping and push force. Within these groups, the median and upper and lower quartiles of the RMI were calculated for each frequency, across all subjects.

For further statistical data evaluation, the magnitude of the RMI, the gripping force, the push force values, and the recorded metadata was transferred to SPSS. According to the Shapiro-Wilk test and visual histogram checking, the transferred data was not normally distributed. Therefore, the Mann-Whitney U test was used to find causalities between the applied coupling forces and the RMI across the applied frequencies. For this purpose, the magnitude of the RMI was defined as the dependent variable, and the gripping force or push force levels were defined as the independent variable. Here, the effect of the gripping force on the RMI at both push force levels and the effect of the push force on the RMI at both gripping force levels were evaluated separately. Overall, four Mann-Whitney U tests were performed. In the first test, the effect of the gripping force on the RMI magnitude was evaluated for the factor levels of $F_{gr} = 14\text{ N}$ and $F_{gr} = 24\text{ N}$, applied at a push force of $F_{pu} = 32.5\text{ N}$. Subsequently, the effect of the gripping force on the RMI magnitude was evaluated for the corresponding gripping force levels, applied at a push force of $F_{pu} = 42.5\text{ N}$. The Mann-Whitney U tests performed on the effect of the push force, on the RMI magnitude, were performed in the same manner. Here, the effect of the push force was evaluated at the gripping forces of $F_{gr} = 14\text{ N}$ and $F_{gr} = 24\text{ N}$ respectively. For all Mann-Whitney U tests, the significance level was set to $\alpha = .05$.

In this context, the effect strength r was considered as small for $r \leq .30$, as moderate for $.30 < r < .50$, and as high for $r \geq .50$ (Cohen, 1992). Figure 7.5 provides a schematic overview of the data evaluation described, structured in nine steps.

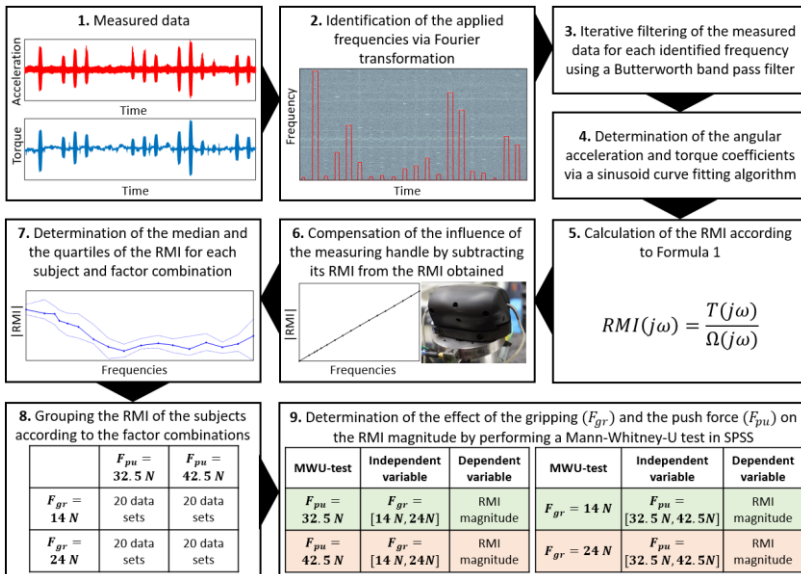


Figure 7.5: Schematic overview of the conducted data evaluation for the determination of the RMI and the influence of the coupling forces.

In addition to this evaluation, the percentage deviation between the requested coupling force levels and the applied coupling forces over all subjects was evaluated. This procedure was performed to see how the applied coupling forces varied to evaluate whether the observed effect on RMI could be clearly attributed to a specific force level. Table 7.3 shows the mean and the maximum percentage deviations between the requested and the applied gripping and push forces.

Table 7.3: The mean and the maximum percentage deviations between the requested gripping and push force levels and the applied gripping and push forces

Level	Push Force $F_{pu} = 32.5\text{ N}$	Push Force $F_{pu} = 42.5\text{ N}$	Gripping Force $F_{gr} = 14\text{ N}$	Gripping Force $F_{gr} = 24\text{ N}$
Mean deviation	0.72 %	0.73 %	0.83 %	0.9 %
Maximum devia-	2.57 %	2.7 %	5.3 %	4.2 %

7.3 Results

7.3.1 Qualitative results on the influence of the gripping and the push forces on the RMI

Figure 7.6 to Figure 7.9 show the influence of the gripping force on the RMI for the various factor combinations. Figure 7.6 and Figure 7.7 show the median plots of the magnitude and phase of the RMI for different gripping force levels, at a push force of $F_{pu} = 32.5 \text{ N}$ and $F_{pu} = 42.5 \text{ N}$. The interquartile range and the median of every factor combination were calculated over all subjects. Hereby, the dots are the actual measured values at the specific frequencies, while the connecting lines between the dots are a linear approximation. In addition, the filled area represents the range between the interquartile ranges between the lower and the upper quartile.

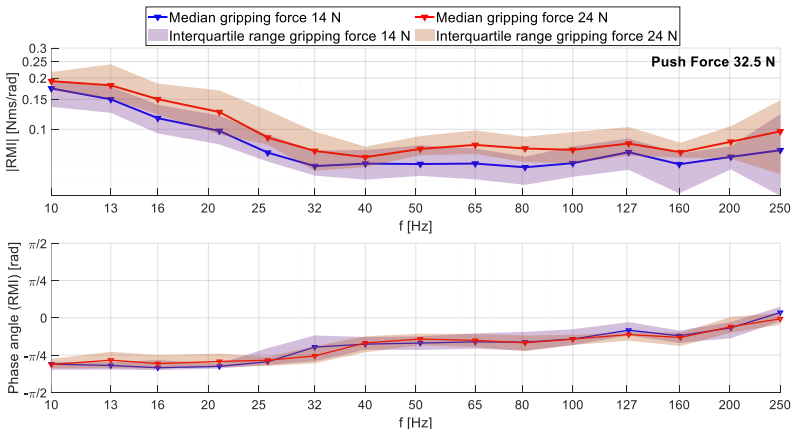


Figure 7.6: The median and interquartile range of the magnitude (above) and the phase angle (below) of the RMI over all subjects. The RMI was measured for the gripping forces of $F_{gr} = 14 \text{ N}$ and $F_{gr} = 24 \text{ N}$ at a gripping force of $F_{pu} = 32.5 \text{ N}$. The RMI was calculated according to equation 2.3²⁸ and refers to steps 7 and 8 of the overview in Figure 7.5

²⁸ In the original publication, the figure refers to Equation 1, which is part of the introduction to the publication and is not cited in this thesis. Therefore, the reference has been changed to Equation 2.3, which is equivalent to the original.

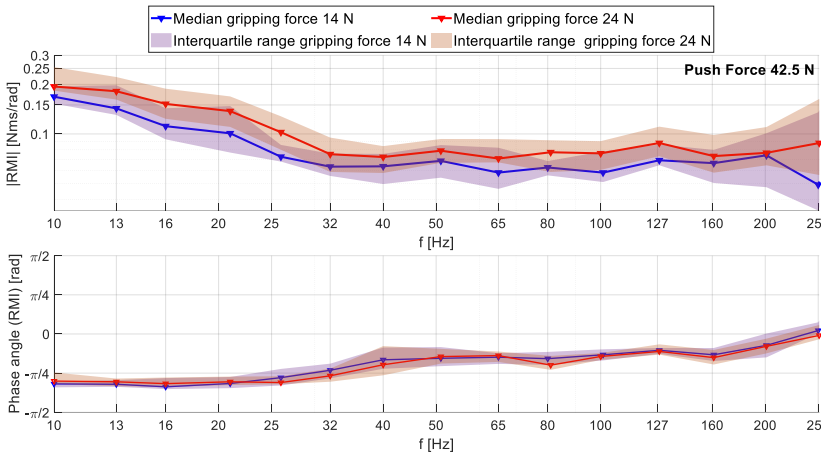


Figure 7.7: The median and interquartile range of the magnitude (above) and the phase angle (below) of the RMI over all subjects. The RMI was measured for the gripping forces of $F_{gr} = 14\text{ N}$ and $F_{gr} = 24\text{ N}$ at a gripping force of $F_{pu} = 42.5\text{ N}$. The RMI was calculated according to equation 2.3 and refers to steps 7 and 8 of the overview in Figure 7.5

In both figures, the plots of the median of the RMI's magnitudes are quite similar to each other. Within the figures, the course of the RMI's magnitude at the different gripping force levels also have a similar course, but the plots of the gripping force level of $F_{gr} = 24\text{ N}$ have an offset to the plots of the gripping force level of $F_{gr} = 14\text{ N}$. The RMI's magnitudes at both gripping forces in both figures decrease to up to 32 Hz and remain almost constant up to 250 Hz. In Figure 7.6, the median plot as well as the interquartile range of the RMI's magnitude is higher for a gripping force of $F_{gr} = 14\text{ N}$ than for a gripping force of $F_{gr} = 24\text{ N}$. In Figure 7.7, the median plot and the interquartile range of the RMI's magnitude are also higher for the higher gripping force level. Regarding the phase angle of the RMI, no difference between the two gripping force levels is visible, regardless of the applied push force. The phase angles for both gripping force levels in both figures are slightly beyond $-\frac{\pi}{4}$ up to 25 Hz, increasing to approximately $-\frac{\pi}{4}$ at 32 Hz to where it remains nearly constant up to 160 Hz, from where it increases linearly up to 0 at 250 Hz.

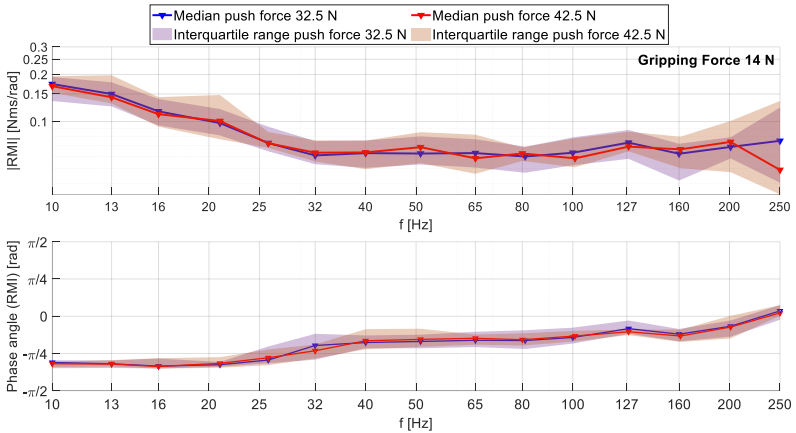


Figure 7.8: The median and the interquartile range of the magnitude (above) and the phase angle (below) of the RMI over all subjects. The RMI was measured for the gripping forces of $F_{pu} = 32.5\text{ N}$ and $F_{pu} = 42.5\text{ N}$ at a gripping force of $F_{gr} = 14\text{ N}$. The RMI was calculated according to equation 2.3 and refers to steps 7 and 8 of the overview in Figure 7.5

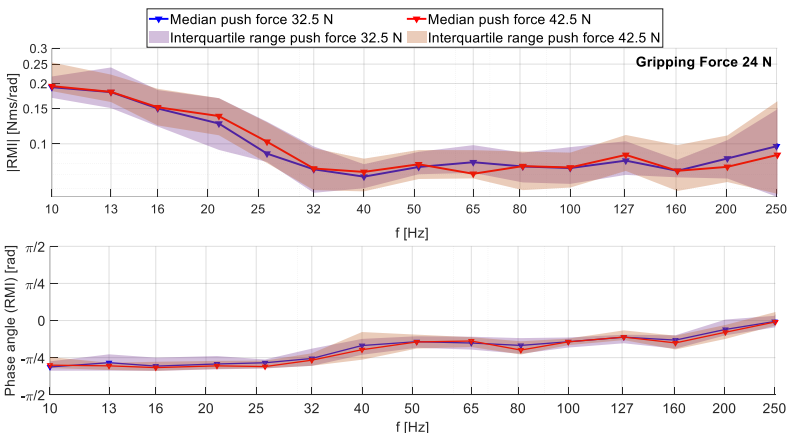


Figure 7.9: The median and the interquartile range of the magnitude (above) and the phase angle (below) of the RMI over all subjects. The RMI was measured for the gripping forces of $F_{pu} = 32.5\text{ N}$ and $F_{pu} = 42.5\text{ N}$ at a gripping force of $F_{gr} = 24\text{ N}$. The RMI was calculated according to equation 2.3 and refers to steps 7 and 8 of the overview in Figure 7.5

The median plots and interquartile ranges of the RMI's magnitude in Figure 7.8 and Figure 7.9 are similar to each other. In both figures, there are no differences between the plots concerning the applied push force levels, and the RMI's magnitudes of both push force levels largely overlap. From 32 Hz, the plots decrease and remain constant up to 250 Hz. As in the case of the magnitudes, the RMI's phase angle plots of both push force levels also largely overlap, regardless of the applied gripping force. Across the applied frequency spectrum, all phase angles in both figures increase stepwise from approximately $-\frac{\pi}{4}$ at 32 Hz to $-\frac{\pi}{8}$ at 160 Hz to 0 at 250 Hz

7.3.2 Statistical results on the influence of the gripping and the push forces on the RMI

Table 7.4 provides the statistical results concerning the effect of the gripping force on the RMI magnitude according to the Mann-Whitney-U test.

Table 7.4: Effect of the gripping force on the magnitude of the RMI, level of significance $p=0.05$, MW-U= Mann-Whitney-U test, r = effect strength. The table refers to step 9 of the overview in Figure 7.5. The effect strength r is considered as small for $r \leq .30$, as moderate for $.30 < r < .50$, and as high for $r \geq .50$ (Cohen, 1992)

Applied Push force:	$F_{pu} = 32.5 N$			$F_{pu} = 42.5 N$		
	Factor levels	$F_{gr} = 14 N$	$F_{gr} = 24 N$	$F_{gr} = 14 N$	$F_{gr} = 24 N$	
Grip- ping force	p	MW-U	r	p	MW-U	r
f [Hz]						
10	.070	-	-	.022*	130	.497
13	.020*	121	.519	.033*	136	.464
16	.028*	126	.490	.021*	129	.502
18	.025*	124	.501	.013*	122	.540
20	.016*	118	.540	.046*	141	.436
25	.012*	114	.560	<.001*	91	.711
32	.026*	125	.496	.193	-	-
40	.165	-	-	.184	-	-
50	.015*	117	.542	.114	-	-
65	.011*	113	.566	.043*	140	.442
80	.013*	115	.554	.062	-	-
100	.058	-	-	.070	-	-
127	.115	-	-	.031*	135	.469
160	.017*	119	.530	.168	-	-
200	.032*	128	.478	.306	-	-
250	.181	-	-	.052	-	-

At the push force level of $F_{pu} = 32.5 \text{ N}$, the effect of the gripping force on the RMI is significant at more frequencies than at the push force level of $F_{pu} = 42.5 \text{ N}$. Here, the effect of the gripping force is significant in the frequency range from 13 Hz to 32 Hz and from 50 Hz to 80 Hz as well as at the frequencies of 160 Hz and 200 Hz. Within these frequency ranges, the effect strength of the gripping force on the RMI mostly varies between moderate and high (Cohen, 1992). At the push force level of $F_{pu} = 42.5 \text{ N}$, the effect of the gripping force on the RMI is also significant at lower frequencies, specifically in the frequency range of 10 Hz to 25 Hz. Furthermore, the effect of the gripping force on the RMI is significant at the frequencies of 65 Hz and 127 Hz. The effect strength of the gripping force at the push force level of $F_{pu} = 42.5 \text{ N}$ is overall lower than at the push force level of $F_{pu} = 32.5 \text{ N}$ and varies between low and moderate. One exception was found at 25 Hz, where its effect strength was found to be quite high (Cohen, 1992).

The results of the Mann-Whitney-U tests that were performed for the evaluation of the effect of the push force on the magnitude of the RMI showed no significant effect of the push force on the RMI at any frequency. These results occur regardless of the gripping force level at which the push forces were applied.

7.4 Discussion

7.4.1 The plots of the magnitude and the phase angle of the RMI across the applied frequency spectrum

The phase angles of the RMI in Figure 7.6 to Figure 7.9 are slightly beyond $-\frac{\pi}{4}$ up to 32 Hz and increase stepwise up to 0 at 250 Hz. This indicates a superimposed spring-damper dynamic of the HAS with an increasing damper component at frequencies beyond 32 Hz. Referring to the simplified example model of the HAS described in Equation 2.10²⁹, the decreasing magnitude plots of the RMI up to 32 Hz support the idea of a spring behavior of the HAS. The magnitude plots of the RMI beyond 32 Hz are almost constant and slightly above 0. The phase angle plots in this frequency range increase and approach zero with increasing frequencies. The

²⁹ In the original publication, the figure refers to Equation 3, which is part of the introduction to the publication and is not cited in this thesis. Therefore, the reference has been changed to Equation 2.10, which is equivalent to the original

course of the magnitude and phase angle indicates an increasing damping component in the dynamics of the HAS across the applied frequencies. A possible explanation for the increasing damper component in the HAS dynamics towards higher frequencies can be found in the hand position and the gripping of the knob-shaped measuring handle. In the case of the knob-shaped handle, the hand rests on the top of the handle and encloses it from above, while the handle oscillates angularly under the palm and fingers with the rotational axis directed through the palm. Due to this hand position and the elliptical shape of the handle, the HAS is connected to the handle via a combination of positive and frictional locking, as the torque of the rotational vibration acts tangentially to the palm and fingers in most parts. This can result in the skin and tissue between the hand and the surface of the handle being sheared and squeezed at high frequencies, as the hand cannot immediately follow the rapid rotational vibration of the handle due to the inertia of the HAS. Consequently, the lateral and normal squeezing of the skin on one's fingers by the rotational vibration movement of the handle may have a damping effect on the phase angle. It can also be assumed that the contact between the hand and the handle is temporarily interrupted in some areas at higher frequencies, as the handle slips under the hand. The combination of tissue shear and local slip in the hand-handle contact possibly results in the increasing damping dynamic of the HAS at higher frequencies. This can be seen in the phase angle plots. As a result, the contact between the hand and the handle works as some kind of frictional damper, whose damping increases with the oscillating speed of the handle. Vice versa, this damping is lower at frequencies below 32 Hz, since the hand can follow these comparatively slower rotational vibrations more easily without the skin being significantly squeezed and sheared or the contact between the hand and the handle partially detaching. Furthermore, the elliptical shape of the measuring handle provides the hand with an additional, positive locking between the hand and the handle. Although this positive locking also exists at high frequencies, it may not be as effective here, due to the faster vibration of the knob-shaped measuring handle. Thus the hand is probably more effectively coupled to the handle at lower frequencies. In doing so, the hand follows the vibrations of the handle by pivoting the hand laterally via the flexion of the wrist. Consequently, a greater amount of vibration would be transmitted to the HAS, and the wrist and forearm would be more affected by the vibration. This vibration exposure of the wrist's tissue and the forearm's muscles may result in the spring dynamics of the HAS at low frequencies, which are visible in the magnitude and the phase angle plots of the RMI. According to this assumption, the additional damping of the hand-handle contact at high frequencies causes the decreasing spring component and the increasing damper component of the magnitude and phase angle plots of the RMI. This additional damping results from the combination of the hand position when gripping the knob-shaped measuring handle and the direction of rotational excitation. This causes a tangential alignment of the direction of rotational vibration to the palm and

fingers. In addition, the added damping may reduce the transmission of vibration to the wrist and forearm, resulting in a decreasing spring component at high frequencies, as the wrist and forearm tissues are less exposed to the vibration.

The obtained results differ in several aspects from those of Lindenmann and Matthiesen (2019), who also excited the HAS rotationally at a similar frequency spectrum with an increasing acceleration (Lindenmann & Matthiesen, 2019). The phase angle of the RMI measured by Lindenmann and Matthiesen (2019) remains around 0 from 10 Hz up to almost 51 Hz. In the following, the phase angle decreases approximately linearly until it reaches the value of $-\pi$ at 201 Hz (Lindenmann & Matthiesen, 2019). Hereinafter, the phase angle shifts to the values of $-\frac{\pi}{2}$ from which it decreases again up to $-\pi$ at 500 Hz. This plot of the phase angle contradicts the phase angle plot presented by this study, as it indicates a damping characteristic of the HAS up to 51 Hz, which changes into a spring-damping dynamic at higher frequencies with an increasing spring component. The magnitude of the RMI measured by Lindenmann and Matthiesen increases across the applied frequency spectrum, indicating a mass-dominant dynamic of the HAS. The differences between the results obtained and the studies of Lindenmann and Matthiesen are probably due to the different excitation axis and the cylindrical measuring handle used by Lindenmann and Matthiesen (Lindenmann & Matthiesen, 2019). Lindenmann and Matthiesen excited the HAS with rotational vibrations around the z_h -axis. With this direction of excitation, the tangential force of the applied torque acts perpendicular to the palm and fingers, resulting in a positive locking between the hand and the cylindrical handle. Due to this stronger coupling between the hand and the handle, the HAS can move with the rotational vibration of the cylindrical handle, even at higher frequencies. This combination of the excitation axis and hand position exposes the forearm more to the rotational vibration of the handle as the hand rotation causes the forearm to twist. The twisting of the forearm increases the mass and inertia attached to the handle, resulting in an increasing mass component in the magnitude of the RMI at high frequencies, as observed by Lindenmann and Matthiesen. The increasing spring component in the phase angle plot of Lindenmann and Matthiesen can also be explained by the greater vibration exposure of the forearm muscles. Due to the positive locking between the hand, the cylindrical measuring handle, and the rotational vibration around the forearm axis, the forearm muscles are more exposed to the vibration. Thus, the stiffness of the muscles may cause the spring component to increase at high frequencies (Lindenmann & Matthiesen, 2019). In contrast, when the HAS is excited around the x_h -axis via a knob-shaped handle, the hand is not as strongly coupled to the handle, due to the applied rotational vibration acting primarily tangential to the fingers and the palm. Based on this conclusion, the results of Lindenmann and Matthiesen support the assumption that the increasing damping component in the phase angle plots in Figure 7.6 to Figure 7.9 is caused by the alignment

between the hand position and the excitation direction. From the studies of Lindenmann and Matthesen, it can be concluded that the vibration exposure of the forearm results in mass- and spring-dominated dynamics of the HAS. However, with reference to Equation 2.10, the magnitude plots in Figure 7.6 to Figure 7.9 indicate a spring characteristic that becomes a damping characteristic at high frequencies. Therefore, it can be assumed that the forearm is not as exposed to the vibration at high frequencies. Hence, it seems plausible that the increasing phase angle plots and the constant magnitude plots at high frequencies indicate a frictional decoupling in the contact between the hand and the knob-shaped measuring handle, which reduces the vibration transmission to HAS at high frequencies.

7.4.2 Influence of the gripping and push force on the RMI

Within the investigated frequency and force ranges, no influence of the push force on the RMI was detected either qualitatively or statistically. The lack of influence of the push force on the RMI could be due to the alignment between the push force direction and the excitation axis. Since the direction of the push force is oriented coaxially to the excitation axis, the rotational vibration movement on the perimeter of the handle acts perpendicular to the direction of the push force. As a result, the push force only increases the friction between the palm and the handle. This higher friction only has a small effect, due to the fact that the majority of the palm is very close to the rotational axis, resulting in a shorter lever arm. Hence, the lack of influence of the push force on the RMI of the HAS may be considered a possibility.

For the gripping force, an influence on the RMI is visible in the plots shown in Figure 7.6 and Figure 7.7, as well as in the results of the Mann-Whitney U test in Table 7.4. Hereby, the plots of the median and the interquartile ranges correspond widely to the statistical results. The plots in Figure 7.6 and Figure 7.7 show that the magnitude of the RMI is higher for a gripping force of $F_{gr} = 24\text{ N}$ than for a gripping force of $F_{gr} = 14\text{ N}$, regardless of the applied push force. The positive effect strength of the gripping force in Table 7.4 supports this observation. However, the influence of the gripping force is significant only at lower frequencies and at a few specific higher frequencies. In this context, the statistical results also correspond to the magnitude plots in Figure 7.6 and Figure 7.7 in that the Mann-Whitney-U test is not significant at frequencies where the interquartile ranges of the plots largely overlap and the medians are closer together.

Furthermore, the statistical results show that the influence of the gripping force plays a significant role at the push force level of $F_{pu} = 42.5\text{ N}$ at fewer frequencies when compared to the push force of $F_{pu} = 32.5\text{ N}$. Hence, the gripping force seems to have a fewer influence on the RMI at higher push forces. A possible reason for this

could be that some parts of the gripping force act parallel to the push force, even if the main part acts perpendicular to the push force against the sides of the knob-shaped handle, as Schröder et al. (2022) show (Schröder et al., 2022). The component of the gripping force that acts parallel to the push force primarily affects the fingertips, which are pulled toward the palm under the protruding bead of the knob-shaped handle. As this component of the gripping force is directed against the direction of the push force applied by the palm, some subjects may also have increased it subconsciously at the higher push force level, leading to a higher preloading of the hand's tissue. Since this component of the gripping force opposes the push force exerted by the palm, some subjects may have unconsciously increased it at the higher push force level, leading to a preload of the hand tissue. Due to this preloading of the hand tissue, the applied gripping force may not affect the RMI as much at a higher push force, because the palm and the fingers are tense.

As already mentioned above in this subchapter concerning the plots of the magnitude and the phase angle of the RMI, the HAS is likely to be coupled more strongly to the handle in lower frequency ranges. Consequently, the gripping force would also have a stronger influence on the RMI magnitude in this range. In consideration of the mainly frictional connection between the hand and the measuring handle, an increase of the magnitude at higher gripping forces seems reasonable. A lower gripping force is likely to result in higher sliding friction in the hand-handle contact, which would lead to greater damping of the excited vibration. A higher gripping force increases the friction between the hand and handle, resulting in a stronger coupling between the hand and handle. Therefore, less sliding friction occurs and the vibration is less damped by dissipation.

However, at certain higher frequencies, the gripping force has no significant influence on the RMI. One possible explanation for this is that the rapid handle movement at these frequencies causes sliding friction regardless of the gripping forces applied, which is why the gripping force has less influence.

In this context, the decreased significance of the gripping force at certain frequencies could also be due to the fact that the requested gripping force levels at these frequencies were more difficult to apply for some subjects. These difficulties may be due to the physical ability of some subjects to apply a constant gripping force at these specific combinations of frequency and excitation magnitude. Although an attempt was made to match the excitation magnitude to the subjects' abilities, as Figure 7.3 shows, this matching may not have been appropriate for all subjects. In this regard, in future studies, the maximal voluntary contraction (MVC) of each subject should be measured to provide an overview and comparability of the subjects' physical constitutions which would allow a more detailed interpretation of the statistical

results. In this context, the gripping force levels could also be adjusted to the personal MVC of each subject, which would allow for a comparison of the RMI in relation to the subjects' physical constitutions.

Another reason for the missing statistical evidence at certain frequencies could be that the applied gripping force levels are very light and only 10 N apart from each other, due to the subjects' physical abilities and the potential comparability to other studies. Hence, at certain frequencies, the gripping force levels may have been too light and too close together to detect significant statistical differences. In future studies, higher gripping force levels should be selected that are further apart from each other. Nevertheless, regarding the central question investigated in this paper, the results show that in the range up to 250 Hz, an increase in the gripping force results in a higher magnitude of the RMI. This overall influence of the gripping force on the RMI corresponds to the influence on the translational MI of the HAS described in the state of research (Aldien et al., 2005; ISO - International Organization for Standardization, 2012; P. Marcotte et al., 2005).

7.4.3 Relevance of the results for hand-arm modeling, power tool applications, and risk assessment

The results obtained provide an experimental basis for the parametrization of HAM for vibration excitation around the x_h -axis. For this purpose, the stiffness, damping, and inertia of the HAS modeled by a rotational single-mass oscillator can be derived from the experimental data, using Equation 2.10. A similar parametrization can also be conducted for a multibody model with more degrees of freedom. In this context, the results obtained contribute to the modeling of the dynamics of the HAS for rotational vibration excitation. Such HAM enables the numerical simulation of the vibrational interaction between the user and the power tool, which can be used in power tool development to detect and prevent harmful vibrations of the power tool under development.

The investigated connection between the hand position and the excitation axis, regarding the application of coupling forces, must also be considered in the development of power tools and the modeling of the HAS. Especially when the hand position results in a mainly frictional connection between the hand and the handle, the dynamics are different from those of a positive locking. In the case of knob-shaped handles and primarily rotational vibration excitation, a frictional connection could reduce the vibration transmission to the HAS. This conclusion may be transferred to power tool handles as such, since a mainly frictional connection between hand and handle could act as an additional way to reduce the vibration exposure of the HAS.

To validate this assumption, further studies with different handle geometries are required.

The significant effect of the gripping force on the RMI at certain frequencies suggests that the gripping of the handle more strongly reduces the frictional decoupling of the hand-handle contact, resulting in a stronger transmission of the vibration to the HAS. With regard to occupational safety and vibrational risk assessment, the RMI, or the MI in general, does not provide specific information about the harmfulness of the applied vibration. However, according to Dong et al. 2005, the MI could be used for the estimation of the absorbed power (Dong et al., 2004). Since Cundiff 1976 (Cundiff, 1976) states that the vibration energy absorption of the HAS can lead to vibration-related diseases, the magnitude of the RMI can be used as an indicator of the risk due to vibration exposure of the HAS. As a result, applying a higher gripping force potentially results in higher power absorption by the HAS, increasing the risk of vibration-related diseases. In this regard, a frictional transmission of vibration between hand and handle, as is the case with the rotational excitation of a knob-shaped handle, could reduce the risk of vibration-related diseases, because the frictional hand-handle contact decouples the vibrations. Therefore, power tools in which the alignment between the axis of vibration excitation and the hand position, resulting in frictional vibration transmission, could have a lower risk of causing vibration-related diseases, unless a strong gripping force is applied. Based on these findings, the power tool handles should possibly be designed to frictionally transmit vibration to the HAS, as this contact can provide additional damping and reduce the vibration exposure of the HAS.

Furthermore, the results suggest that the push force has no influence on the RMI for knob-shaped handles, as long as it is applied coaxially with the axis of excitation of the rotational vibration. In terms of occupational safety, when grinding with a random orbital sander equipped with a knob-shaped handle, a higher push force does not seem to increase the vibration exposure of the HAS, as long as the push force is applied coaxially to the rotation axis of the disc. However, this conclusion only refers to the rotational vibrations caused by the motor and does not take into account the vibrations caused by the grinding disc.

This realization also applies to modeling the dynamics of the HAS under rotational vibration excitation. It can be assumed that for the modeling of rotational HAM, the push force's influence must not be considered when it is applied coaxially to the rotational excitation axis and the hand is in a resting hand position, as is the case with the knob-shaped handle. However, further studies need to investigate whether this assumption regarding the alignment between the hand position and the axis of

excitation of the rotational vibration also applies to other types of power tool handles that emit rotational vibrations.

The current study provides a first approach to measure the RMI of the HAS for excitation around the x_h -axis as well as the influence of the coupling forces. In further studies, this approach must be extended to other hand positions and excitation directions. The additional experimental data of these studies would allow deriving more precise and extensive HAM. Furthermore, the risk assessment on the harmfulness of rotational vibration exposure could be improved with this data, as the assumptions on the influences of the coupling forces and the hand-handle contact could be investigated in more detail.

7.5 Limitations

The influence of the gripping force on the RMI of the HAS could be shown and statistically confirmed for certain frequencies ranging up to 250 Hz. Furthermore, the results show no influence of the push force within this range. For frequencies beyond 250 Hz, further studies have to be conducted to investigate the influence of the coupling force on the RMI at higher frequencies. Taking this into consideration, a greater difference between the gripping force levels could lead to a significant effect of the gripping force on the RMI at an increased range of frequencies. This could also increase the effect strength as well as differences between the plots of the magnitude of the RMI. These considerations regarding the applied gripping force levels also apply to the push force levels, since the lack of effect of the push force could also be caused by the small range of push force levels. Therefore, the assumption that the push force does not influence the RMI, when applied coaxially with the axis of rotation, has to be confirmed for a wider range of push forces. Furthermore, it should be mentioned that the generic design of the knob-shaped measuring handle used in the study was derived from the handle geometry of a random orbital sander. Consequently, a knob-shaped handle with a different geometry could lead to slightly different results concerning the magnitude and the phase angle of the RMI, as well as the influence of coupling forces. In this context, a rounder-shaped handle would possibly result in an even more frictional connection between the hand and the handle.

Regarding the applied coupling forces, the study also does not consider the individual constitution of the subjects and their capability to apply the requested coupling force levels. Therefore, in further studies, the maximal voluntary contraction (MVC) of each subject should be measured before the experiment, which would provide additional information about the constitution of the subjects and help to interpret the

obtained results in more detail. Based on such a measurement, the coupling force levels could be adjusted as a percentage of the MVC for each subject. This would allow for a comparison of the RMI of subjects at different physical fitness levels. Thereby, the number of trials per experiment also limits the validity of the obtained results, since each subject performed only one trial per experiment. The limitation to only one trial per subject was necessary to prevent effects resulting from subject fatigue, due to the long test duration of about 42 minutes per subject. As a result, the intra-subject variability limits the generalization of the results obtained. An attempt to balance out this limitation was done through the number of subjects participating in this study. Therefore, the lack of influence of the push force on the RMI can be regarded as more evident, since it occurred independently of the gripping force level. It can therefore be assumed that the effects of intra-subject variability do probably not cause this lack of influence. Under the assumption that the push force does not influence the RMI, the experiments on the applied gripping force can be grouped together for both push force levels, resulting in virtually two trials per subject. However, this summation is not entirely statistically correct, so more trials per subject should be performed in future studies.

7.6 Conclusion

The study shows that for rotational vibration exposure of the hand-arm system, the gripping posture³⁰ and type of connection between the hand and the vibrating handle influence the rotational mechanical impedance. Herewith, a mostly frictional connection between the hand and handle seems to reduce the vibration transmission to the upper parts of the hand-arm system. During power tool applications, vibration exposure via a frictional hand-handle connection seems to occur often, combined with rotational vibration exposure. For a knob-shaped handle, the results of the study also show that a higher gripping force leads to an increasing magnitude of the rotational mechanical impedance, since the friction between the hand and the rotational vibrating handle increases. The push force instead, does not influence the rotational impedance, at least when it is applied coaxially to the rotational axis of the vibration. Regarding occupational safety against rotational vibration exposure, the results suggest that handle geometries, which are based on the mostly frictional connection between hand and handle, could reduce the vibration exposure of the hand-arm system, while an increasing gripping force seems to increase the vibration exposure.

³⁰ In this context the term “gripping posture” is used synonymously for hand position

When simulating the dynamics of the hand-arm system, the influence of the gripping force as well as the interaction between the gripping posture and the connection between the hand and handle must also be considered.

7.7 Acknowledgment

This work was supported by the German research foundation Deutsche Forschungsgemeinschaft (DFG) under the funding numbers 408254169 and 275571425. The authors of this publication are responsible for its content. We want to thank the DFG for funding and the support of our research, which enabled this publication. We would like to emphasize that the presented results and conclusions do not necessarily reflect the opinion of the DFG."

7.8 Thesis specific conclusion

In the following, it will be assessed whether and to what extent the results and findings of the study presented in this chapter contribute to the investigation of **Hypothesis 2: Rotational impedance around the x_h -axis**. The study was pre-published in the *Journal of Industrial Ergonomics* under the title *Influence of coupling forces on the mechanical impedance of the hand-arm system during rotational vibration excitation around the x_h -axis*. The assessment is based on how the conducted study answer the corresponding sub-research questions of the hypothesis.

Hypothesis 2: Rotational impedance around the x_h -axis

The rotational mechanical impedance for excitations around the x_h -axis in the „hand-grip“ position is influenced by the applied gripping force, push force.

- **Sub-research question 2.1:** What is the course of the magnitude and the phase angle of the RMI for rotational vibration excitation around the x_h -axis via a knob-shaped handle in the “palm” position?
 - Based on the results of the presented study, it was possible to determine the course of the magnitude and the phase angle of the RMI for rotational vibration excitation around the x_h -axis in the “palm” position, as shown in the plots in Figure 7.6 to Figure 7.9. From the course of the magnitude and the phase angle, a superimposed spring-damper dynamic of the HAS with increasing damper component could be concluded. Thus **sub-research question 2.1** can be regarded as answered.

- **Sub-research question 2.2:** How is the magnitude of the RMI influenced by the applied gripping force?
 - The results of the study indicate that a higher gripping force increases the magnitude of the RMI, as shown in the plots in Figure 7.6 to Figure 7.9 and the statistical results in Table 7.4. In the following **sub-research question 2.2** can be regarded as answered.
- **Sub-research question 2.3:** How is the magnitude of the RMI influenced by the applied push force?
 - For the applied push force instead no influence on the magnitude of the RMI could be determined. Based on the obtained results of the study **sub-research question 2.3** can be answered to the effect that the magnitude of the RMI is not influenced by the push force.

By answering these sub-research questions, **Hypothesis 2: Rotational impedance around the x_h –axis** can be considered as investigated. The obtained results show that the RMI for vibration excitation around the x_h –axis in the “palm” position is influenced by the applied gripping force but not by the applied push force. Based on these results, conclusions were drawn, regarding the influence of the hand-handle contact on the RMI. In this context the first approach of an explanation model was developed, describing the damping influence of a primarily frictional hand-handle contact in relation to the RMI as well as the alignment between excitation direction and push force direction.

8 Study on Hypothesis 3: Rotational impedance around the y_h –axis

8.1 Thesis specific introduction

In order to achieve the objective of this thesis, the following chapter will answer the research questions, which is linked to the **Hypothesis 3: Rotational impedance around the y_h –axis**. By answering the sub research questions the hypothesis can be regarded as investigated. The hypothesis and the corresponding research questions from Subchapter 5.1 are:

Hypothesis 3: Rotational impedance around the y_h –axis

The rotational mechanical impedance for excitations around the y_h -axis in the „hand-grip“ position is influenced by the applied gripping force, push force and body posture and the observed effects are comparable to hypothesis 2.

- **Sub-research question 3.1:** What is the course of the magnitude and the phase angle of the RMI for rotational vibration excitation around the y_h –axis in the “hand-grip” position and can this course be related to the excitation around the x_h –axis in the “palm” position?
- **Sub-research question 3.2:** How is the magnitude of the RMI influenced by the applied gripping force and can this influence be related to the excitation around the x_h –axis in the “palm” position?
- **Sub-research question 3.3:** How is the magnitude of the RMI influenced by the applied push force and can this influence be related to the excitation around the x_h –axis in the “palm” position?
- **Sub-research question 3.4:** How is the magnitude of the RMI influenced by the body posture?

According to the structure of the thesis described in Subchapter 1.2 and the research design from Subchapter 5.2 the research questions from Subchapter 5.1 are answered by a subject study in the following Chapter 8. The presented study was pre-published in the Journal *MDPI Vibration* entitled *Influence of Coupling forces and Body Posture on the Rotational Hand-Arm Impedance in y_h –Direction* (Schroter, Lindenmann, & Matthiesen, 2023).

Chapter 8 presents the measurement of the RMI of the HAS for rotational vibration excitation around the y_h -axis in the “hand-grip” position, regarding the influence of the gripping force, the push force and the body posture. In addition Chapter 8 serves as a reference to investigate the transferability of the findings and conclusions of Chapter 7.

These findings here focus on the effects of hand-handle contact on the RMI derived from the influence of gripping force, as well as the lack of influence of the push force on the RMI, which is likely caused by the alignment between hand position and excitation axis. Although the excitation axis is different in the studies from Chapter 7 and Chapter 8, the orientation of the excitation axis to the hand position and the resulting hand-handle contact are comparable. Both when excited around the x_h -axis via the knob-shaped handle and when excited around the y_h -axis via the cylindrical handle, the handle oscillates angularly, in the enclosing hand, with the excitation axis aligned perpendicular to the axis of the forearm. Hence the vibration is mainly transferred to the HAS via the frictional contact between hand and handle. This explained comparability between the two hand positions is shown again schematically in Figure 8.1.

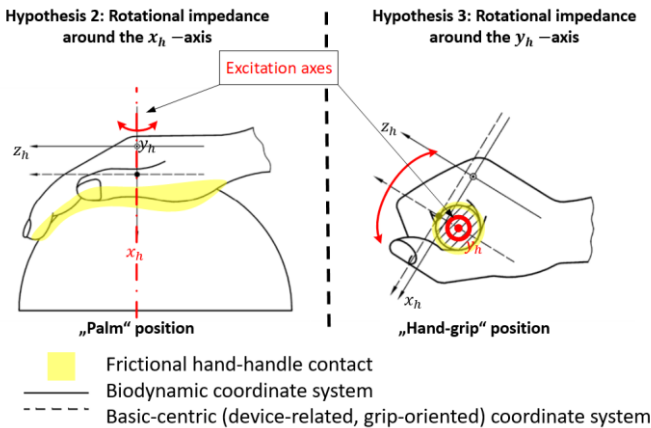


Figure 8.1: Comparison of the frictional closure hand and handle for the rotational excitations in the "palm" position investigated in Chapter 7 and for the excitations in the "hand-grip" position investigated in Chapter 8 based on the figures from DIN EN ISO 5349-1

In Chapter 7 this frictional contact was assumed to have a damping effect on the RMI, while a higher gripping force reduces this damping and leads to higher magnitude of the RMI. However, the knob-shaped handle used in Chapter 7 had an elliptical cross-sectional area, which is why a partially positive connection between the hand and handle can also be assumed. The cross-sectional area of the cylindrical handle is round, so that an exclusively frictional connection between the hand and the handle can be assumed.

If the damping effect on the RMI magnitude is caused by the friction between the hand and the handle, this damping effect must be even higher for the cylindrical handle. The same applies to the influence of the gripping force on the RMI, which must correspond to those observed for excitation via the knob-shaped handle, since it increases the friction in the hand-grip contact. As for the push force, the results of Chapter 7 show that the push force has no influence on the RMI, since it acts coaxially to the excitation axis when the palm pushes against the top of the knob-shaped handle.

Based on this coaxial alignment, it was concluded in Chapter 7 that a higher push force does not lead to a stronger coupling of the HAS against the vibrational motion, therefore the push force has no influence on the RMI. This alignment also applies to the rotational vibration excitation of the HAS around the y_h -axis via the cylindrical measuring handle, as the hand pushes the handle down in the direction of the longitudinal axis of the cylinder. Thus if the assumptions regarding the alignment between excitation axis and the direction of the push force are correct, no influence of the push force in the RMI should be detectable even when the excitation is around the y_h -axis via the cylindrical handle.

In order to extend the knowledge on the RMI in y_h -direction as well as to check the transferability of the findings from Chapter 7 a cylindrical measuring handle was manufactured according to ISO 10819.

The measuring handle consists of GRP with an aluminum plate in each half of the handle, between which two force transducers (8435, Burster GmbH & co kg, Gernsbach, Germany) were mounted. The measuring handle was attached to the measuring flange of the shaker test bench from Matthiesen et al. (2018) via the same aluminum adapter component used for the knob-shaped measuring handle in Chapter 7. When the unloaded, empty handle was measured, a natural frequency at 127 Hz was detected, although this natural frequency was not previously detected in the simulative modal analysis using Ansys (Ansys Inc. Canonsburg, Pennsylvania, USA). For this reason the RMI of the HAS was only analyzed up to a frequency of 100 Hz in the study conducted.

This frequency range is smaller than the one observed for the excitation around the x_h -axis in Chapter 7. Nevertheless, the two studies are comparable up to 100 Hz, especially since the effect of gripping force on RMI in Chapter 7 was significant mainly at frequencies below 100 Hz, as shown in Table 7.4. In Chapter 7, no significant effect on RMI was found for the push force at any frequency, so this lack of significance up to 100 Hz can also be verified and investigated in the following Chapter 8.





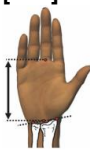

The following subchapters: 8.2 *Methods*, 8.3 *Results*, 8.4 *Discussion*, 8.5 *Limitations*, 8.6 *Conclusion* and are full citations from the publication *Influence of Coupling forces and Body Posture on the Rotational Hand-Arm Impedance in y_h -Direction* (Schröder, Lindenmann, & Matthiesen, 2023). For this purpose, the numbering of the chapters, figures and tables were adapted to the numbering of the thesis. Furthermore, the heading *Material and Methods* of the corresponding subchapter has been changed to just *Methods* in order to keep the headings of the sub-chapters constant within the thesis.

8.2 Methods

8.2.1 Test Subjects

“A total of 15 subjects (4 female, 11 male) participated in the study, with an age range of 20 to 30 years and a median age of 28 years. The height and weight as well as their anthropometric properties were measured according to DIN EN ISO 7250-1 (DIN - Deutsches Institut für Normung, 2017). Accordingly, it was determined that the height of the subjects ranged from 1.66 m to 1.93 m with a median height of 1.85 m. The subjects' weights were within the range from 52 kg to 105 kg, with a median weight of 80 kg. Based on this weight and height distribution, the body mass index of the subjects ranged from 18 kg/m² to 29.7 kg/m², with a median of 24.3 kg/m². Table 8.1 shows the 5th and the 95th percentiles as well as the median of the subjects' anthropometric properties.

Table 8.1: Median, upper and lower quartiles of the subjects' anthropometric properties.

	 Arm length [cm]	 Forearm length [cm]	 Thumb length [mm]	 Hand length [mm]	 Palm length [mm]	 Hand width [mm]
Median	76	37	70	195	105	85
5th percentile	68.5	31.4	65	173	93	76
95th percentile	81.4	41	79	205	115	95

To determine whether the measured weights, heights, and anthropometric properties were representative of the western population, the measured subject data were compared to the country-specific distributions of DIN; CEN; ISO 7250-2 (DIN Deutsches Institut für Normung e. V. & ISO - International Organization for Standardization, 2013). Since the measured anthropometric properties are not available for each country in DIN; CEN; ISO 7250-2, the measured subject data were selectively compared to the nations from which the specific measurements were reported (DIN Deutsches Institut für Normung e. V. & ISO - International Organization for Standardization, 2013). In this context, the measured subject data corresponded to the distributions from the Netherlands, Germany, Austria, and the USA, where the measured values were located between the 5th and 95th percentiles or between the 1st and 99th percentiles (DIN Deutsches Institut für Normung e. V. & ISO - International Organization for Standardization, 2013). Accordingly, the weight, height, and anthropometric properties of the subjects can be regarded as being representative of the western population and thus, most likely, the measured RMI.

8.2.2 Test Apparatus

The test bench used in this study is the same as those described in (Lindenmann et al., 2022; Lindenmann & Matthiesen, 2019; Mangold, 2019; Matthiesen et al., 2018; Schröder, Lindenmann, Resch, et al., 2023) and consists of two independent, electromagnetic shakers (M124M and L125M; ETS Solutions Europe, Loffenau, Germany) that were adjustable in terms of height and tilt angle via a carrier mechanism. The carrier mechanism consists of two spindles driven by two electric motors, which can adjust the height of the shakers from 0 m up to about 2.8 m. The tilt angle could

be adjusted by two electric motors that allow the shakers to be tilted at an angle of 0° to 180°.

Both shakers are attached to a common output shaft, where one shaker (M124M) can vibrate the shaft translationally and the other one can vibrate the shaft rotationally (L125M) via a modally tuned gearbox. The gearbox consists of a rack-and-pinion gear. The rack is mounted on the L125M shaker, while the pinion gear is radially mounted on the output shaft via a splined connection. This arrangement converts the translational vibration of the L125M shaker into a rotational vibration of the output shaft. The splined connection allows for axial movement of the output shaft with simultaneous rotational vibration, allowing the M124M shaker to excite the output shaft translationally parallel to the rotational excitation. This allows the output shaft to be excited with superimposed rotational and translational vibrations. However, in the study conducted, only the L125M shaker was used to apply rotational vibrations to the output shaft. Figure 2.1 shows an annotated schematic of the carrier mechanism and the gearbox with the shaker arrangement.

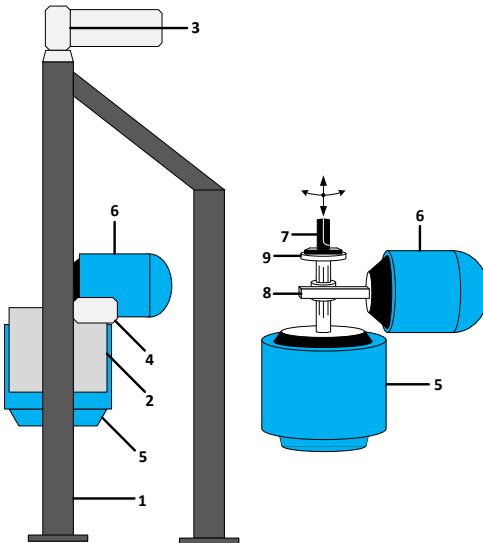


Figure 8.2: Illustrations of the carrier mechanism and the shaker system. **Key:** 1. Frame, 2. holder of the shakers, 3. electric motor for height adjustment, 4. electric motor for tilt angle adjustment, 5. translational shaker, 6. rotational shaker, 7. measuring handle, 8. rack and pinion gear, and 9. measuring flange.

An instrumented measuring flange was attached to the output shaft. The sensors of the measuring flange consist of two 3D force transducers (9027C; Kistler Instrumente AG, Winterthur, Switzerland) and two 3D accelerometers (PCB 356A15; PCB Piezotronics, Depew, NY, USA). The force transducers can measure the torque of the provided vibrations and the push force applied by the subjects. For our study, we equipped the measuring flange with a cylindrical measuring handle, which is depicted in Figure 3. According to the measurement handle design proposed in ISO 10819, we measured the gripping force of the subject by dividing the handle into two half-cylinders and placing two force sensors between them (8435, Burster GmbH & co kg, Gernsbach, Germany) (ISO - International Organization for Standardization, 2013). As proposed in ISO 10819, the division of the cylindrical handle is oriented orthogonally to the axis of the forearm when the handle is gripped. To produce rotational vibration around the y_h -axis according to the coordinate system in Figure 2.4³¹ from ISO 10068, a handle connection position different from that in ISO 10819 was used. ISO 10819 proposes a connection position at the front of the cylindrical handle in the extension of the forearm axis through a bracket-like support. In contrast, we connected the bottom of the cylindrical handle to the flange of the shaker. Hence, the handle oscillated rotationally around its axis when excited. Figure 8.3 shows a photo and a schematic drawing of the measuring handle used in the study.

³¹ In the original publication, the figure refers to Figure 1.1, which is part of the introduction to the publication and is not cited in this thesis. Therefore, the reference has been changed to Figure 2.4, which is equivalent to the original.

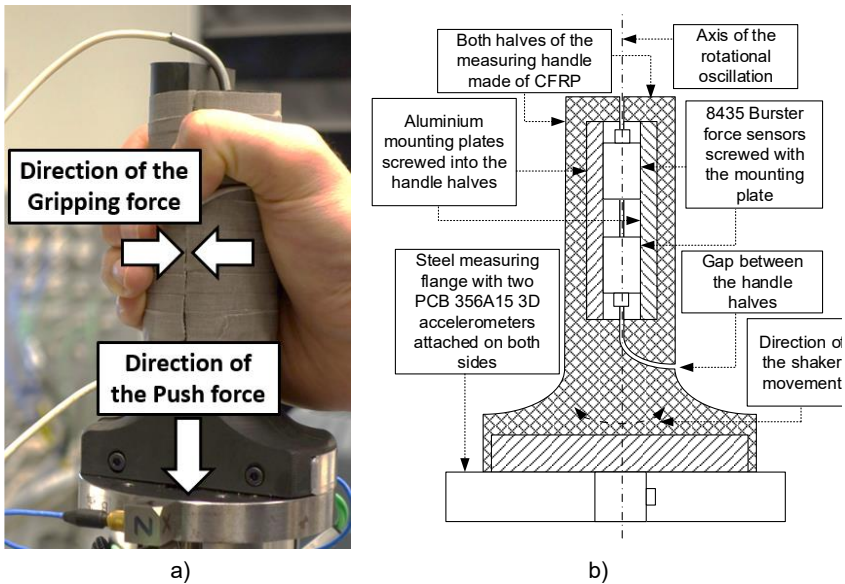


Figure 8.3: a): A photo of the handle used in the study. b): A schematic of the measuring handle

As visible in Figure 8.3 the measuring handle is wrapped with adhesive tape. This was necessary to increase the friction of the handle's surface. To calibrate the measuring handle, we measured the apparent mass of the unloaded measuring handle with the same frequency spectrum and acceleration magnitudes that we later used in the study. The applied frequency spectrum is based on the spectrum described in ISO 10068 and consists of the third octave band frequencies of up to 100 Hz. The pre-studies showed that exciting the measuring handle with a constant acceleration magnitude across the entire frequency spectrum results in a rapid angular deflection of the measuring handle at low frequencies. Due to this angular deflection, subjects had difficulty applying a constant gripping force to the handle at low frequencies. On the other hand, a low acceleration amplitude at high frequencies was very difficult to detect amongst the measurement noise. As a result, the excitation magnitude was adjusted to the applied frequencies to match the subjects' abilities. Therefore, the applied acceleration was increased approximately linearly from an RMS value of $3.2 \frac{m}{s^2}$ ($67.6 \frac{rad}{s^2}$) at 10 Hz to up to an RMS value of $50 \frac{m}{s^2}$ ($1027.5 \frac{rad}{s^2}$) at 100 Hz. A similar acceleration profile has already been used by Schröder, Lindenmann, Resch, et al. (2023) and Lindenmann and Matthiesen (2019), who also adjusted the applied acceleration magnitude to the frequency spectrum due to the rapid angular motion of

the handle at low frequencies (Lindenmann & Matthiesen, 2019; Schröder, Lindenmann, Resch, et al., 2023). Furthermore, comparable approaches were also used in translational MI measurements (Burström, 1997) (DIN Deutsches Institut für Normung e. V., 2019). The calibration of the measuring handle was conducted with the same frequency-weighted magnitudes that we applied to the subjects in the study. For calibration, we vibrated the measuring handle in three trials with these frequency-weighted acceleration magnitudes. The deviation between the three trials in terms of the apparent mass and phase angle of the handle was less than 1 % at each applied frequency. Figure 8.4 shows the magnitude of the measuring handle's apparent mass over the excited frequencies' spectra and the corresponding phase angle.

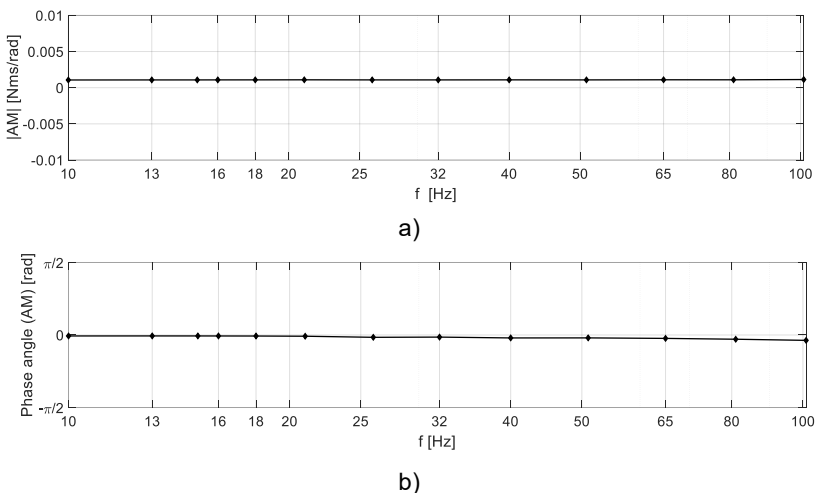


Figure 8.4: Calibration measurement of the measuring handle's apparent mass determined for the frequencies excited in the study. The magnitude (a) and phase angle (b) of the apparent mass indicated the dynamic characteristic of a constant mass, without any natural frequencies, as their value is almost the same for every excited frequency.

Across the entire applied spectrum, the magnitude of the apparent mass in Figure 8.4 is constant at $1.07 \cdot 10^{-3} \frac{Nms}{rad}$ and the phase angle is almost constant at 0. Since both have approximately the same values across at every applied frequency, no natural frequencies of the handle are excited by the applied spectrum. Thus, the

measuring handle has the dynamic characteristic of a constant mass. This vibrational characteristic is suitable for the measurement of the MI, because it does not disturb the measurements according to its resonances.

A graphical display provided a visual feedback of the applied push force and gripping force to the subjects. The display with the visual force feedback is visible in Figure 8.5.

The measured data were recorded using an ADwin Pro II real time measurement and control system (Jaeger Computergesteuerte Messtechnik GmbH, Lorsch, Germany) with a record frequency of 10 kHz.

8.2.3 Test Procedure

This research complied with the tenets of the Declaration of Helsinki, and the subjects' approval was acquired (World Medical Association, 2013). At the beginning of the test procedure, the subjects were informed about the duration and nature of the procedure. Subsequently, the anatomical and anthropometric characteristics of the subject were noted, as described in Subchapter 8.2.1 The RMI values of the subject's HASs were measured for two different body postures. The first posture corresponded to that presented in the work of Dong et al. (2006); here, the subject stood and gripped the handle with an angled arm position of ninety degrees (Dong, Welcome, & McCormick, 2006). In the second posture, the subject sat on a chair and gripped the handle with an outstretched arm. The first posture was chosen as a reference to the literature in order to achieve comparability. The second posture was based on the working position at seated workplaces when working with an inline impact wrench. In this context, the design of the test allowed for the gripping of the measuring handle in a sitting position only if the arm of the subject was extended. To keep the boundary conditions constant for each subject, we adjusted the height of the shaker to the subject's height individually using a carrier mechanism. Both body postures are visible in Figure 8.5.

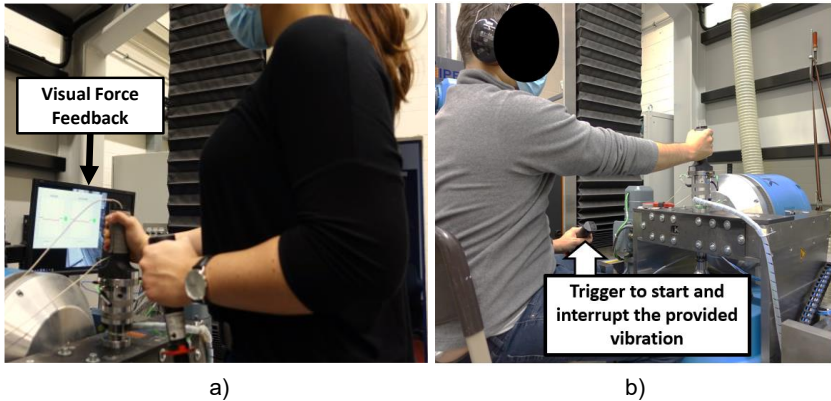


Figure 8.5: Body postures in which the RMI of the subjects was measured: standing posture with angled arm (a), sitting with extended arm (b). The left side also shows the display with the visual force feedback

Before exciting the HAS of the subject with the rotational vibrations, the maximum gripping force of each subject in both body postures was measured. Table 8.2 shows the distribution of the subjects' maximum gripping forces.

Table 8.2: Distribution of the maximum gripping forces of the subjects in each body posture.

Body Posture	Minimum	Lower Quartile	Median	Upper Quartile	Maximum
Sitting	153.0 N	316.4 N	411.7 N	418.9 N	556.6 N
Standing	148.1 N	189.0 N	351.6 N	409.2 N	611.3 N

In each body posture, the magnitude and phase angle of the RMI across the applied frequency spectrum was recorded for five factor combinations of gripping and push forces. Thereby, the five factor combinations had a partwise full-factorial character, combining low and high gripping forces with low and high push forces and vice versa. In addition, each subject applied a factor combination of 24 N gripping force and 50 N push force to extend the number of push force levels examined and determine its influence for a wider range. No further, lower gripping force level was applied at the 50 N push force level since this push force requires a certain amount of gripping force to prevent slippage on the cylindrical grip. Table 8.3 provides an overview of the different factor combinations that the subject had to perform in each posture.

Table 8.3: Overview of the different factor combinations assessed in this study

Level	Body Posture	Gripping Force (F_{gr})	Push Force (F_{pu})
Full factorial			
1	Standing	$F_{gr} = 5.5\text{ N}$	$F_{pu} = 15\text{ N}$
2		$F_{gr} = 24\text{ N}$	$F_{pu} = 32.5\text{ N}$
3		$F_{gr} = 24\text{ N}$	$F_{pu} = 50\text{ N}$
Full factorial			
1	Sitting	$F_{gr} = 10\text{ N}$	$F_{pu} = 15\text{ N}$
2		$F_{gr} = 24\text{ N}$	$F_{pu} = 32.5\text{ N}$
3		$F_{gr} = 24\text{ N}$	$F_{pu} = 50\text{ N}$

In the sitting posture, the value of the gripping force level was increased to $F_{gr} = 10\text{ N}$ since most subjects were not capable of applying the factor combination of 5.5 N gripping force at 32.5 N push force to the cylindrical handle while assuming this position. The additional factor combination of 32.5 N push force and 24 N gripping force was chosen to achieve comparability with the study by Schröder, Lindenmann, Resch, et al., 2023 (Schröder, Lindenmann, Resch, et al., 2023). For each factor combination, the frequencies from Figure 2.2 were applied to the measuring handle in random order as single sine signals with their respective vibration magnitudes. The order of the factor combinations itself was also randomized. Each frequency had a duration of seven seconds with a subsequent pause of 5 s, resulting in 187 s per subject for 1 factor combination and a test duration of 32 min for all 10 factor combinations. To prevent subjects' fatigue, a break of at least 10 min was taken after each factor combination. Furthermore, the subject could interrupt the vibration excitation at any time by releasing a hand trigger. When the subject pressed the trigger again, the vibration excitation continued at the point of interruption. In consideration of the users' fatigue and the experimental time per subject, we performed only one trial per subject and factor combination. Table 8.4 shows the mean percentage deviation between the applied gripping and push forces and the requested force levels of the factor combinations across all frequencies and subjects. For the applied push force levels and the gripping force level of $F_{gr} = 24\text{ N}$, the mean percentage deviation was calculated as common value of both body postures.

Table 8.4: Mean percentage deviation between the applied gripping and push forces and the predefined force levels across all frequencies and subjects. Gripping force: F_{gr} ; push force: F_{pu} .

Specified coupling forces	$F_{pu} = 15\text{ N}$	$F_{pu} = 32.5\text{ N}$	$F_{pu} = 50\text{ N}$
$F_{gr} = 5.5\text{ N}$	$\Delta\bar{F}_{gr} = 2.1\%$	$\Delta\bar{F}_{gr} = 7.3\%$	-
	$\Delta\bar{F}_{pu} = 1.1\%$	$\Delta\bar{F}_{pu} = 4.7\%$	
$F_{gr} = 10\text{ N}$	$\Delta\bar{F}_{gr} = 1.1\%$	$\Delta\bar{F}_{gr} = 2.9\%$	-
	$\Delta\bar{F}_{pu} = 1.8\%$	$\Delta\bar{F}_{pu} = 3.0\%$	
$F_{gr} = 24\text{ N}$	$\Delta\bar{F}_{gr} = 1.3\%$	$\Delta\bar{F}_{gr} = 1.1\%$	$\Delta\bar{F}_{gr} = 1.6\%$
	$\Delta\bar{F}_{pu} = 0.9\%$	$\Delta\bar{F}_{pu} = 2.0\%$	$\Delta\bar{F}_{pu} = 2.6\%$

8.2.4 Data Evaluation

Out of 15 subjects, we evaluated the data from 13, as two subjects ceased their participation in the experiment due to fatigue. Of the remaining 13 subjects, the RMI of the HAS was measured for 10 different factor combinations of gripping force, push force, and body posture, resulting in 130 evaluable experiments. The recorded data were evaluated using MATLAB (The MathWorks, Inc, Natick, MA, USA) and SPSS (IBM SPSS Statistics 25, IBM, Armonk, NY, USA). The calculation of the magnitude and phase angle of the RMI was conducted according to a method described by Lindenmann et al. (2019) (Lindenmann & Matthesen, 2019). First, the excited frequencies were determined using a fast Fourier transformation. Then, the torque and acceleration data were iteratively filtered with a Butterworth band pass filter, whose cutoff frequencies were 0.8 and 1.2 of the determined frequency, respectively. For each frequency, the filtered torque and acceleration data were fitted with a curve-fitting algorithm that determines the corresponding amplitudes as complex values. Based on the results of curve fitting, the magnitude and phase angle of the RMI were calculated for the specific frequency using equation 1. To compensate for the influence of the measuring handle on the calculated RMI, the calibrated RMI of the measuring handle from Figure 4 was subtracted from the results (Dong, Welcome, McDowell, & Wu, 2006). The calculated RMI was grouped according to the applied factor combinations in ten groups. For each group, we determined the arithmetic mean of the RMI's magnitude and phase angle across the applied frequencies. The Shapiro–Wilk test did not indicate a normal distribution of the calculated RMI. Therefore, we used the Mann–Whitney U test (MWU) and the Kruskal–Wallis test (KWT) in SPSS to statistically determine the influence of coupling forces and the body posture on the RMI. The significance level of the tests was $\alpha = .05$. The effect strength r according to was calculated where $r \leq .30$ was considered low, $.30 < r < .50$ was considered moderate, $r \geq .50$ was considered as being high (Cohen, 1992).

8.3 Results

8.3.1 Influence of the Gripping Force on the RMI

Figure 8.6 shows the magnitude of the RMI as boxplots at different gripping force levels applied in the standing and the sitting postures at a push force of $F_{pu} = 15\text{ N}$ and $F_{pu} = 32.5\text{ N}$. Figure 8.7 shows the corresponding boxplots of the phase angle. The factor combination $F_{pu} = 50\text{ N}$ and $F_{gr} = 24\text{ N}$ is not shown in the figures, since only one gripping force level was applied at $F_{pu} = 50\text{ N}$.

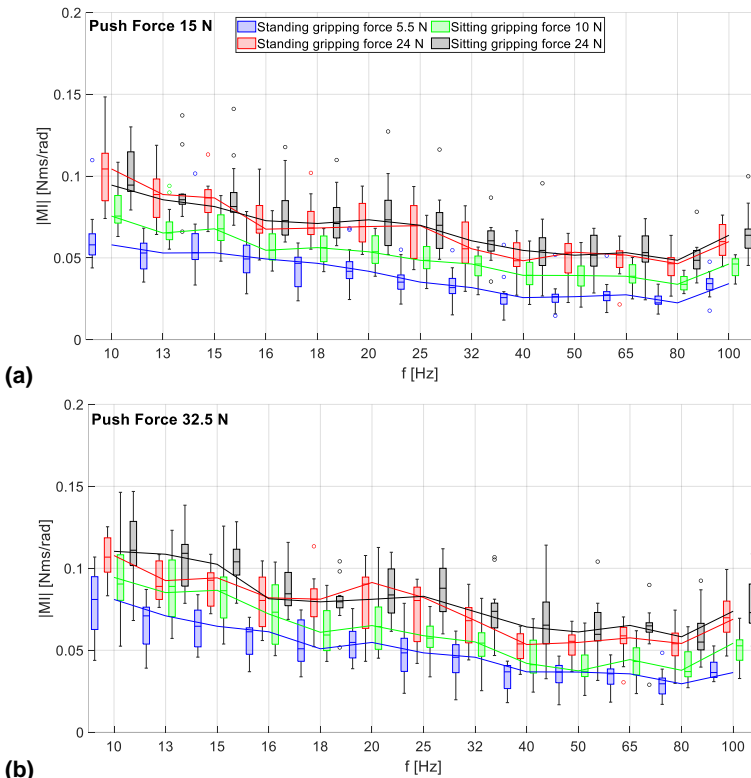


Figure 8.6: Boxplots and median trend lines of the magnitude of the RMI at gripping forces of $F_{gr} = 5.5\text{ N}$ and $F_{gr} = 24\text{ N}$ (standing posture) and $F_{gr} = 10\text{ N}$ (sitting posture) at a push force of $F_{pu} = 15\text{ N}$ (a) and $F_{pu} = 32.5\text{ N}$ (b).

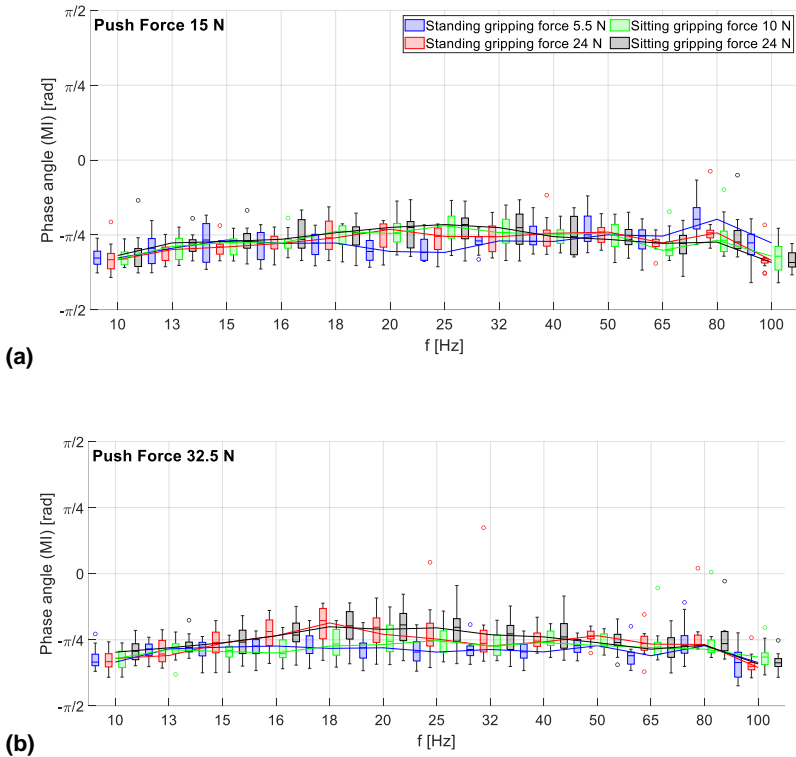


Figure 8.7: Boxplots and median trend lines of the RMI phase angle for gripping forces of $F_{gr} = 5.5\text{ N}$ and $F_{gr} = 24\text{ N}$ (standing posture) and $F_{gr} = 10\text{ N}$ (sitting posture) at a push force of $F_{pu} = 15\text{ N}$ (a) and $F_{pu} = 32.5\text{ N}$ (b).

For all applied factor combinations, the magnitude trend line of the RMI in Figure 8.6 decreases across the frequency spectrum from 10 Hz up to 80 Hz and increases again at 80 Hz. In this case, the magnitudes at a 32.5 N push force are slightly higher overall and have a larger interquartile range than at 15 N push force. Comparing the boxplots in Figure 8.6, the magnitude of the RMI increases at higher gripping force levels, being highest at a gripping force of $F_{gr} = 24\text{ N}$ in the sitting posture and lowest at a gripping force of $F_{gr} = 5.5\text{ N}$ in the standing posture.

In Figure 8.7, the boxplots and the trend lines of the phase angles of all the factor combinations in both plots increase slightly linearly from approximately $-\frac{\pi}{3}$ at 10 Hz to up to $-\frac{\pi}{4}$ at 16 Hz. Subsequently, the plots proceed to increase almost constantly to up to 80 Hz at a value of approximately $-\frac{\pi}{4}$. At 100 Hz, the phase angle plots of all factor combinations drop to a value of approximately $-\frac{\pi}{3}$. The interquartile range and height of the whiskers are roughly similar for all factor combinations and frequencies. Following the boxplots from Figure 8.6, Table 8.5 shows the results of the MWU regarding the influence of the gripping force on the RMI magnitude at the different push force levels and body postures.

Table 8.5: Overview of the different factor combinations performed in the study

Push Force:	$F_{pu} = 15\text{ N}$				$F_{pu} = 32.5\text{ N}$			
	Standing		Sitting		Standing		Sitting	
Body Posture:	$F_{gr} = 5.5\text{ N}$		$F_{gr} = 10\text{ N}$		$F_{gr} = 5.5\text{ N}$		$F_{gr} = 10\text{ N}$	
Gripping Force:	$F_{gr} = 24\text{ N}$		$F_{gr} = 24\text{ N}$		$F_{gr} = 24\text{ N}$		$F_{gr} = 24\text{ N}$	
f [Hz]	p	r	p	r	p	r	p	r
10	<.001*	.769	.002*	.578	<.001*	.704	.081*	-
13	<.001*	.840	.002*	.578	<.001*	.715	.057*	.377
15	<.001*	.699	.002*	.598	<.001*	.704	.014*	.478
16	.001	.629	.001*	.629	.002*	.597	.113*	-
18	<.001*	.840	.001*	.629	<.001*	.672	.002*	.578
20	<.001*	.709	.004*	.548	.001*	.640	.014*	.478
25	<.001*	.769	.002*	.588	.001*	.619	<.001*	.709
32	<.001*	.689	.001*	.619	<.001*	.651	.005*	.538
40	<.001*	.719	.005*	.538	<.001*	.661	.006*	.528
50	<.001*	.699	.006*	.528	<.001*	.725	.005*	.538
65	<.001*	.689	.002*	.588	<.001*	.715	<.001*	.689
80	<.001*	.800	<.001*	.749	<.001*	.736	.005*	.538
100	<.001*	.830	<.001*	.811	<.001*	.779	<.001*	.749

For nearly all factor combinations of push force and body posture, Table 5 shows a significant degree of causality between the gripping force and the RMI up to 100 Hz with a high effect strength. The only factor combination for which significance was not shown at the 13 Hz and 16 Hz frequencies was at a push force of $F_{pu} = 32.5\text{ N}$, applied in a sitting position. The (*) at the bold p-values denotes that the influencing factor has a significant effect on the RMI.

8.3.2 Influence of the Push Force on the RMI

Figure 8.8 shows the RMI's magnitude and phase angle for the push force levels of $F_{pu} = 15\text{ N}$, $F_{pu} = 32.5\text{ N}$, and $F_{pu} = 50\text{ N}$ at a gripping force of $F_{gr} = 24\text{ N}$ exerted in the standing posture as boxplots with the median plotted as a trend line. Besides the plots in Figure 8.8 regarding the standing body posture, the influence of the push force was also evaluated for the sitting position and a gripping force of $F_{gr} = 24\text{ N}$.

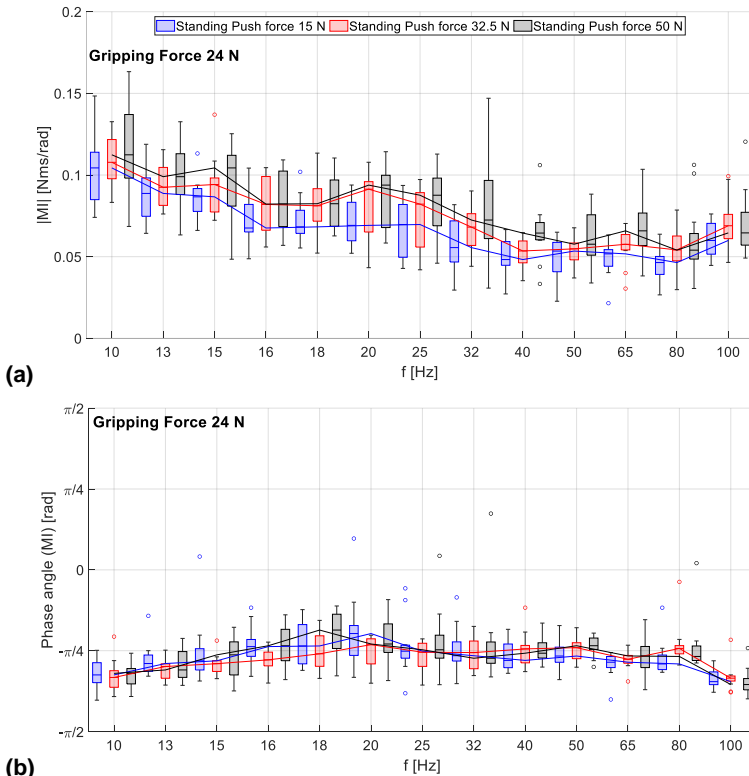


Figure 8.8: Boxplots and median trend line of the RMI's magnitude (a) and phase angle (b) for push forces of 15 N, 32.5 N, and 50 N at a gripping force of $F_{gr} = 24\text{ N}$ provided in the standing posture.

In Figure 8.8, a slight offset between the trend lines and the boxplots of the RMI's magnitude at a 50 N push force and at a 15 N push force is detectable across the entire spectrum. Between the push forces of $F_{pu} = 50\text{ N}$ and $F_{pu} = 32.5\text{ N}$, no clear offset is detectable since the boxplots of both factor combinations overlap. Overall,

the boxplots of the magnitude and the phase angle show larger interquartile ranges and whisker heights at higher push forces, with the boxplots at 50 N of push force showing the largest interquartile range at almost every frequency. In particular, the boxplot of the $F_{pu} = 50\text{ N}$ push force at 32 Hz has a relatively large whisker. Regarding the phase angle of the RMI in Figure 8.8, all three boxplots and the corresponding trend lines increase slightly linearly up to $-\frac{\pi}{4}$ at 16 Hz. From 16 Hz up to 80 Hz, the phase angle plots remain nearly constant at $-\frac{\pi}{4}$. At 100 Hz, all three phase angle plots drop to $-\frac{\pi}{3}$. Regarding the applied factor combinations, the interquartile ranges and the whisker heights of the boxplots of the three phase angles do not show any general differences with respect to one another, neither in their sizes nor in their positions. To check for possible causalities between the push force and the magnitude of the RMI, a KWT was performed with the data plotted in Figure 8.8. The results of the KWT were only significant at the frequencies of 40 Hz, 65 Hz, and 80 Hz. A subsequent Bonferoni-corrected pairwise comparison was significant at the frequencies of 40 Hz and 65 Hz for the change of the push force from $F_{pu} = 15\text{ N}$ to $F_{pu} = 50\text{ N}$. For the sitting posture, no influence of the push force could be detected by the KWT either, even at individual frequencies. However, the plots of the magnitude and phase angle of the RMI across the applied frequency spectrum were similar to those in Figure 8.8 .

8.3.3 Influence of the Body Posture on the RMI

The boxplots in Figure 8.9 visualize the influence of standing and sitting postures on the magnitude and phase angle of the RMI for the factor combination of 24 N of gripping force and 50 N of push force. For the plots represented in Figure 8.9, the highest coupling forces were chosen to show that even with these strong couplings between the HAS and the vibration source, no influence of the body posture is visible. Nevertheless, the influence of body posture on RMI was also evaluated for lower coupling forces.

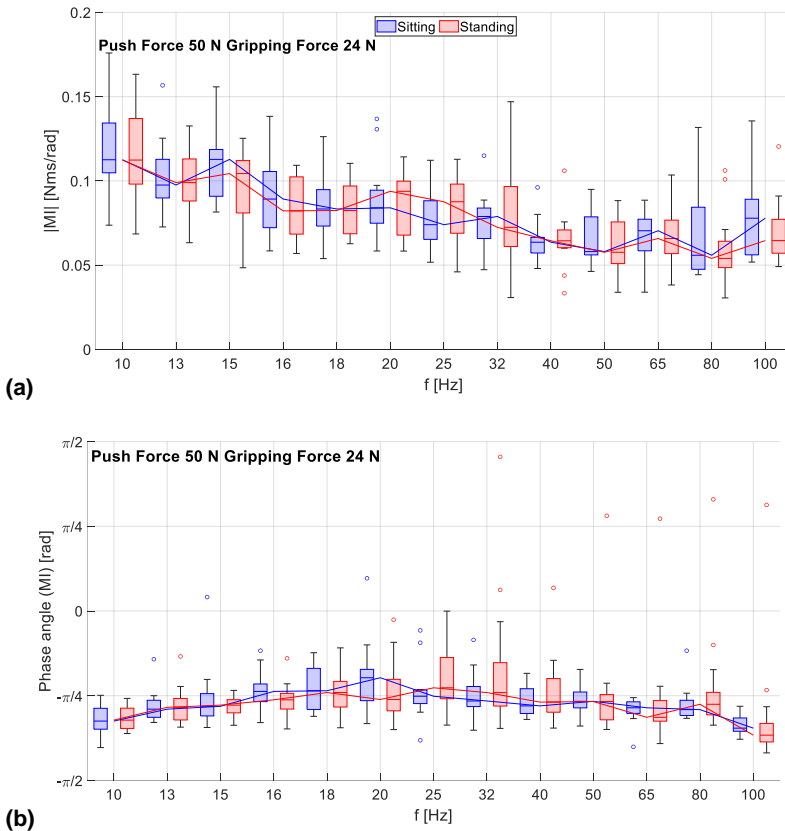


Figure 8.9: Boxplots and median trend line of the RMI's magnitude (a) and phase angle (b) for the standing and the sitting postures at a push force of $F_{pu} = 50\text{ N}$ and a gripping force of $F_{gr} = 24\text{ N}$.

The boxplots and trend lines in Figure 8.9 show no distinct differences in magnitude or phase angle between the plots of the standing and sitting positions. The position, interquartile range, and whisker height of the boxplots are quite similar for both groups across the frequency spectrum. The red boxplots of the magnitude and phase angle corresponding to the standing posture shown in Figure 8.9 are the same as the gray boxplot shown in Figure 8.8, since the factor combination is the same and, consequently, the magnitude and phase angle of the RMI data are too. The whiskers of the boxplots for the sitting posture at 80 Hz and 100 Hz are also

relatively large and shifted towards higher values. The courses of the phase angles' boxplots and trend lines are quite similar for both postures: from 10 Hz to up to 16 Hz, both phase angles increase slightly to up to approximately $-\frac{\pi}{4}$ and remain almost constant up to 80 Hz, while at 100 Hz both phase angles drop to a value of around $-\frac{\pi}{3}$. The results of the MWU regarding the effect of body posture on the magnitude of the RMI correspond to the plots in Figure 8.9, as no significances were found across the frequency spectrum. The influence of body posture on the RMI was also evaluated for the other factor combinations of the coupling forces of 32.5 N of push force and 24 N of gripping force and 15 N of push force and 24 N of gripping force. The MWU was not significant at any frequency for any of these factor combinations. In this context, the course and the distribution of the magnitude and phase angle of the RMI were also plotted for these factor combinations. Regarding the plots of the magnitude and phase angle of the RMI for these factor combinations along the applied frequency spectrum, they were similar to the ones presented in Figure 8.9, with a lower whiskers height at the frequencies of 32 Hz, 80 Hz, and 100 Hz than in Figure 8.9.

8.4 Discussion

8.4.1 How is the Course of the RMI of the HAS for Rotational Vibration Excitation around the y_h -axis?

This subchapter provides a general discussion of both the RMI magnitude and phase results. First, the RMI magnitude is discussed with respect to the frequency. Then, the RMI phase angle results are discussed separately.

The interquartile range of the boxplots and the height of the whiskers of the RMI magnitude in Figure 8.6 to Figure 8.9 show a rather broad distribution of the RMI at each frequency, especially when higher coupling forces are applied. In this context, coupling forces include the gripping and push forces. This distribution may be due to the wide range of anthropometric and physical characteristics of the subjects, as suggested by the range of weights, BMI values, and anthropometric properties in Table 8.1. Consequently, a difference in muscle mass and strength of the subjects can be assumed. The distribution of the maximum gripping forces of the subjects in Table 8.2 also support this assumption. The interquartile range of the maximum applied gripping force in the sitting posture is about 102.5 N and about 220.5 N in the standing body posture, for which the minimum and maximum values are even more distant from each other. These differences indicate a different muscle mass and strength of the subjects.

Therefore, the constant application of higher coupling forces was likely more difficult for some subjects, resulting in a larger interquartile range and whisker height for the specific factor combinations. In this context, the magnitude plots of all the figures show that for factor combinations with a low gripping force level and a high push force level, the interquartile ranges and the whiskers are usually larger. These coupling-force-related differences in the distribution of the RMI magnitude can be seen in Figure 8.6. Here, the interquartile ranges of the RMI boxplots at the gripping forces of $F_{gr} = 5.5\text{ N}$ and $F_{gr} = 10\text{ N}$ are overall larger at a push force of $F_{pu} = 32.5\text{ N}$ than at the same gripping forces at a push force of $F_{pu} = 15\text{ N}$. This observation could be due to the difficulty the subjects experienced in terms of applying these coupling forces, as the hand tends to slide down the surface of the cylindrical handle when it is pushed down and thus only a small gripping force is applied. Consequently, the subjects may have had more difficulty maintaining a constant push and gripping force while keeping their hands in the same position on the vibrating handle when the values of both forces were too far apart. This assumption is supported by the percentage deviations between the requested and applied coupling forces in Table 8.4, in which the highest mean percentage deviations of the gripping and the push force occur at the factor combination of $F_{pu} = 32.5\text{ N}$ and $F_{gr} = 5.5\text{ N}$ followed by the factor combination of $F_{pu} = 32.5\text{ N}$ and $F_{gr} = 10\text{ N}$. As a result, it was probably more difficult for the subjects to keep the muscle tension of the HAS constant while performing these factor combinations because the muscles of the hand had to be mostly relaxed, while the upper arm muscles had to be tense. Due to this unequal distribution of muscle tension, the muscle tension had to be corrected more often by the subject, as suggested by the deviations shown in Table 8.4 suggest. The conscious or unconscious correction of muscle tension resulted in a changing stiffness and damping of the HAS, leading to the observed dispersion of the RMI. In the same context, high coupling forces generally seem to result in a larger interquartile range and whisker height of the RMI magnitude, as can be seen for the coupling forces of $F_{pu} = 50\text{ N}$ and $F_{gr} = 24\text{ N}$ applied while standing and sitting at the frequencies of 32 Hz, 80 Hz, and 100 Hz (Figure 8.9). The shift of the whiskers at 80 Hz and 100 Hz in the sitting position (Figure 8.9) towards higher values could indicate that the degree of coupling between the HAS and the handle is stronger. A possible explanation for this could be that in the sitting position, the requested high coupling forces were more difficult to apply at higher frequencies since the rapid handle movement made it difficult to perceive the applied forces. This difficulty in perception might have led to some subjects using excessive force and thus exceeding the requested force levels, resulting in a stronger coupling of the HAS to the handle. Additionally, the application of the coupling forces in the sitting position could be more difficult in general since each subject's arm was stretched out. The need to adjust the gripping

force level from $F_{gr} = 5.5\text{ N}$ to $F_{gr} = 10\text{ N}$ for the sitting position supports this assumption. Further evidence for this assumption is provided by the distribution of maximum gripping force values in Table 8.2, in which the force values are higher overall in the sitting posture.

Regarding the phase angle plots of the RMI of all factor combinations in Figure 8.7 to Figure 8.9, all phase angles of the RMI increase slightly linearly up to approximately $-\frac{\pi}{4}$ at 16 Hz subsequently remain constant up to 100 Hz. In Figure 8.7 and Figure 8.9, the phase angles of both factor combinations drop to approximately $-\frac{\pi}{3}$ at 100 Hz. Overall, the courses of the phase angles indicate a spring-damper dynamic of the HAS with a slightly predominant spring component at low frequencies, which decreases to as low as 16 Hz and changes to a uniformly distributed spring-damper dynamic at a phase angle of $-\frac{\pi}{4}$ at up to 80 Hz. At 100 Hz, the spring component increases again. The tissue of the wrist and the muscles of the forearm, which are stretched and squeezed by the vibration, possibly generate the spring component of the phase angle plots. In this context, the damper component would result from the specific combination of the rotational vibration direction and the hand orientation. The centerline of the cylindrical measuring handle is coaxial with respect to the excitation axis. Therefore, the torque of vibration acts tangentially to the surface of the palm and the fingers via the frictional contact between the hand and measuring handle. This frictional hand-handle contact may confer a damping effect. In this context, the shear of the skin and the tissue between the hand bones and the handle possibly results in the damper-dominant characteristic of the phase angle plots, as shown by the increasing phase angle between 10 Hz and 16 Hz. At higher frequencies, the frictional contact between the hand and the handle may be temporarily interrupted in some areas due to the rapidly oscillating handle movement. These temporary interruptions of hand-handle contact would also confer a damping effect as the handle slips slightly in the hand. This hypothesis could explain the damper-dominated dynamic of the phase angle beyond 16 Hz, as suggested by the increased phase angle of $-\frac{\pi}{4}$. Accordingly, the angular deflection of the handle at 100 Hz is possibly too small to interrupt the hand-handle contact in certain places. As a result, the damping effect of the frictional contact is reduced, and a greater degree of vibration exposure is transmitted to the wrist again. The exposure of wrist tissue would increase the spring component of the spring-damper dynamic, resulting in a decrease in the phase angle.

The obtained results largely correspond to those by Schröder, Lindenmann, Resch, et al. (2023), who excited the HAS with rotational vibrations up to a frequency of 250 Hz via a knob-shaped measuring handle. Therein, the same shaker test bench was used (and in the same orientation). The human hand gripped the knob-shaped handle from above. The results obtained by Schröder, Lindenmann, Resch, et al. (2023) can be compared to the results of this study since in both studies the HAS was rotationally vibrated via predominantly or exclusively frictional contact between the hand and the measuring handle. The phase angle plots presented by Schröder, Lindenmann, Resch, et al. (2023) also show a spring-damper dynamic of the HAS with a decreasing spring component at higher frequencies (Schröder, Lindenmann, Resch, et al., 2023). Specifically, the phase angle plots by Schröder, Lindenmann, Resch, et al. (2023) show a spring-dominated spring-damper dynamic of the HAS, which changes to a damping-dominated dynamic between 40 Hz and 160 Hz. Beyond 160 Hz, the degree of damping increases further and reaches full damping at 250 Hz (Schröder, Lindenmann, Resch, et al., 2023). In comparison to the results of the present study, the spring component is predominant in Schröder, Lindenmann, Resch, et al. (2023) up to 40 Hz. This difference in the results obtained could be due to the slightly different types of contact between the hand and the measuring handle in the case of a cylindrical and a knob-shaped handle. The knob-shaped measuring handle used by Schröder, Lindenmann, Resch, et al. (2023) was gripped from above in a reclining hand position, with the palm resting on the top of the handle and the fingers enclosing the elliptical geometry of the knob. In this “palm” position, the vibration is transmitted to the HAS via a combination of frictional contact and form-fitting contact between the hand and the handle. The form-fitting contact results from the elliptical geometry of the knob enclosed by the fingers, which prevents the handle from slipping to a certain extent during the propagation of rotational vibrations. Therefore, this additional form-fitting contact may enable vibration transmission to the forearm of the HAS at higher frequencies. As a result, the tissues of the wrist and the muscles of the forearm would also be exposed to higher frequency vibrations, which would increase the spring component of the phase angle at these frequencies. Consequently, the damping effect of the frictional hand-handle contact assumed from the results of the present study would only occur at a higher frequency in the case of the knob-shaped handle.

Schröder, Lindenmann, Resch, et al. (2023) adjusted the acceleration magnitude of the applied vibration in the same way as in the presented study. Therefore, the magnitude plots of the RMI of both studies are comparable. In this context, the magnitude plots of the RMI of the presented study are similar to the magnitude plots presented by Schröder, Lindenmann, Resch, et al. (2023). Since the magnitude plots of the present study correspond to the course of the phase angles and to the results presented by Schröder, Lindenmann, Resch, et al. (2023), it seems that the spring-

damper dynamics of the HAS with a predominant spring component changing to a predominant damping component at high frequencies are valid. Thus, the assumed frictional damping of the vibration propagated via contact between hand and handle could also be considered plausible.

When comparing the obtained plots of the phase angle of the RMI with the plots obtained by Lindenmann and Matthiesen (2019), it is evident that the phase angles differ from each other (Lindenmann & Matthiesen, 2019). Lindenmann and Matthiesen (2019) vibrated the HAS via the measuring handle of the ISO 10819 along the z_h -axis, whereas the handle geometry of the present study also corresponds to the ISO 10819 handle but was excited around the y_h -axis (DIN Deutsches Institut für Normung e. V., 2019; Lindenmann & Matthiesen, 2019). The phase angle plot in the studies conducted by Lindenmann and Matthiesen (2019) also indicates a spring–damper dynamic of the HAS but with an increasing spring component in the frequency range from 10 Hz to up to 201 Hz. In the study conducted by Lindenmann and Matthiesen (2019) the vibration excitation around the z_h -axis causes an exclusive form-fitting connection between the hand and the cylindrical handle since the applied torque acts normally with respect to the palm and the fingers (Lindenmann & Matthiesen, 2019). This positive locking between the hand and the cylindrical handle results in a stronger degree of coupling between the HAS and the vibration source, as the handle cannot slip in the hand at high frequencies. Accordingly, no frictional damping of vibration can occur at high frequencies, as reported in the present study. Instead, the handle pushes with high frequency against the palm of the hand and compresses the tissue of the hand. The compression and rebound of the palm’s tissue may result in the increasing spring component that is observable at high frequencies in the phase angle plot by Lindenmann and Matthiesen (2019).

In addition, rotational excitation around the z_h -axis rotates the hand around the axis of the forearm, which further involves the forearm more in this movement. This vibrational excitation of the forearm and the stronger coupling between hand and handle could be due to the spring-dominated dynamic of the HAS depicted in the phase angle plot presented by Lindenmann and Matthiesen (2019).

By comparing the obtained results with the results by Schröder, Lindenmann, Resch, et al. (2023) and Lindenmann and Matthiesen (2019), it can be concluded that the type of contact between the handle and the HAS has an influence on the vibration transmission to the HAS when it is exposed to rotational vibrations. In this context, frictional hand–handle contact appears to have a damping effect, which reduces the transmission of vibrations to the HAS.

The obtained plots of the magnitude and the phase angle of the RMI differ from those for translational excitation along the y_h -axis represented in ISO 10068 (ISO - International Organization for Standardization, 2012). For comparison the Figure 8.10 shows the magnitude and the phase angle plot of the MI for translational excitation along the y_h -axis from ISO 10068 (ISO - International Organization for Standardization, 2012). The phase angle plot of ISO 10068 shows that the phase angle of the MI for translational excitation along the y_h -axis starts at about $\frac{\pi}{4}$, at which point it decreases to slightly below 0 at 100 Hz. This course differs from the phase angle plot of the RMI and indicates mass-damper dynamics of the HAS with an increasing damping component. A possible explanation for these differences can be found by considering the excitation directions. In this study, the rotational excitation around the y_h -axis rotates the measuring handle within the grip of the hand, resulting in the already-mentioned degree of frictional damping. Alternatively, the translational excitation along the y_h -axis in ISO 10068 makes the hand bounce up and down. Consequently, the applied vibrational motion acts against the inertia of the HAS, thus explaining the mass component in the phase angle. Rotational vibration excitation results in the lateral flexion of the wrist, which decouples the rest of the HAS from this vibration to some extent such that the inertia of the HAS does not affect the phase angle. The phase angle plots of rotational and translational excitation both indicate a damping component. This component may result from the already-mentioned frictional damping of the hand–handle contact, which can also occur during the propagation of translational vibrations of the cylindrical handle along the y_h -axis. The magnitude plots of ISO 10068 and the current study match in terms of their respective phase angle plots. In Figure 8.10, the increasing magnitude plot from ISO 10068 indicates a mass-dominated dynamics of the HAS, thus confirming the mass component in the phase angle plot. As mentioned earlier, the magnitude plots of Figure 8.6 through Figure 8.9 indicate spring-damper dynamics of the HAS, which also matches the phase angle plots of the RMI

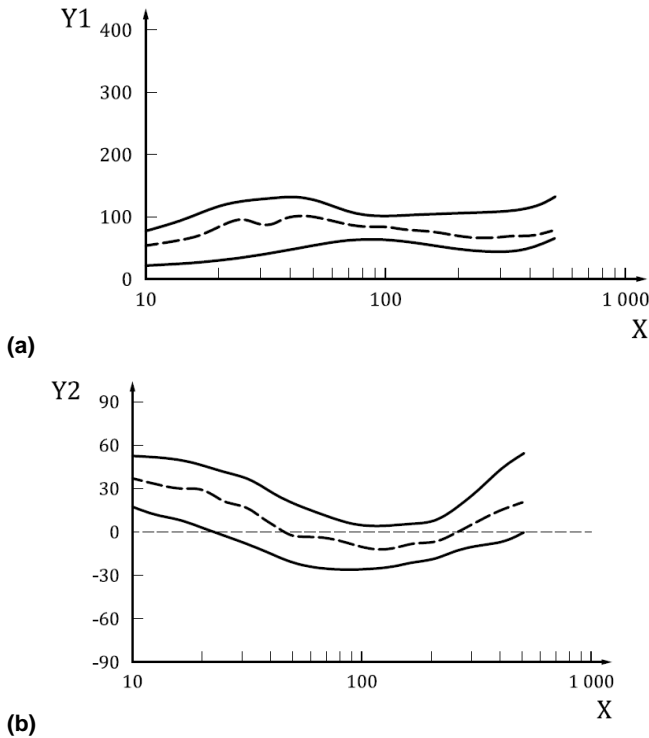


Figure 8.10: a): Magnitude plot of the MI for vibration excitation along the y_h -axis from ISO 10068, b): Phase angle plot of the MI for vibration excitation along the y_h -axis from ISO 10068. **Key:** X: frequency [Hz], Y1: modulus (corresponds to the magnitude) $\left[\frac{Ns}{m}\right]$, Y2: Phase angel (degree) (ISO - International Organization for Standardization, 2012)

8.4.2 How is the RMI in y_h Direction Influenced by the Gripping Forces?

In Figure 8.6 the offset between the boxplots and the median trend lines of the different gripping force levels indicates that applying a higher gripping force results in a higher magnitude of the RMI. These results are supported by the results of the MWU in Table 8.5. According to the MWU, gripping force has a significant effect on

the magnitude of the RMI, with a high positive effect strength at almost every frequency regardless of the applied push force and body posture. An explanation for these results can possibly be found in the alignment between the axis of vibration excitation and the gripping of the cylindrical measuring handle. As mentioned above, the axis of excitation of rotational vibration is coaxial with respect to the centerline of the cylindrical handle. Therefore, vibration is transmitted to the HAS via frictional contact between the handle's surface and the hand. Consequently, a higher gripping force increases this frictional contact, resulting in better vibration transmission, which increases the magnitude of the RMI. Figure 8.11 graphically illustrates the described relationship between the gripping force and the rotational vibration excitation.

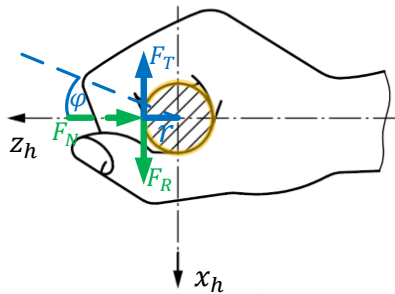


Figure 8.11: Schematic of the relationship between hand position and rotational axis on the basis of the “hand-grip” position from ISO 10068, where yellow indicates contact surface between hand and handle, blue indicates deflection angle and tangential force of excitation, and green indicates normal and friction force, resulting from the gripping force of the test subject (ISO - International Organization for Standardization, 2012). **Key:** r = radius of the handle, φ = deflection angle of rotational vibration excitation, F_T = tangential force on the handle surface conferred by rotational vibration excitation acting on the HAS, F_N = normal force, and F_R = frictional force.

Following the force vectors of Figure 8.11, it can be seen that the tangential force F_T of the rotational vibration excitation acting on the hand counteracts the frictional force F_R between the hand and the handle. Since frictional force F_R is a product of the friction coefficient μ_h and normal force F_N , which depends on gripping force F_{gr} , the following relationship can be derived from Figure 8.11.

$$F_{gr} = F_N = \frac{F_R}{\mu_h} = \frac{F_T}{\mu_h} \quad 8.1$$

As illustrated by the force arrangement shown in Figure 8.11 and the relationship described in equation 8.1 a higher gripping force results in a higher frictional force, allowing for a greater proportion of the tangential force of the vibration to be transmitted to the HAS. Consequently, the vibration exposure as well as the magnitude and HAS generate stronger vibration exposure of the HAS and a higher RMI magnitude.

Overall, the observed influence of the gripping force on the RMI corresponds to the influence of the gripping force on the translational MI (Aldien et al., 2005; Aldien et al., 2006; Dong et al., 2001; Dong et al., 2005; Dong, Welcome, McDowell, & Wu, 2006; ISO - International Organization for Standardization, 2012; Kalra et al., 2015b; Xu et al., 2011). However, the mechanisms of action leading to stronger vibration transmission of rotational vibration excitation in this study may be different from those for translational vibrations (Aldien et al., 2005; Aldien et al., 2006; Dong et al., 2001; Dong et al., 2005; Dong, Welcome, McDowell, & Wu, 2006; ISO - International Organization for Standardization, 2012; Kalra et al., 2015b; Xu et al., 2011). In the case of rotational vibration excitation, Schröder, Lindenmann, Resch, et al. (2023) also describes a similar influence (Schröder, Lindenmann, Resch, et al., 2023). Hence, the observed effect of the gripping force on the RMI corresponds to the state of research (Aldien et al., 2005; Dong et al., 2001; Dong et al., 2005; Dong, Welcome, McDowell, & Wu, 2006; ISO - International Organization for Standardization, 2007, 2012; Kalra et al., 2015b; Lindenmann et al., 2021; Schröder, Lindenmann, Resch, et al., 2023; Xu et al., 2011).

8.4.3 How is the RMI in y_h Direction Influenced by the Push Forces?

The applied push force does not appear to have any influence on the RMI, as the interquartile ranges of the boxplots for the different push force levels in Figure 8.8 largely overlap. The KWT results confirm this conclusion, as they showed no significant effect of the applied push force on the RMI except at frequencies of 40 Hz, 65 Hz, and 80 Hz. However, the significance of these frequencies can be neglected because they were confirmed by pairwise comparison in only two cases. Furthermore, the KWT regarding the influence of the applied push force on the RMI was also insignificant at every analyzed frequency. Therefore, a random correlation corresponding to these frequencies can be assumed. The absent influence of the push force on the RMI of the HAS can be explained by the coaxial alignment between the vector of the push force and the rotational axis of the handle's angular oscillation.

This alignment between the push force and the rotational axis for the torque applied through vibration is shown in Figure 8.12.

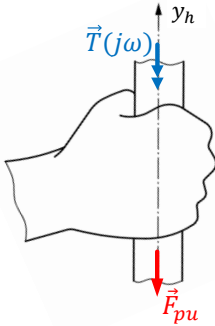


Figure 8.12: Schematic drawing of the relationship between the rotational axis and the direction of the push force on the basis of the “hand-grip” position from ISO 10068, where blue indicates torque of the rotational vibration excitation and red indicates the push force applied by the subject (ISO - International Organization for Standardization, 2012). **Key:** F_{pu} = push force, $T(j\omega)$ = torque of the rotational vibration excitation acting on the hand.

As Figure 8.12 shows, the push force vector is aligned coaxially with the vector of the torque of the rotational vibration acting on the hand. Thus, the push force does not counteract the tangential force resulting from the torque. Consequently, a higher push force would not lead to a stronger degree of coupling between the hand and the handle, as both force vectors are skewed with respect to one another regardless of the direction the handle moves. As a result, more pushing has little or no effect on the coupling of the HAS with the vibration source. Hence, the push force has no verifiable influence on the RMI for rotational vibration excitation around the y_h -axis propagated by a cylindrical handle. These results correspond to those reported by Schröder, Lindenmann, Resch, et al. (2023) concerning the influence of the push force on the RMI in the case of vibration excitation propagated via a knob-shaped handle (Schröder, Lindenmann, Resch, et al., 2023). Nevertheless, Figure 8.8 shows a slight offset between the RMI’s magnitudes at the push forces of $F_{pu} = 15\text{ N}$ and $F_{pu} = 50\text{ N}$ as well as $F_{pu} = 32.5\text{ N}$ and $F_{pu} = 50\text{ N}$ in the frequency range between 25 Hz and 80 Hz, respectively. This offset could be due to the positioning of the hand, as the hand may slip down the cylindrical handle a little, especially with high push forces. This sliding can cause parts of the edge of the hand to lightly touch the flange to which the handle is attached when high push force is applied. This would slightly change the contact area between the hand and the handle, resulting in the observed selective offset of the RMI’s magnitude for higher push forces.

8.4.4 How is the RMI in y_h direction influenced by the Body Posture?

The overlapping interquartile ranges of the boxplots and the median trend lines of the magnitude of the RMI in Figure 8.9 indicate that body posture does not influence RMI. This conclusion is supported by the results of the KWT, which do not indicate any significant effect of body posture on the RMI regardless of the applied coupling forces. These results do not correspond with the influence of posture on translational MI described in the literature (Adewusi et al., 2012; Aldien et al., 2005; Aldien et al., 2006; ISO - International Organization for Standardization, 2012). A possible explanation for the absence of an effect conferred by body posture in the case of rotational vibration excitation can be found by considering the rotational excitation direction and the positioning of the hand. As mentioned above, the overall phase angle and magnitude plots led to the hypothesis that the HAS had a spring-damper dynamic. According to this hypothesis, the tissue of the wrist and the forearm could generate a spring component, while damping can occur partly because of the frictional contact between the hand and the measuring handle. Assuming this hypothesis is correct, the wrist would compensate for vibrations via lateral flexion as the hand follows the motion of the vibrating handle. This flexion would involve the tissue of the wrist and the forearm, as indicated by the described spring component of the phase angle plots. The described frictional hand-handle contact would additionally dampen the transmission of vibrations to the HAS. Since the mobility of the wrist allows the hand to follow the movement of the measuring handle up to a certain frequency and the frictional "hand-grip" position additionally dampens vibration excitation, it is possible that the generated vibrations are not transmitted to the rest of the hand-arm system and the body. Consequently, the RMI of the HAS would not be affected by the stiffness or mass of the upper arm or the body. Therefore, body posture would not influence the RMI.

8.4.5 Relevance of the Results to Industrial Applications

The results of this study extend the body of knowledge regarding the MI of the HAS by providing an approach to the biodynamics of the HAS for rotational vibration excitation, which could be extended by further studies to increase the database concerning the RMI of the HAS. In this context, a larger database would enable the more extensive parametrization of rotational HAMS. These HAMS could be added to the translational models of ISO 10068 to represent the excitation of the HAS by rotational vibrations. For industrial purposes, such models can be used for the vali-

dation and simulation of vibrational human–machine interactions, such as in the development of power tools that transmit rotational vibrations. Furthermore, the results are also relevant in the field of vibration-related occupational health and safety as well as the design of handles for power tools. In this context, the results suggest that a mainly frictional type of contact between hand and handle may reduce the vibrational exposure of the HAS, as the friction between the hand and the handle imparts an additional degree of damping. Regarding the vibration-related occupational health and safety of industrial assembly tasks, power tools with a primarily rotational excitation direction and a cylindrical handle, such as the inline air impact wrench, could confer vibration damping properties due to friction related to hand positioning. However, these assumed damping properties would depend on the applied gripping force, for which a lower gripping force would result in less coupling between the hand and the vibration source. The push force, on the other hand, does not seem to have any influence on the RMI of the HAS as long as it is applied coaxially with respect to the excitation axis of the rotational vibration. In this context, the use of an inline impact wrench with a cylindrical handle aligned coaxially with the axis of rotation would possibly be preferable to an impact wrench with a pistol grip in terms of occupational protection. The results of this study may also form the basis for the design of power tool handles that transmit rotational vibrations. A handle design based mainly on frictional contact between the user's hand and the handle could potentially expose the HAS to less vibration due to frictional damping. Although such a handle design could reduce the vibrational exposure of the HAS, the positioning of the power tool and the force transmission between the user and the power tool must also be considered, for which positive locking might be a better solution.

8.5 Limitations

The results concerning the progression of the RMI and the influences of coupling forces and body posture are limited in terms of their validity for the applied frequency spectrum of up to 100 Hz. Therefore, frequencies beyond 100 Hz need to be investigated in further studies. Accordingly, a preliminary investigation of the natural frequencies for the combination of a handle and the HAS under rotational vibration excitation is required. Other limiting factors that must be considered include the number of subjects and the fact that each subject could only perform one trial per factor combination due to the test's duration and the subjects' fatigue. These limiting factors can be compensated to a certain extent by the fact that the observations and conclusions drawn from the results can be found for different factor combinations, resulting in a larger volume of data on which to base these findings. The plots of the magnitude and phase angle of the RMI are qualitatively similar for all the factor combinations. Consequently, the conclusions drawn from the course of magnitude and

phase angle are based on the plots of each factor combination, resulting in ten plots per subject. The influence of the gripping force on the magnitude of the RMI could also be determined for different push forces and body postures. Since no influence of the push force and body posture on the RMI could be determined, the influence of the gripping force on the RMI can thus be derived from four data sets per subject. In the same manner, the influence of push force and body posture also could not be determined for the sitting position or different coupling forces. Consequently, the observation that the push force or the body posture do not influence RMI is based on two and five data sets per subject, respectively. Nevertheless, in further studies, the number of subjects as well as the number of trials per subject should be increased to confirm the results of this study by using a broader database. In this context, the present study provides an initial exploratory approach covering a broad range of potential factors influencing the RMI. Based on the results of this study, the number of factor combinations can be reduced in future studies on the same excitation direction because factors that do not appear to influence the RMI do not need to be varied. Reducing the variable factors would result in a shorter test duration, thereby enabling more trials per subject and a larger number of subjects.

8.6 Conclusion

The results of this study contribute to the investigation of the biodynamics of the HAS, as the measured RMI of the HAS indicates a spring–damper characteristic for rotational vibration excitation around the y_h -axis. Furthermore, the magnitudes and the phase angles of the RMI indicate that when a rotational vibration is transmitted to the HAS via frictional contact between the hand and a cylindrical measuring handle, this frictional contact is likely to have a damping effect on the transmitted vibration. In this context, the applied gripping force has a significant influence on the magnitude of the RMI of the HAS, as a stronger gripping force increases the friction between the hand and the handle. This influence could be shown qualitatively and statistically for up to 100 Hz with a strong positive effect strength regardless of the applied push force and the posture of the subject. Regarding the push force and body posture, no similar influence on the RMI could be shown. This absent influence could be due to the alignment between the positioning of the hand and the vibration excitation axis. Both the influence of the gripping force on the RMI and the lack of influence of the push force confirm the results obtained by Schröder, Lindenmann, Resch, et al. (2023). In this context, the hypothesis concerning the effect of frictionally engaged gripping positions on vibration transmission reported Schröder, Lindenmann, Resch, et al. (2023) could also be confirmed through the results obtained.

Nevertheless, the observed influences of the coupling force and the body posture on the RMI of the HAS need to be further investigated for other excitation directions and hand positions as well as for the frequency spectrum beyond 100 Hz. In this context, this study constitutes an initial approach to investigating the RMI of the HAS and its influencing factors under rotational vibration excitation along the y_h –axis. Figure 6.1 summarizes the findings regarding the influence of gripping and pressing force, which result from the positioning of the hand and the vibration excitation axis, based on Figure 8.11 and Figure 8.12.

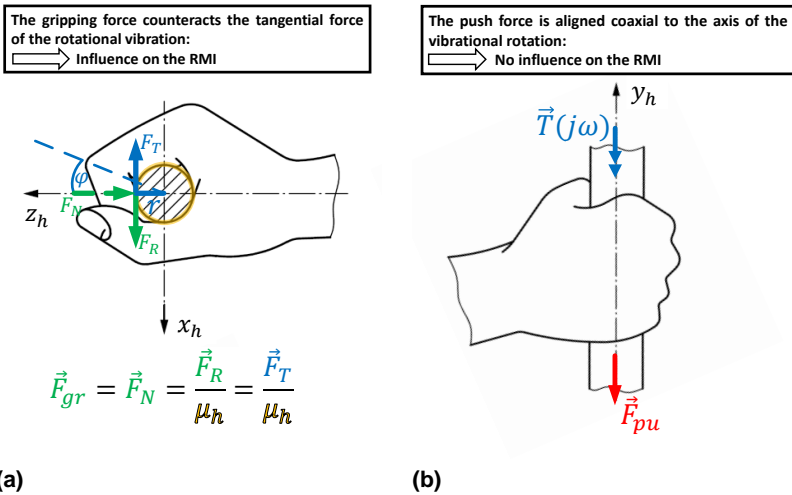


Figure 8.13:

(a) Top view from Figure 4.1 where yellow indicates contact surface between hand and handle, blue indicates deflection angle and tangential force of excitation, and green indicates normal and frictional force resulting from the gripping force of the test subject. (b) Side view from Figure 4.2, where blue indicates torque of the rotational vibration excitation and red indicates push force applied by the subject. **Key:** r = radius of the handle, φ = deflection angle of the rotational vibration excitation, F_T = tangential force on the handle’s surface conferred by rotational vibration excitation acting on the HAS, F_N = normal force, F_R = frictional force, F_{pu} = push force, and $T(j\omega)$ = torque of the rotational vibration excitation acting on the hand”

8.7 Thesis specific Conclusion

In the following, it will be assessed whether and to what extent the results and findings of the study presented in this chapter and pre-published in the Journal *MDPI Vibration* entitled *Influence of Coupling forces and Body Posture on the Rotational Hand-Arm Impedance in y_h -Direction* contribute to the investigation of **Hypothesis 3: Rotational impedance around the y_h -axis**. This assessment is based on how the conducted study answer the corresponding sub-research questions of the hypothesis.

Hypothesis 3: Rotational impedance around the y_h -axis

The rotational mechanical impedance for excitations around the y_h -axis in the „hand-grip“ position is influenced by the applied gripping force, push force and body posture and the observed effects are comparable to hypothesis 2.

- **Sub-research question 3.1:** What is the course of the magnitude and the phase angle of the RMI for rotational vibration excitation around the y_h -axis in the “hand-grip” position and can this course be related to the excitation around the x_h -axis in the “palm” position?
 - The course of the magnitude and the phase angle of the RMI for rotational vibration excitation around the y_h -axis in the “hand-grip” position largely correspond to the results obtained for the excitation of the HAS around the x_h -axis in the “palm” position, since in both cases superimposed spring-damper dynamics are indicated. However, the frequencies at which the spring or damper component in the phase angle plot increases or decreases are shifted, compared to the results from Chapter 7. The magnitude plots the RMI for both excitation direction and hand positions are similar. The observed differences of the phase angle plots can be attributed to the combination of the hand-position and the excitation direction, which lead to a higher frictional damping in the hand-handle contact in the study presented in this chapter. Thus the course of the magnitude and the phase angle of the RMI for rotational vibration excitation around the y_h -axis in the “hand-grip” position can be related to the excitation around the x_h -axis in the “palm” position and **sub-research question 3.1** can be considered as answered.

- **Sub-research question 3.2:** How is the magnitude of the RMI influenced by the applied gripping force and can this influence be related to the excitation around the x_h –axis in the "palm" position?
 - The results presented in Figure 8.6 and Figure 8.7 as well as in Table 8.5 indicate that a higher gripping force results in an increasing magnitude of the RMI. These results are consistent with the results of Chapter 7 and support the assumption that a higher gripping force decreases the frictional damping in the hand-handle contact, resulting in a higher vibration transmission to the HAS. Thus the influence of the applied gripping force observed in Chapter 7 and Chapter 8 can be related and **sub-research question 3.2** can be considered as answered.
- **Sub-research question 3.3:** How is the magnitude of the RMI influenced by the applied push force and can this influence be related to the excitation around the x_h –axis in the "palm" position?
 - As with the x_h –axis excitation in the "palm" position in Chapter 7, no influence of the push force on the magnitude of the RMI was found for the y_h –axis excitation in the "hand-grip" position in the study of this chapter. The absence of this influence supports the conclusions drawn in Chapter 7 regarding the alignment between the direction of the applied shear force and the direction of excitation. In the studies in both chapters the parallel alignment between the excitation axis and the direction in which the push force is applied results in the push force having no influence on the RMI. Consequently, the influence of the applied push force on the RMI for excitation around the y_h –axis in the "hand-grip" position can be related to the influence of the push force applied for the excitation around the x_h –axis in the "palm" position, to the effect that it has no influence in either cases. Hence **sub-research question 3.3** can be considered as answered.
- **Sub-research question 3.4:** How is the magnitude of the RMI influenced by the body posture?
 - For the body posture no influence on the magnitude of the RMI could be detected in the study presented, even at the highest coupling forces applied, as shown in Figure 8.9. Therefore, the answer to Research Question 3.4 is that the obtained results do not indicate an influence of body posture on the RMI for excitation around the y_h –axis in the "hand-grip" position.

On the basis of the **sub-research questions 3.1 to 3.4 Hypothesis 3: Rotational impedance around the y_h –axis** can be considered as investigated. In this context the assumed influence of the applied gripping force was shown in the results of the

study, while the influence of the push force and the body posture was not. The effects observed in this chapter are related to the effects observed in the investigation of **Hypothesis 2: Rotational impedance around the x_h -axis** in terms of the relationship between the frictional hand-handle contact and the transmitted vibration. In this regard the explanation model from Chapter 7 was confirmed and extended to the “hand-grip” position.

9 Summary Overall Discussion and Outlook

The aim of this chapter is to complete the thesis by a short summary that provides an overview of the central aspects, the obtained results and findings. This is followed by an overall discussion of the results and findings obtained in Chapters 6 to 8, and an outlook for further research on the basis of these results and findings.

9.1 Summary

The research problem introduced in Chapter 1.1 was motivated by the investigation and simulation of vibration-related human-machine interaction as it occurs in the context of power tool development. Here a lack of research on the rotational mechanical impedance (RMI) of the hand-arm system (HAS) was identified, resulting in the following **research problem**:

Research Problem

The state of research lacks data on the rotational mechanical impedance of the human hand-arm system, which is required for the parametrization and the development of hand-arm models, such as those used in power tool development.

The knowledge on the RMI of the HAS enables the complete description and simulation of the vibration biodynamics of the HAS, especially in the case of multidirectional vibration excitation. In addition, the research on the RMI is motivated by the validation of power tools within the power tool development, with the RMI providing a basis for the development HAM, which simulate the biodynamics of the HAS under rotational vibration excitation.

For the excitation around the x_h -axis and the y_h -axis, the thesis referred to the random orbital sander and the assembly screwdriver, as exemplary power tools, which emit rotational vibrations around the corresponding axes. The gripping of these exemplary power tools refer to the “palm” and the “hand-grip” position according to DIN EN ISO 5349-1 and ISO 10068. Consequently, those hand positions were chosen for the excitation around the corresponding axes. However, both combinations of excitation axis and hand position additionally have in common that the hand-handle contact is largely or complete frictional. Therefore, the results of both combinations are comparable and suggest a similar effect of this frictional contact on the RMI. Accordingly, the following **objective** of the thesis has been derived:

Objective

The objective of this thesis is the investigation of the rotational mechanical impedance of the human hand-arm-system for rotational excitations around the x_h -axis in the „palm“ position, and around the y_h -axis in the „hand-grip“ position.

Regarding the excitation around the x_h –axis in the “palm” position the challenge here was that in the state of research, no suitable measuring handles existed so far. However, since such a handle was mandatory for measuring the influence of the coupling forces on the RMI the thesis also aimed for the development of a knob-shaped measuring handle.

Thus, the objective of the thesis was divided into three research hypothesis related to the development of a knob-shaped measuring handle, the investigation of the RMI around the x_h –axis in the “palm” position, and the investigation of the RMI around the y_h –axis in the “hand-grip” position:

Hypothesis 1: Derivation of the measuring handle design

From the distribution of gripping forces on a knob-shaped power tool handle, a measuring handle for excitations in the "palm" position can be derived, which is suitable for measuring gripping forces.

Hypothesis 2: Rotational impedance around the x_h -axis

The rotational mechanical impedance for excitations around the x_h -axis in the „hand-grip“ position is influenced by the applied gripping force, push force.

Hypothesis 3: Rotational impedance around the y_h –axis

The rotational mechanical impedance for excitations around the y_h -axis in the „hand-grip“ position is influenced by the applied gripping force, push force and body posture and the observed effects are comparable to hypothesis 2.

These three hypotheses were addressed in the thesis in three studies, presented in Chapter 6, Chapter 7, and Chapter 8, with each study pre-published as a journal article.

To investigate **Hypothesis 1: Derivation of the measuring handle design**, a new method for designing a knob-shaped measurement handle for RMI measurements was presented in Chapter 6. Chapter 6 confirmed the first hypothesis to the extent that the main gripping force direction when gripping a knob-shaped handle in the "palm" position is different from the main gripping force direction in the "hand-grip" position. To this end, a knob-shaped measurement handle was developed as a first approach to close the gap in the state of research regarding the lack of an appropriate measuring handle for MI measurements in the "palm" position. Thereby, the newly developed knob-shaped measuring handle not only provides a handle geometry suitable for measuring the vibration excitation of the HAS in the "palm" position, but also enables the measurement of gripping forces in this hand position which is important for understanding the effects on the RMI. In this context the knob-shaped measuring handle extends the state of research by enabling measurements of MI and the influence of gripping force in the "palm" position. In the investigation of the gripping force distribution on knob-shaped handles effects were also found with regard to the relationship between handedness and gripping force direction

To investigate **Hypothesis 2: Rotational impedance around the x_h –axis**, the course of the RMI was measured Chapter 7 investigated when excited around the x_h –axis in the "palm" position und the influence of the gripping and push force on the RMI. For this purpose, the knob-shaped measuring handle from Chapter 6 was used. The obtained results indicated a spring- damper dynamic of the HAS for rotational vibration excitation up to 250 Hz. Furthermore, an influence of the gripping force on the RMI with an overall moderate effect strength could be detected at a push force of 32.5 N up to the frequency of 200 Hz and at a push force of 42.5 N up to 127 Hz. For the influence of the push force on the RMI no statistical significance was found at any frequency. Consequently, the second hypothesis can be confirmed with regard to the influence of the gripping force on the RMI, but must be falsified with regard to the influence of the push force on the RMI.

In order to investigate **Hypothesis 3: Rotational impedance around the y_h –axis**, the course of the RMI was measured in Chapter 8 with excitation around the y_h –axis in the "hand grip" position, determining the influence of the gripping and push force as well as the body posture. For the conducted study, a modified version of the cylindrical measuring handle from ISO 10819 was used. The results obtained in Chapter 8 provide plots of the magnitude and phase angle of the RMI, which also indicate a spring-damper dynamic of the HAS. Regarding the influence of the grip-ping force on the RMI, a significant effect was found for all applied frequencies with an overall high positive effect strength, regardless of the applied push force or body posture. In contrast, no significant influence could be detected for the influence of the push force and the body posture. Consequently, the third hypothesis can be

confirmed regarding the influence of gripping force, but not regarding the influence of push force and body posture.

9.2 Overall Discussion

Based on the obtained results from Chapter 7 and Chapter 8 the objective of the thesis, can be considered as fulfilled since an initial approach to the investigation of the RMI for excitations around the x_h – and y_h –axis in the “palm” and the “hand-grip” positions has been provided. Fulfilling the objective of the thesis expands the knowledge and data on the rotational impedance of the hand-arm system and thus contributes to solving the research problem introduced. The study on the RMI for excitation around the x_h –axis in the “palm” position in Chapter 7 is a new approach, which has not been investigated in the state of research so far.

The same applies for the measurement of RMI for rotational vibration excitations around the y_h –axis, in the “hand-grip” position in Chapter 8 for which no data have been published yet either. Referring to the introduced statement of Dong et al. (2013): “Not directly accounting for the cross-axis responses and rotational responses in these models may also contribute to discrepancies.” (Dong et al., 2013, p. 1139) this data provides a basis for the development of more accurate hand-arm models (HAM). The acquisition of RMI data using the example of power tools thus contributes to a field of product development where this knowledge is particularly in demand, as shown by Dong et al. (2012): “Powered hand tools are known to generate and transmit multi-axes vibrations. Due to the non-uniform distributions of the mass, elastic, and viscous properties in the human hand-arm system, it could respond to such multi-axes vibrations in a highly complex manner a long all the translational and rotational axes.” In this context the investigated influences of the applied coupling forces and of the body posture on the RMI are specifically relevant for the field of power tool development. Power tools are guided by hand and the applied gripping and push forces can affect the work result achieved with the power tool.

Based on the results obtained in Chapter 7 to investigate **Hypothesis 2: Rotational impedance around the x_h –axis**, an **explanation model** was derived. According to this explanation model the spring-damper dynamics of the magnitude and phase angle plots of the RMI is caused by the partial frictional hand-handle contact that results from the geometry of the knob-shaped handle. This frictional contact has a damping effect, as the handle can partially slip under the hand during rotational vibrations. Higher gripping force increases the friction between the hand and the vibrating measuring handle, which is why the gripping force has a significant influence on the RMI. The lack of influence of the push force can be explained, according to

the explanation model, by the fact that the push force is aligned coaxial to the excitation axis. Due to this alignment, the push force vector and the tangential vector of the rotational vibration are aligned perpendicularly to each other and are therefore independent of each other. As a result the push force has no influence on the RMI.

The investigations on **Hypothesis 3: Rotational impedance around the y_h –axis** also confirmed the explanatory model derived from the investigations on **Hypothesis 2: Rotational impedance around the x_h –axis**. Due to the round shape of the cylindrical measuring handle used in the study in Chapter 8, the hand-handle contact was completely frictionally engaged during excitations around the y_h –axis. Here the plots of the magnitude and the phase angle indicate an even stronger spring-damper dynamic than in the study in Chapter 7. The explanation model about the frictional damping effect of the hand-handle contact is also confirmed by the high positive effect strength of the gripping force which occurs at all frequencies. Thus, it can be confirmed that a higher gripping force increases the friction between the hand and the handle, resulting in a stronger coupling of the HAS to the vibrating measuring handle, which increases the magnitude of the RMI and reduces the damping effect of the frictional hand-grip contact. The assumption made in Chapter 7 that the push force has no influence on the RMI due to the coaxial alignment of the excitation axis and push force direction could also be confirmed in Chapter 8. In the study in Chapter 8 the push force direction was also coaxially aligned to the excitation axis and no influence on the RMI could be detected either. Thus, overall, the explanation model established in Chapter 7 could be confirmed by the results of the study in Chapter 8. Figure 9.1 summarizes the derived explanation model of both chapters graphically.

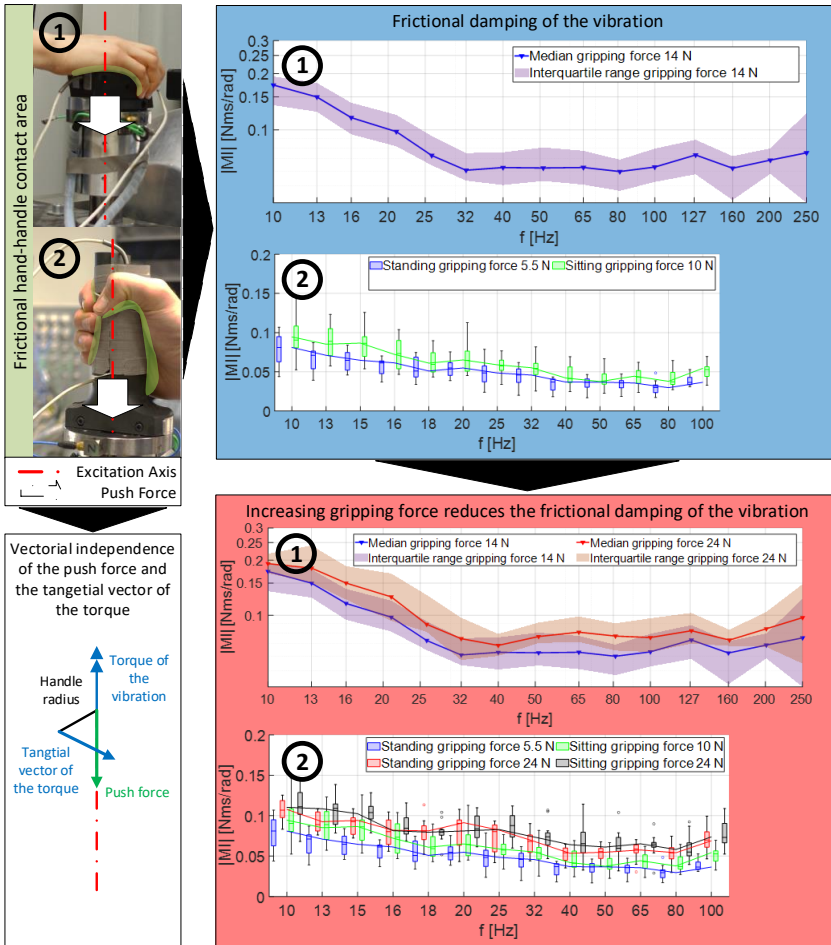


Figure 9.1: Graphical illustration of the explanation model derived from the findings of Chapter 7 and Chapter 8 presented in this thesis.

The explanation model shown in Figure 9.1 could provide a basis for designing power tool handle geometries that can transmit a lower vibration exposure due to a predominantly frictional hand-handle contact. The explanation model is supported by the studies conducted in the state of research on vibration reducing handles and gloves, as these devices also aim to provide additional damping in hand-handle contact. This additional damping is usually realized by adding a gel-, air- or textile-

based structure as a layer between the hand and the handle. Corresponding to the results and findings of Chapter 7 and Chapter 8 and the derived explanation model, the amount of damping due to these additional layers also depends on the coupling forces as well as on the excitation frequencies (ISO - International Organization for Standardization, 2013; Singh & Khan, 2014; D. E. Welcome et al., 2014). In this regard damping from a mostly frictional hand-handle contact, as suggested by the explanation model of the thesis, maybe provides an additional damping option that can be combined with the described coating methods. In this regard, damping from a predominantly frictional handle contact, as suggested by the explanation model of the thesis, potentially provides an additional damping option that can be combined with the handle coatings and the vibration reducing gloves from the state of re-search.

However, it must be acknowledged that a predominantly frictional handle contact may have a negative effect on the control of the power tool in terms of push and guide force. For this purpose, the method presented in Chapter 6 used to deal with **Hypothesis 1: Derivation of the measuring handle design** could help to develop an appropriate handle design that balances reduced vibration with sufficient user control. In this context the method used for developing the knob-shaped measuring handle could be transferred to other generic handle geometries and thus contributes to the investigation of gripping force distribution and the development of new measuring handles. The development of new measuring handles would enable a more extensive investigation of the relationship between hand position, power tool handle design and vibration exposure.

As the state of research presented in Chapter 2 and Chapter 3 of the thesis shows, the gripping force has a mandatory influence of the vibration transmission between the power tool handle and the HAS. For the investigation of the gripping force distribution on the surface of the power tool handle, the use of force measuring foils is an established method (Kalra et al., 2015b; Lemerle et al., 2008; Lindenmann et al., 2021). However, force measurement foils are not only used for field studies on real power tools, but also for gripping force measurements under laboratory conditions, such as on vibrating handles of shaker test benches or static loads (Gurram et al., 1993; D. Welcome et al., 2004). Hence several investigations on the development of corresponding measuring foils and gripping force measurement systems exist in the state of research (Pierre Marcotte et al., 2011; Yao et al., 2017). The method used in Chapter 6 to derive the design of the knob-shaped handle from the gripping force distribution contributes to this research. In this context the method establishes a link between the measurement gripping forces in field studies with power tool and the measurement of the MI in laboratory studies.

The results of such studies using the proposed method of Chapter 6 can be used in the field of ergonomic handle design. With regard to the handle design of power tools and the resulting force application as well as the user comfort, several studies on the pistol grip and the cylinder grip are available (Björing et al., 1999; Oh & Radwin, 1993; Wang & Cai, 2017). Here the method from Chapter 6 can be used to determine the main direction of the gripping force on generic power tool handles and set it into context to the anthropometric properties of the user as well as to the other forces the user applies to the handle. Such an approach can lead to more comfortable and less vibrating handling of the power tool, as well as safer handling.

9.3 Overall Conclusion on the obtained Results

The results of the work contribute to the solution of the presented research problem, as the obtained results provide data and knowledge about the rotational mechanical impedance (RMI) of the hand-arm system (HAS) for excitations around the x_h -axis and the y_h -axis. In preparation for this, a new knob-shaped measuring handle was developed for measuring gripping forces in impedance studies. This measuring handle also extends the state of the research by providing a new measuring instrument. An explanation model was derived from the measured RMI data to help understand vibration transmission in the hand-handle contact. For the industrial development of power tools, this explanation model provides a basis for a vibration reduced handle design. In this context, the method used for the data-driven design of the developed knob-shaped measuring handle can be applied to other handles gain knowledge about the gripping force distribution at different handle geometries in order to achieve a suitable compromise between low vibration transmission and sufficient usability of the power tool.

9.4 Outlook

From the results achieved and findings obtained in this thesis, the following topics arise for further research.

1. Establishment of the developed knob-shaped measuring handle in the state of research and standardization as an appropriated design.
2. Establish the method of data driven design for the positioning of the force transducers in measuring handles with a generic handle geometry.
3. Further investigations of the MI of the HAS and establishment of an online database for experimental biodynamic vibration data of the HAS.
4. Use of the experimental obtained data for the development, vibrational and musculoskeletal HAM.
5. Transfer obtained results and findings on the RMI to standardization.
6. Further investigations on the relationship between excitation axis, hand-handle contact and vibration transmission based on the derived explanation model.

Establishment of the developed knob-shaped measuring handle in the state of research and standardization as an appropriated design

In order to establish the proposed knob-shaped handle design in the state of research and standardization, it is required to extend the frequency spectrum up to which the handle has no natural frequencies. In the thesis this requirement could only be fulfilled up to 250 Hz, but it would make sense to eliminate all natural frequencies of the handle up to at least 500 Hz, which corresponds to the highest frequency of the third octave band from ISO 10068. One possible option for the frequency optimization of the handle could be to change the material of the measuring handle from GRP to aluminum. Furthermore the observed effect of the subject's handedness on the angular orientation on the division of the measuring handle should be addressed in future research. For this purpose, it is recommended to conduct a similar study as in Chapter 6 with only left-handed subjects. In this context also the assumption about the stabilizing effect of the push force on the angular orientation of the separation plane could be evaluated. It should also be noted that the developed measuring handle was derived only from the knob-shaped handle of one particular random orbital sander. Therefore, it is recommended to conduct comparable studies with other power tools that have a knob-shaped handle, to verify the derived division of the measuring handle by a larger quantity of power tools.

Establish the method of data driven design for the positioning of the force transducers in measuring handles with a generic handle geometry

The method for deriving the angular position of the force transducers from the gripping force distribution on handle's surface can be transferred to other handles with a generic handle geometry. Especially when regrading handles, for which the main direction of the gripping force is not as obviously visible as in the case of the cylindrical handle the method supports the determination of the gripping force direction. With regard to vibration measurement at test benches the method thus enables the use of more realistic measuring handles that represent the actual geometry of the real power tool handle. Such measuring handles open a new aspect in research on vibration transmission and gripping force measurement, as the suitability of different handle geometries can be investigated with regard to vibration transmission and force application. This applies also for the field of ergonomic handle design, where the method can be used to identify areas of particularly high gripping forces. The areas identified in this way could allow conclusions to be drawn about the handling and gripping comfort of a particular handle design. In this context, it is proposed to use the term "Handle Design by Force Distribution" or the acronym "HDFD-method" to describe and refer to this newly developed method in the future.

Further investigations of the MI of the HAS and establishment of an online database for experimental biodynamic vibration data of the HAS.

The investigations on the RMI presented in this thesis can be regarded as a first approach to extend the knowledge on the rotational biodynamics of the HAS. Nevertheless, further research is needed to expand the knowledge on the RMI and to confirm the results of this thesis. This applies in particular for rotational vibration excitation around the x_h – and y_h –axes at frequencies beyond 250 Hz and 100 Hz. In this context it should also be investigated, whether the determined influences of the coupling forces and the body posture also apply at higher frequencies and for excitations around the z_h –axis. The same applies to the determined influences itself, as the range of the coupling force should be extended and the body posture further varied.

Another approach would be to combine the rotational excitation of the HAS with an additional translational excitation. In this case the HAS would be multiaxially excited and the cross axial biodynamic response of the HAS could be measured. This type of biodynamic response to vibration would be closer to the real biodynamic response of the HAS when exposed to vibration from power tools. In addition, the results obtained with this multiaxial excitation could be used to extend the modeling of the HAS and validate the existing HAM in the state of the research. In this context, it is

recommended that an open-access online database of experimental data on HAS biodynamics be created. This would have the advantage of summarizing the data already available in the state of the research, allowing missing data to be better identified and targeted for investigation. Also, the results of different studies could be compared to draw general conclusions about the vibrational biodynamics of the HAS, thus increasing the knowledge of its physical description. This would contribute to communication between the different researchers in the field of hand-arm vibration and lead to a common understanding of the biodynamics of the hand-arm system. Furthermore, such a data base would provide a huge basis for the parametrization of HAM.

Use of the experimental obtained data on the RMI for the development of vibrational and musculoskeletal HAM

As mentioned in subchapter 1.1 the measured data can be used to parametrize corresponding HAM. As shown by equation 2.10 the RMI can be used to derive the inertia, stiffness and damping parameters of the HAS. These physical quantities allow the parametrization of corresponding HAM. Hereby the corresponding HAM include mechanical substitute models as well as simulative multibody models and musculoskeletal models.

In the case of mechanical substitute models the dynamic properties derived from the RMI can be used as reference values to which the springs, dampers and inertias of the HAM are adjusted. The basic structure of the rotational hand-arm model developed by Mangold (2019) could possibly also be used for excitations around the x_h – or y_h –axis. For this purpose, however, the springs and dampers would have to be adjusted to the values resulting from the RMI measurements of this thesis. Therefore it is recommended to use adjustable springs and dampers, as Lindemann (2023) did for a translational HAM. This would allow different rotational excitation directions to be represented by a physical HAM.

Beside mechanical substitute models the RMI data of this thesis could also be used for the parametrization of simulative HAM. As introduced in subchapter 1.1, the RMI data of the HAS enable the simulation of a corresponding rotational HAM as well as the physical description of the biodynamics of the HAS under multiaxial excitation. Consequently, the RMI data obtained in this thesis contribute to the parameterization of simulative HAM to simulate the biodynamics of the HAS under multiaxial vibration excitation. A corresponding application has already been submitted to the German Research Foundation (DFG). In this application the development of a vibrational HAM for six excitation directions (six translational and six rotational) is proposed. For the parametrization of this HAM the RMI data measured presented in

this thesis are used together with additional data. The proposed HAM should also be able to simulate the influence of the coupling forces on the MI, to which the RMI data of this thesis also contributes.

A further approach of using the data obtained is to parametrize the HAS of **musculoskeletal body models**. From the investigated RMI data the stiffness, damping and inertia of the HAS can be derived. Combined with the additional data from other studies on the biodynamics of the HAS, these dynamic properties could be attributed to specific anatomic structures of the HAS. This applies in particular to the MI data obtained for different gripping and push forces, since here differences may be due to the tension of specific forearm muscles. In this context, the online database mentioned above would provide a suitable data pool from which such data could be obtained. Since the musculoskeletal system of the HAS is very complex, the analytical derivation of the dynamic properties of certain anatomical structures in the hand-arm system from the experimental biodynamic data is limited. For this reason it is recommended to use an AI-based approach to analyze the biodynamic data and derive the dynamic properties of specific muscles and bones of the musculoskeletal HAM. In such an approach a machine learning algorithm would be trained by the data obtained in this thesis and other experimental biodynamic data to parametrize a given a musculoskeletal HAM under the physical conditions of human motion kinematics. The advantage of this approach would be that a larger amount of experimental data could be used to automatically parameterize the model, resulting in higher accuracy of the HAM when simulating the HAM. Once trained, such an AI-based parameterization of the musculoskeletal HAM could be regularly updated by the experimental biodynamic data newly uploaded to the before mentioned online database, iteratively increasing the accuracy of the musculoskeletal HAM.

Transfer obtained results and findings on the RMI to standardization

The current state of standardization ISO 10068 and the standards based on it do not cover rotational excitation with regard to RMI. Since the several power tools emit rotational vibrations and the consideration of the RMI is also required for the complete physical description of the biodynamics of the HAS an extension of the standardization regarding the RMI is recommended. This extension should also contain the influence of hand position. The results presented in the thesis suggest that the "palm" and the "hand-grip" position result in a different course of the RMI, therefore similar differences regarding the MI can also be assumed. It is therefore recommended that the standardization for MI also be supplemented to include the "palm" position. The extension regarding the "palm" position would also be beneficial with regard to DIN EN ISO 5349-1, where the "palm" position is already mentioned. For this reason consideration of the "palm" position in ISO 10068 would complement

vibration related standardization. However, to expand MI-related standardization, several additional studies and investigations on the RMI and the influence of the "palm" position are required to create a larger data base. The aspects and boundary conditions to be investigated in this context are mentioned above in the third topic for further research.

Further investigations on the relationship between excitation axis, hand-handle contact and vibration transmission based on the derived explanation model.

The results from Chapter 7 and Chapter 8 presented in this thesis can be summarized in an explanation model, which suggests that vibration transmission via a frictional hand-handle contact could reduce the vibration exposure of the HAS. This explanation model has to be verified and extend by further studies on the relationship between excitation axis, hand-handle contact and vibration transmission. In these studies it should be investigated, whether damping effect of a frictional hand-handle contact also applies for other excitation directions, vibration types, hand positions and frequency ranges. Together with the findings of this thesis the results of such studies could contribute to the development of a low-vibration handle design of power tools. Since the frictional handle contact presumably acts as a friction damper, this effect could be used purposefully in the design of new handle geometries of power tools. However it has to be considered that while frictional contact between the hand and handle may reduce vibration exposure, it may restrict the application of guiding forces to the handle. In a positive hand-handle contact, the forces applied by the user act normal to the surface of the handle. In a frictional hand-handle contact, the forces are applied tangentially to the surface of the handle, which limits the amount of force applied because the hand could slip off the handle. In addition, the handling of the handle could also be negatively influenced in terms of precision by a frictional hand-handle contact, since the force feedback of the power tool only acts indirectly via the frictional contact. In this context, the method for determining gripping force distribution presented in Chapter 6 of the thesis could potentially be used as a tool for analyzing the handling and force transmission of different handle geometries. Thus, the results and findings of the thesis can also be used to design low-vibration power tool handle geometries that also enable safe and precise handling.

References

- Adewusi, S., Rakheja, S., & Marcotte, P. (2012). Biomechanical models of the human hand-arm to simulate distributed biodynamic responses for different postures. *International Journal of Industrial Ergonomics*, 42(2), 249–260. <https://doi.org/10.1016/j.ergon.2012.01.005>
- Aldien, Y., Marcotte, P., Rakheja, S., & Boileau, P. É. (2005). Mechanical Impedance and Absorbed Power of HandArm under xh–Axis Vibration and Role of Hand Forces and Posture. *Industrial Health*, 2005(43), 495–508. <https://doi.org/10.2486/indhealth.43.495>
- Aldien, Y., Marcotte, P., Rakheja, S., & Boileau, P. E. (2006). Influence of hand-arm posture on biodynamic response of the human hand-arm exposed to zh-axis vibration. *International Journal of Industrial Ergonomics*, 36(1), 45–59. <https://doi.org/10.1016/j.ergon.2005.07.001>
- Besa, A. J., Valero, F. J., Suñer, J. L., & Carballeira, J. (2007). Characterisation of the mechanical impedance of the human hand–arm system: The influence of vibration direction, hand–arm posture and muscle tension. *International Journal of Industrial Ergonomics*, 37(3), 225–231. <https://doi.org/10.1016/j.ergon.2006.10.019>
- Björing, G., Johansson, L., & Hägg, G. M. (1999). Choice of handle characteristics for pistol grip power tools. *International Journal of Industrial Ergonomics*, 24(6), 647–656. [https://doi.org/10.1016/S0169-8141\(98\)00069-9](https://doi.org/10.1016/S0169-8141(98)00069-9)
- Burström, L. (1997). The influence of biodynamic factors on impedance of the hand and arm. *International Arch Occup Environ Health*, 1997(69), 437–446. <https://doi.org/10.1007/s004200050172>
- Chang, C. H., & Wang, M. J. (2000). Evaluating factors that influence hand-arm stress while operating an electric screwdriver. *Applied Ergonomics*, 31(3), 283–289. [https://doi.org/10.1016/S0003-6870\(99\)00048-4](https://doi.org/10.1016/S0003-6870(99)00048-4)

- Chang, C.-H., Wang, M.-J. J., & Lin, S.-C. (1999). Evaluating the effects of wearing gloves and wrist support on hand–arm response while operating an in-line pneumatic screwdriver. *International Journal of Industrial Ergonomics*, 24(5), 473–481. [https://doi.org/10.1016/S0169-8141\(98\)00053-5](https://doi.org/10.1016/S0169-8141(98)00053-5)
- Chang, C.-H., & Wang, M.-J. J. (2001). Evaluating the effects of activation mode, torque and horizontal operating distance on hand–arm response while operating pneumatic screwdrivers. *International Journal of Industrial Ergonomics*, 28(3-4), 171–179. [https://doi.org/10.1016/S0169-8141\(01\)00030-0](https://doi.org/10.1016/S0169-8141(01)00030-0)
- Cohen, J. (1992). Quantitative methods in psychology: A power primer. *Psychological Bulletin*(112), 155–159. <http://citeseerx.ist.psu.edu/viewdoc/summary?doi=10.1.1.1043.9095>
- Concettoni, E., & Griffin, M. (2009). The apparent mass and mechanical impedance of the hand and the transmission of vibration to the fingers, hand, and arm. *Journal of Sound and Vibration*, 325(3), 664–678. <https://doi.org/10.1016/j.jsv.2009.03.033>
- Cundiff, J. S. (1976). Energy dissipation in human hand-arm exposed to random vibration. *The Journal of the Acoustical Society of America*, 59(1), 212–216. <https://doi.org/10.1121/1.380850>
- DIN - Deutsches Institut für Normung (August 2013). *DIN CEN ISO/TR 7250-2 DIN SPEC 91279:2013: Wesentliche Maße des menschlichen Körpers für die technische Gestaltung – Teil 2: Anthropometrische Datenbanken einzelner nationaler Bevölkerungen: Basic human body measurements for technological design – Part 2: Statistical summaries of body measurements from national populations (DIN CEN ISO/TR 7250-2)*. Berlin. Beuth Verlag GmbH.
- DIN - Deutsches Institut für Normung (Dezember 2017). *DIN EN ISO 7250-1:2017: Wesentliche Maße des menschlichen Körpers für die technische Gestaltung – Teil 1: Körpermaßdefinitionen und -messpunkte: Basic human body measurements for technological design – Part 1: Body measurement definitions and landmarks (DIN EN ISO 7250-1)*. Berlin. Beuth Verlag GmbH.

- DIN Deutsches Institut für Normung e. V. (Januar 2001a). *Mechanische Eingangsimpedanz des menschlichen Hand-Arm-Systems* (DIN 45677). Berlin. Beuth Verlag GmbH.
- DIN Deutsches Institut für Normung e. V. (Dezember 2001b). *DIN EN ISO 5349-1:2001-12: Mechanische Schwingungen - Messung und Bewertung der Einwirkung von Schwingungen auf das Hand-Arm-System des Menschen Teil 1: Allgemeine Anforderungen*: [Mechanical vibration – Measurement and evaluation of human exposure – Part 1: General requirements] (DIN EN ISO 5349-1). Berlin. Beuth Verlag GmbH.
- DIN Deutsches Institut für Normung e. V. (2002). *DIN 1311-2:2002-08, Schwingungen und schwingungsfähige Systeme – Teil 2: Lineare, zeitinvariante schwingungsfähige Systeme mit einem Freiheitsgrad*. Berlin: Beuth Verlag GmbH.
- DIN Deutsches Institut für Normung e. V. (Mai 2010a). *DIN EN ISO 28927-3:2010-05: Handgehaltene motorbetriebene Maschinen - Messverfahren zur Ermittlung der Schwingungsemission Teil 3: Poliermaschinen sowie Rotationsschleifer, Schwingschleifer und Exzentrerschleifer (ISO 28927-3:2009)*: [Hand-held portable power tools – Test methods for evaluation of vibration emission – Part 3: Polishers and rotary, orbital and random orbital sanders (ISO 28927-3:2009)] (DIN EN ISO 28927-3). Berlin. Beuth Verlag GmbH.
- DIN Deutsches Institut für Normung e. V. (Mai 2010b). *DIN EN ISO 28927-3:2010-5: Handgehaltene motorbetriebene Maschinen - Messverfahren zur Ermittlung der Schwingungsemission - Teil 3: Poliermaschinen sowie Rotationsschleifer, Schwingschleifer und Exzentrerschleifer (ISO 28927-3:2009)*: [Hand-held portable power tools – Test methods for evaluation of vibration emission – Part 3: Polishers and rotary, orbital and random orbital sanders (ISO 28927-3:2009)] (DIN EN ISO 28927-3). Berlin. Beuth Verlag GmbH.
- DIN Deutsches Institut für Normung e. V. (Februar 2013). *DIN 45679:2013-02: Mechanische Schwingungen - Messung und Bewertung der Ankopplungskräfte zur Beurteilung der Schwingungsbelastung des Hand-Arm-Systems*: [Mechanical vibration - Measurement and evaluation of coupling forces to assess the vibration load on the hand-arm system] (DIN 45679). Berlin. Beuth Verlag GmbH.

- DIN Deutsches Institut für Normung e. V. (Dezember 2015). *Mechanische Schwingungen – Messung und Bewertung der Einwirkung von Schwingungen auf das Hand-Arm-System des Menschen – Teil 2: Praxisgerechte Anleitung zur Messung am Arbeitsplatz (ISO 5349-2:2001 + Amd 1:2015)*; (DIN EN ISO 5349-2). Berlin. Beuth Verlag GmbH.
- DIN Deutsches Institut für Normung e. V. (Mai 2019). *DIN EN ISO 10819:2019-5: Mechanische Schwingungen und Stöße – Hand-Arm-Schwingungen – Messung und Bewertung der Schwingungsübertragung von Handschuhen in der Handfläche: Mechanical vibration and shock - Hand-arm vibration - Measurement and evaluation of glove palm vibration transmission* (DIN EN ISO 10819). Berlin. Beuth Verlag GmbH.
- DIN Deutsches Institut für Normung e. V.; ISO - International Organization for Standardization (August 2013). *DIN CEN ISO 7250-2: Wesentliche Maße des menschlichen Körpers für die technische Gestaltung – Teil 2: Anthropometrische Datenbanken einzelner nationaler: Basic human body measurements for technological design – (DIN; CEN; ISO 7250-2)*. Berlin. Beuth Verlag GmbH.
- DIN Deutsches Institut für Normung e.V. (August 1997). *DIN EN ISO 266:1997-8: Normfrequenzen* (DIN EN ISO 266). Berlin. Berlin: Beuth Verlag GmbH.
- Dong, R. G., Rakheja, S., Schopper, A. W., Han, B., & Smutz, W. P. (2001). Hand-transmitted vibration and biodynamic response of the human hand-arm: A critical review. *Critical Reviews in Biomedical Engineering*, 29(4), 393–439. <https://doi.org/10.1615/critrevbiomedeng.v29.i4.20>
- Dong, R. G., Welcome, D. E., & McCormick, R. E. (2006). 3-D laboratory simulation of hand-transmitted vibration. In *Conference Proceedings of the Society for Experimental Mechanics Series*.
- Dong, R. G., Welcome, D. E., McDowell, T. W., & Wu, J. Z. (2006). Measurement of biodynamic response of human hand-arm system. *Journal of Sound and Vibration*, 294(4), 807–827. <https://doi.org/10.1016/j.jsv.2005.12.047>
- Dong, R. G., Welcome, D. E., McDowell, T. W., & Wu, J. Z. (2013). Modeling of the biodynamic responses distributed at the fingers and palm of the hand in three orthogonal directions. *Journal of Sound and Vibration*, 332(4), 1125–1140. <https://doi.org/10.1016/j.jsv.2012.10.003>

- Dong, R. G., Welcome, D. E., & Wu, J. Z. (2005). Estimation of Biodynamic Forces Distributed on the Fingers and the Palm Exposed to Vibration. *Industrial Health*, 43(3), 485–494. <https://doi.org/10.2486/indhealth.43.485>
- Dong, R. G., Welcome, D. E., Xu, X. S., Warren, C., McDowell, T. W., Wu, J. Z., & Rakheja, S. (2012). Mechanical impedances distributed at the fingers and palm of the human hand in three orthogonal directions. *Journal of Sound and Vibration*, 331(5), 1191–1206. <https://doi.org/10.1016/j.jsv.2011.10.015>
- Dong, R. G., Wu, J. Z., McDowell, T. W., Welcome, D. E., & Schopper, A. W. (2004, May). Distribution of mechanical impedance at the fingers and the palm of the human hand. *Journal of Biomechanics*, 2005(38), 1165–1175. <https://doi.org/10.1016/j.jbiomech.2004.05.021>
- European Commission, Directorate-General for Research and Innovation, Breque, M., Nul, L. de, & Petridis, A. (2021, January 5). Industry 5.0 : towards a sustainable, human-centric and resilient European industry. Publications Office.
- Forsteneichner, C., Paetzold, K., & Metschkoll, M. (2015). Methodische Vorgehensweise zur Verifikation und Validierung komplexer Systeme. In D. Krause, K. Paetzold, & S. Wartzack (Eds.), *Design for X: Beiträge zum 26. Dfx-Symposium, Oktober 2015*. TuTech Verl.
- Griffin, M. J. (1996). *Handbook of human vibration* (1st pbk. ed.). Academic Press.
- Gurram, R., Gouw, G. J., & Rakheja, S. (1993). Grip pressure distribution under static and dynamic loading. *Experimental Mechanics*, 33(3), 169–173. <https://doi.org/10.1007/BF02322568>
- ISO - International Organization for Standardization (April 1973). *ISO 3:1973: Preferred numbers- Series of preferred numbers* (ISO 3). Geneva. ISO copyright office.
- ISO - International Organization for Standardization (July 2007). *ISO 15230:2007(E): Mechanical vibration and shock — Coupling forces at the man-machine interface for hand-transmitted vibration* (ISO 15230). Geneva. ISO copyright office.

References

- ISO - International Organization for Standardization (December 2012). *ISO 10068:2012(E): Mechanical vibration and shock - Mechanical impedance of the human hand-arm system at the driving point* (ISO 10068). Geneva. ISO copyright office.
- ISO - International Organization for Standardization (July 2013). *ISO 10819:2012-7: Mechanical vibration and shock — Hand-arm vibration - Measurement and evaluation of the vibration transmissibility of gloves at the palm of the hand* (ISO 10819). Geneva. ISO copyright office.
- Joshi, A., Guttenberg, R., Leu, M., & Murray, S. (2008). Modeling of the hand–arm system for impact loading in shear fastener installation. *International Journal of Industrial Ergonomics*, 38(9), 715–725. <http://dx.doi.org/10.1016/j.ergon.2007.10.012>
- Kalra, M., Rakheja, S., Marcotte, P., Dewangan, K. N., & Adewusi, S. (2015a). Measurement of coupling forces at the power tool handle-hand interface. *International Journal of Industrial Ergonomics*, 50, 105–120. <https://doi.org/10.1016/j.ergon.2015.09.013>
- Kalra, M., Rakheja, S., Marcotte, P., Dewangan, K. N., & Adewusi, S. (2015b). Measurement of coupling forces at the power tool handle-hand interface. *International Journal of Industrial Ergonomics*(50), 105–120. <https://doi.org/10.1016/j.ergon.2015.09.013>.
- Kaulbars, U., & Lemerle, P. (2007). Messung der Ankopplungskräfte zur Beurteilung der Hand-Arm-Schwingungen–Weiterentwicklung eines Messsystems: [Measurement of coupling forces for the evaluation of hand-arm vibrations-Further development of a measurement system (author's transl.)]. *VDI-Berichte*, 2002, 99–111.
- Kuijt-Evers, L. F. M., Bosch, T., Huysmans, M. A., Looze, M. P. de, & Vink, P. (2007). Association between objective and subjective measurements of comfort and discomfort in hand tools. *Applied Ergonomics*, 38(5), 643–654. <https://doi.org/10.1016/j.apergo.2006.05.004>
- Kuijt-Evers, L. F. M., Vink, P., & Looze, M. P. de (2007). Comfort predictors for different kinds of hand tools: Differences and similarities. *International Journal of Industrial Ergonomics*, 37(1), 73–84. <https://doi.org/10.1016/j.ergon.2006.09.019>

- Lemerle, P., Klinger, A., Cristalli, A., & Geuder, M. (2008). Application of pressure mapping techniques to measure push and gripping forces with precision. *Ergonomics*, *51*(2), 168–191. <https://doi.org/10.1080/00140130701528602>
- Lin, J. H., Radwin, R. G., & Richard, T. G. (2003). A single-degree-of-freedom dynamic model predicts the range of human responses to impulsive forces produced by power hand tools. *Journal of Biomechanics*, *36*(12), 1845–1852. [https://doi.org/10.1016/S0021-9290\(03\)00214-8](https://doi.org/10.1016/S0021-9290(03)00214-8)
- Lindenmann, A. (2023). Analyse der Schwingungseigenschaften des menschlichen Hand-Arm-Systems in translatorischer Richtung und deren Abbildung in einem einstellbaren physischen Hand-Arm-Modell. In A. Albers & S. Matthiesen (Eds.), *Forschungsberichte des IPEK - Institut für Produktentwicklung: Systeme, Methoden, Prozesse* (Bd. 166). Karlsruhe: Karlsruher Institut für Technologie (KIT) <https://doi.org/10.5445/IR/1000161145>
- Lindenmann, A., & Matthiesen, S. (2019). The Rotational Mechanical Impedance of the Hand-Arm System: A Preliminary Study. In Institut für Arbeitsschutz der Deutschen Gesetzlichen Unfallversicherung (Ed.), *14th International Conference on Hand-Arm-Vibration: - Abstracts -* (Vol. 14, pp. 75–76). Deutsche Gesetzliche Unfallversicherung (DGUV). <https://publikationen.bibliothek.kit.edu/1000095936>
- Lindenmann, A., Schröder, T., Germann, R., Gwosch, T., & Matthiesen, S. (2022). Effect of high level grip-and push force and elevated arm posture on the zh-axis hand-arm impedance. *International Journal of Industrial Ergonomics*, *92*, 103375. <https://doi.org/10.1016/j.ergon.2022.103375>
- Lindenmann, A., Uhl, M., Gwosch, T., & Matthiesen, S. (2021). The influence of human interaction on the vibration of hand-held human-machine systems – The effect of body posture, feed force, and gripping forces on the vibration of hammer drills. *Applied Ergonomics*, *95*, 103430. <https://doi.org/10.1016/j.apergo.2021.103430>
- Looze, M. P. de, Urlings, I., Vink, P., van Rhijn, J. W., Miedema, M. C., Bronkhorst, R. E., & van der Grinten, M. P. (2001). Towards successful physical stress reducing products: An evaluation of seven cases. *Applied Ergonomics*, *32*(5), 525–534. [https://doi.org/10.1016/S0003-6870\(01\)00018-7](https://doi.org/10.1016/S0003-6870(01)00018-7)

- Makita Werkzeug GmbH. (2021). *DBO180Z - Akku-Exzentrerschleifer Datenblatt*. <https://www.makita.de/product/dbo180z.html>
- Mangold, S. (2019). Erfassung heterogener passiver Anwendereigenschaften und deren Abbildung in einem einstellbaren Hand-Arm Modell am Beispiel eines Impulsschraubers. Dissertation: Acquisition of user's heterogeneous biodynamic response and possibilities to model those in an adjustable hand-arm model using the example of an impulse wrench. In A. Albers & S. Matthiesen (Eds.), *Forschungsberichte des IPEK - Institut für Produktentwicklung*. ISSN: 1615-8113 (Vol. 125).
- Marcotte, P., Aldien, Y., Boileau, P. É., Rakheja, S., & Boutin, J. (2005). Effect of handle size and hand-handle contact force on the biodynamic response of the hand-arm system under zh-axis vibration. *Journal of Sound and Vibration*, 283(3-5), 1071–1091. <https://doi.org/10.1016/j.jsv.2004.06.007>
- Marcotte, P., Boutin, J., & Jasinski, J. (2010). Development of a hand-arm mechanical analogue for evaluating chipping hammer vibration emission values. *Journal of Sound and Vibration*, 329(10), 1968–1980. <https://doi.org/10.1016/j.jsv.2009.10.042>
- Marcotte, P., Adewusi, S., & Rakheja, S. (2011). Development of a low-cost system to evaluate coupling forces on real power tool handles. *Canadian Acoustics*, 39(2), 36–37. <https://jcaa.caa-aca.ca/index.php/jcaa/article/view/2345>
- Matthiesen, S., Bruchmueller, T., Grauberger, P., & Wettstein, A. (2015). Modellunterstützte Reduktion von Störgrößen in einem Messsystem zur Erfassung der Geräte-Werkstück-Wechselwirkungen. In D. Krause, K. Paetzold, & S. Wartzack (Eds.), *Design for X: Beiträge zum 26. Dfx-Symposium, Oktober 2015* (pp. 157–168). TuTech Verl.
- Matthiesen, S., Lindenmann, A., & Bruchmueller, T. (2018). Anforderungen an ein Messsystem zur Ermittlung der Rotationsimpedanz von Hand-Arm Systemen. In VDI - Wissensforum GmbH (Ed.), *VDI-Berichte: Vol. 2322, 7. Vdi-Tagung Humanschwingungen 2018* (pp. 91–106). VDI Verlag GmbH.
- Matthiesen, S., Mangold, S., Bruchmüller, T., & Marko, A.-M. (2014). Der Mensch als zentrales Teilsystem in Wechselwirkung mit handgehaltenen Geräten – Ein problemorientierter Ansatz zur Untersuchung dieser Schnittstelle: [The human as a central subsystem interacting with hand-held devices -

- A problem-oriented approach to the study of this interface (author's transl.). In *Design for X: Beiträge zum 25. DfX-Symposium, Oktober 2014* (pp. 193–204). TuTech-Verlag.
- Matthiesen, S., Mangold, S., & Schaefer, T. (2012). Modellierung und Simulation des Hand-Arm-Systems bei stoßartiger Anregung. In D. Krause, K. Paetzhold, & S. Wartzack (Eds.), *Design for X: Beiträge zum 23. DfX-Symposium Oktober 2012* (pp. 113–124). TuTech-Verl.
- Matthiesen, S., Mangold, S., & Zumstein, T. (2016). Ein anpassbares Hand-Arm Modell mit rotatorischem Freiheitsgrad zur Validierung handgehaltener Geräte. In *VDI-Berichte: Vol. 2277. 6. VDI-Tagung Humanschwingungen 2016: Würzburg, 26.-27. April 2016* (pp. 95–109). VDI Verlag GmbH. An adjustable hand-arm model with rotational degree of freedom for power tool validation usage.
- Matthiesen, S., & Uhl, M. (2017a). Methodical Approach for the Analysis of the Active User Behavior during the Usage of Power Tools. In D. Krause, K. Paetzold, & S. Wartzack (Eds.), *Design for X: Beiträge zum 28. DfX-Symposium Oktober 2017* (1st ed., pp. 1–12). TuTech Verlag.
- Matthiesen, S., & Uhl, M. (2017b). Methodical Approach for the Analysis of the Active User Behavior during the Usage of Power Tools. In D. Krause, K. Paetzold, & S. Wartzack (Eds.), *Design for X: Beiträge zum 28. DfX-Symposium Oktober 2017* (1st ed., pp. 1–12). TuTech Verlag.
- Matysek, M., & Kern, T. A. (2009). *Entwicklung Haptischer Geräte: Ein Einstieg für Ingenieure [Haptic device development: an introduction for engineers (author's transl.)]*. Springer Berlin Heidelberg.
- Meldrum, D., Cahalane, E., Conroy, R., Fitzgerald, D., & Hardiman, O. (2007). Maximum voluntary isometric contraction: Reference values and clinical application. *Amyotrophic Lateral Sclerosis : Official Publication of the World Federation of Neurology Research Group on Motor Neuron Diseases*, 8(1), 47–55. <https://doi.org/10.1080/17482960601012491>
- Oh, S., & Radwin, R. G. (1993). Pistol grip power tool handle and trigger size effects on grip exertions and operator preference. *Human Factors*, 35(3), 551–569. <https://doi.org/10.1177/001872089303500311>

- Päivinen, M., & Heinimaa, T. (2009). The usability and ergonomics of axes. *Applied Ergonomics*, *40*(4), 790–796. <https://doi.org/10.1016/j.apergo.2008.08.002>
- Pan, D., Xu, X. S., Welcome, D. E., McDowell, T. W., Warren, C., Wu, J., & Dong, R. G. (2018). The relationships between hand coupling force and vibration biodynamic responses of the hand-arm system. *Ergonomics*, *61*(6), 818–830. <https://doi.org/10.1080/00140139.2017.1398843>
- Radwin, R. G., & Armstrong, T. J. (1985). Assessment of hand vibration exposure on an assembly line. *American Industrial Hygiene Association Journal*, *46*(4), 211–219. <https://doi.org/10.1080/15298668591394680>
- Rakheja, S., Wu, J. Z., Dong, R. G., & Schopper, A. W. (2002). A Comparison of biodynamic Models of the human Hand–Arm System for Applications to Hand-held Power Tools. *Journal of Sound and Vibration*, *249*(1), 55–82. <https://doi.org/10.1006/jsvi.2001.3831>
- Reynolds, D. D., & Soedel, W. (1972). Dynamic response of the hand-arm system to a sinusoidal input. *Journal of Sound and Vibration*, *352*.
- Schröder, T., Lindenmann, A., Hehmann, S., Uhl, M., Gwosch, T., & Matthiesen, S. (2020). A Method of Determining the Separation Plane of a Knob-Shaped Measuring Handle for the Measurement of Hand-Arm-Impedances. In VDI - Wissensforum GmbH (Ed.), *VDI-Berichte: Vol. 2370. 8. VDI-Tagung Humanschwingungen 2020* (Vol. 2323). VDI Verlag GmbH.
- Schröder, T., Lindenmann, A., Hehmann, S., Wettstein, A., Germann, R., Gwosch, T., & Matthiesen, S. (2022). Use of data-driven design for the development of knob-shaped handles in the context of impedance measurements. *Applied Ergonomics*, *2022*(98), 103575. <https://doi.org/10.1016/j.apergo.2021.103575>
- Schröder, T., Lindenmann, A., & Matthiesen, S. (2023). Influence of Coupling Forces and Body Posture on Rotational Hand–Arm Impedance in yh Direction. *Vibration*, *6*(2), 375–397. <https://doi.org/10.3390/vibration6020023>
- Schröder, T., Lindenmann, A., Resch, A., Matthiesen, S., & Gwosch, T. (2023). Influence of coupling forces on the mechanical impedance of the hand-arm

- system during rotational vibration excitation around the xh-axis. *International Journal of Industrial Ergonomics*, 95. <https://doi.org/10.1016/j.ergon.2023.103427>
- Shi, L., & Sun, B. (2018). Modeling and optimization of vibration response characteristics of the orbital sander based on surrogate model. *Structural and Multidisciplinary Optimization*, 57(6), 2259–2271. <https://doi.org/10.1007/s00158-017-1856-4>
- Shi, L., & Sun, B. (2019). 36th International Conference on Vibroengineering in Dubai, United Arab Emirates, March 15-17th, 2019. *Vibroengineering PROCEDIA*, 22, 176–181. <https://doi.org/10.21595/vp.2018.20466>
- Singh, J., & Khan, A. A. (2014). Effect of coating over the handle of a drill machine on vibration transmissibility. *Applied Ergonomics*, 45(2), 239–246. <https://doi.org/10.1016/j.apergo.2013.04.007>
- Tarabini, M., Saggin, B., Scaccabarozzi, D., & Moschioni, G. (2013). Hand-arm mechanical impedance in presence of unknown vibration direction. *International Journal of Industrial Ergonomics*, 43(1), 52–61. <https://doi.org/10.1016/j.ergon.2012.10.005>
- U. Kaulbars (2006). Schwingungen fest im Griff: [Vibrations firmly under control (author's transl.)]. *Technische Überwachung Düsseldorf*, 47(6), 35–40. https://www.dguv.de/medien/ifa/de/pub/grl/pdf/2006_081.pdf
- Wakula, J., Berg, K., Schau, K., & Bruder, R. (2009). *Der montagespezifische Kraftatlas: [the assembly-specific force atlas (author's transl.)]*. BGIA-Report: Vol. 2009,3. Technische Informationsbibliothek u. Universitätsbibliothek; BGIA. <https://publikationen.dguv.de/widgets/pdf/download/article/1913>
- Wang, C., & Cai, D. (2017). Hand tool handle design based on hand measurements. *MATEC Web of Conferences*, 119, 1044. <https://doi.org/10.1051/mateconf/201711901044>
- Welcome, D., Rakheja, S., Dong, R., Wu, J. Z., & Schopper, A. W. (2004). An investigation on the relationship between grip, push and contact forces applied to a tool handle. *International Journal of Industrial Ergonomics*, 34(6), 507–518. <https://doi.org/10.1016/j.ergon.2004.06.005>

- Welcome, D. E., Dong, R. G., Xu, X. S., Warren, C., & McDowell, T. W. (2014). The effects of vibration-reducing gloves on finger vibration. *International Journal of Industrial Ergonomics*, 44(1), 45–59. <https://doi.org/10.1016/j.ergon.2013.10.003>
- World Medical Association. (2013). *Declaration of Helsinki*. World Medical Association. <https://www.uni-goettingen.de/de/document/download/a91ef4324cf47306d6dbf334687e70dc.pdf/helsinki.pdf> <https://doi.org/10.1515/9783110874488-033>
- Xu, X., Welcome, D. E., McDowell, T., Wu, J. Z., Wimer, B., & Warren, C. (2011). The vibration transmissibility and driving-point biodynamic response of the hand exposed to vibration normal to the palm. *International Journal of Industrial Ergonomics*, 41(5), 418–427. <https://doi.org/10.1016/j.ergon.2011.05.007>
- Yao, Y., Rakheja, S., Marcotte, P., & Yang, F. (2017). Calibration and verification of a thin flexible film hand sensor. In *2017 International Conference on Advanced Mechatronic Systems: December 6-9, 2017, Huaqiao University, Xiamen, China* (pp. 501–505). IEEE. <https://doi.org/10.1109/I-CAMechS.2017.8316525>
- Zhang, W., Wang, Q., Xu, Z., Xu, H., Li, H., Dong, J., & Ma, X. (2021). An Experimental Study of the Influence of Hand-Arm Posture and Grip Force on the Mechanical Impedance of Hand-Arm System. *Shock and Vibration*, 2021, 1–11. <https://doi.org/10.1155/2021/9967278>

Student theses that were co-supervised by the author in the context of this dissertation at the IPEK Institute for Product Development at the Karlsruhe Institute of Technology (KIT)

- Nouri, N. (2019). *Entwicklung eines Modells zur Korrelation von Sensormodul und externer Sensorik am Beispiel von Beschleunigungsmessungen an Power-Tools: Development of a model for the correlation of sensor module and external sensors using the example of acceleration measurements on power-tools* (IPEK-Abschlussarbeit 3981) [Unveröffentlichte Masterarbeit]. Karlsruher Institut für Technologie (KIT), Karlsruhe.

Glossary

Term	Definition
Hand-arm system (HAS)	The human hand-arm system consists of the body parts arm and hand.
Hand-arm model (HAM)	A vibrational substitute model of the human hand-arm system. According to ISO 10068
Mechanical impedance (MI)	The complex-valued ratio of excitation force and deflection velocity at the excitation point as a function of excitation frequency. According to ISO 10068
Apparent mass (AM)	The complex-value ratio of excitation force and acceleration in the direction of force at the excitation point as a function of excitation frequency. According to ISO 10068
Apparent stiffness (AS)	The complex-valued ratio of excitation force and deflection in the direction of force at the excitation point as a function of excitation frequency. According to Dong, Welcome, McDowell, and Wu (2006)
Rotational Mechanical impedance (RMI)	The complex-valued ratio of excitation torque and angular velocity at the excitation point as a function of excitation frequency. According to Matysek and Kern (2009)
Rotational apparent mass (RAM)	The complex-valued ratio of excitation torque and angular acceleration at the excitation point as a function of excitation frequency. According to Matysek and Kern (2009)
Rotational apparent stiffness (AS)	The complex-valued ratio of excitation torque and rotation angel at the excitation point as a function of excitation frequency. According to Matysek and Kern (2009)
Basic centric coordinate system	Coordinate system related to the machine or power tool, whose origin is in the vibrating machine or its handle, which are gripped by the hand. According to DIN EN ISO 5349-1
Biodynamic coordinate system	Coordinate system related to the human hand, with the origin at the finger base of the third metacarpal. According to DIN EN ISO 5349-1

Coupling forces	All forces, which the user applies to a vibrating surface or handle. According to ISO 15230
Gripping force	A clamp-like force, which occurs when the hand encloses a handle. According to ISO 15230
Grip force	A synonym for gripping force
Push force	The resulting force, the user applies with each hand on a vibrating surface that is not compensated within the coupling surface of the hand. According to ISO 15230
Pressing force	A synonym for push force
Guiding force	A force applied by the user that moves a machine in a planar or horizontal movement. According to ISO 15230
„palm“ position	Hand position in which the hand rests on the top of a spherical, ball-like or knob-shaped handle geometry, with the fingers gripping enclosingly from above. According to DIN EN ISO 5349-1
„hand-grip“ position	Hand position in which the hand grips a cylindrical or elliptical handle geometry enclosing. According to DIN EN ISO 5349-1
Separation plane	Virtual plane rotated by angle α around the central axis in the 3D handle model's centric base coordinate system, dividing the handle model into two parts. According to Schröder et al. (2020)
A-group	The sensor positions located in the base-centric coordinate system of the 3D handle model inside the angular range of $\alpha \leq \vartheta_i \leq \alpha + \pi$. According to Schröder et al. (2020)
B-group	The sensor positions located in the base-centric coordinate system of the 3D handle model outside the angular range of $\alpha \leq \vartheta_i \leq \alpha + \pi$. According to Schröder et al. (2020)
Power tool	A synonym for handheld machine

Appendix A

Appendix A refers to the original appendix of the first publication of Schröder et al. (2022) cited in this thesis, as described in footnot 22

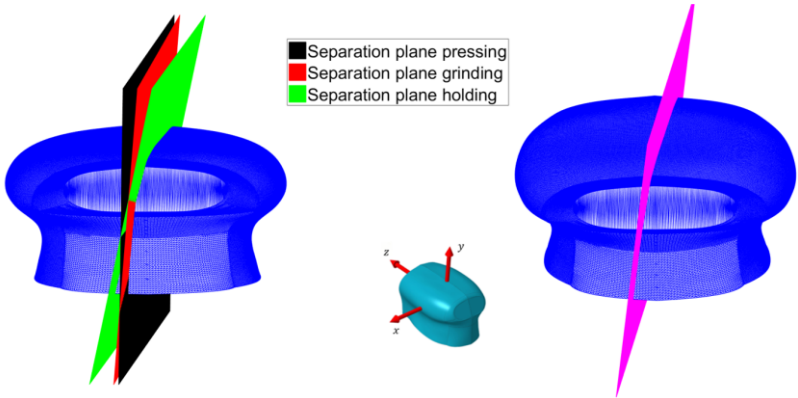
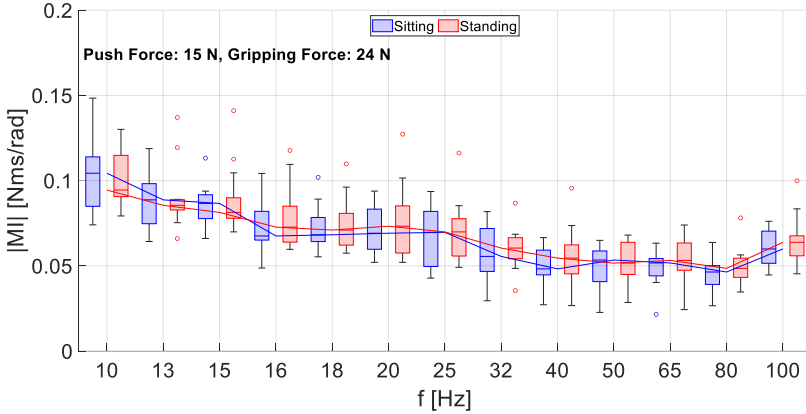


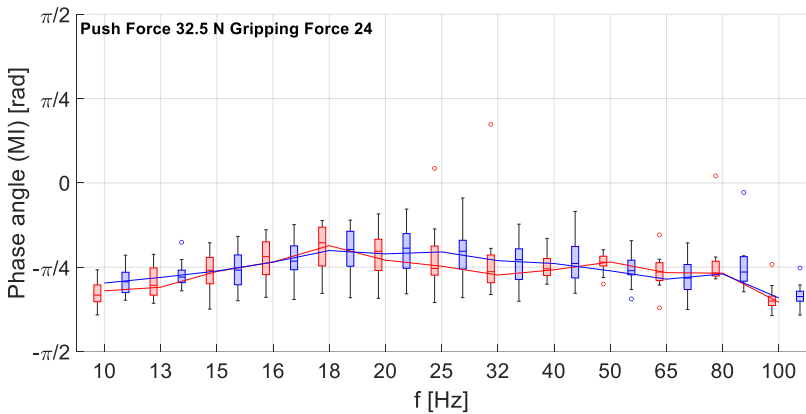
Figure A-1: “**Appendix A:** 3D-representation of the mean separation plane for each task passing through the 3D-scan of the orbital sander’s handle (left side). Overall separation plane calculated by the arithmetic mean over all three tasks.”

Appendix B

Appendix B contains additional plots of RMI magnitude and phase angle measured but not yet published as part of the third publication.

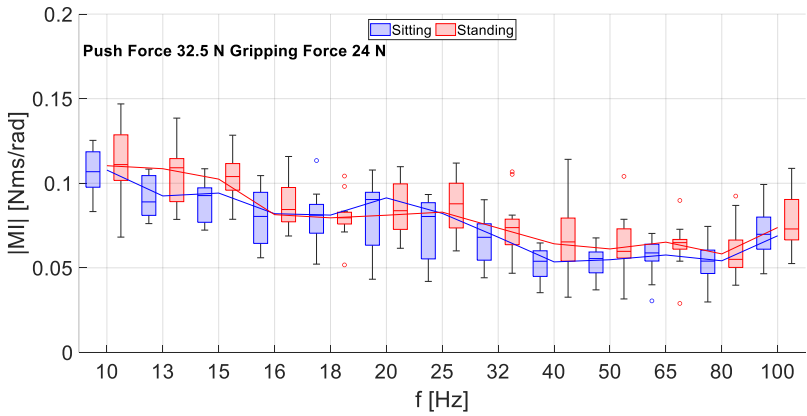


(a)

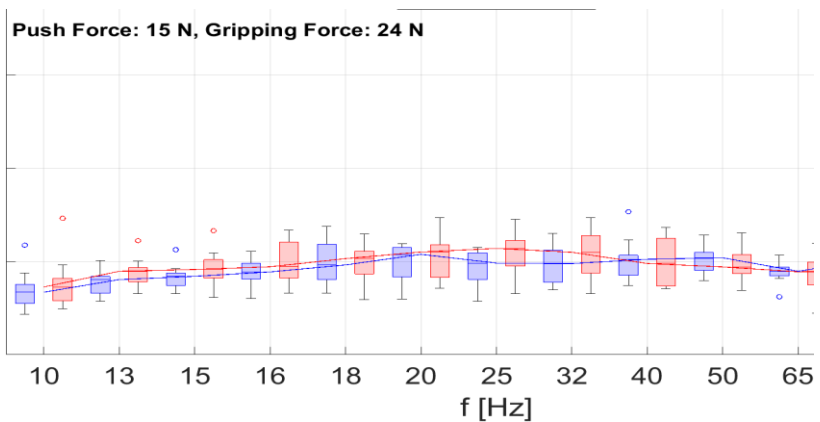


(b)

Figure B-1: Boxplots and median trend line of the RMI's magnitude (a) and phase angle (b) for the standing and the sitting postures at a push force of $F_{pu} = 32.5 N$ and a gripping force of $F_{gr} = 24 N$.



(a)



(b)

Figure B-2: Boxplots and median trend line of the RMI's magnitude (a) and phase angle (b) for the standing and the sitting postures at a push force of $F_{pu} = 32.5\text{ N}$ and a gripping force of $F_{gr} = 24\text{ N}$.

Publikationen die unter der Mitautorenschaft des Autors dieser Forschungsarbeit entstanden sind:

Fotler, D., Schröder, T., Germann, R., & Matthiesen, S. (27 and 2021, September 28). Objective evaluation of vibration comfort through the design of a vibration filter - Implementation of a study design for vibration comfort evaluation. In Proceedings of the 32nd Symposium Design for X. The Design Society. <https://doi.org/10.35199/dfx2021.06>.

Selbstständig erbrachter Teil: Schriftliche Ausarbeitung Einleitung, Review

Fotler D., Schröder T., Lindenmann, A., & Matthiesen, S. (2023). Aufbau einer Studienumgebung zur Bewertung von Vibrationsdiskomfort am Hand-Arm-System. In VDI-Berichte: Vol. 2411. Humanschwingungen 2023: 9. Vdi-Fachtagung : Vibrations- und Schwingungseinwirkungen auf den Menschen : 09. Und 10. Mai 2023, Würzburg (Vol. 9, pp. 137–148). VDI VERLAG GMBH. <https://doi.org/10.51202/9783181024119>.

Selbstständig erbrachter Teil: Konzept, Schriftliche Ausarbeitung Einleitung, Review

Lindenmann, A., Schröder, T., Germann, R., Gwosch, T., & Matthiesen, S. (2022). Effect of high level grip-and push force and elevated arm posture on the zh-axis hand-arm impedance. International Journal of Industrial Ergonomics, 92, 103375.

Selbstständig erbrachter Teil: Schriftliche Ausarbeitung, Review

Schröder, T., Lindenmann, A., Hehmann, S., Uhl, M., Gwosch, T., & Matthiesen, S. (2020). A Method of Determining the Separation Plane of a Knob-Shaped Measuring Handle for the Measurement of Hand-Arm-Impedances. In VDI - Wissensforum GmbH (Ed.), VDI-Berichte: Vol. 2370. 8. VDI-Tagung Humanschwingungen 2020 (Vol. 2323). VDI VERLAG GMBH.

Selbstständig erbrachter Teil: Methodenentwicklung, Experiment Durchführung, Datenauswertung, Schriftliche Ausarbeitung & Korrektur

Publikationen die unter der Mitautorenschaft des Autors dieser Forschungsarbeit entstanden sind:

Schröder, T., Lindenmann, A., Hehmann, S., Wettstein, A., Germann, R., Gwosch, T., & Matthiesen, S. (2022). Use of data-driven design for the development of knob-shaped handles in the context of impedance measurements. *Applied Ergonomics*, 2022(98), 103575. <https://doi.org/10.1016/j.apergo.2021.103575>.

Selbstständig erbrachter Teil: Methodenentwicklung, Experiment Durchführung, Datenauswertung, Schriftliche Ausarbeitung & Korrektur

Schröder, T., Lindenmann, A., & Matthiesen, S. (2023). Influence of Coupling Forces and Body Posture on Rotational Hand–Arm Impedance in yh Direction. *Vibration*, 6(2), 375–397. <https://doi.org/10.3390/vibration6020023>.

Selbstständig erbrachter Teil: Methodenentwicklung, Experiment Durchführung, Datenauswertung, Schriftliche Ausarbeitung & Korrektur

Schröder, T., Lindenmann, A., Resch, A., Matthiesen, S., & Gwosch, T. (2023). Influence of coupling forces on the mechanical impedance of the hand-arm system during rotational vibration excitation around the xh-axis. *International Journal of Industrial Ergonomics*, 95, 103427. <https://doi.org/10.1016/j.ergon.2023.103427>.

Selbstständig erbrachter Teil: Methodenentwicklung, Experiment Durchführung, Datenauswertung, Schriftliche Ausarbeitung & Korrektur

Schröder, T., Gwosch, T., & Matthiesen, S. (2020). Comparison of Parameterization Methods for Real-Time Battery Simulation Used in Mechatronic Powertrain Test Benches. *IEEE Access*, 8, 87517–87528. <https://doi.org/10.1109/ACCESS.2020.2989724>.

Selbstständig erbrachter Teil: Methodenentwicklung, Experiment Durchführung, Datenauswertung, Schriftliche Ausarbeitung & Korrektur

Schröder T., Spengler C., Lindenmann, A., & Matthiesen, S. (2023). Einfluss der Ankopplungskräfte auf die rotatorische Impedanz des menschlichen Hand-Arm-Systems bei Rotationsschwingungen um die zh-Achse. In *VDI-Berichte: Vol. 2411. Humanschwingungen 2023: 9. Vdi-Fachtagung : Vibrations- und Schwingungseinwirkungen auf den Menschen : 09. Und 10. Mai 2023, Würzburg (Vol. 9, pp. 125–134)*. VDI VERLAG GMBH. <https://doi.org/10.51202/9783181024119>

Selbstständig erbrachter Teil: Methodenentwicklung, Experiment Durchführung, Datenauswertung, Schriftliche Ausarbeitung & Korrektur